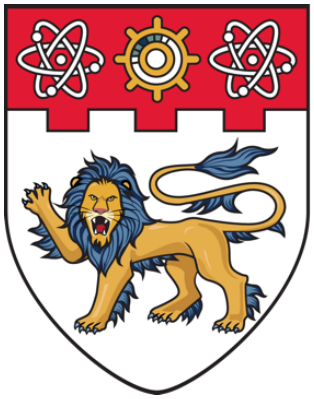

NANYANG TECHNOLOGICAL UNIVERSITY

SINGAPORE

THE ROLE OF N-WASP AND TXNIP IN SKIN CANCER CELL PROLIFERATION

CHUNG YAT JOONG

SCHOOL OF BIOLOGICAL SCIENCES

2019

THE ROLE OF N-WASP AND TXNIP IN SKIN CANCER CELL PROLIFERATION

CHUNG YAT JOONG

SCHOOL OF BIOLOGICAL SCIENCES

A thesis submitted to Nanyang Technological University
in partial fulfilment of the requirement for
the degree of Doctor of Philosophy

2019

Statement of Originality

I hereby certify that the work embodied in this thesis is the result of original research done by me except where otherwise stated in this thesis. The thesis work has not been submitted for a degree or professional qualification to any other university or institution. I declare that this thesis is written by myself and is free of plagiarism and of sufficient grammatical clarity to be examined. I confirm that the investigations were conducted in accord with the ethics policies and integrity standards of Nanyang Technological University and that the research data are presented honestly and without prejudice.

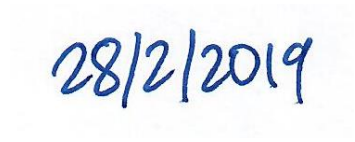

. . . . . .

Date

. . . . . .

Chung Yat Joong

Supervisor Declaration Statement

I have reviewed the content and presentation style of this thesis and declare it of sufficient grammatical clarity to be examined. To the best of my knowledge, the thesis is free of plagiarism and the research and writing are those of the candidate's. I confirm that the investigations were conducted in accord with the ethics policies and integrity standards of Nanyang Technological University and that the research data are presented honestly and without prejudice.

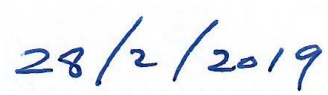

. . . . . .

Date

. . . . . .

Assoc Prof Thirumaran Thanabalu

Authorship Attribution Exclusion Statement

I have excluded the Authorship Attribution Statement declaration because the thesis does not contain any published material.

. . . . . .

Chung Yat Joong

Date: 28/2/2019

. . . . . .

Assoc Prof Thirumaran Thanabalu

Date: 28/2/2019

Acknowledgments

This thesis would not have been possible without the help of many people. I want to first thank the School of Biological Sciences, Nanyang Technological University for allowing me to pursue my PhD program. I want to next thank Assoc Prof Thirumaran Thanabalu for his patience, continuous guidance and feedback regarding the progress of this project, and also Assoc Prof Andrew Tan and Asst Prof Lu Lei, my Thesis Advisory Committee members who provided feedback and comments for my project amid their busy schedules.

I want to thank my lab colleagues, past and present, who have been there to help me in my endeavour and also simply being a source of joy, laughter and personal good times. Dr Bhawana George and Dr Neeraj Jain were past colleagues who had assisted me with several lab methodologies in both cell culture and dry lab practices. Dr Amrita Salvi was my greatest senior who knew the most of N-WASP and gave the most help, training and education where possible in about virtually anything I asked. Dr Payal Mitra was a good spot who was a fun benchmate, had a good sense of humour and also helped in various experiments.

Tai Pei Chee was a nice former Project Officer, and her replacement Tan Hui Bing was a brilliant hardworking fellow Malaysian who helped whenever I had time management issues. The current postdoctoral fellow Dr Pazhani Kalailingam is a great help especially for his non-stop positive outlook on things, his help regarding protein and RNA analysis, and the Ingenuity software usage. Apoorva Verma is a fine lady who can be trusted for some laughs when sharing humour, and has been helpful with several assays I have done.

I also want to thank lab colleagues from the neighbouring lab of Asst Prof Lu Lei's. Dr Chen Bing is my batch mate whom I had the pleasure of being friends with in sharing lab and duty experiences. Dr Shi Meng was an interesting and knowledgeable fellow whom I will discuss politics and work with occasionally. Dr Divyanshu Mahajan and Tie Hieng Chong are two intellectuals whom I could derive knowledge outside my field and some good times from sharing hobbies and entertainment tastes. Dr Viswanadh Madugula also assisted me in a few lab methodology practices and occasional work and non-serious discussions.

I want to thank again Assoc Prof Andrew Tan for allowing me access to the Ingenuity Pathway Analysis online software for part of my studies. There are members of his lab who were helpful for me (unfortunately I cannot remember their full names): I want to thank Mr Ming Jie for his help in providing the original HSC-5 cells for cell culture work, I want to thank Mr Jeremy and Mr Eddie for their availability previously to discuss some antibody technical details and using the Ingenuity software, and lastly I want to thank Mr PC whom I discussed with concerning FAK expression in cancer cell lines.

Lastly, I want to thank my parents, my younger brother and his wife, and my sisters, my Belgian and Malaysian soul mates and numerous other friends who were there for me during emotional and mental ups and downs, constantly giving me love and support when they were most needed on my part. I feel very fortunate to have everyone around me throughout the journey of completing the PhD program and completing this dissertation.

Table of Contents

List of Figures

List of Tables

List of Abbreviations

4E-BP1	Eukaryotic translation initiation factor 4E-binding protein 1 (EIF4EBP1)
5HT4	5-hydroxytryptamine receptor 4
ADP	Adenosine diphosphate
AKT	Protein kinase B (PKB)
AMPK	5' adenosine monophosphate-activated protein kinase
APS	Ammonium persulphate
AraC	Cytosine arabinoside
Arp	Actin-related protein
ARRDC	Arrestin domain-containing protein
ASK1	Apoptotic signal kinase 1
ATP	Adenosine triphosphate
B	Basic
BCC	Basal cell carcinoma
BCL2L11	B-cell lymphoma 2-like protein 11
BMX	Bone marrow X protein-tyrosine kinase (Etk) (BMX (Etk))
$CaCl_2$	Calcium chloride
CAS	Crk-associated protein
CBP/p300	CREB-binding protein/p300
CC	Coiled-coils
CCND1	Cyclin D1
CD24	Cluster of differentiation 24
CDC42	Cell division control protein 42 homolog
CDK1/2	Cyclin-dependent kinase 1/2

CDK4	Cyclin-dependent kinase 4
CDKN1A	Cyclin-dependent kinase inhibitor 1A ($p21^{cip1}$)
CDKN1B	Cyclin-dependent kinase inhibitor 1B ($p27^{kip1}$)
CDKN2A	Cyclin-dependent kinase inhibitor 2A
cDNA	Complementary DNA
cMyc	Cellular homolog of retroviral v-Myc oncogene
CNTF	Ciliary neurotrophic factor
CO_2	Carbon dioxide
CR16	Corticosteroid and regional expression 16
CSNK1A1	Casein kinase 1 alpha 1
CTGF	Connective tissue growth factor
DAPI	4',6-diamidino-2-phenylindole, dihydrochloride
DBD	DNA-binding domain
DCFDA	2',7'-dichlorofluorescin acetate
ddH_2O	Double-distilled water
DEPC	Diethyl pyrocarbonate
DMEM	Dulbecco's Modified Eagle's Medium
DMSO	Dimethyl sulfoxide
DNA	Deoxyribonucleic acid
dNTP	Deoxynucleoside triphosphate
DTT	Dithiothreitol
DYRK1A	Dual-specificity tyrosine-phosphorylation-regulated kinase 1A
E-cadherin	Epithelial cadherin
ECL	Enhanced chemiluminescence

ECM	Extracellular matrix
EDTA	Ethylenediaminetetraacetic acid
EGF	Epidermal growth factor
EGFR	EGF receptor
EIF2	Eukaryotic translation initiation factor 2
EMT	Epithelial-mesenchymal transition
ERK	Extracellular signal-regulated kinase
ERM	Ezrin, radixin and moesin
F-actin	Filamentous actin
FAD	Flavin adenine dinucleotide
$FADH_2$	Flavin adenine dinucleotide hydroquinone
FAK	Focal adhesion kinase (PTK2)
FASL	Fas ligand (CD95L)
FBS	Fetal bovine serum
FGF	Fibroblast growth factor
FGF7	Keratinocyte growth factor
FHD	Forkhead box DNA-binding domain
FITC	Fluorescein isothiocyanate
FOX	Forkhead box
FOXO	Forkhead box protein class O
FPKM	Fragments per kilobase of transcript per million mapped read
G1 phase	Gap 1 phase
GABA-B	Gamma-aminobutyric-B
G-actin	Globular actin

GAPDH	Glyceraldehyde 3-phosphate dehydrogenase
GBD	GTPase-binding domain
GDP	Guanosine diphosphate
GFP	Green fluorescent protein
GPCR	G-protein-coupled receptor
GRB2	Growth factor receptor-bound protein 2
GTPase	Guanosine triphosphate-ase
HCl	Hydrochloric acid
HEK293T	Human embryonic kidney cells 293 with SV-40 Large T-antigen (293T)
HEPES	4-(2-hydroxyethyl)-1-piperazineethanesulfonic acid
HGF	Hepatocyte growth factor
HRP	Horseradish peroxidase
HSC-5	Human skin squamous cell carcinoma 5
HSF1	Heat shock factor 1
HTLV-1	Human T-cell lymphotropic virus type 1
IGF-1	Insulin growth factor 1
IgG	Immunoglobulin protein G
ILK	Integrin-linked kinase
IKKβ	Inhibitor of nuclear factor kappa-B kinase subunit beta
IL-8	Interleukin-8
IRS1	Insulin receptor substrate 1
ITGA2	Integrin α2
ITGA3	Integrin α3
ITGA6	Integrin α6

ITGB1	Integrin β1
ITGB4	Integrin β4
JHD1	JmjC domain-containing protein domain 1
JHD2	JmjC domain-containing protein domain 2
JMY	Junction mediating and regulatory protein
JAK1	Janus kinase 1
JNK	c-Jun N-terminal kinase
KCl	Potassium chloride
KD	Knockdown
KDM5B	Lysine-specific demethylase 5B
KH_2PO_4	Monobasic potassium phosphate
LB	Luria-Bertani
LC	Liquid chromatography
LC-MS/MS	Liquid chromatography-mass spectrometry/mass spectrometry
MAPK	Mitogen-activated protein kinase
MAP2K	Mitogen-activated protein kinase kinase
MAP3K	Mitogen-activated protein kinase kinase kinase
MCS	Multiple cloning site
MDM2	Mouse double minute 2 homolog
MEF	Mouse embryonic fibroblast
MEK	Mitogen-activated protein kinase kinase (MAP2K)
Mek	Protein phosphatase 4 regulatory subunit 3A (PPP4R3A) (Smek1)
Met	Hepatocyte growth factor receptor tyrosine kinase
$MgCl_2$	Magnesium chloride

mRNA	Messenger RNA
MRPL27	Mitochondrial 39S ribosomal protein L27
MST1	Macrophage-stimulating 1
MT-2	Metallothionein 2
mTOR	Mammalian target of rapamycin
mTORC	mTOR complex
Na_2HPO_4	Sodium hydrogen phosphate
Na_3VO_4	Sodium orthovanadate
NaCl	Sodium chloride
NADPH	Nicotinamide adenine dinucleotide phosphate
$NaHCO_3$	Sodium bicarbonate
NCK1	Non-catalytic region of tyrosine kinase adaptor protein 1
NES	Nuclear export sequence
NF2	Neurofibromatosis type 2
NLS	Nuclear localization sequence
N-WASP	Neural Wiskott-Aldrich syndrome protein
OE	Overexpression
p38 MAPK	p38 mitogen-activated protein kinase (p38) (MAPK11)
p70S6K	Ribosomal protein S6 kinase beta-1
PAK	p21 (CDKN1A) activated protein kinases
PBS	Phosphate-buffered saline
PBS-T	Phosphate-buffered saline with Triton X-100
PCR	Polymerase chain reaction
PDGF	Platelet-derived growth factor

PDK4	Pyruvate dehydrogenase lipoamide kinase isozyme 4
PEI	Polyethyleneimine
PGR	Progesterone receptor
PI	Propidium iodide
PIP_3	Phosphatidylinositol (3,4,5)-trisphosphate
PI3K	phosphoinositide 3-kinase
PKCl	Protein kinase C lambda/iota
PKM2	Pyruvate kinase muscle isozyme M2
PMSF	Phenylmethylsulfonyl fluoride
PP	Polyproline-rich region
Prx	Peroxiredoxin
PTCH1	Protein patched homolog 1
PTEN	Phosphatase and tensin homolog
PTM	Post-translational modification
PTPD1	Protein-tyrosine phosphatase D1
RAF	RAF proto-oncogene serine/threonine protein kinase (RAF-1)
RAS	Transforming protein 21 (Ras)
RB	Retinoblastoma
RETSAT	All-trans-retinol 13,14-reductase
RFP	Red fluorescent protein
RhoGDI	Rho GDP dissociation inhibitor
RIPA	Radioimmunoprecipitation assay
RNA	Ribonucleic acid
RNAi	RNA inteference

RNA-Seq	RNA sequencing
ROS	Reactive oxygen species
RSK	Ribosomal protein S6 kinase
RTK	Receptor tyrosine kinase
SCC	Squamous cell carcinoma
SDS	Sodium dodecyl sulphate
SDS-PAGE	Sodium dodecyl sulphate protein agarose gel electrophoresis
Se	Selenium
Ser	Serine residue
SFK	SRC-family tyrosine kinases
SGK1	Serum and glucocorticoid-regulated kinase 1
SHD	Spa2 homology domain
shRNA	Short hairpin RNA
SKP2	S-phase kinase-associated protein 2
SMARCA4	Transcription activator BRG1
SMO	Smoothened
SOS1	Son of sevenless homolog 1
SOX4	SRY-box 4
SRC	Proto-oncogene tyrosine-protein kinase Src (Src)
STAT1	Signal transducer and activator of transcription 1 alpha
TAD	Transactivation domain
TAE	Tris-Acetate-EDTA
TAZ	Transcriptional coactivator with PDZ-binding motif
TBP-2	Thioredoxin-binding protein 2

TBS	Tris-buffered saline
TC10	RAS homolog family member Q (RHOQ)
TEAD	TEA domain family member protein
TEMED	Tetramethylethylenediamine
TF	Transcription factor
Thr	Threonine residue
TNFSF10	Tumour necrosis factor superfamily member 10
TP53	Tumour protein 53
TP63	Tumour protein 63
Trx	Thioredoxin
TrxR	Thioredoxin reductase
TXNIP	Thioredoxin interacting protein
Tyr	Tyrosine residue
UV	Ultraviolet
V	Verproline
VCA	Verproline-Central-Acidic
VDUP1	Vitamin D3-upregulated protein 1
VEGF	Vascular endothelial growth factor
VV-A	Verproline-Verprolin-Acidic
VVCA	Verproline-Verprolin-Central-Acidic
WAS	Wiskott-Aldrich syndrome
WASH	WASP and Scar homolog
WASP	Wiskott-Aldrich syndrome protein
WAVE	WASP-family verproline homologous protein 1

WH1	WASP homology domain 1
WHAMM	WASP homolog associated with actin, membranes and microtubules
WHD1	N-terminal WASH homology region domain 1
WHD2	N-terminal WASH homology region domain 2
WHDC1	WASP homology region 2 domain-containing 1
WICH	WIP and CR16 homologous protein
WIP	WASP interacting protein
WIRE	WIP-related protein
WISH	WASP interacting SH3 protein
XRCC3	X-ray repair complementing defective repair in Chinese hamster cells 3
YAP	Yes-associated protein

Abstract

The ubiquitously-expressed neural Wiskott-Aldrich syndrome protein (N-WASP) regulates actin cytoskeleton remodelling. N-WASP messenger ribonucleic acid (mRNA) levels was found to be reduced in skin squamous cell carcinoma (SCC) samples compared to matched perilesional samples of 33 patients, suggesting it plays a role in skin carcinogenesis. The SCC cell line human skin squamous cell carcinoma 5 (HSC-5) was used to generate control HSC-5 (HSC-5^{CTR}) cells HSC-5 cells overexpressing N-WASP (HSC-$5^{N\text{-}WASP}$) cells. HSC-$5^{N\text{-}WASP}$ cells had increased epithelial cadherin (E-cadherin) and vinculin localizations but reduced cell migration, paxillin localization, cell proliferation and protein kinase B (AKT) signalling compared to HSC-5^{CTR} cells.

Ingenuity Pathway Analysis (IPA) comparative analysis of proteomics, protein microarray and RNA sequencing (RNA-Seq) data suggested that N-WASP probably regulates Integrin-mediated signalling, forkhead box protein class O1 (FOXO1)-mediated signalling to reduce cell proliferation in HSC-5 cells. Experimental validation found altered Integrin-mediated signalling, whereby HSC-$5^{N\text{-}WASP}$ cells had reduced signalling of focal adhesion kinase (FAK), proto-oncogene tyrosine-protein kinase Src (SRC) and growth factor receptor-bound protein 2 (GRB2), but increased signalling of son of sevenless homolog 1 (SOS1) compared to HSC-5^{CTR} cells. It was also found that increased FOXO1 cytoplasmic translocation and degradation may be responsible for reduced HSC-$5^{N\text{-}WASP}$ cell proliferation. The activity of extracellular signal-regulated kinase 2 (ERK2) may be responsible for FOXO1 cytoplasmic translocation and degradation. Inhibition of ERK2 in HSC-$5^{N\text{-}WASP}$ cells restored cell proliferation rate, E-cadherin, vinculin and paxillin localizations, and cell migration to that of HSC-5^{CTR} cells.

Thioredoxin-interacting protein (TXNIP) is a FOXO1 target gene that negatively regulates the thioredoxin system and its ROS-scavenging activity. TXNIP levels were increased in HSC-$5^{N\text{-}WASP}$ cells compared to HSC-5^{CTR} cells, suggesting cell proliferation is reduced due to increased reactive oxygen species (ROS) levels. TXNIP knockdown in HSC-$5^{N\text{-}WASP}$ cells restored cell proliferation rate, E-cadherin, vinculin and paxillin localizations, and cell migration to that of HSC-5^{CTR} cells. These results suggest that in skin carcinogenesis, reduced N-WASP protein levels keep FOXO1 in the nucleus via reduced ERK2-dependent phosphorylation. TXNIP expression is repressed,

allowing unhindered thioredoxin system-mediated ROS scavenging, increasing cell migration and proliferation via altered Integrin-mediated FAK-SRC-GRB2-SOS1 and AKT signalling pathways. These *in vitro* results could be translated into *in vivo* solutions for skin cancer treatment and prevention.

Chapter 1: Introduction

1.1 The skin

The skin is the largest organ of the human body; it protects the body and all constituent organs from foreign particles, pathogens and harm in general [1]. The skin is divided into two layers, separated by a layer of basement membrane: the epidermis and the dermis. The epidermis is a layer of stratified squamous epithelial cells composed of keratinocytes, melanocytes, Langerhans cells and Merkel cells [2], and also subcategorized into five layers, which are the *stratum basale*, *stratum spinosum*, *stratum granulosum*, *stratum lucidum* and *stratum corneum* [3] (Fig. 1).

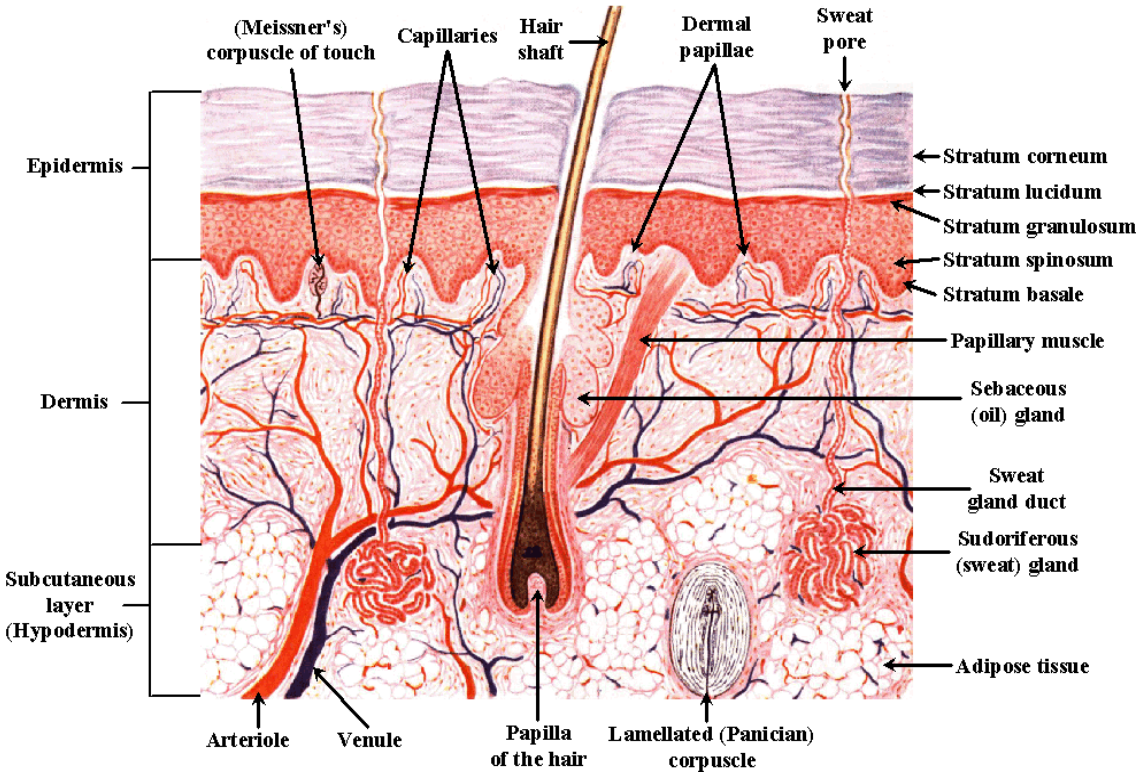

Figure 1: Illustration of the skin, consisting of the epidermis and dermis. Also shown are the five strata of the epidermis of which keratinocytes are the majority cell type. Adapted from Health, Medicine and Anatomy Reference Pictures [4].

Keratinocytes are the major cell types in the epidermis and protect the body against foreign pathogens and particles [5]. The Langerhans cells participate in the immune system via capture of antigens from pathogens and foreign particles and present them to T cells for immune recognition and response [6]. The melanocytes are responsible for production of melanin which gives the skin its hue and filters ultraviolet (UV) light [7].

Merkel cells are situated in the deepest part of the epidermis and enable the registration of the sensation of touch by the somatosensory system [8].

The *stratum basale* is the innermost layer of the epidermis, consisting of proliferating and non-proliferating cells that maintain epidermis' connection to the dermis [2]. The next layer, *stratum spinosum*, consists of multi-layered keratinocytes that provide for the skin's strength, support and elasticity. The *stratum granulosum* secretes lamellar bodies containing proteins and lipids that enable the skin's biological sealant property [3]. The *stratum lucidum* consists of several layers of dead keratinocytes that allow the skin to resist friction, and the outermost layer the *stratum corneum*, which similarly consists of layers of dead cells to be shed, is embedded in a mixture of ceramides, cholesterol and fatty acids that serve as the skin's protection against chemicals, infections and dehydration [9].

1.2 Skin cancer

Normal cells accumulate genetic changes that dysregulate metabolic and self-protection mechanisms over a long time, causing cancerous development. These changes occur at many levels, from loss and gain of entire chromosomes to single mutations anywhere in the chromosome, causing aberrant protein expression and dysregulation of factors regulating gene expression [10]. Cancer cells are capable of self-sufficient growth signalling, uncontrolled cell division, apoptotic evasion and insensitivity to anti-growth signals [11]. Cancer of the skin is divided into two types: melanoma and non-melanoma skin cancer, which in turn is divided to basal cell carcinoma (BCC) and SCC.

1.2.1 Melanoma

Melanoma is a highly prevalent skin cancer, caused mainly by high exposure to UV radiation [12] and mainly in countries such as Australia, New Zealand and those in Europe and North America due to low levels of melanin in the resident populations there [13]. It is fatal if undetected in early stages, and it is responsible for over 75% of reported deaths from skin cancer [14]. Melanoma is caused by UV-radiation-induced deoxyribonucleic acid (DNA) nucleotide dimerization and its incidence is increasing [15]. Other causes include mutations in cyclin-dependent kinase 4 (CDK4) and cyclin-dependent kinase inhibitor 2A (CDKN2A) which regulate cell cycle progression [16], mutations of any genes for involved pathways that regulate or promote cell proliferation

such as the transforming protein 21 (Ras) (RAS)-RAF proto-oncogene serine/threonine protein kinase (RAF)-ERK and phosphoinositide 3-kinase/phosphatase and tensin homolog (PI3K/PTEN) pathways, or abnormal expressions of genes that induce proliferation signalling such as AKT [17].

1.2.2 Non-melanoma skin cancer

More than 70% of reported cases of non-melanoma skin cancer are due to BCCs, with the remainder less than 30% due to SCCs. However, BCCs are rarely metastatic and are thus rarely fatal compared to SCCs [18]. This is because SCCs have the ability to develop multiple tumour foci with eventual highly metastatic ability, coupled with increased proliferative ability [19]. Similar to melanoma, excessive exposure to UV radiation is the main cause of both BCCs and SCCs [12]. BCCs are caused by mutations in tumour suppressor genes such as tumour protein 53 (TP53) [20], and mutations in the protein patched homolog 1 (PCTH1) and Smoothened (SMO) genes of the hedgehog pathway which regulate gene transcription and expression [21]. Mutations in the DNA repair gene X-ray repair complementing defective repair in Chinese hamster cells 3 (XRCC3) appears to be characteristic of BCCs as well [20]. In SCCs, mutations in TP53 and genes of the PI3K/AKT pathway are also a cause, while increased protein levels in integrins α5β1 and αvβ6 as well as the loss of other integrins [22], and increased protein levels of cellular homolog of retroviral v-Myc oncogene (cMyc), Src-family tyrosine kinases (SFK) and epidermal growth factor receptor (EGFR)-induced signalling are all implicated in SCC development [23].

1.3 Cytoskeleton

The cytoskeleton is an intracellular network of polymerized protein filaments that maintain a cell's form, shape and polarity, and to detect and respond to external stimuli. This makes the cytoskeleton crucial for activities such as embryogenesis, cell division, cell extensions, organelle transport and positioning, cell movement and migration and wound healing [24]. The three constituents of the cytoskeleton are actin filaments, intermediate filaments and microtubules, which interact intensively with each other and the numerous cellular components throughout the body of the cell and the plasma membrane. These interactions, as well as the recycling and reassembly of cytoskeletal

constituents throughout the cellular body, are responsible for normal cellular function and growth [25].

1.4 Actin cytoskeleton

Actin filaments constitute a major component of the cytoskeleton network. It consists of the globular G-actin form and the filamentous F-actin form [26], and its recycling and reassembly are what drives the formation of actin-based protrusive structures such as lamellipodia, filopodia and invadopodia [27]. Actin has also been shown to be present in the nucleus, suggesting a possible role for chromatin remodelling, gene transcription and expression [28].

Actin reorganization is mediated by actin-binding proteins that are classified based on functions such as capping, severing, nucleating, sequestering, cross-linking and monomer-binding proteins [29]. Thymosin-β4 sequesters G-actin and prevents G-actin polymerization to F-actin [30]; cofilin severes and disassembles existing F-actin branches for redistribution elsewhere in the cell [31]. The Actin-related protein (Arp) 2/3 complex is composed of Arp2, Arp3 and five subunit proteins; they provide the actin nucleus for the formation of F-actin from G-actin [32], with G-actin being recruited by nucleation promoting factors [33]. Nucleation promoting factors of interest to this dissertation belong to the Wiskott-Aldrich syndrome protein (WASP) family of proteins [34]. The process of actin cytoskeleton remodelling is summarized visually (Fig. 2). Given the actin cytoskeleton's importance in cell division and proliferation, coordination of actin recycling, reassembly and cellular processes such as cell-cell adhesion and cell motility is required.

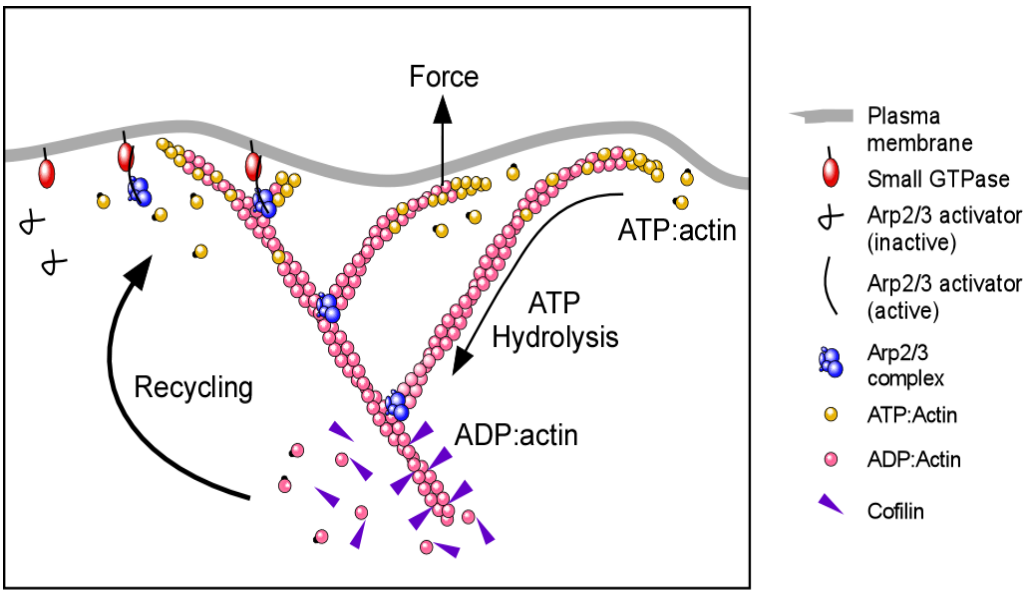

Figure 2: The Arp2/3 complex nucleates actin filament formation. The Arp2/3 complex nucleates actin following the hydrolysis of ATP form to ADP form, allowing formation of daughter filaments from the main actin branch which assert force on the plasma membrane and influencing changes in cell shape. Actin regulators such as cofilin determine how and where actin branches are formed, disassembling actin constituents to be recycled as needed elsewhere in the cell. Adapted from Dayel [35].

1.4.1 Cell-cell adhesion

For cells to break away to grow, proliferate or even metastasize, the connections between cells at the membrane must be removed [36]. Molecules responsible for cell-cell adhesion include transmembrane glycoproteins such as cadherins and integrins, and intermediary molecules or complexes that tie receptors to F-actin and cellular machinery [36]. The structures responsible for these interactions are the gap junctions, tight junctions and anchoring junctions. Gap junctions employ structures called connexon complexes that permit the passing of ions and small molecules between cells without leakage into extracellular fluids around the cells [37]. Tight junctions are intercellular junctions that hold epithelial cells together as layers and ensure that water, ions and small molecules pass through cells in order to move through tissues [38]. Anchoring junctions, which hold cells together and provide joint structural cohesion, are divided into three types: desmosomes use the intermediate filament-based cytoskeleton and cadherins to hold to other cells, hemidesmosomes use the intermediate filament-based cytoskeleton and integrins to hold cells to the extracellular matrix (ECM), and adherens junctions utilize the actin cytoskeleton and cadherins for cell-cell adhesion [39].

1.4.2 Cell motility

The cell's ability to migrate is essential for development and metastasis. Changes in cytoskeletal dynamics and interactions by adhesion molecules allow cells to migrate [40], which is usually done either as single cell movements or in a collective manner by a sheet of cells on the ECM [41]. The process is cyclic in manner, where a repetition of protrusion, adhesion and retractions occur and allow cell movement in a desired direction. The cell first establishes polarity, with a defined trailing edge and leading edge, and protrusions at the leading edge occur after actin polymerization either in a broad sheet-like manner (lamellipodia) or thin finger-like microspikes (filopodia) [42] in response to chemical gradients or other stimuli. Integrins and other adhesion molecules at the end of these protrusions attach to the ECM, giving the cell a solid traction forward [43]. Active cell division control protein 42 homolog (CDC42) and Rac guanosine triphosphate-ases (GTPases) remodel the actin cytoskeleton and reposition organelles and the nucleus forward [44,45], followed by cellular retractions from the ECM at the trailing edge, caused by signals from active Rho GTPase and other molecules such as SRC kinase, ERK and FAK [43].

1.5 WASP family of proteins

The WASP protein was first identified in studies of mutations in the Wiskott-Aldrich syndrome (WAS) gene responsible for said syndrome [46]. The syndrome is a rare, inherited X-linked disease causing eczema, immunodeficiencies due to impaired hematopoietic cells, neutropenia and thrombocytopenia [47]. Mutations of WAS generally occur throughout the gene, although more than 50% are known to be in exons 1 to 3 that encode the WASP homology domain 1 (WH1) [48]. Further studies on WASP allowed for the discovery of other member proteins, including N-WASP and the WASP-family verproline homologous protein 1 (WAVE) proteins 1 to 3 of the Scar/WAVE subfamily group [49], and those more recently discovered that recruit the Arp2/3 complex for actin polymerization such as WASP and Scar homolog (WASH) and WASP homolog associated with actin, membranes and microtubules/WASP homology region 2 domain-containing 1 (WHAMM/WHDC1) [47], and the WHDC1-like protein junction mediating and regulatory (JMY) [50]. A comparison of the common constituent domains of the WASP family of proteins is shown (Fig. 3).

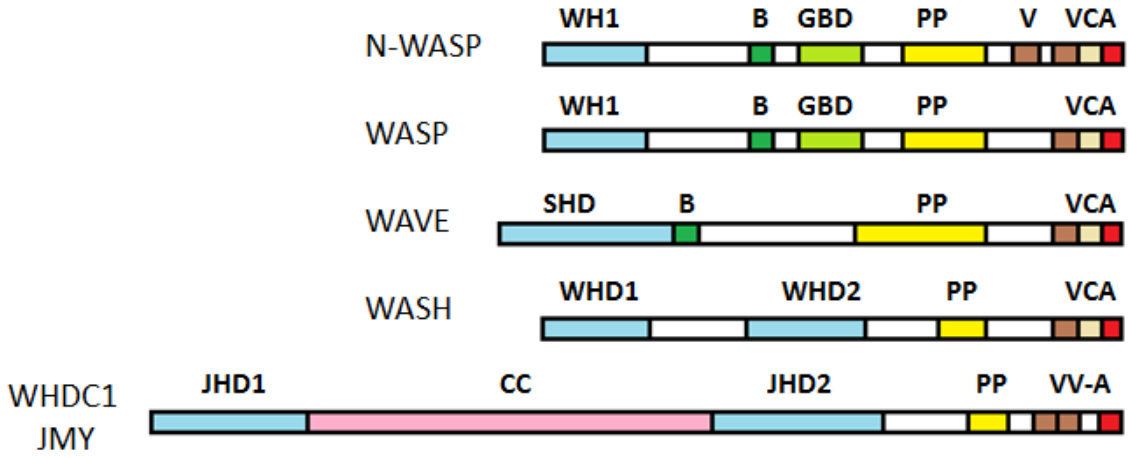

Figure 3: Comparison of domains of various members of the WASP family of proteins. The WASP and N-WASP proteins almost share an identical domain composition, but differences abound in WAVE and WASH proteins, and most significantly the recently discovered WHDC1 and JMY proteins. All member proteins contain the WH1, PP, and VCA domains to some degree. WH1, WASP homology domain 1; B, basic, GBD, GTPase-bding domain; PP, polyproline-rich region; V, verproline; VVCA, verproline-verproline-central-acidic, VV-A, verproline-verproline-acidic; SHD, Spa2 homology domain; WHD1, N-terminal WASH homology region domain 1; WHD2, N-terminal WASH homology region domain 2; JHD1, JmjC domain-containing protein domain 1; JHD2, JmjC domain-containing protein domain 2; CC, coiled-coils domain. Adopted from Institut für Molekulare Zellbiologie [51].

1.5.1 N-WASP domains and functions

N-WASP was first isolated as a bovine WASP isoform and initially presumed to be mainly expressed in neural cells at high levels [49]. N-WASP was then found to be ubiquitously expressed, in contrast to WASP which was only expressed in hematopoietic cells [52]. N-WASP has a similar protein homology with WASP, containing the WH1, Basic (B), GTPase-binding domain (GBD), poly-proline (PP) and Verprolin-Central-Acidic (VCA) domains, with an additional verprolin region (Fig. 3). The WH1 domain interacts with verprolin family proteins including WASP-interacting protein (WIP), corticosteroid and regional expression 16 protein (CR16), and the WIP homolog WIP and CR16 homologous protein/WIP-related protein (WICH/WIRE) [53-55]. The B and GBD domains interact with GTPases such as CDC42, Rac and the RAS homolog family member Q (TC10) [56]. The PP domain interacts with profilin and SH3-containing proteins such as cortactin, non-catalytic region of tyrosine kinase adaptor protein 1 (NCK1), GRB2 and WASP interacting SH3 protein (WISH) [57]. The VVCA domains interact with G-actin and the Arp2/3 complex [58]. N-WASP exists in an autoinhibited state due to its closed conformation from intramolecular interactions between the VVCA

and B domains, similar to WASP [47]. When active Cdc42 binds to the GBD domain [56] or FAK phosphorylates the tyrosine (Tyr)-256 residue [59], N-WASP is relieved from the autoinhibited state, allowing the VVCA domain to interact with the Arp2/3 complex and G-actin to promote actin polymerization [56]. N-WASP dimerization at the VVCA domain has been reported when interacting with Arp2/3 complex in order to facilitate actin polymerization [60].

N-WASP-Arp2/3 complex activity from the VVCA domain is vital for cellular activities such as cell migration and division [61]. N-WASP has been shown to be necessary for clathrin dependent endocytosis, vesicle fission and departure from the nucleus [61,62]. N-WASP also assists in RNA polymerase II-mediated transcription in the nucleus and chromosomal alignment in mitosis [63,64]. N-WASP knockout in mice was shown to be embryonically lethal with neural tube and cardiac tissue defects [65,66], and its presence has been demonstrated in actin-rich cellular protrusion structures like lamellipodia, dorsal ruffles, filopodia and invadopodia [67-69]. In muscle cells, N-WASP cooperates with nebulin to cause actin polymerization in a manner similar to yet independent of Arp2/3 complex, alongside with myosin filament assembly, for myofibrillogenesis [70]. N-WASP also cooperates with WIRE and E-cadherin at the epical zonula adherens, an adherens junction subdomain, to maintain cell junction integrity [71]. N-WASP is being increasingly linked to cancer progression and invasion. It was found to be up-regulated in colorectal cancer cells that metastasized and formed lesions in the liver [72]. N-WASP appears to play a role in lung cancer cell proliferation, growth and metastasis, and correlates with poor patient survival rate [73]. N-WASP was also reported to play a critical role in ovarian tumour growth and migration via interaction with the EGFR signalling axis [74]. Our laboratory has found N-WASP expression to be reduced in 33 SCC patient samples compared to matched skin perilesionals (Swagata's unpublished data) (Fig. 4), suggesting that N-WASP plays a role in skin carcinogenesis.

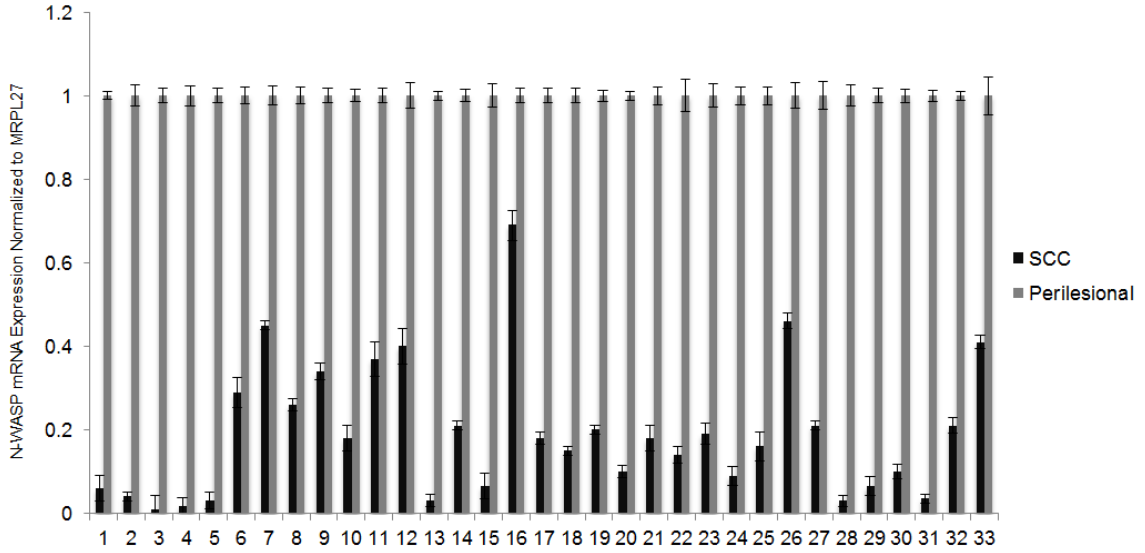

Figure 4: N-WASP expression is reduced in 33 patient SCC samples compared to matched skin perilesionals. Total ribonucleic acid (RNA) was extracted from paraffin-embedded SCC and matched perilesional samples obtained from 33 SCC patients from the National Skin Centre of Singapore, followed by generation of complementary DNA (cDNA) and real-time polymerase chain reaction (PCR). Equal amounts of cDNA were used for real-time PCR for N-WASP expression, normalized to mitochondrial 39S ribosomal protein L27 (MRPL27), and compared to the individual matched skin perilesional values. Experiments were performed in triplicates.

In blood peripheral monocytes, upon stimulation of EGFR, N-WASP has been shown to be recruited for receptor-mediated endocytosis of human cytomegalovirus and for mediating cell motility [75]. Although T cells require mainly WASP for activation, they require the activities of both WASP and N-WASP for development [76]. Wiskostatin is a well-known chemical inhibitor of N-WASP [73]. The ezrin, radixin and moesin (ERM) proteins, which link the plasma membrane and actin cytoskeleton, as well as the neurofibromatosis type 2 (NF2) tumour suppressor protein Merlin are capable of inhibiting N-WASP *in vitro* and *in vivo* [77]. N-WASP has been shown to be phosphorylated at threonine (Thr)-196, -202 and -259 residues by dual-specificity tyrosine-phosphorylation-regulated kinase 1A (DYRK1A), which restores intramolecular interactions of GBD and VVCA domains and N-WASP's autoinhibited state, thus negatively regulating actin polymerization and the relevant cellular processes [78].

1.5.2 N-WASP and cell signalling

N-WASP expression was found to be reduced in breast and colorectal cancers, which is believed to reduce patient survival rate in both cancers [79,80]. N-WASP was found to play an important role in hypoxia-induced epithelial-mesenchymal transition (EMT) and

is necessary for metastasis [81]. N-WASP is present in the lamellipodia and invadopodia of cancer [82,69]. It plays a role in cell motility and maintenance of amoeboid cell morphology [83]. Breast cancer cells utilize N-WASP at invadopodia to promote trafficking of matrix metalloproteases there for degradation of the ECM [84]. These suggest that N-WASP plays a role in carcinogenesis in numerous cell types.

As stated earlier, our laboratory found N-WASP mRNA levels to be reduced in SCC samples from skin cancer patients compared to matched perilesional samples (Fig. 4), suggesting N-WASP is down-regulated in skin carcinogenesis. Cancer development is caused by dysregulation of or acquired mutations in normal metabolic and signalling pathways [10]. The role of N-WASP in epithelial skin cancer has yet to be characterized. Therefore, the study of cell signalling pathways influenced by N-WASP is considered vital as detailed mechanisms of N-WASP's role in carcinogenesis is not fully understood [85]. Four candidate pathways have been chosen for N-WASP studies, including their justifications.

The Integrin signalling pathway is responsible for cell growth, proliferation, migration and cell adhesion [86]. It works primarily by utilizing focal adhesion complex member proteins such as talin, vinculin, paxillin and FAK to connect signals from integrins to F-actin, inward to the cell [87]. FAK phosphorylates N-WASP at the Tyr256 residue in the GBD domain and converts N-WASP into an active state that stimulates cell migration in mouse embryonic fibroblasts (MEF) [59]. The SRC-Crk-associated protein (CAS)-Crk signalling axis, controlled by this pathway, was found to influence N-WASP activity towards cell migration and adhesion activity in MEF cells [88]. It is of interest if similar findings can be repeated by studying this pathway in epithelial skin cancer cells.

The epidermal growth factor (EGF) signalling pathway transmits signalling from activated EGFR to the RAS-RAF-mitogen-activated protein kinase kinase (MAP2K) (MEK)-mitogen-activated protein kinase (MAPK) signalling axis to regulate cell cycle progression or the PI3K/AKT signalling axis to regulate cell proliferation [89]. EGF signalling has been shown to stimulate and regulate Drosophila intestinal stem cell proliferation via the c-Jun N-terminal kinase (JNK) signalling axis in response to stress and maintains epithelial regeneration after tissue damage [90]. EGF stimulation was also found to stimulate increases in N-WASP levels and induce epithelial-mesenchymal

transition (EMT) in A431 carcinoma cells, with induced cells exhibiting increased cell migration [81]. As stated earlier, in both monocytes and ovarian cancer cells, active EGFR recruits N-WASP to mediate effects such as cell motility, migration and receptor-mediated endocytosis [74,75]. It is thus of interest to determine if N-WASP regulates EGF signalling in epithelial skin cancer cells, or vice-versa.

The Wnt signalling pathway is responsible for axis patterning, cell migration, proliferation, cell fate specification and tissue regeneration [91]. Mutations have caused diseases including prostate and breast cancers, glioblastoma and type-2 diabetes among others [92]. Three pathways have been identified that utilize signalling from the Frizzled receptor and its ligand Dishevelled protein; two non-canonical pathways do not utilize β-catenin [93], and one canonical pathway utilizes β-catenin and depends on β-catenin accumulation to activate gene transcription [92]. The role of Wnt signalling in skin cancer is not clear and insufficiently studied. One study found N-WASP knockout mice exhibited reduced β-catenin-dependent nuclear activity and cell hyperproliferation [65]. This suggests that N-WASP may influence or is influenced by Wnt signalling in epithelial skin cancer cells.

The Hippo signalling pathway was recently discovered in a *Drosophila* screen for tumour suppressor genes [94-97] and, similar to other pathways, is conserved in humans and responsible for cell growth, proliferation and size control [98]. The Hippo signalling pathway regulates transcription of growth genes via the Yes-associated protein (YAP)/Transcriptional coactivator with PDZ-binding motif (TAZ)-TEA domain family member protein (TEAD) complex in the nucleus [99,100]. Overexpression of YAP transcription factor in mice caused enlargement of liver more than twice the size that of control [101]. Knockdown of the Hippo target gene connective tissue growth factor (CTGF) reduced chondrocyte proliferation and resulted in skeletal dysmorphisms in mice [102]. Our own observation was that the tumorigenic human SCC model HSC-5 cells are larger in size than non-cancerous, non-tumorigenic human skin cell model HaCaT cells. These suggest that the Hippo pathway may play a role in growth and size control in epithelial skin cancer cells.

1.6 Transcription factors

Transcription factors (TFs) regulate transcription and gene expression, by binding to specific DNA sequences via specific DNA-binding domains (DBDs) [103]. Control is asserted by individual TFs or in a complex with various effectors to promote or repress RNA polymerase II activity [104]. Mutations in TFs cause aberrant TF activity, and in response to stimuli further leads to abnormal cell growth and cancer development [105]. TFs are categorized based on the sequence similarity and tertiary structures of their DNA-binding domains, of which 5 superclasses are known: superclass 1 basic domain, superclass 2 zinc-coordinating DBDs, superclass 3 helix-turn-helix, superclass 4 β-scaffold factors and superclass 0 others [106,107]. An example of a TF family currently undergoing intensive research is superclass 3 class 3 forkhead/winged helix family 1 developmental regulators – the forkhead box (FOX) protein.

1.6.1 FOXO family of transcription factors

FOX proteins are TFs responsible for cell metabolism, growth, proliferation, longevity and embryonic development [108], and all share forkhead box motif that loops in a butterfly-like manner [109]. A protein *fkh* was first isolated in a *Drosophila* mutagenesis screen [110], after which subsequent studies expanded the collection of proteins to mammals and yeast and necessitated a unified FOX naming nomenclature and categories from class A to S [111]. Of interest for this dissertation are the O class proteins, specifically FOXO1. A comparison of the domains of all four FOXO proteins is shown (Fig. 5).

FOXO1 contains a forkhead box DNA-binding domain (FHD), a nuclear localization sequence (NLS), a nuclear export sequence (NES) and a transactivation domain (TAD) [112]. As mentioned, the FHD domain is necessary for binding of FOXO protein to target genes [109]. Phosphorylation of residues in the NES in FOXO1 by kinases such as AKT and serum and glucocorticoid-regulated kinase 1 (SGK1) causes recruitment of the 14-3-3 protein for FOXO protein shuttling from nucleus to cytoplasm for proteasomal degradation [112,113]. It was also reported that FOXO1 degradation is caused by polyubiquitination by E3 ligases such as mouse double minute 2 homolog (MDM2) in the nucleus and S-phase kinase-associated protein 2 (SKP2) in the cytoplasm [114]. The TAD domain, usually located at the carboxy-terminus, is the region that interacts with

other effectors of the transcription complex, and either promotes or represses gene transcription [115].

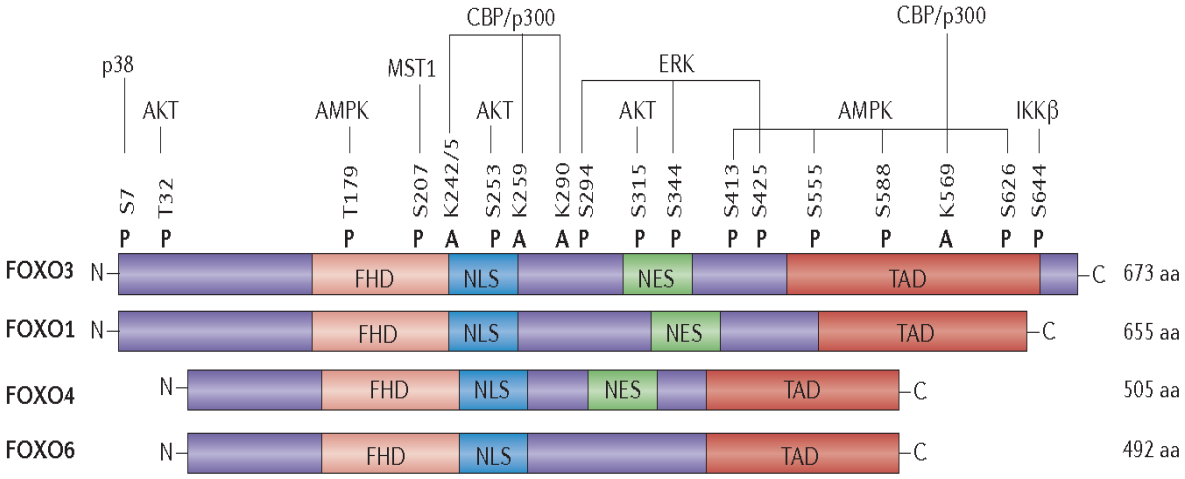

Figure 5: Comparison of FOXO family member proteins and their domains. All member proteins contain at least the FHD domain, NLS and NES. Shown are the various serine and threonine residues that are phosphorylated (P) by various kinases, and the lysine residues that are acetylated (A) by CREB-binding protein/p300 (CBP/p300) on FOXO3 only. A rough equivalent residue site of kinase or acetylase action exists on the other FOXO proteins, though not shown. FHD, forkhead box DNA-binding domain; NLS, nuclear localization sequence; NES, nuclear export sequence; TAD, transactivation domain; AMPK, 5' adenosine monophosphate-activated protein kinase; MST1, macrophage-stimulating 1; p38, p38 MAPK; IKKβ, inhibitor of nuclear factor kappa-B kinase subunit beta. Adapted from Lam *et al.* [112].

1.6.2 FOXO1 and interactions

All FOXO proteins are ubiquitously-expressed. FOXO1 is found most highly expressed in the spleen, heart, kidney, brain and adipose tissues [115], although studies about its metabolic function have been performed mainly in the liver and pancreas [116]. AKT, SGK1, ERK, JNK and PTEN phosphorylate FOXO proteins and target them for degradation, but macrophage-stimulating 1 (MST1) and 5' adenosine monophosphate-activated protein kinase (AMPK) phosphorylate FOXO proteins and convert them to an active form; CREB-binding protein (CBP)/p300 alone acetylates and deacetylates FOXO1 into its inactive and active forms, respectively, although how this mechanism works is not well known [112,117].

Unlike other FOX proteins, FOXOs negatively regulate cell proliferation by repressing Cyclin D1 (CCND1) and promoting cyclin-dependent kinase inhibitors 1A and 1B (CDKN1A and CDKN1B), retarding cell cycle progression [112]. Faced with external

stimuli, FOXO1 activates pro-apoptotic genes including Fas ligand (FASL), B-cell lymphoma 2-like protein 11 (BCL2L11) and tumour necrosis factor superfamily member 10 (TNFSF10) [115,118]. FOXO1 knockout mice exhibited cardiovascular deformities, progressive cell apoptosis and embryonic lethality [119], showing how crucial FOXO1 is for life. Chromosomal breaks in FOXO1 and fusion of its TAD domain to DNA-binding domains of other transcriptional effectors have been found to cause rhadomyosarcoma growth, due to lack of control by AKT inactivation [120]. FOXO1 is known to regulate gluconeogenesis, glycogenolysis and adipogenesis [113]. JNK phosphorylates FOXO1 in pancreatic cancer HCT-115 cells, causing FOXO1 to be translocated to the cytoplasm for degradation, which leads to cell apoptosis [116]. These suggest that FOXO1 performs multiple metabolic control functions in different cells. FOXO1 has been reported to play a role in skin epidermal morphogenesis and repair processes [121]. FOXO1 is also reported to regulate proliferation of *stratum basale* keratinocytes via inhibition of tumour protein 63 (TP63) by stimulus from the insulin/insulin growth factor 1 (IGF-1) pathway [122]. It is therefore possible that FOXO1 plays a role in skin carcinogenesis.

1.7 Cell redox system

Oxygen usage as part of cellular metabolism is necessary for the growth and development of multicellular organisms. However, in the form of ROS, it poses a threat to said development. ROS is produced as a result of metabolic processes as well as stimuli such as exposure to UV light, radiation, foreign contaminants and allergens, infection by viruses and even smoking [123]. In low and natural concentrations, they pose little threat to cells and are even beneficial, but in high concentrations, they result in oxidative stress, can be detrimental to DNA, lipids and proteins, and cause cell damage [124,125]. A cell has in-built mechanisms to scavenge intracellular ROS for self-protection and biological safety. Three reduction-oxidation (redox) systems are usually employed by cells which scavenge ROS and both modulate and stimulate signalling axes – the glutathione, pyridine nucleotide, and thioredoxin redox systems [126].

1.7.1 Thioredoxin system

The thioredoxin system, conserved in many bacteria, plants and mammals, consists of nicotinamide adenine dinucleotide phosphate (NADPH), thioredoxin (Trx), thioredoxin reductase (TrxR) and peroxiredoxin (Prx) [127]. This system often cooperates with the glutathione system to scavenge ROS and modulate signalling axes, and both the

thioredoxin and glutathione systems depend on NADPH for their reduction reactions [126]. Prx consists of 6 isoforms, aptly numbered from 1 to 6 [128], while both Trx and TrxR exist in isoforms 1 and 2. Trx1 and TrxR1 localize in the cytoplasm, and Trx2 and TrxR2 localize in the mitochondria [123]. NADPH serves as a reservoir for hydrogen ions, while TrxRs are flavoproteins containing an NADPH binding site, a conserved Cys-Val-Asn-Val-Gly-Cys catalytic site necessary for receiving NADPH hydrogen ions and a C-terminal cysteine-selenocysteine site that receiving the hydrogen ions and reduces TrxR [129]. In both cytoplasm and mitochondria, the reactions are as follows: Prx first renders ROS harmless, and the oxidized Prx or any other oxidized protein are reduced by Trx, resulting in an oxidized Trx which is then reversibly reduced by TrxR and NADPH hydrogen ion donation [123,127] (Fig. 6).

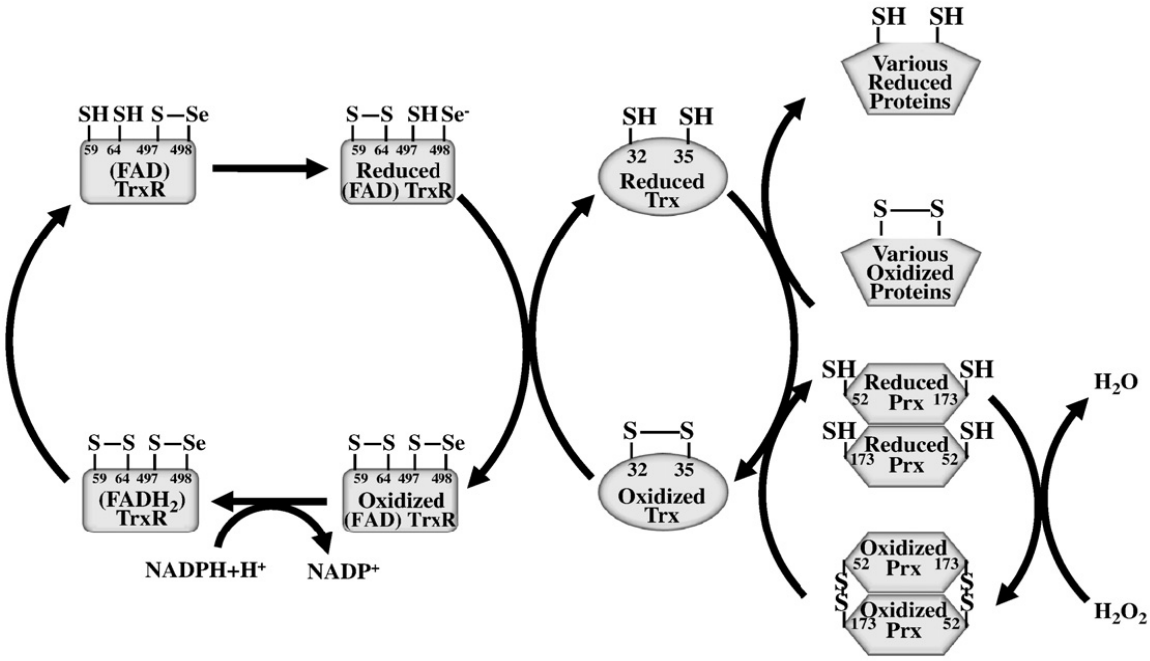

Figure 6: Thioredoxin redox system exchange of hydrogen ions to scavenge ROS. Prx is oxidized in order to reduce ROS to harmless forms, and both dithiol-oxidized proteins and oxidized Prx depend on the oxidation of Trx to render themselves reduced. The oxidized Trx is then recycled into its reduced form to be used for further hydrogen ion donations by NADPH donation of hydrogen ions catalysed by TrxR. Numbers indicate the positions of cysteine residues related to dithiol/disulfide reactions. Prx, peroxiredoxin; Trx, thioredoxin; TrxR, thioredoxin reductase; FAD, flavin adenine dinucleotide; $FADH_2$, flavin adenine dinucleotide hydroquinone; Se, selenium. Adapted from Watanabe *et al.* [123].

1.7.2 TXNIP and interactions

TXNIP was first identified from yeast two-hybrid studies and at first named independently as thioredoxin-binding protein 2 (TBP-2) [130] and Vitamin D3-upregulated protein 1 (VDUP1) [131]. Initially isolated from HL-60 cells, TXNIP is later found to be ubiquitously-expressed and localizes in the nucleus, cytoplasm and mitochondria [123]. It is considered a member of the α-arrestin family of proteins due to it sharing arrestin-like domains with α-arrestin domain-containing proteins (ARRDC) 1 to 5, all known to modulate glucose metabolism – although TXNIP is the only one that interacts with Trx [132]. TXNIP is a negative regulator of Trx, whereby its Cys-247 residue forms a disulfide bridge with thioredoxin's Cys-32 residue, thus inactivating it [133]. This interaction, or lack thereof, has been suggested to be responsible for development of many diseases and even carcinogenesis in many cell types.

The combination of reduced TXNIP and increased Trx was shown to increase muscle insulin sensitivity and glucose uptake, reduce the chances of neuropathy, cardiac hypertrophy and neurodegenerative pathogenesis [127]. However, a review by Zhou *et al*. [134] showed that either loss-of-function of reduced levels of TXNIP correlated with progression and development of cancers including breast, bladder, prostate and colorectal. Increased TXNIP levels in pancreas reduced Trx levels and reduced cell proliferation via apoptosis by apoptotic signal kinase 1 (ASK1) signalling [135]. The same phenotype was observed in podocytes via p38 MAPK signalling [136]. *In vitro* overexpression of TXNIP caused reduced Trx and increased intracellular ROS levels [130,137]. The treatment of metastatic neuroblastomas with the fibrate-class drug fenofibrate repressed cell proliferation and migration activity via increased TXNIP levels [138]. Increased TXNIP has been found to repress mammalian target of rapamycin (mTOR) signalling in HeLa, H1299 and H460 cells, possibly reducing chances of carcinogenesis [139]. Increased TXNIP correlated with increased CDKN2A levels to induce Gap 1 phase (G1) cell cycle arrest in human T-cell lymphotropic virus type 1 (HTLV-1)-infected metllothionein 2 (MT-2) cells [140]. *In vivo* HcB-19 mouse models of TXNIP nonsense mutation found increased occurrence of familial combined hyperlipidemia, including hypercholesterolemia and hypertriglyceridemia [141], while another HcB-19 mouse model with TXNIP mutations correlated with increased occurrence of hepatocellular carcinoma [142]. Thus, it is possible that TXNIP activity is beneficial to the health of some cell types, but detrimental to others. To our knowledge,

there are no known reports on the role of TXNIP in skin cancers, and this dissertation aims to determine if TXNIP does play a role in skin carcinogenesis.

1.8 Objectives

WASP family of proteins, such as N-WASP, are critical for actin cytoskeleton remodelling via Arp2/3 complex activation for subsequent actin polymerization. N-WASP expressions in breast and colorectal cancers are found to be reduced. This was similarly found in SCCs, when a comparison of skin cancer samples was made to matched perilesional controls in 33 patients (Swagata's unpublished data). So far, the role of N-WASP in skin cancer has yet to be elucidated. The study of N-WASP in tumorigenic and non-tumorigenic cells, represented by HSC-5 (established from human SCCs) and HaCaT cell lines respectively, and how N-WASP influences HSC-5 cell proliferative activity are the focuses of this dissertation. The objectives of this dissertation are thus:

1) To characterize the function of N-WASP in normal skin cells, skin cancer cells and skin cancer cells overexpressing N-WASP
2) To identify the signalling pathways or functional molecules responsible for N-WASP-mediated changes in skin cancer cells overexpressing N-WASP by means of proteomics analysis, protein microarray and RNA-Seq
3) To validate identified candidate signalling pathways and functional molecules via Western blotting or knockdown studies

Chapter 2: Materials and Methods

2.1 Materials

2.1.1 Plasmids and commercial vectors

pUC19 (Invitrogen) vector was used for DNA subcloning. pLKO.1 TRC vector (Addgene #10878), a gift from Prof David Root (Broad Institute of MIT and Harvard, USA) [143], was used for generation of queried short hairpin RNA (shRNA) sequences. pTT1-Puro vector was constructed by replacing EGFP sequences of pLJM1-EGFP vector (Addgene #19319), a gift from Prof David Sabatini (Massachusetts Institute of Technology, USA) [144], with a multiple cloning site (MCS) for future DNA subcloning. pTT2-Neo vector was constructed by replacing sequences for puromycin resistance of pTT1-Puro with sequences for neomycin resistance. pTT1-Puro vector was used for protein expression, and pTT2-Neo vector was used for both knockdown of genes via RNA interference (RNAi) and protein expression.

2.1.2 Bacterial strains

The bacterial strain of *Escherichia coli* (*E. coli*) DH5α (Invitrogen) was used for plasmid DNA amplification and subcloning. Another *E. coli* strain, Stabl3 (Thermo Fischer), was used for shRNA plasmid DNA amplification.

2.1.3 Mammalian cells

The human embryonic kidney 293 cells with SV40 Large T-antigen (HEK293T) (or 293T) cell line was purchased from American Type Culture Collection (ATCC, USA). The human tumorigenic keratinocyte cell line HSC-5 and non-tumorigenic keratinocyte cell line HaCaT were both gifts from Assoc Prof Andrew Tan (School of Biological Sciences, Nanyang Technological University).

2.1.4 Bacterial culture media

2.1.4.1 Luria-Bertani (LB) broth

1% (w/v) Bacto-Tryptone powder (BD Biosciences), 0.5% (w/v) Bacto-Yeast extract powder (BD Biosciences) and 0.5% (w/v) sodium chloride (NaCl) (BD Biosciences) were weighed and dissolved in double-distilled water (ddH_2O) and autoclaved. Prior to usage for bacterial culture, the broth is supplemented with 50 μg/ml ampicillin (Sigma).

2.1.4.2 LB agar plates

2% (w/v) Bacto-Agar (BD Biosciences) was added to LB broth and autoclaved. The medium was allowed to cool in room temperature to a warm touch, supplemented with 50 μg/ml ampicillin (Sigma) and 10 ml was poured into plastic plates, and allowed to cool to solidify.

2.1.5 Cell culture media and plasticware

Dulbecco's Minimal Eagle's Medium (DMEM) (Hyclone) was used for maintenance of mammalian cells. Additives such as fetal bovine serum (FBS), penicillin/streptomycin antibiotic, puromycin and neomycin antibiotics, and sodium bicarbonate ($NaHCO_3$) were purchased from Gibco, Thermo Fisher and Sigma. Plasticware such as Eppendorf tubes, mammalian cell culture plates and centrifuge tubes were bought from Corning, Nunc, Costar and Eppendorf.

2.1.6 Antibodies

2.1.6.1 Primary antibodies

Antibodies used for Western blot and immunohistochemistry experiments are specified in Table 1 below.

Table 1: Primary antibodies and respective dilutions used for Western blot study and immunohistochemistry.

Primary antibody	Source	Dilution for Western blot	Blocking condition	Dilution for immunohisto-chemistry
Rabbit Anti-N-WASP polyclonal antibody	Homemade	1:1000	5% skim milk	N/A
Mouse Anti-GAPDH (glyceraldehyde 3-phosphate dehydrogenase) monoclonal antibody	Ambion	1:10000	3% skim milk	N/A
Mouse Anti-E-cadherin monoclonal antibody	BD Transduction	1:1000	3% skim milk	1:50
Mouse Anti-Vinculin monoclonal antibody	Sigma	1:500	3% skim milk	1:500

Mouse Anti-Paxillin monoclonal antibody	BD Transduction	1:50	3% skim milk	1:50
Mouse Anti-FOXO1 monoclonal antibody	Santa Cruz	1:500	3% skim milk	1:500
Mouse Anti-TXNIP monoclonal antibody	Santa Cruz	1:200	3% skim milk	N/A
Rabbit Anti-AKT monoclonal antibody	Cell Signalling	1:1000	5% skim milk	N/A
Rabbit Anti-phospho Ser473/4/2 AKT monoclonal antibody	Cell Signalling	1:1000	5% skim milk	N/A
Rabbit Anti-PTEN monoclonal antibody	Cell Signalling	1:1000	5% skim milk	N/A
Rabbit Anti-phospho Ser380/Thr382/383 PTEN monoclonal antibody	Cell Signalling	1:1000	5% skim milk	N/A
Rabbit Anti-ERK1/2 monoclonal antibody	Cell Signalling	1:500	5% skim milk	N/A
Rabbit Anti-phospho Thr202/Tyr204 ERK1/2 monoclonal antibody	Cell Signalling	3:1000	5% skim milk	N/A
Rabbit Anti-FAK monoclonal antibody	Sigma	1:1000	5% skim milk	N/A
Rabbit Anti-phospho Tyr398 FAK monoclonal antibody	Sigma	1:500	5% skim milk	N/A
Mouse Anti-GRB2 monoclonal antibody	Santa Cruz	1:500	3% skim milk	N/A
Rabbit Anti-SRC monoclonal antibody	Cell Signalling	1:1000	3% skim milk	N/A
Rabbit Anti-SOS1 monoclonal antibody	Santa Cruz	1:500	3% skim milk	N/A
Mouse Anti-CCND1 monoclonal antibody	Santa Cruz	1:1000	3% skim milk	N/A
Rabbit Anti-mTOR monoclonal antibody	Santa Cruz	1:1000	3% skim milk	N/A
Rabbit Anti-phospho Ser2448 mTOR monoclonal antibody	Cell Signalling	1:1000	3% skim milk	N/A

Rabbit Anti-4E-BP1 (eukaryotic translation initiation factor 4E-binding protein 1) monoclonal antibody	Santa Cruz	1:1000	3% skim milk	N/A
Rabbit Anti-phospho Thr37/46 4E-BP1 monoclonal antibody	Cell Signalling	1:1000	3% skim milk	N/A

2.1.6.2 Secondary antibodies

Horseradish peroxidase (HRP) conjugated antibodies, which are used for Western blot and immunohistochemistry experiments, are specified in Table 2 below.

Table 2: Secondary antibodies and respective dilutions used for Western blot study and immunohistochemistry.

Secondary antibody	Source	Dilution for Western blot	Dilution for immunohistochemistry
Alexa568 phalloidin	Molecular Probes	N/A	1:100
Anti-Mouse Alexa488	Molecular Probes	N/A	1:500 or 1:250
DAPI (4',6-diamidino-2-phenylindole, dihydrochloride)	Molecular Probes	N/A	1:1000
Anti-Mouse IgG (immunoglobulin protein G)-HRP	Sigma	1:10000	N/A
Anti-Rabbit IgG-HRP	Sigma	1:10000	N/A

2.1.7 Enzymes and biological kits

Necessary restriction endonucleases and their appropriate buffers used for DNA subcloning were from New England Biolabs. T4 DNA ligase and ligation buffer for DNA subcloning were from Fermentas. Amplified DNA was extracted from transformed *E. coli* cells with the TianGen MiniPrep Kit from TianGen. DNA fragments from agarose gel were extracted with the TIANgel Midi Purification Kit from TianGen. 5X Protein Assay Dye Reagent used for Bradford assays was from BioRad. Trizol solution used for RNA isolation from mammalian cells was from Invitrogen. Protein band

detection for Western blot via enhanced chemiluminescence (ECL) was done with Millipore Immobilon Western solutions from Millipore.

KAPA2G Robust polymerase and its PCR kit used for simple PCR were from KAPA Biosystems, while the reverse transcriptase, its 5X buffer and oligo dT primers used for RNA conversion to cDNA were from Promega. Deoxynucleoside triphosphate (dNTP) mixture used for PCR was from Invitrogen. SYBR Green Master Mix used for real-time PCR was from Fermentas. Mammalian protein microarray was done with the Kinex KAM-880 Antibody Microarray Kit from Kinexus Bioinformatics. Study of apoptotic or necrotic mammalian cells was done with the FITC (fluorescein isothiocyanate) Annexin V Apoptosis Detection Kit with PI from Biolegend. Study of generation of ROS levels in mammalian cells was done with the Total ROS Detection Kit from ENZO.

2.1.8 Chemicals and reagents for DNA work

6X DNA loading buffer and DNA molecular-weight 1 kbp ladder used were from New England Biolabs, ampicillin powder used to make ampicillin solution for LB culture was from Sigma and 10000X Gel Red used to label DNA in resolving agarose gel electrophoresis was from Biotium.

2.1.9 Chemicals and reagents for protein work

The phosphatase inhibitor sodium orthovanadate (Na_3VO_4), the proteasome inhibitor MG132 and the protease inhibitor phenylmethylsulfonyl fluoride (PMSF) used during cell lysis were from Sigma, dithiothreitol (DTT) used to reduce protein disulfide links in cell lysates was from BioRad, the protein molecular-weight (kDa) ladder used in SDS-PAGE was from New England Biolabs and the nitrocellulose membrane used for protein transfer was from BioRad. Dimethyl sulfoxide (DMSO) used was from Sigma.

2.1.10 General buffers and solutions

2.1.10.1 DNA subcloning

2.1.10.1.1 50X Tris-acetate-EDTA (TAE)

40 mM Tris-acetate (Promega) was mixed with 1.0 mM ethylenediaminetetraacetic acid (EDTA) (Sigma). A 1X TAE buffer was made by dilution with ddH_2O, to be used as running buffer and making agarose gel.

2.1.10.1.2 Agarose gel

10 g agarose powder (Promega) was mixed with 1000 ml 1X TAE buffer to make 1% agarose solution, and subsequently microwaved for 10 minutes to make agarose gel. The agarose solution was stored in an oven at 60°C to maintain its liquid form.

2.1.10.1.3 DNA loading buffer

1.5 µl 10000X Gel-Red (biotium) was mixed with 1 ml 6X DNA loading buffer (New England Biolabs), and can be kept as such for prolonged periods of time in 4°C until used by mixing Gel-Red DNA loading buffer with any solution containing DNA in a 1:4 (v/v) ratio.

2.1.10.2 Western blotting

2.1.10.2.1 10% sodium-dodecyl-sulphate (SDS)

10 g SDS powder (Sigma) was dissolved with 100 ml ddH_2O.

2.1.10.2.2 10% ammonium persulphate (APS)

1 g APS powder (Biorad) was dissolved with 10 ml ddH_2O.

2.1.10.2.3 10X Tris-glycine electrophoresis buffer

0.25 M Tris (Promega), 1.92 M glycine (Sigma) and 1% SDS (Sigma) were mixed with ddH_2O, and the solution pH was adjusted to 8.3. A 1X solution for SDS-polyacrylamide gel electrophoresis (SDS-PAGE) was made by diluting 10X stock with ddH_2O.

2.1.10.2.4 5X membrane transfer buffer

25 mM Tris (pH 8.3) (Promega), 192 mM glycine (Sigma), 0.1% SDS (Sigma) and 20% methanol (Sigma) were mixed with ddH_2O. A 1X solution for transfer was made by diluting 5X stock with ddH_2O.

2.1.10.2.5 2X SDS-PAGE loading buffer

Loading buffer was first made with 100 mM Tris-hydrohloric acid (HCl) (Promega) (pH 6.8), 4% SDS (Sigma), 0.2% bromophenol blue (Sigma) and 20% glycerol (Sigma) mixed with ddH_2O. The solution was kept in room temperature, and 200 mM DTT (Biorad) was added only to make fresh buffer for making mammalian cell lysates.

2.1.10.2.6 1M Tris buffer

121.12 g Tris (Promega) was dissolved in ddH_2O, and the solution pH was adjusted to 8.0.

2.1.10.2.7 5M NaCl buffer

292 g NaCl (BD Biosciences) was dissolved with ddH_2O.

2.1.10.2.8 10X phosphate-buffered saline (PBS) buffer

1.37 M NaCl (BD Biosciences), 0.027 M potassium chloride (KCl) (BD Biosciences), 0.018 M monobasic potassium phosphate (KH_2PO_4) and 0.1 M sodium hydrogen phosphate (Na_2HPO_4) were mixed in ddH_2O, and the solution pH was adjusted to 7.5. A 1X PBS solution was made by diluting 10X stock with ddH_2O.

2.1.10.2.9 10X Tris-buffered saline (TBS) buffer

200 mM Tris (Promega) and 5 M NaCl (BD Biosciences) were mixed in ddH_2O, and the solution pH was adjusted to 7.5. A 1X TBS solution was made by diluting 10X stock with ddH_2O.

2.1.10.2.10 Blocking solution

5%, 3% or 1% non-fat skim milk powder (Cowhead) was dissolved in 1X PBS or TBS solution.

2.1.10.2.11 Washing solution

10% Triton X-100 (Biorad) solution was mixed with 1X PBS to make 0.05% or 0.1% PBS-T. Tween (Biorad) solution was mixed with 1X TBS to make 0.05%, 0.01% or 0.001% TBS-Tween.

2.1.10.3 Mammalian cell culture

2.1.10.3.1 Freezing media

FBS and DMSO were mixed in a 9:1 (v/v) ratio. It was kept in -20°C till need for use.

2.1.10.3.2 1X PBS buffer

A 10X PBS solution was first made, the solution pH was adjusted to 7.0 and then autoclaved. A 1X PBS buffer was made by diluting 10X stock with autoclaved ddH_2O.

2.1.10.3.3 RIPA lysis buffer

A radioimmunoprecipitation assay (RIPA) solution containing 50 mM Tris-HCl (Promega) (pH 7.5), 200 mM NaCl (BD Biosciences), 1% Triton X-100 (Biorad), 0.1% SDS (Sigma), 0.5% sodium deoxycholate (Sigma), 10% glycerol (Sigma) and 1 mM EDTA (Sigma) was made. Only before cell lysis was 1 mM PMSF with or without 1 mM phosphatase inhibitor Na_3VO_4 added to the lysis buffer for usage.

2.1.10.3.4 Transfection reagent

A 2 mg/ml polyethyleneimine (PEI, linear) (Sigma) solution was prepared with ddH_2O, then filter-sterilized by passing through a 0.2 μm filter. It was kept in 4°C till need for use.

2.2 Methods

2.2.1 *E. coli* cell manipulation

2.2.1.1 Growth conditions and maintenance

E. coli cells were cultured in LB broth and grown on LB agar plates at 37°C. These cultures and plates can be stored in 4°C for prolonged periods of time. Any *E. coli* cells transformed with plasmids containing ampicillin resistance marker requires LB broth and agar plates be supplemented with ampicillin.

2.2.1.2 Glycerol stock

An 80% glycerol solution was made with ddH_2O. For long term preservation of select *E. coli* cells, a single *E. coli* colony was grown in 5 ml LB broth supplemented with ampicillin to mid-log phase. 800 μl of culture was mixed with 200 μl 80% glycerol solution in a cryo-vial and stored in -20°C.

2.2.1.3 Preparation of *E. coli* competent cells ($CaCl_2$ method)

A bacterial colony was picked from an LB agar plate and cultured in 5 ml LB broth overnight at 37°C, after which 1 ml culture was added to a flask of 200 ml fresh LB broth

and incubated at 37°C until an OD_{600} of approximately 0.5 was achieved. The culture was transferred to sterile centrifuge tubes, placed in ice to be chilled, and then spun down at 5000 *g* at 4°C for 10 minutes. All supernatant were discarded, the pellets were resuspended in 100 ml ice cold sterile 100 mM magnesium chloride ($MgCl_2$) solution and spun down again. All supernatant were discarded, the pellets were resuspended in 10 ml ice cold sterile 100 mM calcium chloride ($CaCl_2$) and kept in ice for 2 hours to render them competent. 2 ml ice cold sterile 50% glycerol solution was mixed with the cell suspension, and stored as 250 µl aliquots in -80°C. All cells and reagents, when used, were always kept on ice.

2.2.1.4 Transformation of plasmid DNA into *E. coli*

Frozen competent cells were thawed on ice. 100 ng DNA was added to 50 µl competent cells for DNA amplification, and 20 µl of ligation reaction was added to 100 µl competent cells for DNA subcloning work. Tubes were kept on ice for 15 minutes, heat-shocked in a 42°C water bath for 90 seconds, and kept on ice again for 15 minutes. Cells were then plated on LB agar plates supplemented with selective antibiotics and incubated at 37°C overnight.

2.2.1.5 Isolation of plasmid DNA from *E. coli*

A bacterial colony was picked from the LB agar plate and cultured in 5 ml LB broth with supplemented antibiotic overnight at 37°C. The culture was centrifuged at 5000 *g* at 4°C for 5 minutes. The supernatant was discarded, and plasmid DNA was isolated from the cell pellet according to instructions in the TianGen MiniPrep kit.

2.2.2 DNA manipulation

2.2.2.1 Agarose gel electrophoresis

1X agarose solution was poured into a cast, left to set, and then placed in a gel electrophoretic tank with 1X TAE solution. DNA samples were mixed with Gel-Red DNA loading buffer and loaded into the respective gel wells. DNA was resolved by running at 135 V with 400 mA for 35 minutes, and then visualized under long wavelength UV light.

2.2.2.2 DNA extraction from agarose gel

After visualizing of DNA bands under UV light, the bands of desired molecular weight were excised with a scalpel and transferred to an Eppendorf tube. DNA extraction was performed according to instructions in the TIANgel Midi DNA Purification Kit.

2.2.2.3 DNA subcloning

Purified plasmid DNA was set in a mixture of compatible restriction endonuclease buffer with appropriate restriction endonucleases for 2 hours at 37°C. The digested DNA was resolved with gel electrophoresis, the bands of interest were excised and extracted using the TIANgel Midi DNA Purification Kit. The purified DNA insert and DNA vector were ligated in room temperature for 30 minutes by T4 DNA ligase in a ligation mixture made according to manufacturer instructions. The ligation mixture was then introduced to competent *E. coli* cells for transformation.

2.2.2.4 DNA precipitation

To a 25 µl solution containing DNA, 2.5 µl 3 M sodium acetate (Sigma) (0.1X DNA volume) and 50 µl 100% ethanol (Merck) (2X DNA volume) were added, mixed and kept in -20°C for 30 minutes at minimum. The tube was centrifuged at 5000 g for 10 minutes, the supernatant was discarded, the pellet was washed with 70% ethanol and centrifuged again. The supernatant was discarded, the pellet was air-dried and subsequently dissolved in appropriate volume of ddH_2O or 1X Tris-EDTA buffer for further usage.

2.2.2.5 Verification of recombinant DNA plasmid constructs

DNA plasmids were digested with restriction enzymes that cut at unique sites internal or external of the open reading frame or unique to the plasmid alone. Digested DNA was then resolved with agarose gel electrophoresis, and the presence and specific order of bands a DNA plasmid was predicted to possess after DNA subcloning were checked.

2.2.2.6 DNA quantification

1 µl DNA solution was used to determine DNA concentration, against 1 µl DNA solvent as a blank, using the NanoDrop apparatus and software (Thermo Fischer). DNA quality

was checked by observing the OD_{260}/OD_{280} ratio, of which ideal quality is represented by ratios 1.8 to 2.0.

2.2.2.7 Polymerase chain reaction (PCR)

PCR was done to amplify specific DNA in large amounts from small amounts. All reactions were done with the Peltier Thermal Cycler PTC-100 (Biorad). Each reaction was 25 µl, consisting of 5 µl 5X KAPA2G Robust Reaction Buffer, 5 µl Enhancer, 0.1 µl 1U/µl KAPA2G Robust DNA polymerase, 0.5 µl dNTP (KAPA Biosystems), 0.75 µl 10 µM 5' primer, 0.75 µl 10 µM 3' primer, 0.5 µl template DNA, with remainder volume topped up with ddH_2O.

Cycle conditions were as such: initial denaturation of 95°C for 10 minutes, denaturation of 95°C for 1 minute, annealing of 55°C for 1 minute, extension of 72°C for 30 second every 1kb of desired DNA product (for 35 cycles), and a final extension of 72°C for 5 minutes. PCR products are later resolved by agarose gel electrophoresis.

2.2.2.8 RNA isolation

Total RNA was isolated from a cell line of interest using Trizol reagent (Invitrogen) according to the manufacturer instructions. 1 µl RNA solution was used to determine RNA concentration, against 1 µl diethyl pyrocarbonate (DEPC) water as a blank, using the NanoDrop apparatus and software (Thermo Fischer). RNA quality was checked by observing the OD_{260}/OD_{280} ratio, of which ideal quality is represented by a ratio of 2.0 or higher.

2.2.2.9 Conversion of RNA to cDNA

Following harvest of fresh RNA from mammalian cell lines, 2 µg RNA was used and mixed with 0.5 µl 0.5 µg/µl oligo dT primers (Promega), topped up to 10 µl with nuclease-free DEPC water and incubated at 70°C for 5 minutes. After incubating in ice for 5 minutes, 6 µl 5X reaction buffer (Promega), 3 µl 0.1 M DTT (Biorad), 0.5 µl 25 mM dNTP (Promega) and 9 µl DEPC water were all added to the mixture, incubated at 37°C for 5 minutes and then incubated in ice for 3 minutes. 0.5 µl reverse transcriptase enzyme (Promega) was added to the tube, the mixture resuspended to mix and was then

incubated at 42°C for 1 hour. The tube containing cDNA was kept on ice for real-time PCR use or stored in -20°C till usage.

2.2.2.10 Real-time PCR

25 µl real-time PCR reactions were set up as follows: 12.5 µl SYBR Green Master Mix (Fermentas), 2.5 µl 5X-diluted cDNA, 2.5 µl 5' and 3' primers (working concentration 50nm each), and remainder volume topped up with DEPC water. Each reaction was done in triplicates with primers used as detailed in Appendix 3. The real-time PCR was performed using the Applied Biosystems 7500 Real-Time PCR system, using the comparative C_T method of a cell line's gene of interest normalized to a control. The formula is as follows: $Ct_{Target} = 2^{(CtEndogenous - CtGene)}$, of which $Ct_{Endogenous}$ is the value of control gene expression in a cell line, Ct_{Gene} is the value of gene of interest expression in a cell line, and Ct_{Target} is the value of expression of gene of interest normalized to control in a cell line.

2.2.2.11 RNA sequencing (RNA-Seq)

100 ng RNA isolated from cell lines of interest was aliquoted into RNAstable tubes (Biomatrica) and shipped to Omega Bioservices (Georgia, USA) for total RNA-Seq method. The RNA integrity number was analyzed with the Agilent RNA600 Pico kit. mRNA enrichment was performed with Oligo (dT) magnetic beads and then fragmented into short fragments as templates for cDNA synthesis using the Illumina TruSeq Total RNA kit coupled with eukaryotic (human/mouse/rat) Ribo-Zero rRNA depletion for removing ribosomal RNA (rRNA). The resulting library was sequenced using the Illumina Hi-Seq 2500 platform and the 2x100bp run mode to achieve 20 million total reads, and differential gene expressions were identified by aligning RNA-Seq data with the *Homo sapiens* genome reference in the Illumina BaseSpace cloud server.

2.2.3 Culture of mammalian cells

2.2.3.1 Culturing mammalian cells

The HSC-5, HaCaT and 293T cell lines were maintained in complete growth medium (DMEM supplemented with 10% FBS, 100 IU/ml penicillin and 100 IU/ml streptomycin) (Gibco) at 37°C in an incubator with a 5% carbon dioxide (CO_2) atmospheric condition.

2.2.3.2 Thawing mammalian cells

Cryo-vials with cell lines of interest were taken from -80°C and resuspended in complete DMEM. The solution of thawed cells were transferred to a centrifuge tube and then centrifuged at 100 *g* in room temperature for 3 minutes. The supernatant was discarded and the pellet resuspended in complete DMEM, which was then added to a 10-cm culture dish with complete DMEM. Cells were incubated to grow autonomously.

2.2.3.3 Passage and culture of mammalian cells

A 10-cm culture dish of approximately 70% confluency was aspirated of complete DMEM and washed with 1X PBS buffer. The buffer was aspirated and cells were detached from the dish by incubation with 1 ml trypsin-EDTA (Gibco) solution spread across the dish surface. The solution was mixed with 5 ml complete DMEM, all transferred to a centrifuge tube and centrifuged at 100 *g* in room temperature for 3 minutes. The pellet of cells was resuspended in fresh complete DMEM and cells were seeded at a desired confluency in a new culture dish. The new dish of cells was incubated in 37°C and 5% CO_2.

2.2.3.4 Freezing and stocks of mammalian cells

Cells were trypsinized and resuspended in complete DMEM. The solution was centrifuged at 100 *g* in room temperature for 3 minutes, the supernatant discarded and the pellet resuspended in appropriate volume of freezing media. The cell solutions were aliquoted to cryo-vials and the vials were stored in -80°C.

2.2.3.5 Culture of cells prior to microscopic analysis and PEI transfection

Cells were trypsinized and resuspended in complete DMEM. Cells were either determined of its population count using a hemocytometer (Marienfeld) before subsequently seeding, or were seeded in a manner that enables desired cell confluency 24 hours after seeding. For microscopic analysis, culture plates may require laying of coverslips before seeding of cells.

2.2.3.6 Lentiviral preparation and induction of 293T cells

293T cells were transfected with lentiviral plasmids to produce retroviruses able to express exogenous proteins in mammalian cells or produce knockdown of genes via

RNAi using PEI method. 293T cells were ensured to be at 90% confluency in 10-cm culture dishes. Prior to transfection, 293T cells were washed with 8 ml serum-free media. Two 5 ml serum-free media solutions were prepared: one containing 3.75 μg pCMV-VSV-G, 3.125 μg pCMV-REV, 6.25 μg pCMV-GAG-POL and 18.75 μg pTT1-Puro or pTT2-Neo, and another containing 99.6 μg PEI. They were mixed gently and allowed to stand for 20 minutes before being added to the 293T cells. The lentiviral solution was left alone for 4 hours and then replaced with complete DMEM. After a first 24 hours, the media was collected and passed through a 0.45 μm filter to harvest the retroviruses. Aliquots are made to be either stored in -80°C or used immediately for mammalian cell infection. This was repeated again 24 hours later. 293T cells may be lysed to determine protein expression or discarded after second lentiviral harvest.

2.2.3.7 Lentiviral infection of HSC-5 and HaCaT cells

In 6-well culture plates already seeded with HSC-5 or HaCaT cells the previous day, a 500 μl fresh complete DMEM solution supplemented with 2 μl 5 mg/ml polybrene (Sigma) was added, followed by addition of 500 μl lentiviral harvest spread all over the surface. This was repeated 24 hours later for a second round.

2.2.3.8 Generation and maintenance of stable cell lines

Lentiviral-infected cell lines to either produce exogenous proteins or generate knockdown of genes via RNAi were selected with 2 μg/ml puromycin for 2 days or 1 mg/ml neomycin for 5 days. If both puromcyin and neomycin selections are employed, the duration of antibiotic selection was 5 days. This method of antibiotic selection was done to also eliminate uninfected cells. Maintenance of stable cell lines was done by employing 1 μg/ml puromycin or 0.5 mg/ml neomycin or both in complete DMEM.

2.2.3.9 Lysis of mammalian cells

Cells were trypsinized and resuspended in complete DMEM. The number of viable cells was determined using a hemocytometer (Marienfeld) and Trypan Blue (Gibco) exclusion method. 1 x 10^6 cells were centrifuged at 3000 *g* for 4 minutes, the media aspirated and cells were washed with 1X PBS buffer. The supernatant was discarded and cells were lysed with an appropriate volume of cell lysis buffer. The tube was left in ice for 1 hour and unlysed cellular components were removed by centrifugation at 14500 *g* for 10

minutes. 1 µl was used to quantify protein concentration according to the Bradford protein assay protocol (Biorad).

2.2.4 Mammalian cell assays

2.2.4.1 Cell proliferation assay

Cells were trypsinized, and the appropriate volume containing 7.5 x 10^3 viable cells was determined using a hemocytometer (Mariendfeld) and the Trypan Blue (Gibco) exclusion method. The cells were seeded in triplicates in 24-well culture plates for a period of 5 days. At the end of 5 days, cells were trypsinized and resuspended with complete DMEM to a total volume of 1 ml, of which 10 µl was loaded to the hemocytometer and cell count was performed. An average value from triplicates of each cell line was obtained in terms of ratio of number of cells to 7.5 x 10^3 cells.

2.2.4.2 Wound healing assay

Cells seeded in 6-well culture plates are ensured to reach 100% confluency prior to starting this assay (estimated viable cell number of 1 x 10^6). Three scratches were made in each well using a 2.5 µl micropipette for a cell line. The media was aspirated, the cells washed with 1X PBS buffer and fresh complete DMEM was added to each well. Images of each scratch were taken at 0 hours and 24 hours using the Olympus IX51 fitted with Cool SNAP^{HQ} camera and the MetaVue program, with additional time-points if necessary. Wound surface areas were quantified using the ImageJ program, and an average value from triplicates of each cell line was obtained for comparison.

2.2.4.3 Immunohistochemistry

Cells seeded onto coverslips in 6-well culture plates were ensured of appropriate confluency before immunohistochemistry was performed. Cells were fixed with 3.7% formaldehyde for 20 minutes, washed with 1X PBS buffer thrice, permeabilized with 0.2% PBS-T for 20 minutes, washed with 0.1% PBS-T thrice and blocked with 1% BSA 1X PBS for 1 hour, all in room temperature. Cells were probed with appropriate primary antibodies in 1% BSA 1X PBS for 1 hour, washed with 0.1% PBS-T thrice, incubated with Alexa488 green fluorescent protein (GFP) conjugated secondary antibody and Alexa568 red fluorescent protein (RFP) phalloidin for 1 hour, and washed thrice with 0.1% PBS-T, all in room temperature. Coverslips with stained cells were mounted with

Dako mounting media to glass slides, and fluorescence imagery of desired protein expression was performed with the Olympus IX51 fitted with Cool SNAP^{HQ} camera and the MetaVue program. The E-cadherin fluorescence intensity was quantified by using freehand icon in ImageJ to draw regions of interest for all cell membranes of a randomly-chosen cell, the fluorescence quantified, each value was divided by 2, and these values were then averaged. The average fluorescence intensity of 20 randomly-chosen cells was determined.

2.2.4.4 Cell lysate fractionation

Fractionation of cell lysates was performed to determine protein expression in the cytosol and nucleus. Two solutions were made as follows and then kept on ice: Buffer A (3 ml solution containing 300 µl 0.1 M 4-(2-hydroxyethyl)-1-piperazineethanesulfonic acid (HEPES) pH 7.9, 90 µl 0.05 M $MgCl_2$, 300 µl 0.1 M KCl, 1.5 µl 1 M DTT, 7.5 µl 200 mM PMSF, remainder topped with ddH_2O), and Buffer C (3 ml solution containing 600 µl 0.1 M HEPES pH 7.9, 90 µl 0.05 M $MgCl_2$, 1.26 ml 1M NaCl, 1 ml 75% glycerol, 1.5 µl 1 M DTT, 7.5 µl 200 mM PMSF, 1.2 µl 0.5 M EDTA pH 8.0, remainder topped with ddH_2O). Adherent cells on a 10-cm culture dish were scraped, transferred to an Eppendorf tube and centrifuged at 400 *g* at 4°C for 5 minutes. The supernatant was discarded, the pellet was resuspended in ice cold 2.5X volume Buffer A and incubated in ice for 30 minutes. The solution was centrifuged again at 400 *g* at 4°C for 10 minutes, the supernatant was discarded and the pellet resuspended in 1X volume Buffer A with Nonidet P-40 (Thomas Scientific) (working concentration 0.1%). The solution was lysed with 25G needle syringe and then centrifuged at 14500 *g* at 4°C for 20 minutes. The supernatant was transferred to an Eppendorf tube labelled 'Cytosol' and kept on ice for further Bradford assay or stored in -20°C till usage. The cell pellet was washed thrice with 2X volume Buffer A and centrifuged at 14500 *g* at 4°C for 5 minutes to wash any cytosolic residue. The cell pellet was then resuspended in 1.75X volume Buffer C, incubated in ice for 30 minutes, the solution was lysed with 30G needle syringe, centrifuged at 21500 *g* at 4°C for 45 minutes, and the resulting supernatant was transferred to an Eppendorf tube labelled 'Nucleus' and kept on ice for further Bradford assay (Biorad) or stored in -20°C till usage.

2.2.4.5 Protein microarray

Protein microarray study of mammalian cells was performed according to instructions in the Kinex KAM-880 Antibody Microarray Kit (Kinexus Bioinformatics). Mammalian cells were grown in 10-cm culture dishes and subjected to the microarray protocol. The microarray was read with the GenePix 4000B reader using the Gene Pix Pro 6.0 program, with microarray format provided from the KAM-880 GAL file. The protein expression ratio of test cell line to control cell line was calculated to determine proteomic up- or down-regulation.

2.2.4.6 Annexin-V/PI microscopy

Identification and determination of cell death by apoptosis or necrosis was done according to instructions in the BioLegend FITC Annexin V Apoptosis Detection Kit with PI. Cells were first seeded in 24-well culture plates in such a way that a cell confluency of 70% was obtained after 24 hours and staining protocol was immediately performed, with slight modifications. After washing of cells with 1X Annexin V Binding Buffer, Annexin V and propidium iodide (PI) in cells were visualized with the Olympus IX51 fitted with Cool SNAP^{HQ} camera and MetaVue program.

2.2.4.7 Reactive oxygen species (ROS) study

Detection of ROS in mammalian cells was performed according to instructions in the ENZO Total ROS Detection Kit, using not the provided 2',7'-dichlorofluorescin acetate (DCFDA) but one bought from Sigma to generate the optimized concentration of 25 μM for staining. Cells were first seeded in 24-well culture plates so a confluency of 70% was obtained after 24 hours and staining protocol was immediately performed. After washing with 1X Wash Buffer the cells' fluorescence reading (against blank 1X Wash buffer well) was done using the TECAN Infinite 200 Pro multiplate reader and software.

2.2.5 Western blotting

2.2.5.1 Cell lysate preparation

After lysis of cells, a Bradford assay was performed according to manufacturer instructions to quantify protein levels in samples. Fresh 2X SDS-PAGE loading buffer containing 200 mM DTT was added in equal volume to lysate volume, and the mixture

was boiled at 100°C for 5 minutes. Lysate were kept in ice for immediate use or stored in -20°C until eventual use.

2.2.5.2 SDS protein agarose gel electrophoresis (SDS-PAGE)

A 10% SDS-PAGE gel was prepared by first casting a resolving gel, and then a stacking gel with wells. A 5 ml resolving gel was made with 1900 µl ddH_2O, 1700 µl 30% acrylamide/bis-acrylamide (Biorad), 1300 µl 1.5 M Tris-HCl (pH 8.8) (Sigma), 50 µl 10% SDS (Sigma), 50 µl 10% APS (Biorad) and 2 µl tetramethylethylenediamine (TEMED) (Biorad). A 3 ml stacking gel was made with 2100 µl ddH_2O, 500 µl 30% acrylamide/bis-acrylamide (Biorad), 380 µl 1.0 M Tris-HCl (pH 6.8) (Sigma), 30 µl 10% SDS (Sigma), 30 µl 10% APS (Biorad) and 3 µl TEMED (Biorad). The same amount of proteins were loaded into gel wells and resolved in an electrophoretic tank (Biorad) with 1X Tris-glycine buffer at 210 V and 400 mA for 45 minutes.

2.2.5.3 SDS-PAGE transfer

The resolved SDS-PAGE gel was transferred to a transfer apparatus tank (Biorad) with 1X membrane transfer buffer. The transfer was performed at 100 V and 400 mA for 1 hour at 4°C. The 0.45 µm nitrocellulose membrane (Biorad) was retrieved, stained with 1 ml Ponceau S solution (Biorad) to confirm protein transfer from the SDS-PAGE gel, washed with ddH_2O twice with the Ponceau S solution discarded twice as well.

2.2.5.4 Western blotting and chemiluminescence

The nitrocellulose membrane was first blocked with the appropriate blocking solution, then probed with primary antibody either for overnight at 4°C or for several hours in room temperature. The membrane was then washed thrice with appropriate washing solution, then probed with secondary antibody conjugated with HRP for 1 hour in room temperature. The membrane was washed thrice again. Visualization of the secondary antibody via ECL was performed with Millipore Immobilon ECL reagent with the Fujifilm LAS-4000 apparatus and software.

2.2.6 Bioinformatics analysis

2.2.6.1 Proteomics, LC-MS/MS and PANTHER

300 μg protein was obtained from lysis of each mammalian cell line, and were delivered to the School Biological Sciences' Proteomic Core Facility. Protein separation, digestion and analysis via one dimensional SDS-PAGE, in-gel digestion and liquid chromatography-mass spectrometry/mass spectrometry (LC-MS/MS) was performed by staff member Ms Belinda Chen, employing slightly-modified protocols from those established [145]. Chromatogram and mass spectrum results were uploaded into the MascotCluster software for comparison with human proteomic database in UniProt. Relative abundance of proteins in test cell lines to control cell line was measured to determine down- or up-regulation of protein expression. Gene and signalling pathway annotation was done with the PANTHER software [146] under the *Homo sapiens* setting.

2.2.6.2 Microarray, RNA-Seq and Ingenuity Pathway Analysis

Protein microarray results from the Kinex KAM-880 Antibody Microarray Kit and RNA-Seq results from Omega Biosciences services and Illumina Hi-Seq 2500 software were organized, and together with proteomics data were further analyzed with the Ingenuity Pathway Analysis (Ingenuity) software; any access to it was courtesy of Assoc Prof Andrew Tan. Analysis of either protein microarray or RNA-Seq data by PANTHER software was also performed.

2.2.7 Statistics

All experiments were performed in triplicates, unless stated otherwise. Average values and standard deviation values are displayed. A Student's *t*-test was done to quantify significance in differences between control and experimental values, represented by * ($p<0.05$), ** ($p<0.01$) and *** ($p<0.001$).

Chapter 3: Results Part 1 – Characterizing the Role of N-WASP in Skin Cancer

3.1 Comparison of N-WASP levels and phenotypes in HSC-5 and HaCaT cells

N-WASP regulates actin polymerization and actin cytoskeleton remodelling [56]. N-WASP is shown to play a critical role in cell motility and spreading [147]. N-WASP expression is reduced in both breast and colorectal cancers, and they both correlate inversely with cancer progression [79,80]. Our laboratory has found N-WASP expression to be reduced in SCCs compared to matched perilesional samples in 33 skin cancer patients (Swagata's unpublished data) (Fig. 4). These suggest that N-WASP may be a tumour suppressor and plays a negative role in skin carcinogenesis. N-WASP plays a critical role in development since classic N-WASP knockouts resulted in embryonic lethality [67]. To our knowledge, its role in skin carcinogenesis has not been characterized.

3.1.1 N-WASP expression is reduced in HSC-5 cells compared to HaCaT cells

The early-stage human SCC skin cell line HSC-5 generated by Hozumi *et al*. [148] was used as a skin cancer cell model against the non-tumorigenic spontaneously-immortalized human skin keratinocyte cell line HaCaT, which behaves similarly to normal human skin keratinocytes [149]. A Western blot analysis of N-WASP expression in HSC-5 and HaCaT cells suggested that HSC-5 cells have approximately half the N-WASP levels of that of HaCaT cells (Fig. 7A). Densitometric quantification of N-WASP bands against GAPDH bands showed HSC-5 cells had significantly lower N-WASP protein levels compared to HaCaT cells (Fig. 7B). A real-time PCR was performed on cDNA converted from RNA extracted from both cell lines to determine if mRNA levels correlated with protein levels. HSC-5 cells were found to have significantly lower N-WASP mRNA levels compared to HaCaT cells (Fig. 7C), suggesting that N-WASP mRNA levels correlated with protein levels in skin cells.

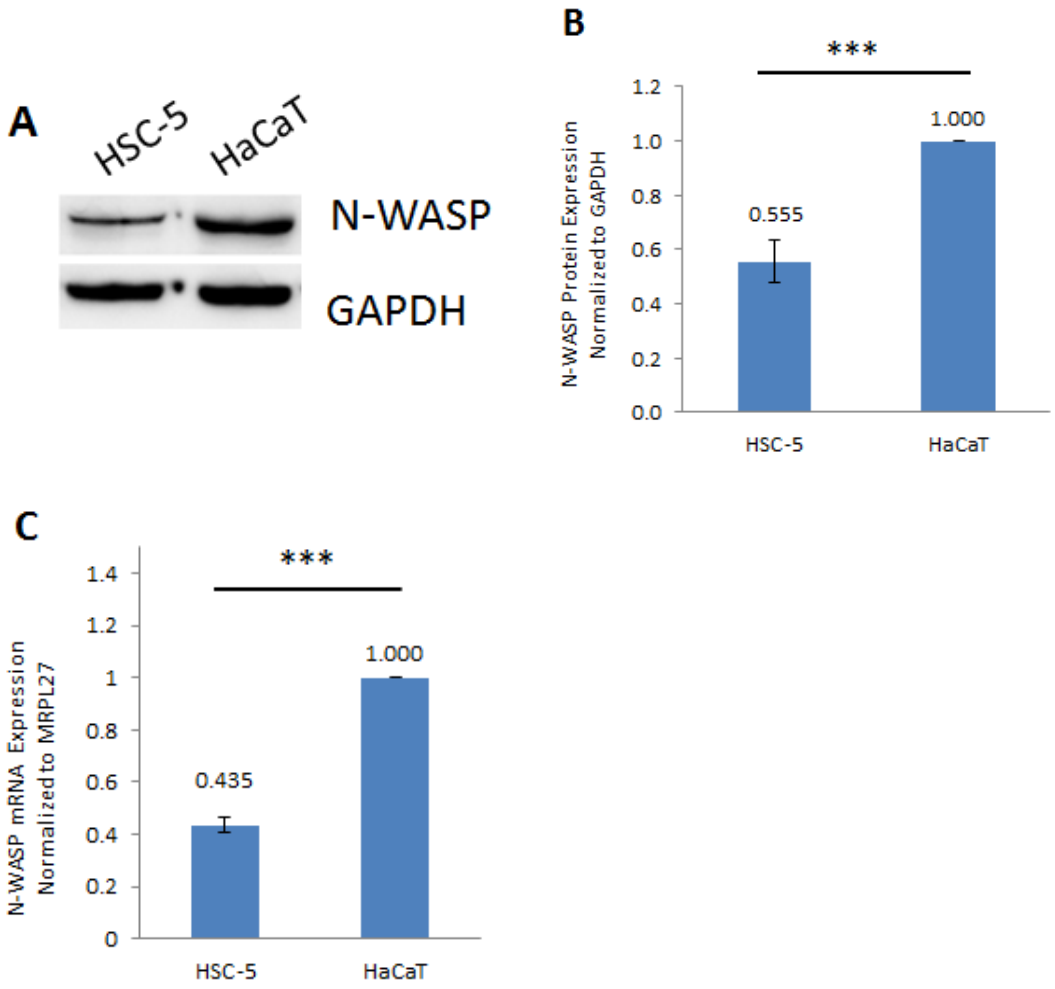

Figure 7: N-WASP expression is reduced in HSC-5 cells compared to HaCaT cells. A) Equal amounts of HSC-5 and HaCaT cell protein lysates were loaded for Western blot analysis using anti-N-WASP and anti-GAPDH antibodies. B) Densitometric quantifications show significant reduction of N-WASP protein levels in HSC-5 compared to HaCaT cells. C) Equal amounts of cDNA from HSC-5 and HaCaT cells were subjected to real-time PCR analysis of N-WASP cDNA, normalized to MRPL27, showing significant reduction of N-WASP mRNA levels in HSC-5 cells compared to HaCaT cells. Experiments were performed in triplicates. Significance: ***P<0.001 (Student's *t*-test).

3.1.2 HSC-5 cells have reduced cell proliferation compared to HaCaT cells

HRT18 human colorectal cancer cells overexpressing N-WASP had reduced cell proliferation activity compared to control cells [80], suggesting a possible role for N-WASP in reducing cell proliferation. Proliferation assays of viable HSC-5 and HaCaT cells were performed, and HSC-5 cells were found to proliferate at a significantly lower rate compared to HaCaT cells (Fig. 8).

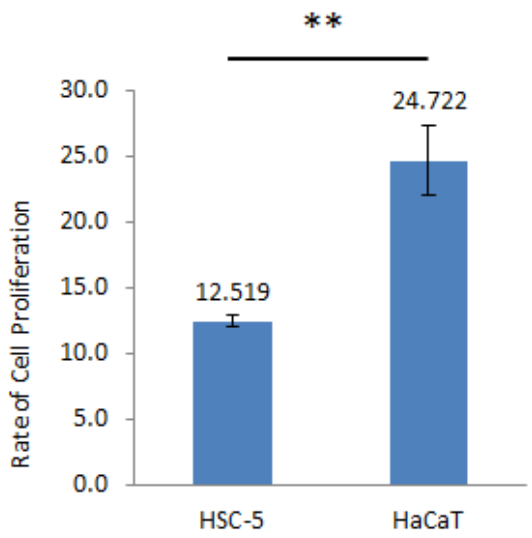

Figure 8: HSC-5 cells have reduced cell proliferation compared to HaCaT cells. 7.5 x 10^3 cells of each cell line were seeded in 24-well plates, incubated for 5 days, trypsinized and counted using a hemacytometer. The rate of proliferation was obtained by comparing total cell counted after 5 days against the number of cells seeded. Experiments were performed in triplicates. Significance: $^{**}P<0.01$ (Student's *t*-test).

3.1.3 E-cadherin localizations are reduced in HSC-5 cells compared to HaCaT cells

Localization of E-cadherin usually occurs in the adherens junctions [39,150] and the interaction of E-cadherin extracellular domains are necessary for cell-cell adhesion [151]. Immunohistochemistry to visualize E-cadherin localization and actin in HSC-5 and HaCaT cells was performed. HSC-5 cells had lower E-cadherin fluorescence intensity at the cell cortex compared to HaCaT cells, suggesting reduced localization (Fig. 9A). This was elaborated with the quantification of E-cadherin fluorescence, showing HSC-5 cells with significantly reduced average fluorescence compared to HaCaT cells (Fig. 9B). A Western blot analysis of HSC-5 and HaCaT cells for E-cadherin expression was done to determine if protein levels correlated with localization intensities. Both cell lines had similar E-cadherin expression (Fig. 10A), and densitometric quantification of E-cadherin bands against GAPDH bands showed no significant difference in E-cadherin protein levels between both cell lines (Fig. 10B). This suggests that reduced E-cadherin localization in skin cells is not due to reduced protein levels.

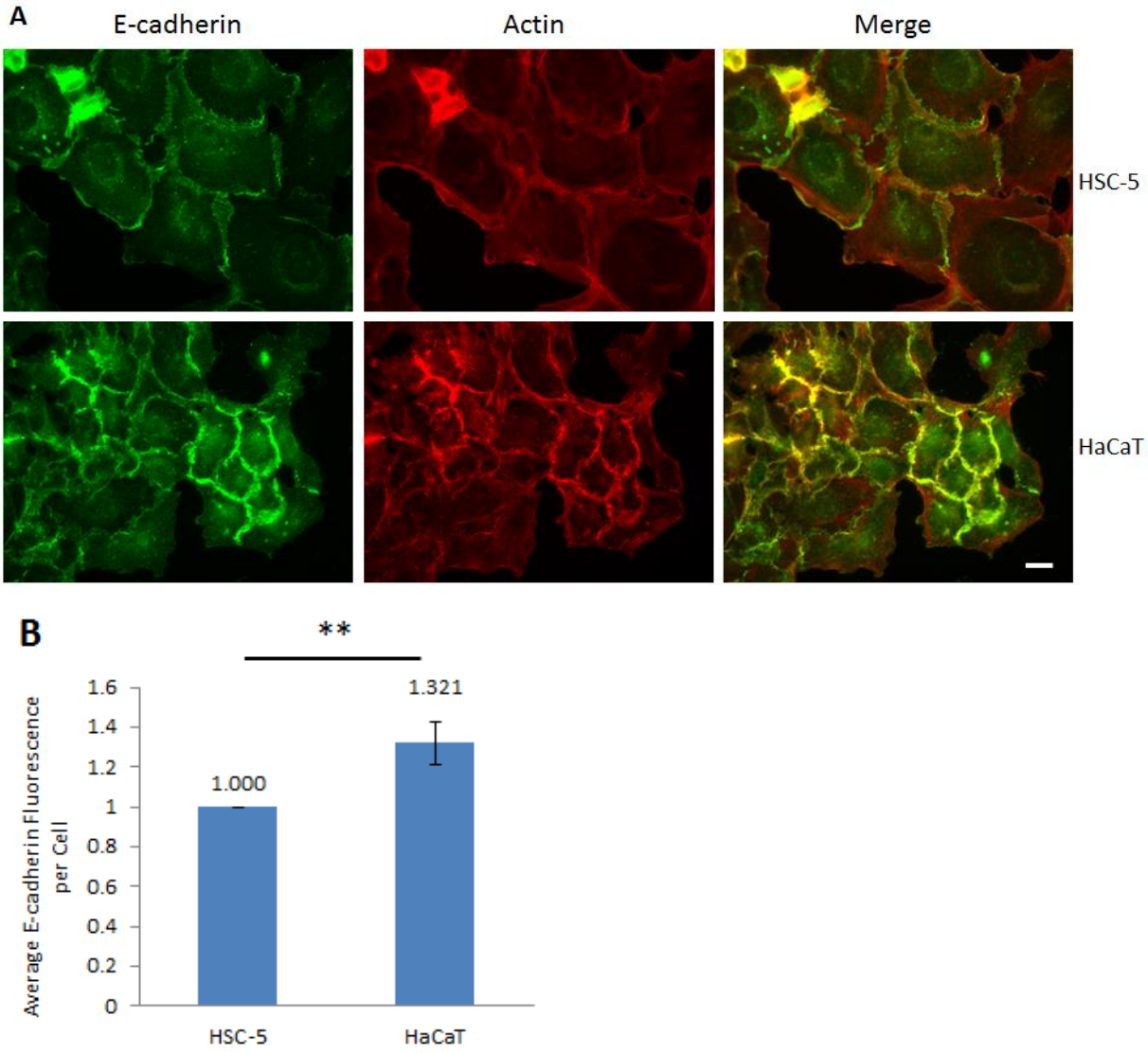

Figure 9: E-cadherin localizations are reduced in HSC-5 cells compared to HaCaT cells. A) HSC-5 and HaCaT cells were seeded on coverslips in 6-well plates, incubated, then fixed and probed with anti-E-cadherin (1°) antibody and Alexa488 conjugates (2°), and with Alexa568 conjugated phalloidin, and viewed under a 40X objective lens. Note the difference in green fluorescence in both cell lines; the intensity correlating with levels of E-cadherin localization. Scale bar represents 20 µm. B) E-cadherin fluorescence was quantified by quantifying the fluorescence in hand-drawn regions of interest for each cell, each fluorescence value was divided by 2, and the total values were then averaged. The average fluorescence intensity was obtained from 20 random cells. Experiments were performed in triplicates. Significance: $^{**}P<0.01$ (Student's *t*-test).

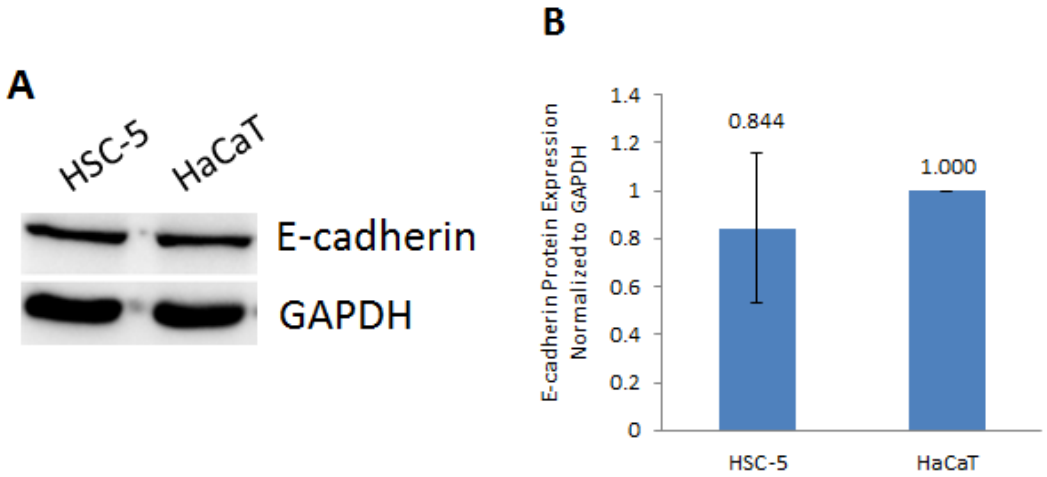

Figure 10: HSC-5 cells and HaCaT cells have similar E-cadherin expressions. A) Equal amounts of HSC-5 and HaCaT cell protein lysates were loaded for Western blot analysis using anti-E-cadherin and anti-GAPDH antibodies. B) Densitometric quantifications show no significant difference of E-cadherin protein levels in HSC-5 cells compared to HaCaT cells. Experiments were performed in triplicates. Significance: $P>0.05$ (Student's *t*-test).

3.1.4 HSC-5 cells migrated faster than HaCaT cells

N-WASP plays a role in MEF cell adhesion, since MEF N-WASP knockout cells exhibited increased cell migration compared to control cells [147]. Wound healing assays were done to determine which cell line migrates and closes the wound gap the fastest. HSC-5 cells migrated and closed the wound faster than HaCaT cells at 24 hours (Fig. 11A). Wound surface areas of both cells were similar at 0 hours, but HaCaT cells had significantly larger wound surface areas compared to HSC-5 cells at 24 hours (Fig. 11B).

3.1.5 Vinculin localizations are reduced in HSC-5 cells compared to HaCaT cells

Cell adhesion to the ECM is mediated by focal adhesion complexes rich in vinculin along with various constituents such as talin and actinin [151,152]. Reduced cell adhesion was observed due to reduced vinculin patch localization in cells [147]. Immunohistochemistry to visualize vinculin localization and actin and cell vinculin patch counts in HSC-5 and HaCaT cells were performed. HSC-5 cells were found to have reduced vinculin patches at the focal adhesion compared to HaCaT cells (Fig. 12A). HSC-5 cells had a significantly lower cell vinculin patch count than HaCaT cells (Fig. 12B). A Western blot of HSC-5 and HaCaT cells for vinculin expression was done to determine if protein levels correlated with patch counts. Both cell lines had similar

vinculin expression (Fig. 13A), and densitometric quantification of vinculin bands against GAPDH bands showed no significant difference in vinculin protein levels between both cell lines (Fig. 13B), suggesting that reduced vinculin localization in skin cells is not due to reduced protein levels.

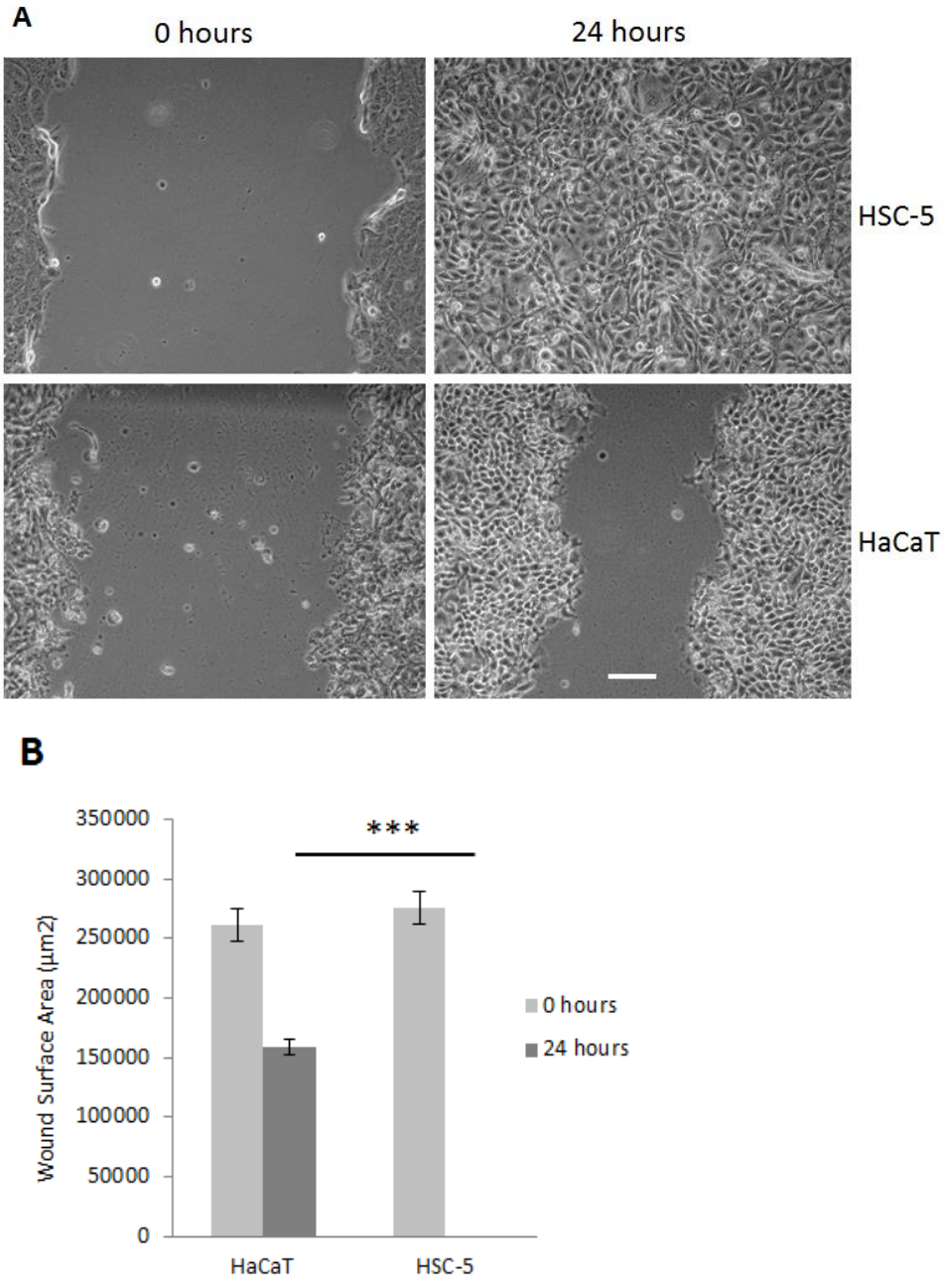

Figure 11: HSC-5 cells migrated faster than HaCaT cells. A) Cells were seeded such that prior to wound healing assay, the cell confluency would be 100%. Images were taken of the cells 0 hours and 24 hours after the scratches were made on the cells under view of a 10X objective lens. Scale bar represents 50 µm. B) Surface areas of wounds were measured at respective time points and compared, whereby HSC-5 cells closed the gap significantly faster than HaCaT cells. Experiments were performed in triplicates. Significance: ****P*<0.001 (Student's *t*-test).

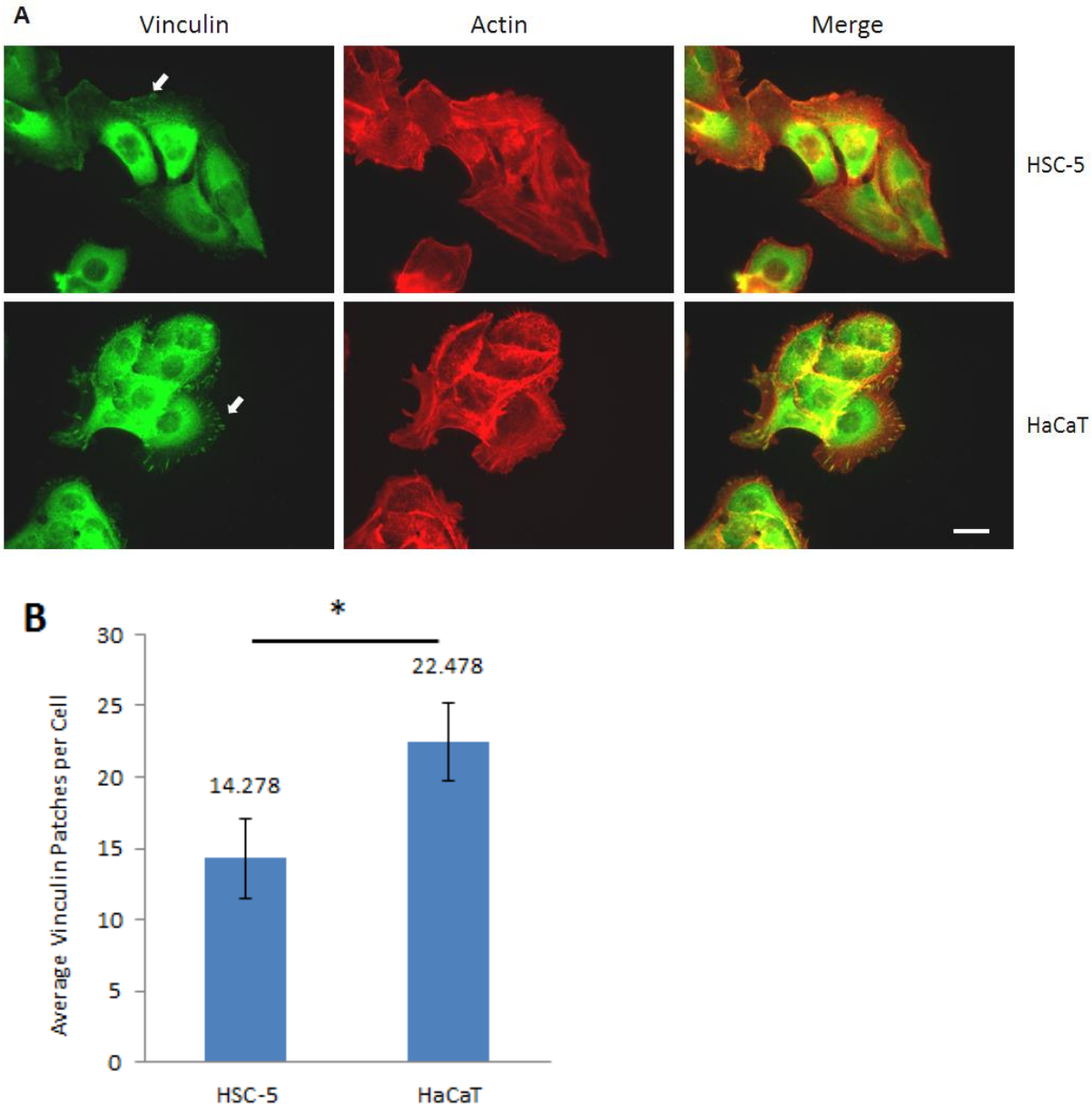

Figure 12: HSC-5 cells have fewer vinculin patches than HaCaT cells. A) HSC-5 and HaCaT cells were seeded on coverslips in 6-well plates, incubated, then fixed and probed with anti-vinculin (1°) antibody and Alexa488 conjugates (2°), and with Alexa568 conjugated phalloidin, and viewed under a 40X objective lens. Note the difference in the number of observable green fluorescence streaks and dots at the cell membrane. Scale bar represents 20 µm. B) Vinculin patch count was performed by counting number of observable vinculin patches in 30 random cells, averaged, and compared to each other. Experiments were performed in triplicates. Significance: **P*<0.05 (Student's *t*-test).

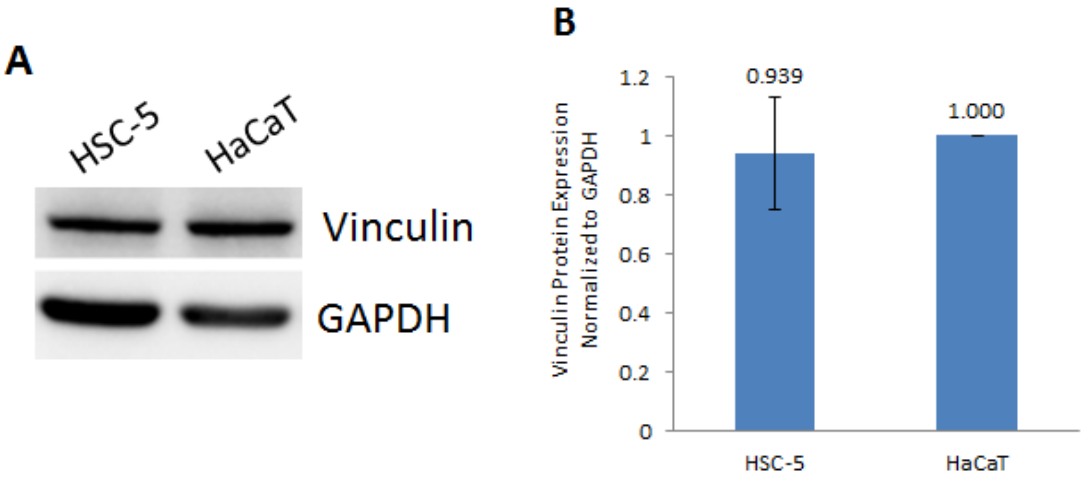

Figure 13: HSC-5 cells and HaCaT cells have similar vinculin expressions. A) Equal amounts of HSC-5 and HaCaT cell protein lysates were loaded for Western blot analysis using anti-vinculin and anti-GAPDH antibodies. B) Densitometric quantifications show no significant difference of vinculin protein levels in HSC-5 cells compared to HaCaT cells. Experiments were performed in triplicates. Significance: $P>0.05$ (Student's *t*-test).

3.1.6 Paxillin localizations are increased in HSC-5 cells compared to HaCaT cells

Paxillin is another focal adhesion complex protein that regulates cell migration, but has been noted to work in a manner in contrast to vinculin [153]. Increased paxillin expression was correlated with cell invasive ability [154]. Immunohistochemistry to visualize paxillin localization and actin and cell paxillin patch counts in HSC-5 and HaCaT cells were performed. HSC-5 cells were found to have increased paxillin patches at the focal adhesion compared to HaCaT cells (Fig. 14A). HSC-5 cells had a significantly higher cell paxillin patch count than HaCaT cells (Fig. 14B). A Western blot of HSC-5 and HaCaT cells for paxillin expression was done to determine if protein levels correlated with patch counts. Both cell lines had similar paxillin expression (Fig. 15A), and densitometric quantification of paxillin bands against GAPDH bands showed no significant difference in paxillin protein levels between both cell lines (Fig. 15B), suggesting that increased paxillin localization in skin cells is not due to increased protein levels.

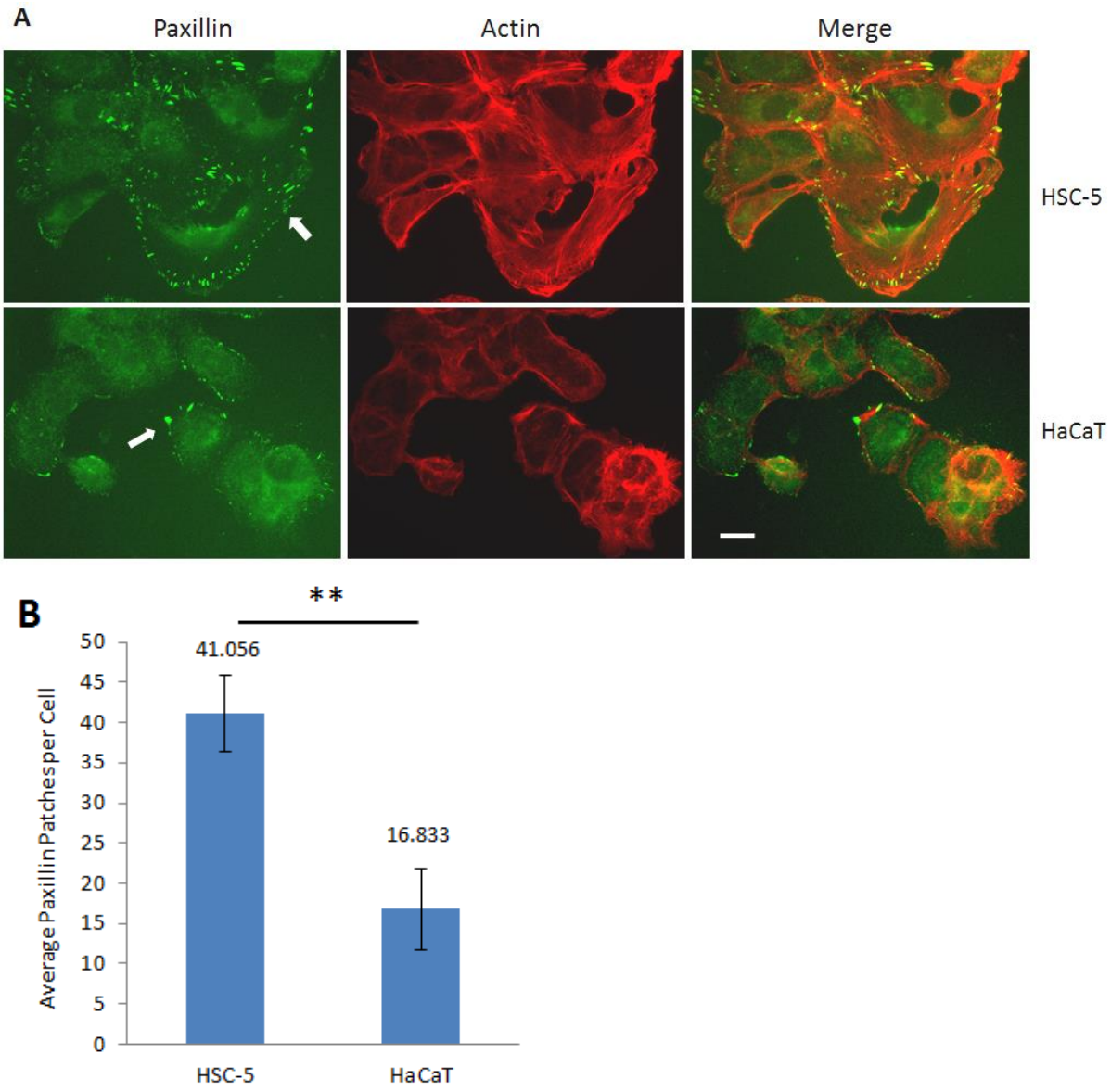

Figure 14: HSC-5 cells have more paxillin patches than HaCaT cells. A) HSC-5 and HaCaT cells were seeded on coverslips in 6-well plates, incubated, then fixed and probed with anti-paxillin (1°) antibody and Alexa488 conjugates (2°), and with Alexa568 conjugated phalloidin, and viewed under a 40X objective lens. Note the difference in the number of observable green fluorescence streaks and dots at the cell membrane. Scale bar represents 20 µm. B) Paxillin patch count was performed by counting number of observable paxillin patches in 30 random cells, averaged, and compared to each other. Experiments were performed in triplicates. Significance: $^{**}P<0.01$ (Student's *t*-test).

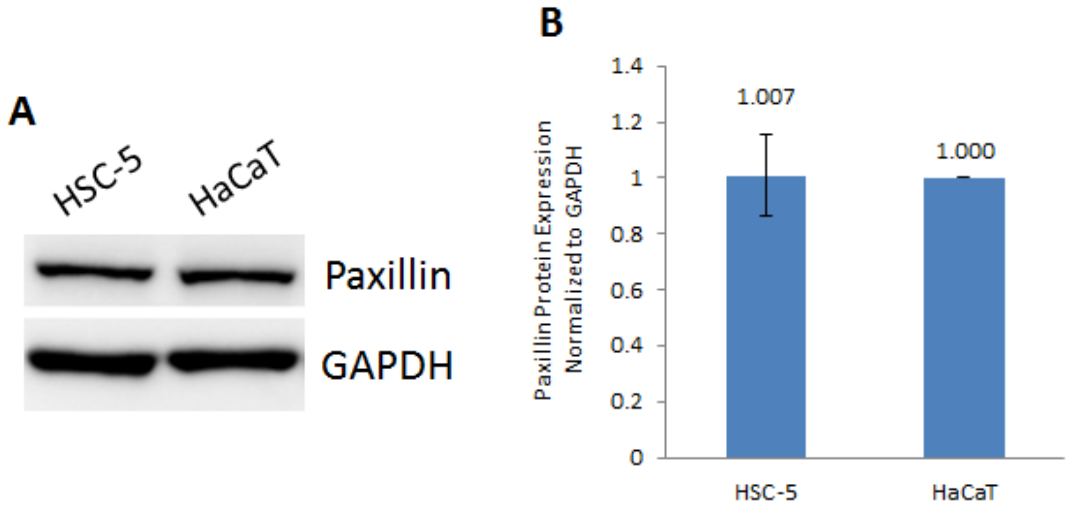

Figure 15: HSC-5 cells and HaCaT cells have similar paxillin expressions. A) Equal amounts of HSC-5 and HaCaT cell protein lysates were loaded for Western blot analysis using anti-paxillin and anti-GAPDH antibodies. B) Densitometric quantifications show no significant difference of paxillin protein levels in HSC-5 cells compared to HaCaT cells. Experiments were performed in triplicates. Significance: $P>0.05$ (Student's *t*-test).

3.1.7 Summary

Reduced N-WASP levels were previously implicated in breast and colorectal carcinogenesis. N-WASP levels were found to be reduced in SCC samples compared to matched skin perilesional samples in 33 patients (Swagata's unpublished data), suggesting a role for N-WASP in skin carcinogenesis. HSC-5 skin cancer cells had reduced N-WASP expression compared to HaCaT normal skin cells, and mRNA levels correlated with protein levels. Further studies suggest that N-WASP expression may correlate with cell proliferation, E-cadherin localization and cell migration ability due to increased paxillin but reduced vinculin patches in skin cells. Cellular localizations of E-cadherin, vinculin and paxillin do not correlate with protein expressions. It is possible these *in vitro* studies correlate with observed N-WASP phenotypes in clinical *in vivo* scenarios.

3.2 Characterization of N-WASP levels and phenotypes in HSC-5 sublines

Studies comparing phenotypes of HSC-5 and HaCaT cells have found that HSC-5 cells have reduced N-WASP protein levels and mRNA levels (Fig. 7). HSC-5 cells proliferated slower (Fig. 8), migrated faster (Fig. 11) and have reduced E-cadherin localizations (Fig. 10) and vinculin patches (Fig. 12) but increased paxillin patches (Fig. 14) compared to HaCaT cells. Both HSC-5 and HaCaT cells were derived from different individuals with different genetic backgrounds and mutations, so any phenotypic differences observed cannot be correlated to N-WASP protein levels in both cell lines. The role of N-WASP in skin cancer cells was characterized by generating HSC-5 cells capable of expressing N-WASP similar to HaCaT cells, followed by similar phenotypic characterization studies.

3.2.1 Generation of HSC-5 sublines overexpressing N-WASP

HSC-5 cells were infected with third-generation lentivirus derived from empty pTT1-Puro vector (HSC-5^{CTR}) or pTT1-N-WASP-Puro to overexpress exogenous N-WASP (HSC-$5^{N\text{-}WASP}$). Single cell HSC-$5^{N\text{-}WASP}$ colonies were isolated following infection and puromycin selection, and a Western blot for N-WASP expression was done on HSC-$5^{N\text{-}WASP}$ clones to identify the clone with N-WASP expression similar to that of HaCaT cells. Densitometric quantification of N-WASP bands against GAPDH bands showed HSC-$5^{N\text{-}WASP}$ clones 64, 86, 89 and 56 with N-WASP protein levels at 94%, 100%, 119% and 125% respectively, that of HaCaT cells (Fig. 16). The HSC-$5^{N\text{-}WASP\text{-}86}$ clone was used as HSC-$5^{N\text{-}WASP}$, as it had N-WASP protein levels similar to HaCaT cells, for the rest of the study.

Further Western blots of HSC-5^{CTR}, HSC-$5^{N\text{-}WASP}$ and HaCaT cells for N-WASP was performed. HSC-$5^{N\text{-}WASP}$ and HaCaT cell N-WASP protein levels are similar and higher than that of HSC-5^{CTR} cells (Fig. 17A). The HSC-$5^{N\text{-}WASP}$ cell N-WASP protein levels was found to be significantly higher (Fig. 17B). Real-time PCR for N-WASP cDNA was performed on both HSC-5 sublines to determine if mRNA levels correlated with protein levels. HSC-$5^{N\text{-}WASP}$ cells had easily 358% the mRNA levels of HSC-5^{CTR} cells (Fig. 17C), suggesting that N-WASP mRNA levels do not correlate with protein levels proportionately in skin cancer cells probably due to post-transcriptional regulation of N-WASP.

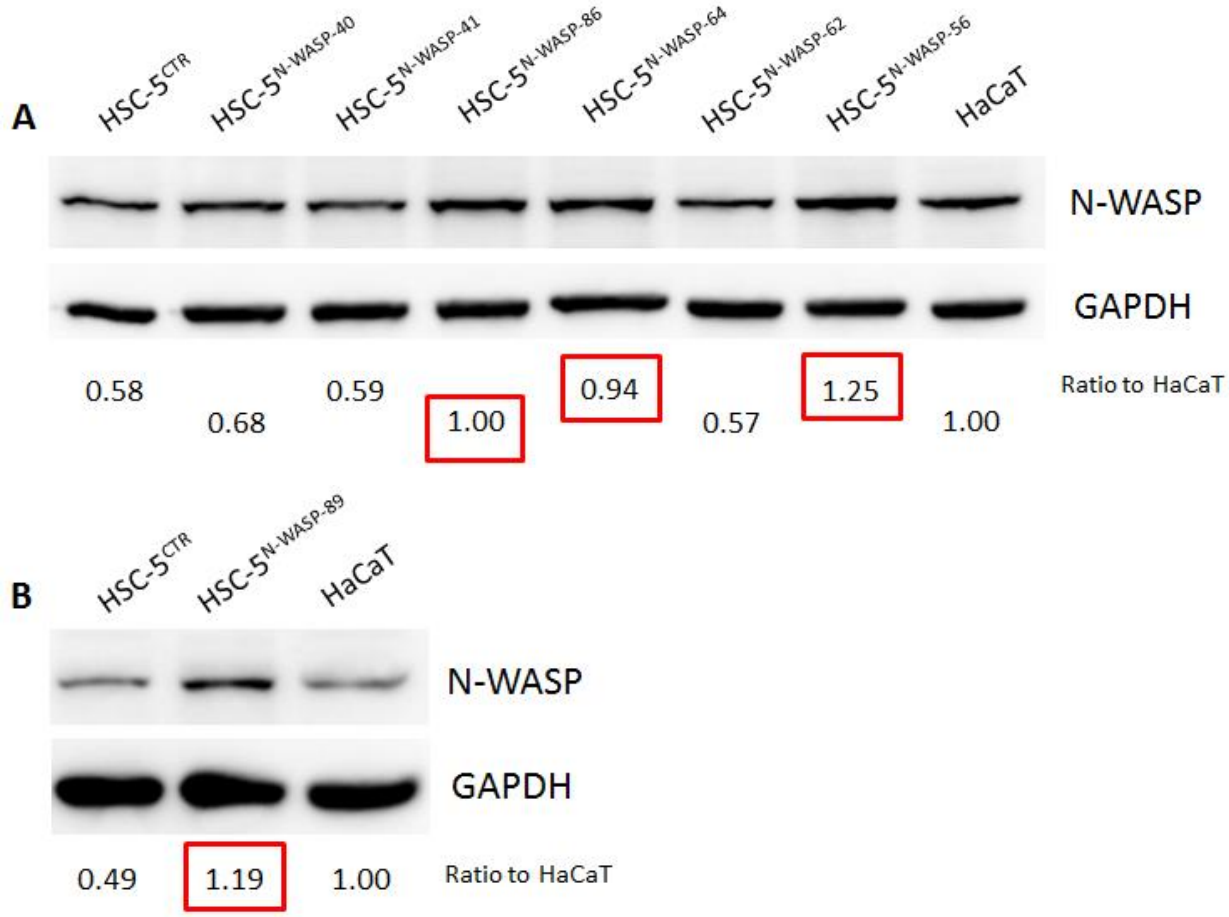

Figure 16: Western blot analysis of N-WASP expressions of HSC-5$^{N\text{-}WASP}$ clones. Equal amounts of HSC-5^{CTR}, HSC-5$^{N\text{-}WASP}$ and HaCaT cell protein lysates were loaded for Western blot analysis using anti-N-WASP and anti-GAPDH antibodies. Densitometric quantifications show A) several HSC-5$^{N\text{-}WASP}$ clones expressing exogenous N-WASP similar or exceeding that of HaCaT cells, and B) one HSC-5$^{N\text{-}WASP}$ clone expressing exogenous N-WASP exceeding that of HaCaT cells (1.00 = 100% that of HaCaT, highlighted in red boxes). The HSC-5$^{N\text{-}WASP\text{-}86}$ clone was used as HSC-5$^{N\text{-}WASP}$ for the rest of the study. This Western blot screen was done only once.

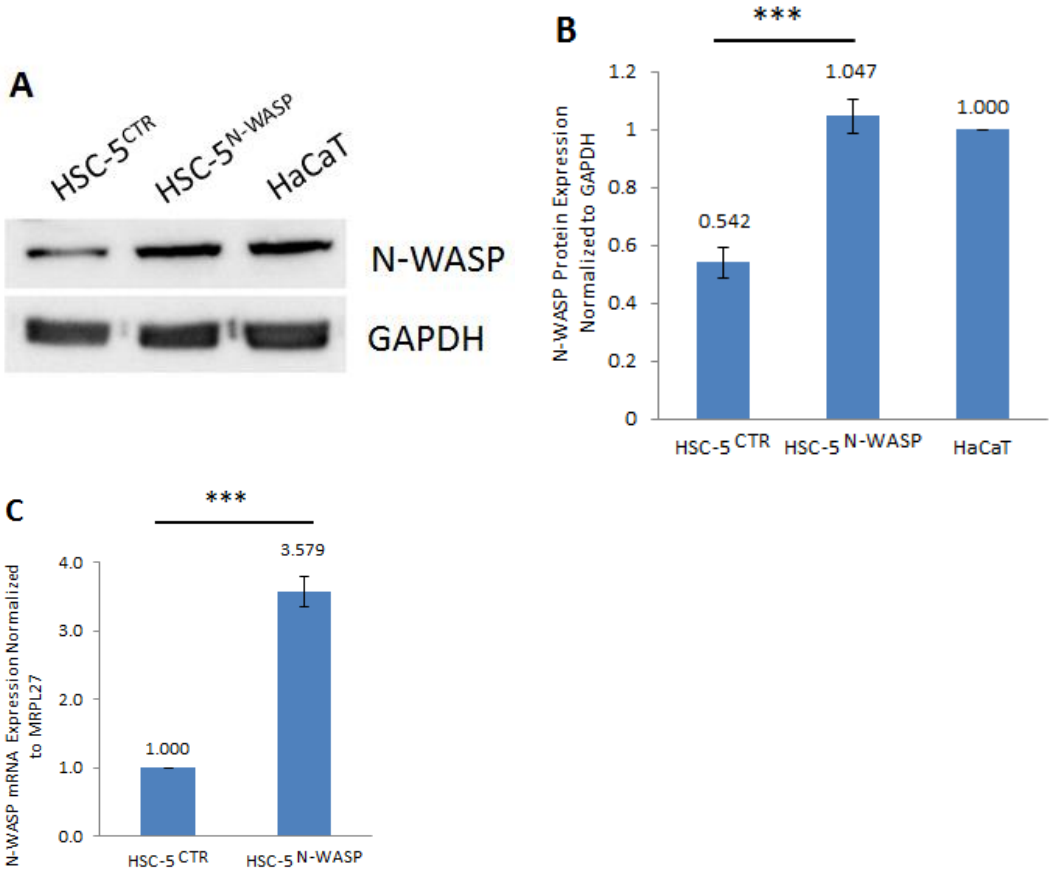

Figure 17: HSC-5$^{N\text{-}WASP}$ cells and HaCaT cells have similar N-WASP expressions. A) Equal amounts of HSC-5^{CTR}, HSC-5$^{N\text{-}WASP}$ and HaCaT cell protein lysates were loaded for Western blot analysis using anti-N-WASP and anti-GAPDH antibodies. B) Densitometric quantifications show significant increase of N-WASP protein levels in HSC-5$^{N\text{-}WASP}$ compared to HSC-5^{CTR} cells, similar to HaCaT cells. C) Equal amounts of cDNA from HSC-5^{CTR} and HSC-5$^{N\text{-}WASP}$ cells were subjected to real-time PCR analysis of N-WASP cDNA, normalized to MRPL27, showing significant increase of N-WASP mRNA levels in HSC-5$^{N\text{-}WASP}$ cells compared to HSC-5^{CTR} cells. Experiments were performed in triplicates. Significance: ***P<0.001 (Student's t-test).

3.2.2 HSC-5$^{N\text{-}WASP}$ cells have reduced cell proliferation compared to HSC-5^{CTR} cells

HSC-5 cells proliferated slower than HaCaT cells (Fig. 8), possibly due to its reduced N-WASP expression. Human HRT18 colorectal cancer cells overexpressing N-WASP exhibited reduced cell proliferative activity compared to control cells [80]. Cell proliferation assays were performed on HSC-5^{CTR} and HSC-5$^{N\text{-}WASP}$ cells to study N-WASP effects on cell proliferation. HSC-5$^{N\text{-}WASP}$ cells had significantly reduced cell proliferation compared to HSC-5^{CTR} cells (Fig. 18A). The assay was repeated with the HSC-5$^{N\text{-}WASP}$ clones 64, 89 and 56 to determine if the reduction in cell proliferation is N-WASP-dependent. HSC-5$^{N\text{-}WASP}$ cell proliferation was reduced further compared to HSC-5^{CTR} cells with increasing significance and with increasing N-WASP expression

(Fig. 18B), suggesting that cell proliferation rates are dependent on N-WASP protein levels in skin cancer cells.

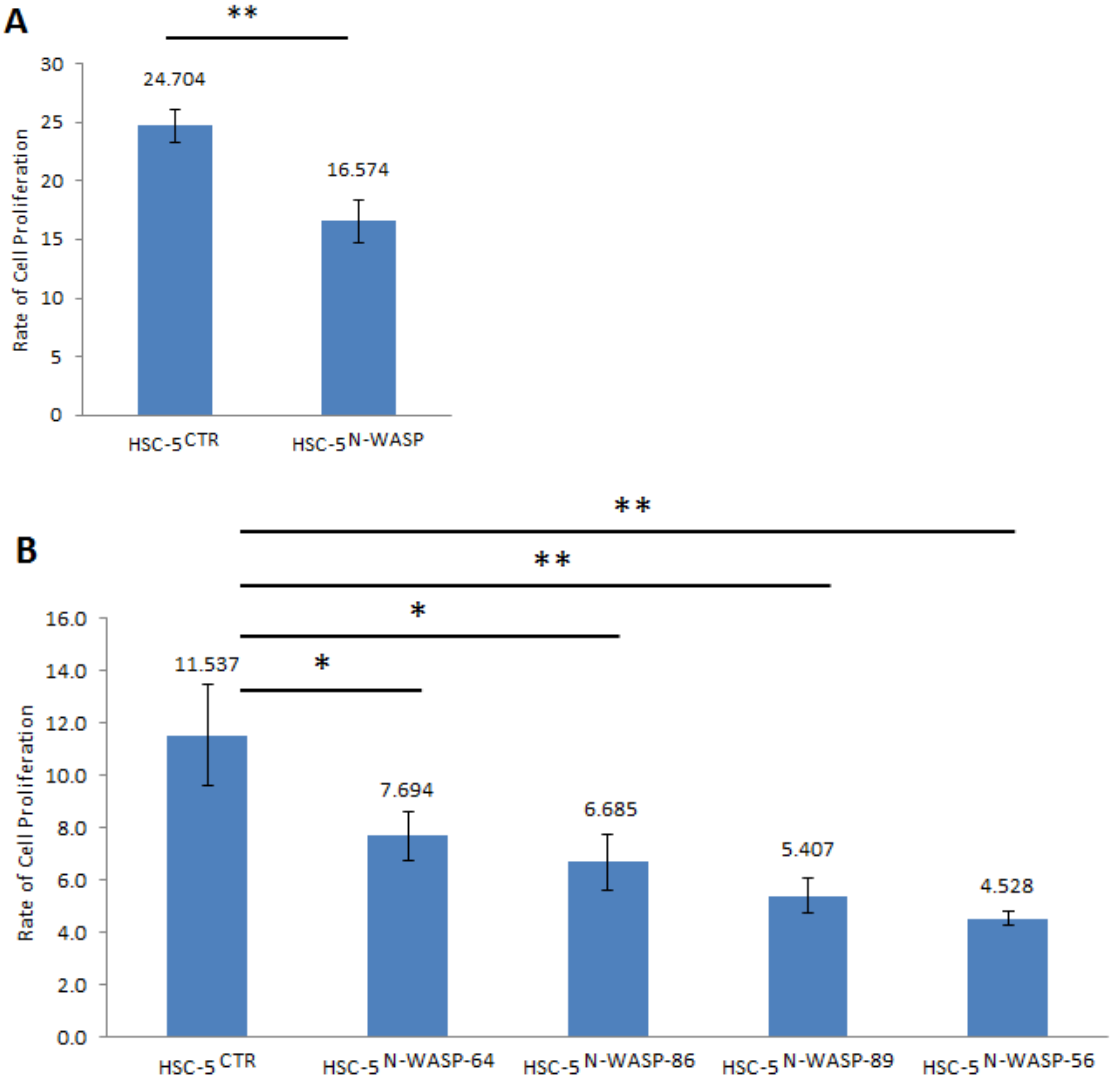

Figure 18: HSC-5$^{N\text{-}WASP}$ cells have reduced cell proliferation compared to HSC-5^{CTR} cells. 7.5 x 10^3 cells of each cell line were seeded in 24-well plates, incubated for 5 days, trypsinized and counted using a hemacytometer. The rate of proliferation was obtained by comparing total cell counted after 5 days against the number of cells seeded. Cell proliferation assays were performed either A) with HSC-5^{CTR} and HSC-5$^{N\text{-}WASP}$ cells alone, or B) with HSC-5^{CTR} and all four HSC-5$^{N\text{-}WASP}$ clones generated earlier. Experiments were performed in triplicates. Significance: *P<0.05, **P<0.01 (Student's t-test).

3.2.3 Cyclin D1 expression is reduced in HSC-5$^{N\text{-}WASP}$ cells compared to HSC-5^{CTR} cells

Cyclin D1 (CCND1) is a well-known marker for cell proliferation activity. Increased CCND1 levels correlates with increased phosphorylation of retinoblastoma (RB) protein, which pushes cell cycle transit past G1 phase [155]. HSC-5$^{N\text{-}WASP}$ cells proliferated at slower rates than HSC-5^{CTR} cells (Fig. 18A). A Western blot of the HSC-5 sublines for CCND1 was performed to characterize CCND1 expression. HSC-5$^{N\text{-}WASP}$ cells had reduced CCND1 expression compared to HSC-5^{CTR} cells (Fig. 19A). Densitometric quantification of CCND1 bands against GAPDH bands showed the reduction of CCND1 protein levels was significant (Fig. 19B). These suggest that CCDND1 expression correlated with cell proliferative activity in skin cancer cells.

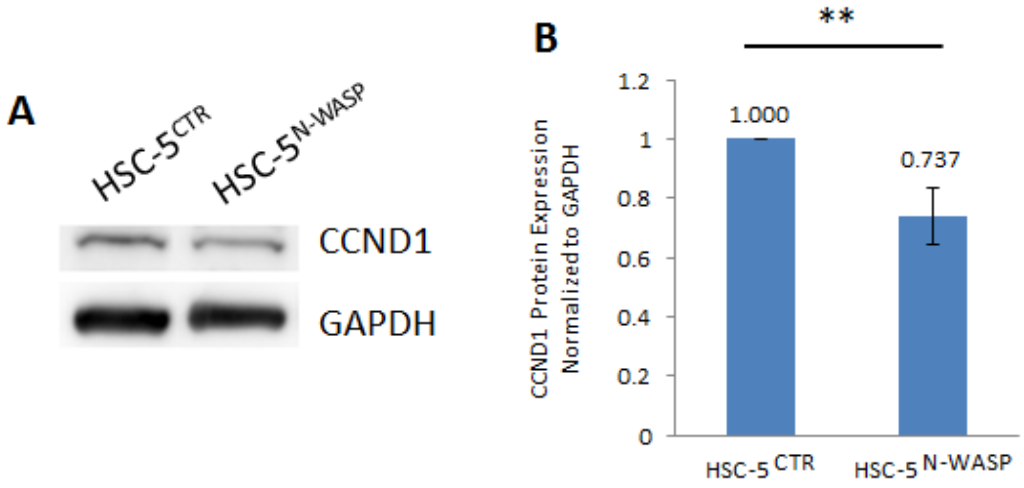

Figure 19: CCND1 expression is reduced in HSC-5$^{N\text{-}WASP}$ cells compared to HSC-5^{CTR} cells. A) Equal amounts of HSC-5^{CTR} and HSC-5$^{N\text{-}WASP}$ cell protein lysates were loaded for Western blot analysis using anti-CCND1 and anti-GAPDH antibodies. B) Densitometric quantifications show significant reduction of CCND1 protein levels in HSC-5$^{N\text{-}WASP}$ cells, compared to HSC-5^{CTR} cells. Experiments were performed in triplicates. Significance: $^{**}P<0.01$ (Student's *t*-test).

3.2.4 E-cadherin localizations are increased in HSC-$5^{N\text{-}WASP}$ cells compared to HSC-5^{CTR} cells

HSC-5 cells had reduced E-cadherin localizations compared to HaCaT cells (Fig. 9), possibly due to reduced N-WASP expression. Immunohistochemistry to visualize E-cadherin and actin in HSC-5^{CTR} and HSC-$5^{N\text{-}WASP}$ cells was performed to study N-WASP effects on E-cadherin localization. HSC-$5^{N\text{-}WASP}$ cells had increased E-cadherin localization at the cell cortex (Fig. 20A) and significantly increased average E-cadherin fluorescence intensity (Fig. 20B) compared to HSC-5^{CTR} cells, which are similar to when comparing HaCaT cell E-cadherin localization and fluorescence intensity to that of HSC-5 cells (Fig. 9). A Western blot of both HSC-5 sublines for E-cadherin expression was performed to determine if E-cadherin protein levels correlated with localization intensities. E-cadherin expressions of both HSC-5 sublines were similar (Fig. 21A). Densitometric quantification of E-cadherin bands against GAPDH bands showed no significant difference in E-cadherin protein levels between both cell lines (Fig. 21B), suggesting that increased E-cadherin localization is not due to increased protein levels in skin cancer cells.

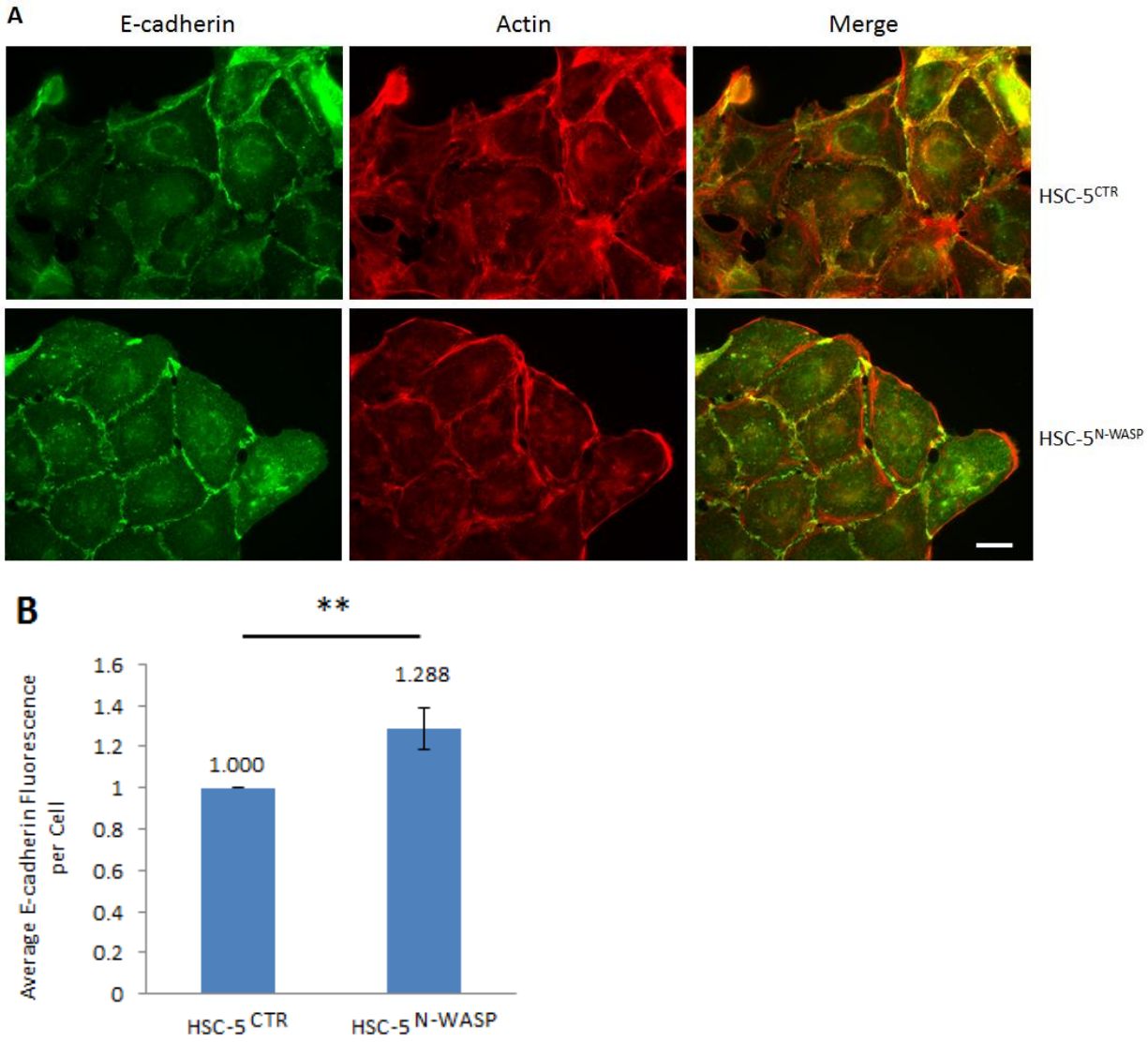

Figure 20: E-cadherin localizations are increased in HSC-5$^{N\text{-}WASP}$ cells compared to HSC-5^{CTR} cells. A) HSC-5^{CTR} and HSC-5$^{N\text{-}WASP}$ cells were seeded on coverslips in 6-well plates, incubated, then fixed and probed with anti-E-cadherin (1°) antibody and Alexa488 conjugates (2°), and with Alexa568 conjugated phalloidin, under the view of 40X objective lens. Note the difference in green fluorescence in both cell lines; the intensity correlating with levels of E-cadherin localization. Scale bar represents 20 µm. B) E-cadherin fluorescence was quantified by quantifying the fluorescence in hand-drawn regions of interest for each cell, each fluorescence value was divided by 2, and the total values were then averaged. The average fluorescence intensity was obtained from 20 random cells. Experiments were performed in triplicates. Significance: $^{**}P<0.01$ (Student's *t*-test).

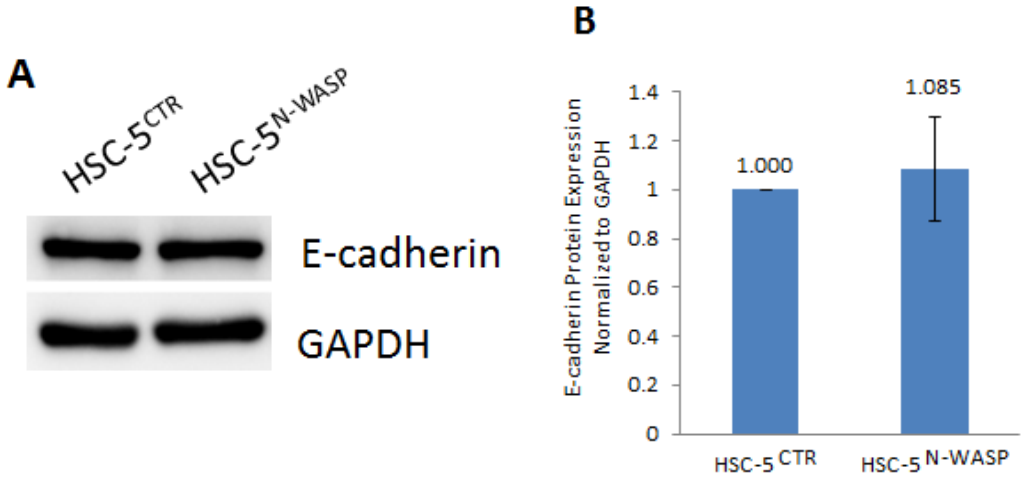

Figure 21: HSC-5^{CTR} and HSC-5$^{N\text{-}WASP}$ cells have similar E-cadherin expressions. A) Equal amounts of HSC-5^{CTR} and HSC-5$^{N\text{-}WASP}$ cell protein lysates were loaded for Western blot analysis using anti-E-cadherin and anti-GAPDH antibodies. B) Densitometric quantifications show no significant difference of E-cadherin protein levels in HSC-5$^{N\text{-}WASP}$ cells compared to HSC-5^{CTR} cells. Experiments were performed in triplicates. Significance: $P>0.05$ (Student's *t*-test).

3.2.5 HSC-5$^{N\text{-}WASP}$ cells migrated slower than HSC-5^{CTR} cells

A cell's ability to migrate depends on its adhesion to the surrounding ECM [156]. HSC-5 cells migrated faster than HaCaT cells (Fig. 11), possibly due to reduced N-WASP expression. Wound healing assays were performed on HSC-5^{CTR} and HSC-5$^{N\text{-}WASP}$ cells to study N-WASP effects on cell migration. HSC-5$^{N\text{-}WASP}$ cells migrated and closed the wound slower than HSC-5^{CTR} cells (Fig. 22A), similar to when comparing HaCaT cell migration to that of HSC-5 cells (Fig. 11A). Wound surface areas of both HSC-5 sublines were similar at 0 hours, but HSC-5$^{N\text{-}WASP}$ cells showed significantly larger wound surface areas compared to HSC-5^{CTR} cells at 24 hours (Fig. 22B).

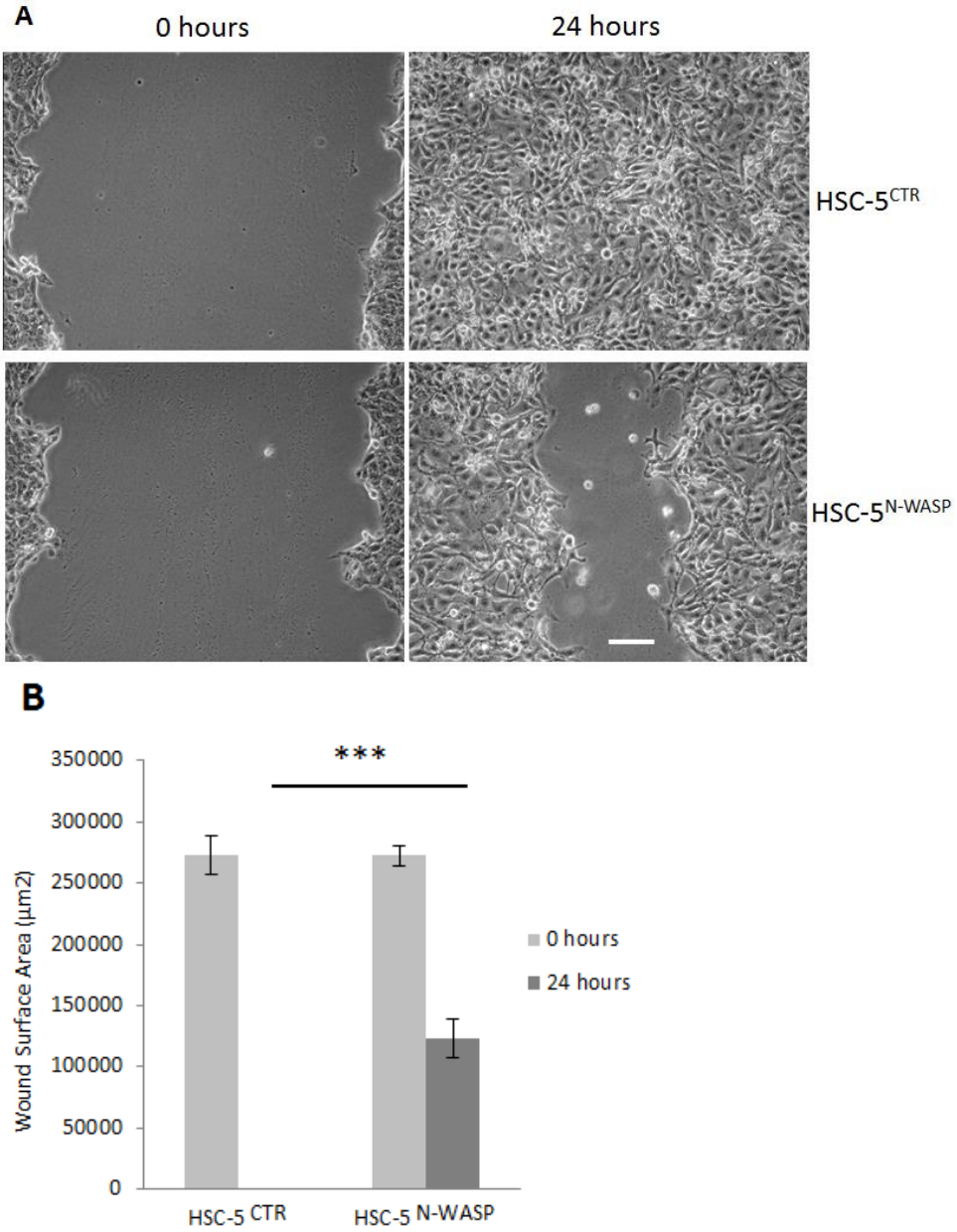

Figure 22: HSC-5$^{N\text{-}WASP}$ cells migrated slower than HSC-5^{CTR} cells. A) Cells were seeded such that prior to wound healing assay, the cell confluency would be 100%. Images were taken of the cells 0 hours and 24 hours after the scratches were made on the cells under view of a 10X objective lens. Scale bar represents 50 µm. B) Surface areas of wounds were measured at respective time points and compared, whereby HSC-5$^{N\text{-}WASP}$ cells closed the gap slower than HSC-5^{CTR} cells. Experiments were performed in triplicates. Significance: ***P<0.001 (Student's t-test).

3.2.6 Vinculin localizations are increased in HSC-5$^{N\text{-}WASP}$ cells compared to HSC-5^{CTR} cells

As stated earlier, vinculin is a key component of the focal adhesion complex that regulates cell adhesion [152], with protein localization correlating inversely to cell migration [147]. HSC-5 cells had reduced vinculin patches compared to HaCaT cells (Fig. 12), possibly due to reduced N-WASP expression. Immunohistochemistry to visualize vinculin and actin and cell vinculin patch counts in HSC-5^{CTR} and HSC-5$^{N\text{-}WASP}$ cells were performed to study N-WASP effects on vinculin localization. HSC-5$^{N\text{-}WASP}$ cells had increased vinculin patches at the focal adhesion compared to HSC-5^{CTR} cells (Fig. 23A). HSC-5$^{N\text{-}WASP}$ cells had a significantly higher cell vinculin patch count than HSC-5^{CTR} cells (Fig. 23B). This is similar to a comparison of vinculin localizations between HaCaT and HSC-5 cells (Fig 12). A Western blot of both HSC-5 sublines for vinculin expression was done to determine if protein levels correlated with patch counts. Both cell lines had similar vinculin expressions (Fig. 24A), and densitometric quantification of vinculin bands against GAPDH bands showed no significant difference in vinculin protein levels between both cell lines (Fig. 24B), suggesting that increased vinculin localization is not due to increased protein levels in skin cancer cells.

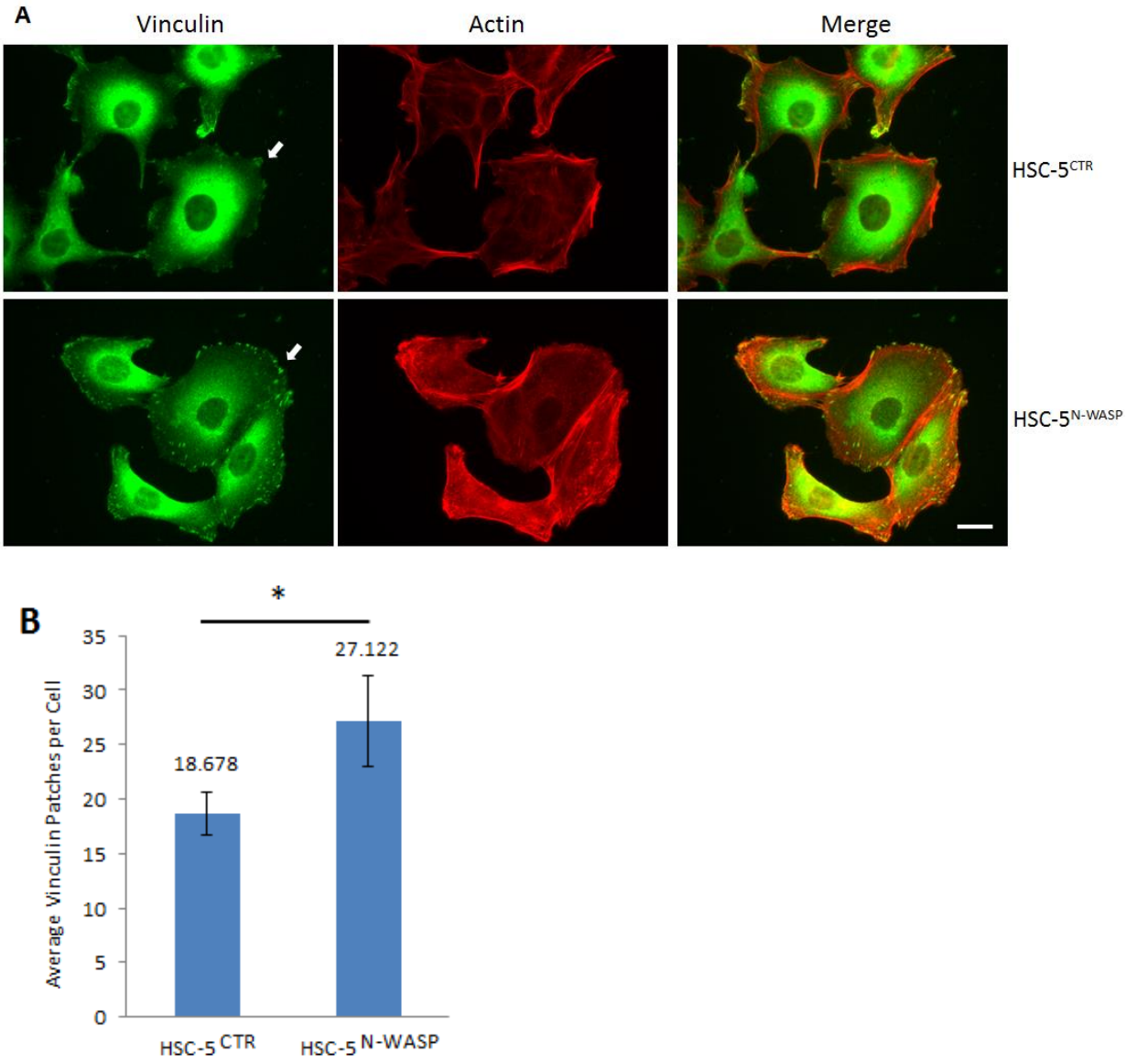

Figure 23: HSC-5$^{N\text{-}WASP}$ cells have more vinculin patches than HSC-5^{CTR} cells. A) HSC-5^{CTR} and HSC-5$^{N\text{-}WASP}$ cells were seeded on coverslips in 6-well plates, incubated, then fixed and probed with anti-vinculin (1°) antibody and Alexa488 conjugates (2°), and with Alexa568 conjugated phalloidin, under view of a 40X objective lens. Note the difference in the number of observable green fluorescence streaks and dots at the cell membrane. Scale bar represents 20 µm. B) Vinculin patch count was performed by counting number of observable vinculin patches in 30 random cells, averaged, and compared to each other. Experiments were performed in triplicates. Significance: *P<0.05 (Student's t-test).

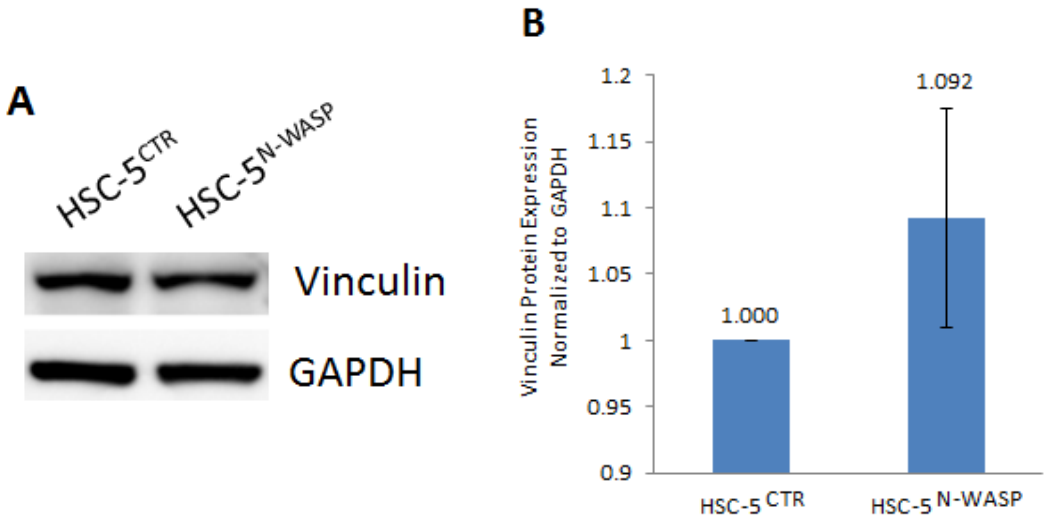

Figure 24: HSC-5^{CTR} and HSC-5$^{N\text{-}WASP}$ cells have similar vinculin expressions. A) Equal amounts of HSC-5^{CTR} and HSC-5$^{N\text{-}WASP}$ cell protein lysates were loaded for Western blot analysis using anti-vinculin and anti-GAPDH antibodies. B) Densitometric quantifications show no significant difference of vinculin protein levels in HSC-5$^{N\text{-}WASP}$ cells compared to HSC-5^{CTR} cells. Experiments were performed in triplicates. Significance: $P>0.05$ (Student's *t*-test).

3.2.7 Paxillin localizations are reduced in HSC-5$^{N\text{-}WASP}$ cells compared to HSC-5^{CTR} cells

As stated earlier, paxillin is another component of focal adhesion complex that operates in a manner opposite to that of vinculin [153], with its expression correlating to cancer cell ability to migrate or metastasize [154]. HSC-5 cells had increased paxillin patches compared to HaCaT cells (Fig. 14), possibly due to reduced N-WASP expression. Immunohistochemistry to visualize paxillin and actin and cell paxillin patch counts in HSC-5^{CTR} and HSC-5$^{N\text{-}WASP}$ cells were performed to study N-WASP effects on paxillin localization. HSC-5$^{N\text{-}WASP}$ cells had reduced paxillin patches at the focal adhesion compared to HSC-5^{CTR} cells (Fig. 25A). HSC-5$^{N\text{-}WASP}$ cells had a significantly lower cell paxillin patch count than HSC-5^{CTR} cells (Fig. 25B). This is similar to a comparison of paxillin localizations between HaCaT and HSC-5 cells (Fig 14). A Western blot of both HSC-5 sublines for paxillin expression was done to determine if protein levels correlated with patch counts. Both cell lines had similar paxillin expressions (Fig. 26A), and densitometric quantification of paxillin bands against GAPDH bands showed no significant difference in paxillin protein levels between both cell lines (Fig. 26B), suggesting that reduced paxillin localization is not due to reduced protein levels in skin cancer cells.

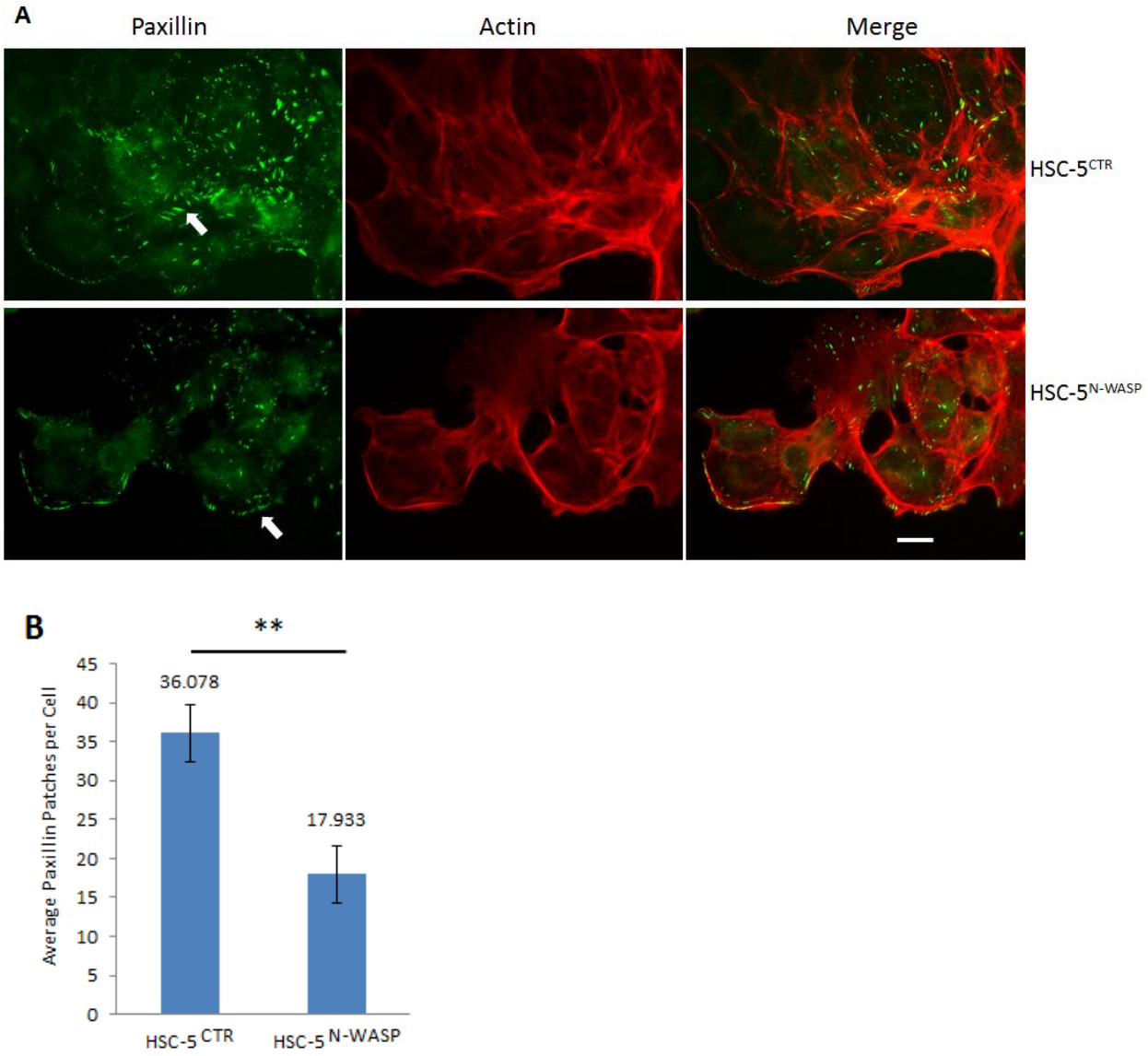

Figure 25: HSC-5$^{N\text{-}WASP}$ cells have fewer paxillin patches than HSC-5^{CTR} cells. A) HSC-5^{CTR} and HSC-5$^{N\text{-}WASP}$ cells were seeded on coverslips in 6-well plates, incubated, then fixed and probed with anti-paxillin (1°) antibody and Alexa488 conjugates (2°), and with Alexa568 conjugated phalloidin, under view of a 40X objective lens. Note the difference in the number of observable green fluorescence streaks and dots at the cell membrane. Scale bar represents 20 µm. B) Paxillin patch count was performed by counting number of observable paxillin patches in 30 random cells, averaged, and compared to each other. Experiments were performed in triplicates. Significance: $^{**}P<0.01$ (Student's *t*-test).

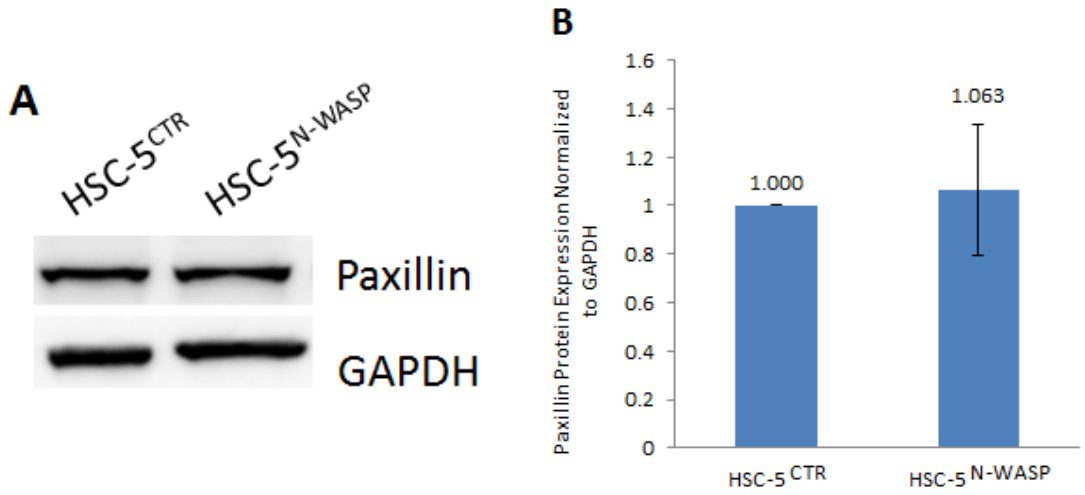

Figure 26: HSC-5^{CTR} and HSC-5^{N-WASP} cells have similar paxillin expressions. A) Equal amounts of HSC-5^{CTR} and HSC-5^{N-WASP} cell protein lysates were loaded for Western blot analysis using anti-paxillin and anti-GAPDH antibodies. B) Densitometric quantifications show no significant difference of paxillin protein levels in HSC-5^{N-WASP} cells compared to HSC-5^{CTR} cells. Experiments were performed in triplicates. Significance: $P>0.05$ (Student's *t*-test).

3.2.8 The AKT pathway is dysregulated in HSC-5^{N-WASP} cells compared to HSC-5^{CTR} cells

AKT proteins are known to promote cancer development by stimulating proliferative signals and repressing apoptosis [157]. Three AKT isoforms exist, aptly named AKT1 to 3. Efforts to study AKTs focus more on AKT1 and AKT2 than AKT3, as AKT1 and AKT2 are known to be overexpressed or amplified in numerous cancers [158]. HSC-5^{N-WASP} cells proliferate at lower rates than HSC-5^{CTR} cells (Fig. 18), so it is possible that AKT activity, in the form of phospho-protein, is reduced in HSC-5^{N-WASP} cells. A Western blot of both HSC-5 sublines for phospho-serine (Ser) 473/4/2 AKT1/2/3 and pan-AKT1/2/3 was performed. HSC-5^{N-WASP} cells had similar phospho-AKT expressions but increased pan-AKT expressions compared to HSC-5^{CTR} cells (Fig. 27A). Densitometric quantification of AKT phospho-to-pan-specific bands against GAPDH bands showed a significant reduction of AKT activity (Fig. 27B).

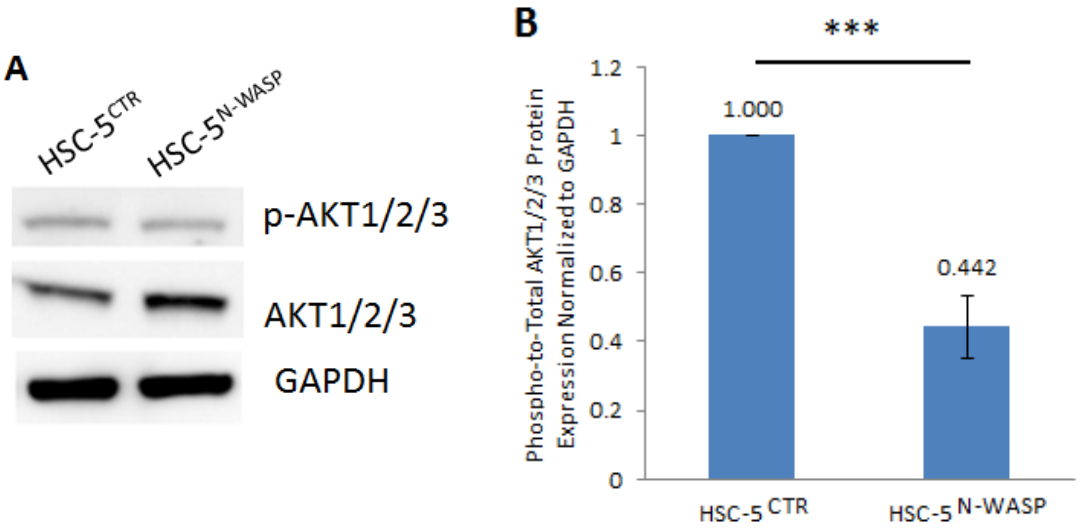

Figure 27: HSC-5$^{N\text{-}WASP}$ cells have reduced AKT activity compared to HSC-5^{CTR} cells. A) Equal amounts of HSC-5^{CTR} and HSC-5$^{N\text{-}WASP}$ cell protein lysates were loaded for Western blot analysis using anti-phospho-Ser473/4/2 AKT1/2/3, anti-pan-AKT1/2/3 and anti-GAPDH antibodies. B) Densitometric quantifications show significant reduction of active AKT levels in HSC-5$^{N\text{-}WASP}$ cells compared to HSC-5^{CTR} cells. Experiments were performed in triplicates. Significance: ***P<0.001 (Student's t-test).

PTEN negatively regulates AKTs by dephopshorylating PI3K-generated phosphatidylinositol (3,4,5)-trisphosphates (PIP_3), which activate AKTs [159]. PTEN mutations and deletions are known to deregulate AKT action and spur cancer development [159]. A recent model suggested that high phosphorylation levels of PTEN inactivates PTEN, prevents PIP_3 dephosphorylation, allows uncontrolled AKT activation, permitting cancer development [160]. A Western blot of both HSC-5 sublines for phospho-Ser380/Thr382/3 PTEN and pan-PTEN was performed to assess PTEN activity. Phospho- and pan-PTEN expressions are increased in HSC-5$^{N\text{-}WASP}$ cells (Fig. 28A), but densitometric quantification of PTEN phospho-to-pan-specific bands against GAPDH bands showed significantly reduced PTEN phosphorylation levels in HSC-5$^{N\text{-}WASP}$ cells compared to HSC-5^{CTR} cells (Fig. 28B). This suggests an increase in PTEN activity, increased PIP_3 dephosphorylation and thus reduced AKT phospho-activity, which may be reducing HSC-5 cell proliferation when N-WASP is overexpressed.

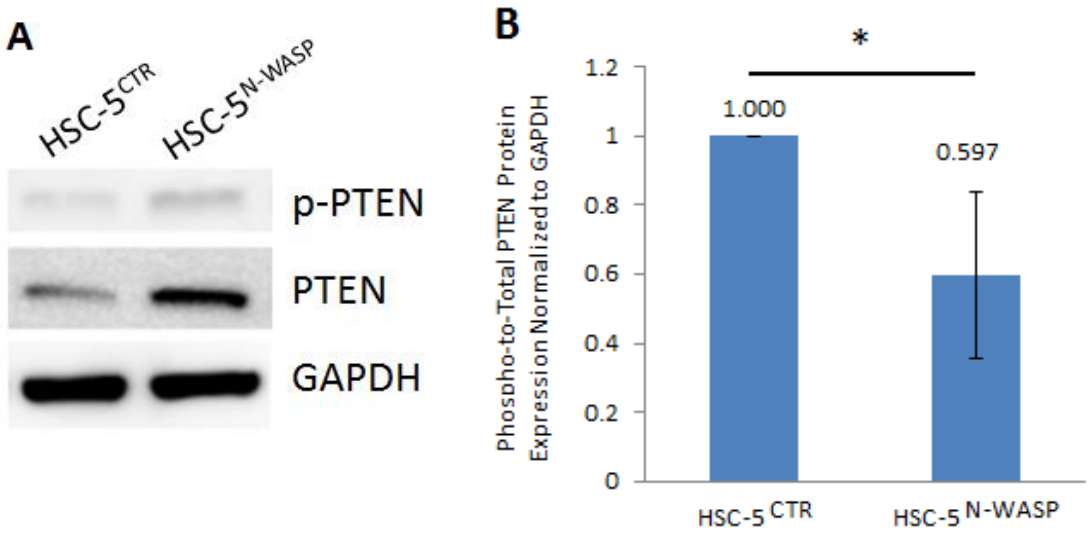

Figure 28: HSC-5$^{N\text{-}WASP}$ cells have reduced PTEN phosphorylation levels compared to HSC-5^{CTR} cells. A) Equal amounts of HSC-5^{CTR} and HSC-5$^{N\text{-}WASP}$ cell protein lysates were loaded for Western blot analysis using anti-phospho-Ser380/Thr382/3 PTEN, anti-pan-PTEN and anti-GAPDH antibodies. B) Densitometric quantifications show significant reduction of phospho-PTEN levels in HSC-5$^{N\text{-}WASP}$ cells compared to HSC-5^{CTR} cells. Experiments were performed in triplicates. Significance: **P*<0.05 (Student's *t*-test).

3.2.9 Summary

Phenotypic differences between HSC-5 and HaCaT cells cannot be attributed to differences in N-WASP expression as these cells have varied genetic background and mutations. HSC-5^{CTR} and HSC-5$^{N\text{-}WASP}$ cells were generated to study the role of N-WASP in skin cancer cells. N-WASP mRNA levels correlate with protein levels. HSC-5$^{N\text{-}WASP}$ cells had reduced cell proliferation rates that are N-WASP-dependent compared to HSC-5^{CTR} cells, and had reduced CCND1 levels as well. HSC-5$^{N\text{-}WASP}$ cells had increased E-cadherin localization, reduced cell migration, increased vinculin and reduced paxillin patches compared to HSC-5^{CTR} cells, which are similar to when comparing phentoypes of HaCaT cells to HSC-5 cells. Cellular localizations of E-cadherin, vinculin and paxillin do not correlate with changes to protein levels. These suggest that N-WASP operates in the same manner in HSC-5 and HaCaT for these phenotypes. The sole exception is that HSC-5$^{N\text{-}WASP}$ cells had reduced cell proliferation compared to HSC-5^{CTR} cells, which correlated with the observed reduction of HSC-5$^{N\text{-}WASP}$ cell AKT activity.

3.3 Molecular analyses of the role of N-WASP in HSC-5 sublines

N-WASP is a protein crucial for actin cytoskeleton formation and remodelling [56], and has been suggested to play a role in cell carcinogenesis [79,80]. When comparing HSC-5^{CTR} and HSC-$5^{N\text{-}WASP}$ cells, N-WASP has been shown to influence cellular processes such as E-cadherin (Fig. 20), vinculin (Fig. 23) and paxillin (Fig. 25) localizations, cell proliferation (Fig. 18) and cell migration (Fig. 22). HSC-$5^{N\text{-}WASP}$ cell proliferation was reduced in an N-WASP-dependent manner (Fig. 18) possibly to due reduced AKT phospho-activity (Fig. 27, 28). A series of studies were performed to identify the putative signalling pathways and functional molecules involved whereby overexpression of N-WASP reduces HSC-5 cell proliferation.

3.3.1 Proteomic analysis of HSC-5 sublines

A study of cell proteome was performed to characterize changes in HSC-5 cell signalling axes when N-WASP was overexpressed. HSC-5^{CTR} and HSC-$5^{N\text{-}WASP}$ cell lysate proteins were concentrated in an SDS-PAGE resolving gel and submitted to Ms Belinda Chen of Nanyang Technological University's School of Biological Sciences Proteomic Core Facility for in-gel digestion, tryptic peptide solubilisation and LC-MS/MS based on established protocols [145]. The LC-MS/MS chromatographic raw data (Fig. 29) and dissociated peptide mass spectra raw data (Fig. 30) of both HSC-5^{CTR} and HSC-$5^{N\text{-}WASP}$ cells are shown.

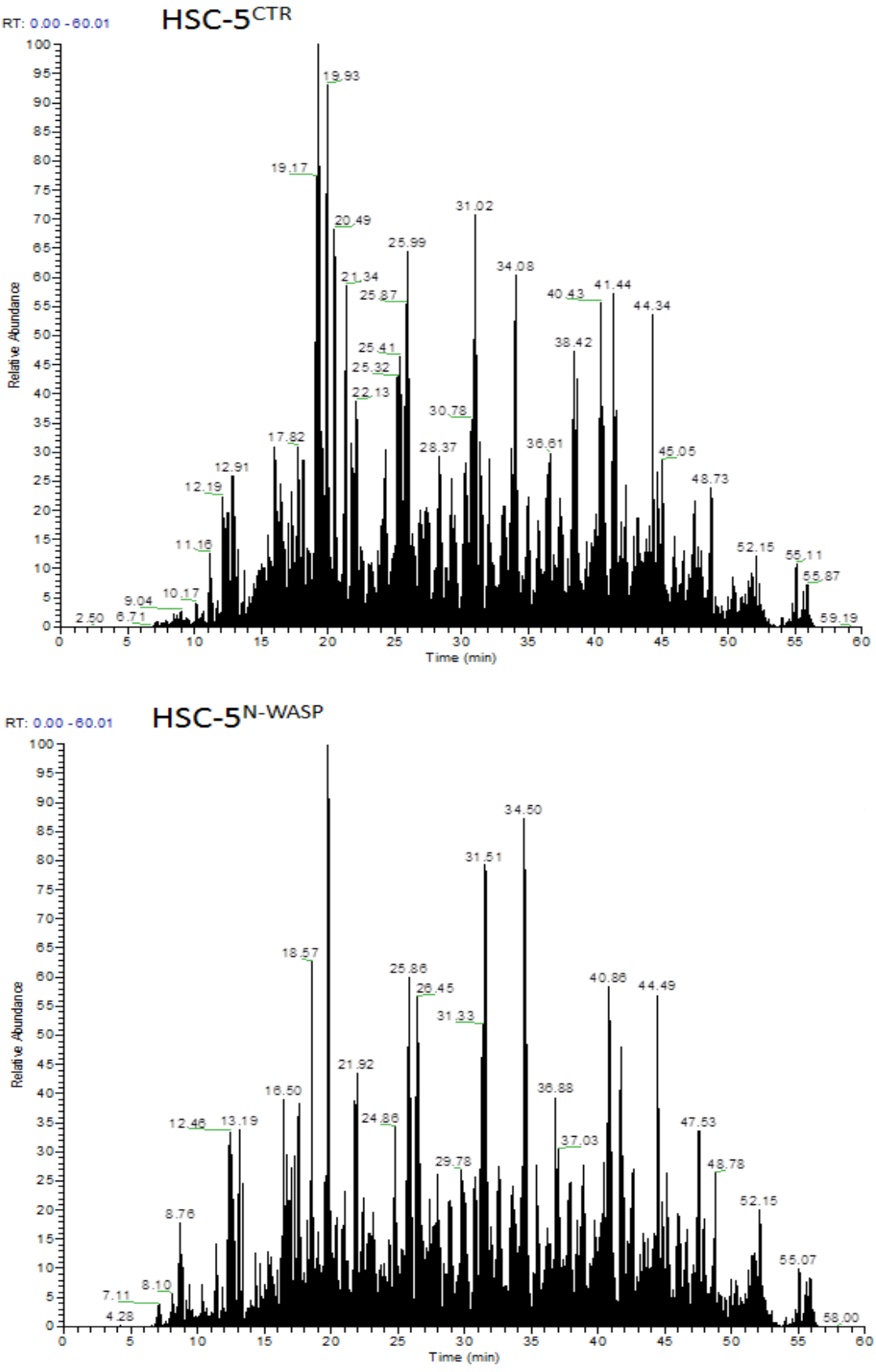

Figure 29: LC-MS/MS chromatograms of HSC-5^{CTR} (top) and HSC-5$^{N\text{-}WASP}$ (bottom) cell protein samples. LC chromatograms of both cells are shown, with X-axis representing time of mobile phase elution and Y-axis the protein relative abundance.

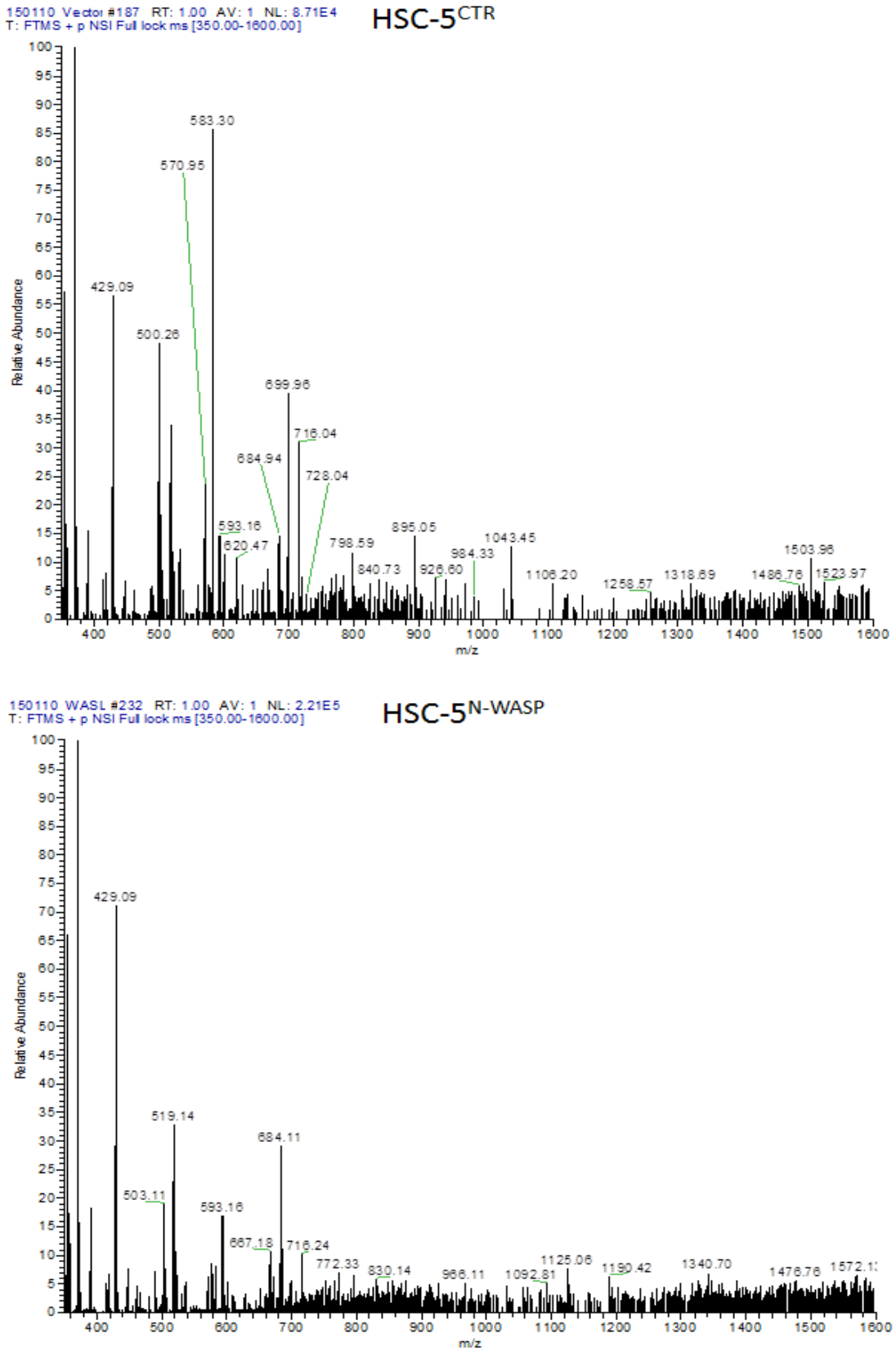

Figure 30: LC-MS/MS mass spectra of HSC-5^{CTR} (top) and HSC-5$^{N\text{-}WASP}$ (bottom) cell protein samples. Mass spectrums of dissociated peptides of both cells are shown, with X-axis representing mass-to-charge (m/z) ratio, and Y-axis the protein relative abundance.

Analysis of raw data with MascotCluster software allowed the determination of the relative abundance of detected proteins compared to those from the UniProt human proteomic database in the form of emPAI values. Proteins considered up-regulated or down-regulated in HSC-$5^{N\text{-}WASP}$ cells compared to HSC-5^{CTR} cells must have an emPAI HSC-$5^{N\text{-}WASP}$/HSC-5^{CTR} value ratio of equal or more ($\geq$) than 1.5 and equal or less ($\leq$) than 0.5, respectively. A total of 1131 proteins were identified in both HSC-$5^{N\text{-}WASP}$ and HSC-5^{CTR} cells. 260 proteins were found to be up-regulated and 109 proteins were found to be down-regulated.

Both up-regulated and down-regulated proteins identified were analyzed with the PANTHER software [146]. It is an online annotation software used for identifying protein cellular localization, molecular function, biological activity, class and signalling axis. The software was used to identify signalling pathways influenced by N-WASP overexpression in HSC-5 cells. 54 signalling pathways were identified from up-regulated protein hits (Fig. 31) and 19 signalling pathways were identified from down-regulated protein hits (Fig. 32). Four candidate pathways – Integrin, EGF, Wnt, Hippo – were chosen since they are responsible for cell proliferation. A comparison of signalling pathways identified by PANTHER database correlated all candidate pathways as possible mechanisms of action when HSC-5 cells overexpress N-WASP, with the exception of Hippo signalling pathway.

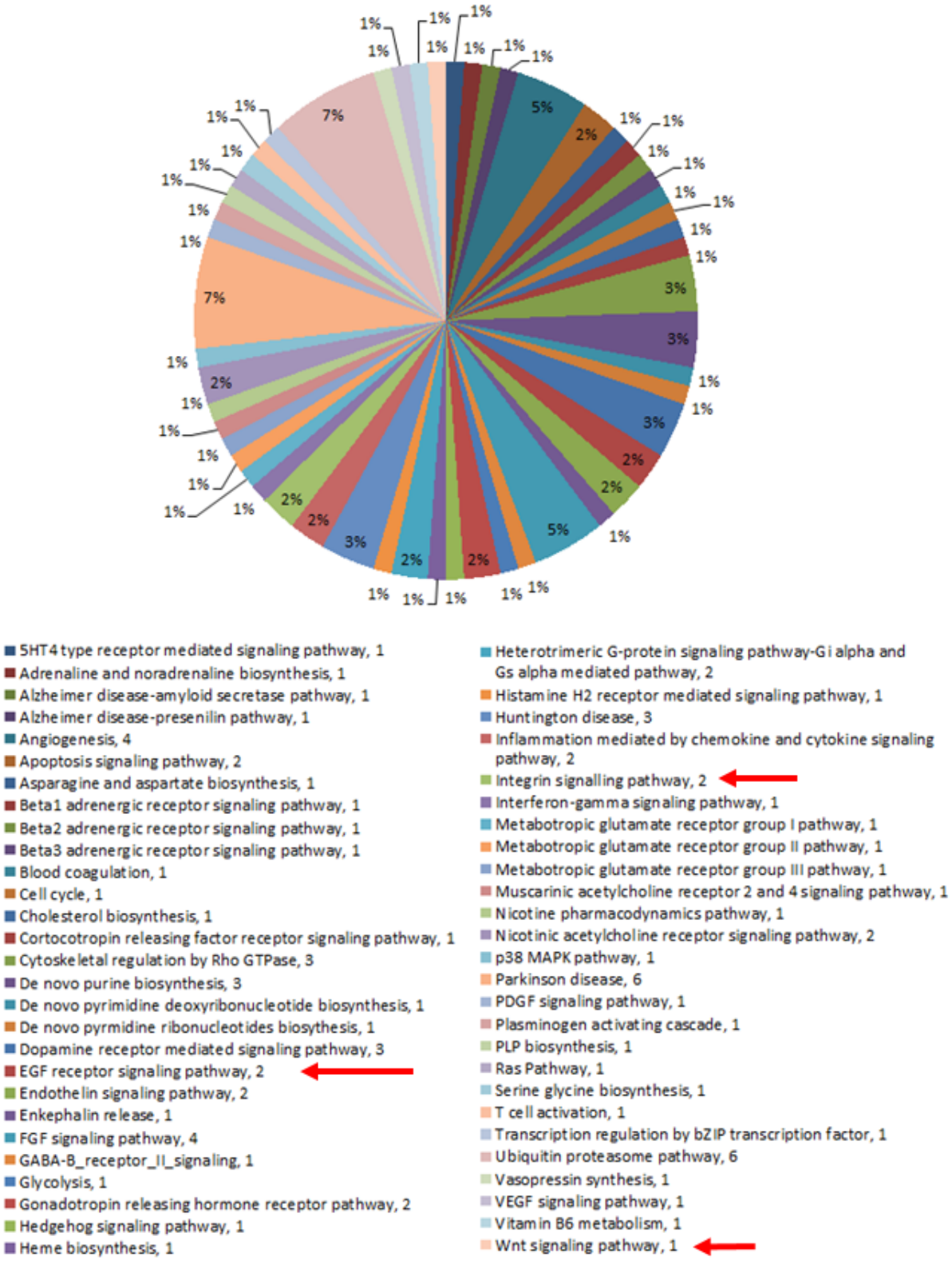

Figure 31: PANTHER analysis of 54 cell signalling pathways influenced by proteins up-regulated in HSC-5$^{N\text{-}WASP}$ cells compared to HSC-5^{CTR} cells from proteomics. Percentages in pie chart represent number of proteins against total identifications. "5HT4 type receptor mediated signalling pathway, X" signify X number of proteins identified for 5HT4 type receptor mediated signalling pathway. Red arrows highlight the detected EGF, Integrin and Wnt signalling pathways.

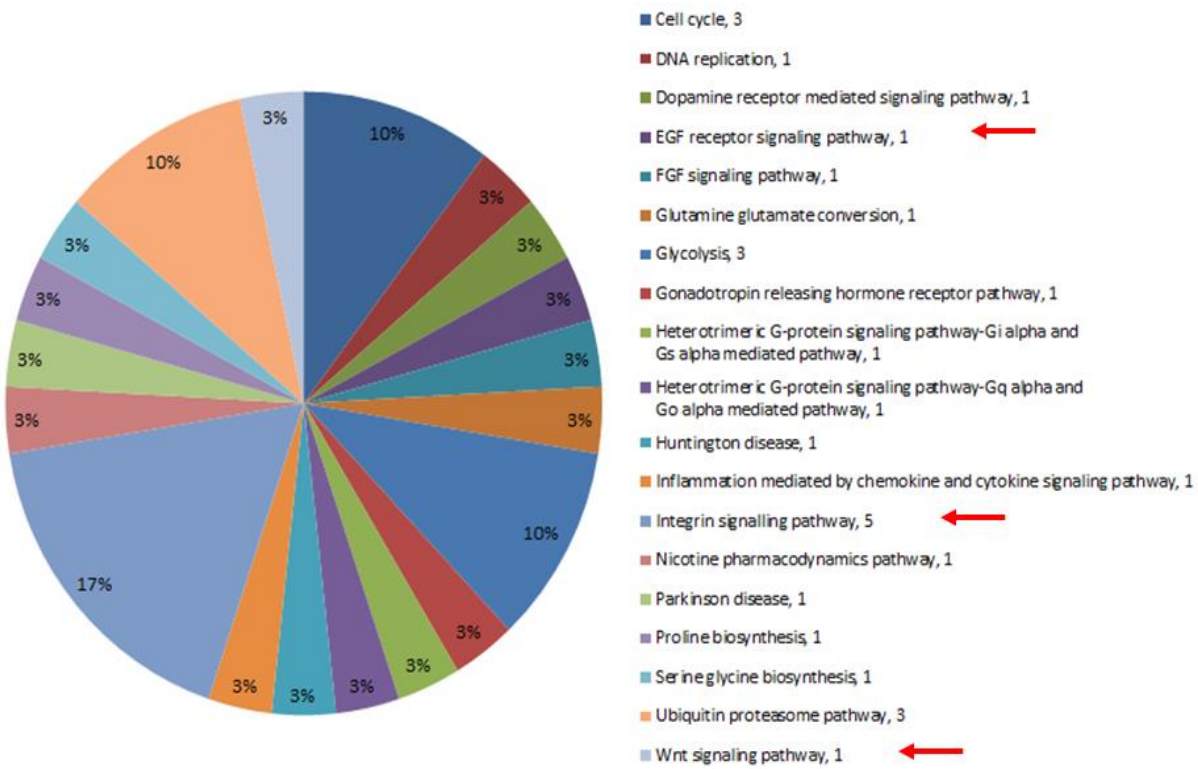

Figure 32: PANTHER analysis of 19 cell signalling pathways influenced by proteins down-regulated in HSC-5$^{N\text{-}WASP}$ cells compared to HSC-5^{CTR} cells from proteomics. Percentages in pie chart represent number of proteins against total identifications. "Cell cycle, X" signify X number of proteins identified for cell cycle pathway. Red arrows highlight the detected EGF, Integrin and Wnt signalling pathways.

3.3.2 Protein microarray of HSC-5 sublines

Post-translational modification (PTM) occurs after gene transcription and protein synthesis, on strategic, critical amino acids and is essential for producing functional proteins [161]. Phosphorylation, the addition of a phosphoryl group to certain amino acids, is the most common PTM used for regulating protein function [162]. The Kinex KAM-880 microarray kit is able to detect 518 pan-specific proteins and 359 phospho-specific proteins identified as critical in cell signalling axes. HSC-5^{CTR} and HSC-5$^{N\text{-}WASP}$ cell lysate proteins were harvested and subjected to the protein microarray according to manufacturer instructions.

Proteins considered up-regulated or down-regulated in HSC-5$^{N\text{-}WASP}$ cells compared to HSC-5^{CTR} cells must have an HSC-5$^{N\text{-}WASP}$/HSC-5^{CTR} value ratio of equal or more ($\geq$) than 1.5 and equal or less ($\leq$) than 0.5, respectively. Depending on the context of the pan- or phospho-specific protein, signalling axes can be either promoted or repressed. The individual microarray images of HSC-5^{CTR} cell (Fig. 33) and HSC-5$^{N\text{-}WASP}$ cell (Fig.

34) protein samples are shown. An overlap of pseudocolour comparisons of both cell microarrays (Fig. 35) was performed with the ImageJ software. 13 pan- and phospho-proteins were identified as being up-regulated (Table 3), and 5 pan- and phospho-proteins were identified as being down-regulated (Table 4). The biological processes associated with up-regulated microarray protein hits (Fig. 36) and down-regulated microarray protein hits (Fig. 37) was identified with the PANTHER database under *Homo sapiens* setting.

Interesting proteins to note include up-regulation of T(hr)-421/S(er)-424 phospho-ribosomal protein S6 kinase β1 (p70S6K), T(hr)-183/Y(Tyr)-185 phospho-JNK1/2/3, S(er)-65 phospho-4E-BP1, T(hr)-573 phospho-ribosomal protein S6 kinase 1/2/3 (RSK1/2/3) and S(er)-319 phospho-FOXO1 (listed in Table 3 as FKHR), and the down-regulation of T(hr)-412 phospho-p70S6K and pan-RSK1. All are proteins involved in cell signalling that regulate cell growth, proliferation, metabolism and protein biosynthesis [112,163-165]. Of note also were the up-regulated S(er)-727 signal transducer and activator of transcription 1α (STAT1), Y(Tyr)-40 bone marrow X protein-tyrosine kinase (BMX), Y(Tyr)-1230/4/5 Met (hepatocyte growth factor (HGF) receptor tyrosine kinase) and T(hr)-567 Ezrin proteins and down-regulation of pan-specific protein-tyrosine phosphatase D1 (PTPD1) and pan-protein-serine kinase C lambda/iota (PKCl).

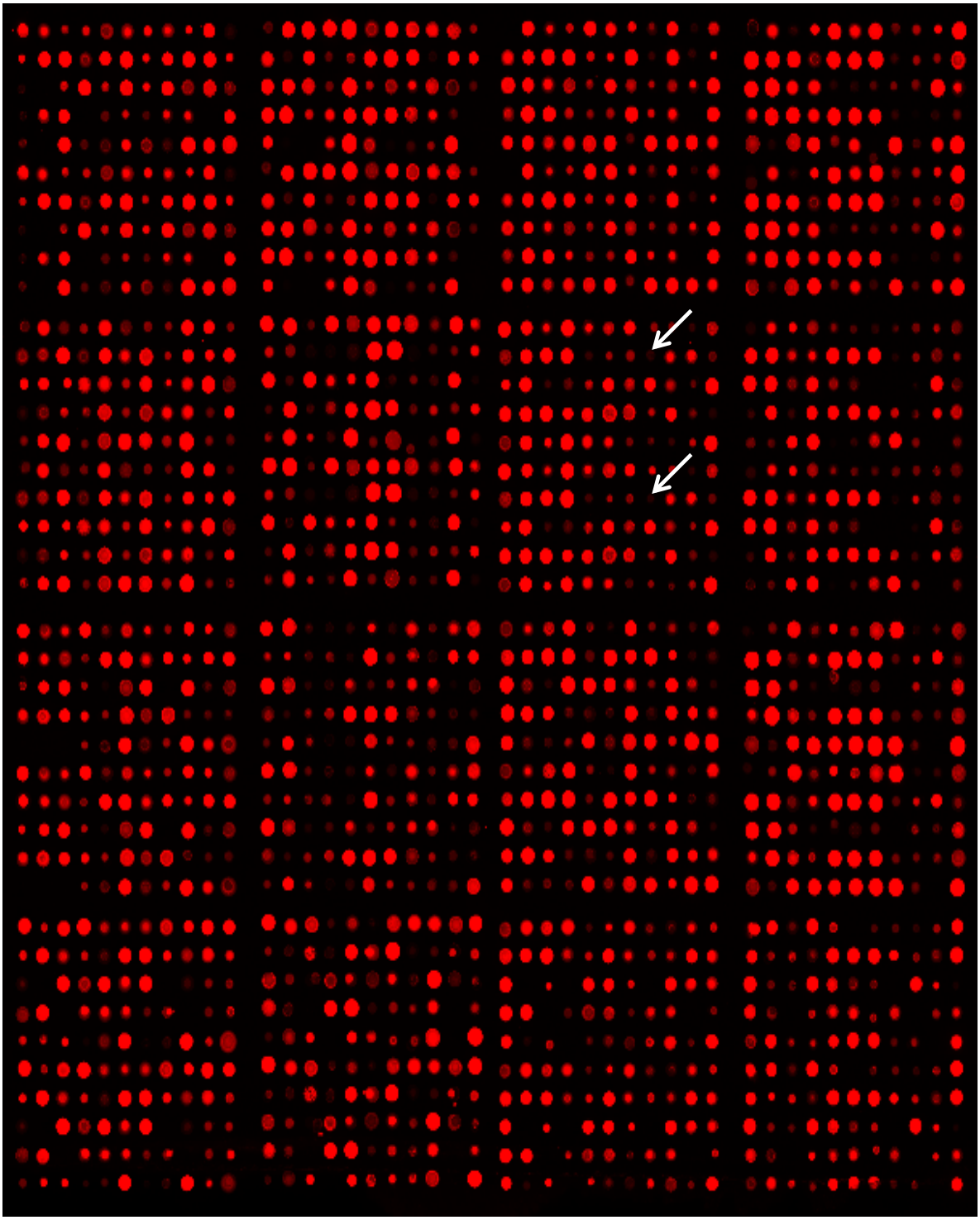

Figure 33: Protein microarray of HSC-5^{CTR} cells. Cell protein lysates were obtained according to instructions in the KAM-880 microarray kit manual, and microarray was imaged and individual protein values deciphered with the Gene Pix Pro 6.0 program. Microarray was given false colour of red to measure intensity. The arrows pinpoint the duplicate location for detection of phospho-Ser319 FOXO1; the context of which details are elaborated on in Section 4.1.6.

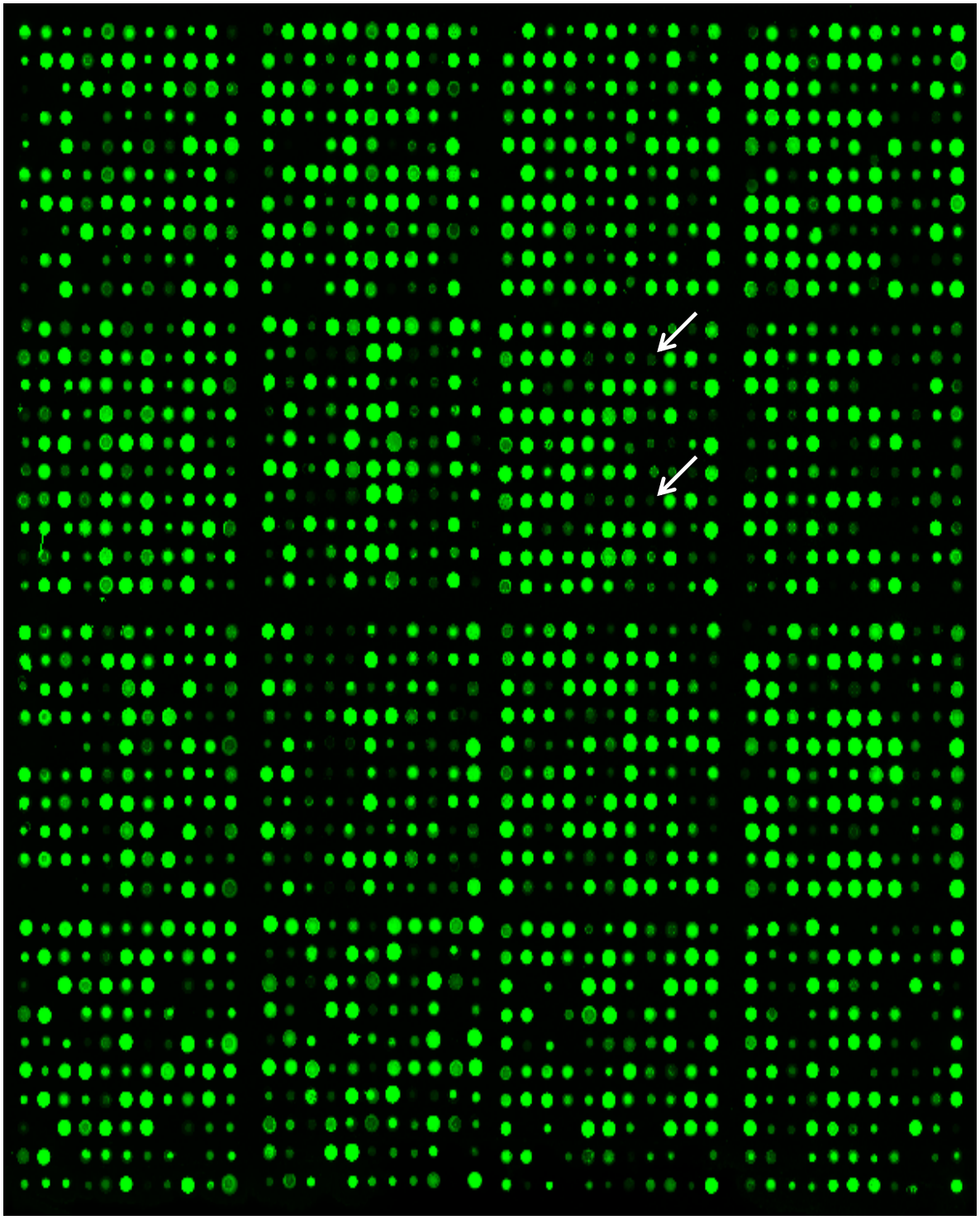

Figure 34: Protein microarray of HSC-5$^{N\text{-}WASP}$ cells. Cell protein lysates were obtained according to instructions in the KAM-880 microarray kit manual, and microarray was imaged and individual protein values deciphered with the Gene Pix Pro 6.0 program. Microarray was given false colour of green to measure intensity. The arrows pinpoint the duplicate location for detection of phospho-Ser319 FOXO1; the context of which details are elaborated on in Section 4.1.6.

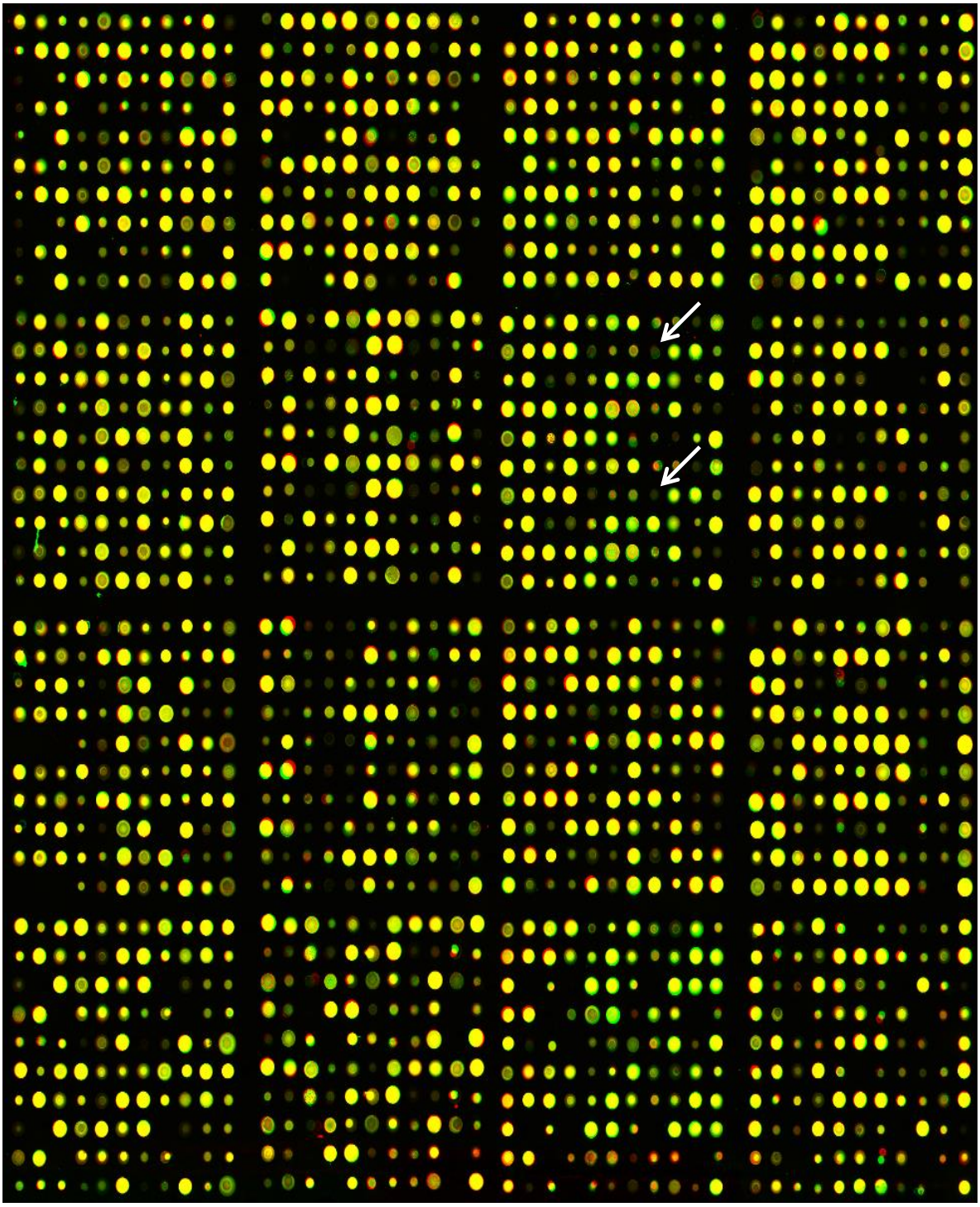

Figure 35: A comparison of HSC-5^{CTR} and HSC-5$^{N\text{-}WASP}$ protein microarrays. Both protein microarrays were overlaid to determine which protein is up-regulated or down-regulated in HSC-5$^{N\text{-}WASP}$ cells compared to HSC-5^{CTR} cells. The arrows pinpoint the duplicate location for detection of phospho-Ser319 FOXO1; the context of which details are elaborated on in Section 4.1.6.

Table 3: List of proteins up-regulated in microarray detection for HSC-5$^{N\text{-}WASP}$ cells in comparison to HSC-5^{CTR} cells, with pan- or phospho-specific details.

Target Protein Name	Phospho Site (Human)	Full Target Protein Name	HSC-5^{CTR} Detection Value	HSC-5$^{N\text{-}WASP}$ Detection Value	HSC-5$^{N\text{-}WASP}$/HSC-5^{CTR} Ratio
p70S6K	T421/ S424	Ribosomal protein S6 kinase beta-1	0.181	0.356	**1.970**
STAT1	S727	Signal transducer and activator of transcription 1 alpha	2.099	4.081	**1.944**
BMX (Etk)	Y40	Bone marrow X protein-tyrosine kinase	1.175	2.210	**1.881**
Met	Y1230/ Y1234/ Y1235	Hepatocyte growth factor (HGF) receptor-tyrosine kinase	2.307	4.175	**1.809**
JNK 1/2/3	T183/ Y185	Jun N-terminus protein-serine kinase (stress-activated protein kinase (SAPK)) 1/2/3	2.594	4.613	**1.778**
4E-BP1	S65	Eukaryotic translation initiation factor 4E binding protein 1 (PHAS1)	1.527	2.570	**1.683**
RSK1/2/3	T573	Ribosomal S6 protein-serine kinase 1/2/3	1.744	2.905	**1.666**
Ezrin	T567	Cytovillin 2	1.529	2.535	**1.658**
FKHR	S319	Forkhead box protein O1	2.286	3.700	**1.619**
Caveolin 1	Pan-specific	Caveolin 1	1.911	3.042	**1.592**
Tyrosine Hydroxylase	S40	Tyrosine hydroxylase isoform a	0.429	0.671	**1.565**
IRS1	S312	Insulin receptor substrate 1	2.532	3.898	**1.539**
CDK1/2	Y15	Cyclin-dependent protein-serine kinase 1/2	2.210	3.357	**1.519**

Table 4: List of proteins down-regulated in microarray detection for HSC-5$^{N\text{-}WASP}$ cells in comparison to HSC-5^{CTR} cells, with pan- or phospho-specific details.

Target Protein Name	Phospho Site (Human)	Full Target Protein Name	HSC-5^{CTR} Detection Value	HSC-5$^{N\text{-}WASP}$ Detection Value	HSC-5$^{N\text{-}WASP}$/HSC-5^{CTR} Ratio
p70S6K	T412	Ribosomal protein S6 kinase beta-1	0.147	0.004	**0.029**
PKCl	Pan-specific	Protein-serine kinase C lambda/iota	0.187	0	**0**
PTPD1	Pan-specific	Protein-tyrosine phosphatase non-receptor type 21	0.222	0	**0**
RSK1	Pan-specific	Ribosomal S6 protein-serine kinase 1	0.009	0	**0**
Yes	Pan-specific	Yamaguchi sarcoma proto-oncogene-encoded tyrosine kinase	0.102	0	**0**

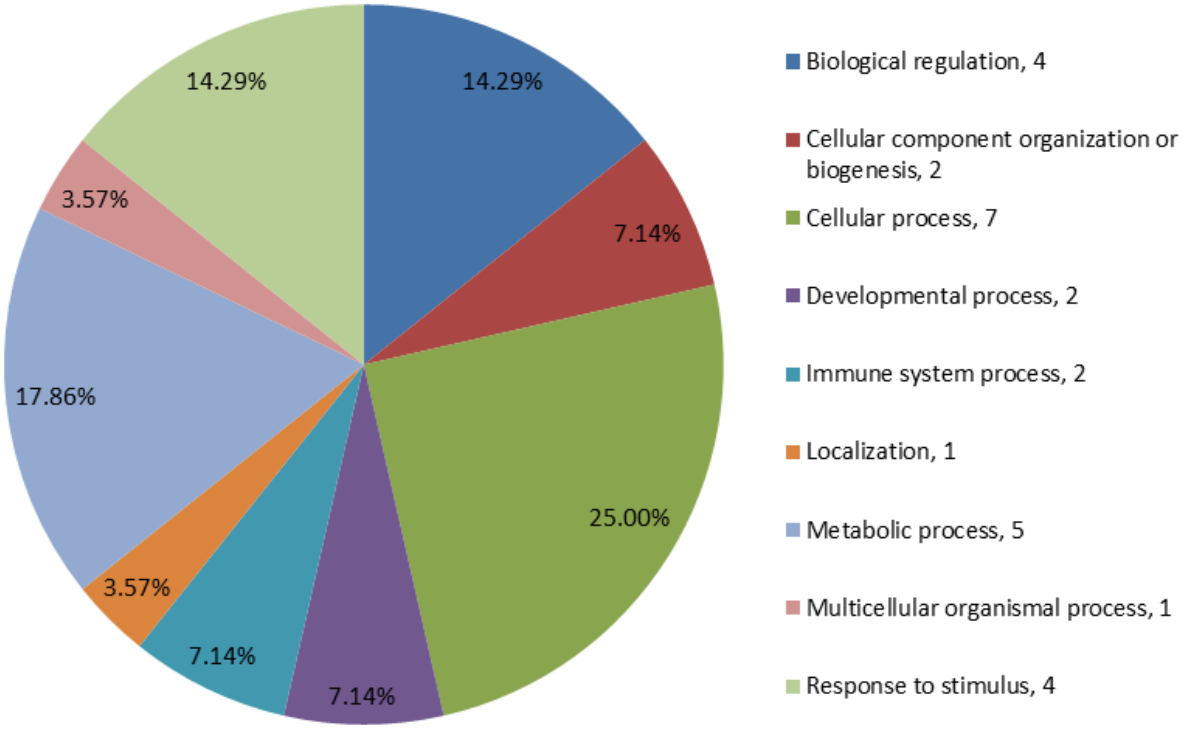

Figure 36: PANTHER analysis of biological processes associated with proteins up-regulated in HSC-5$^{N\text{-}WASP}$ cells compared to HSC-5^{CTR} cells from protein microarray. Percentages in pie chart represent number of genes of interest against total identifications. "Biological regulation, X" signify X number of genes of interest identified for the biological process of biological regulation.

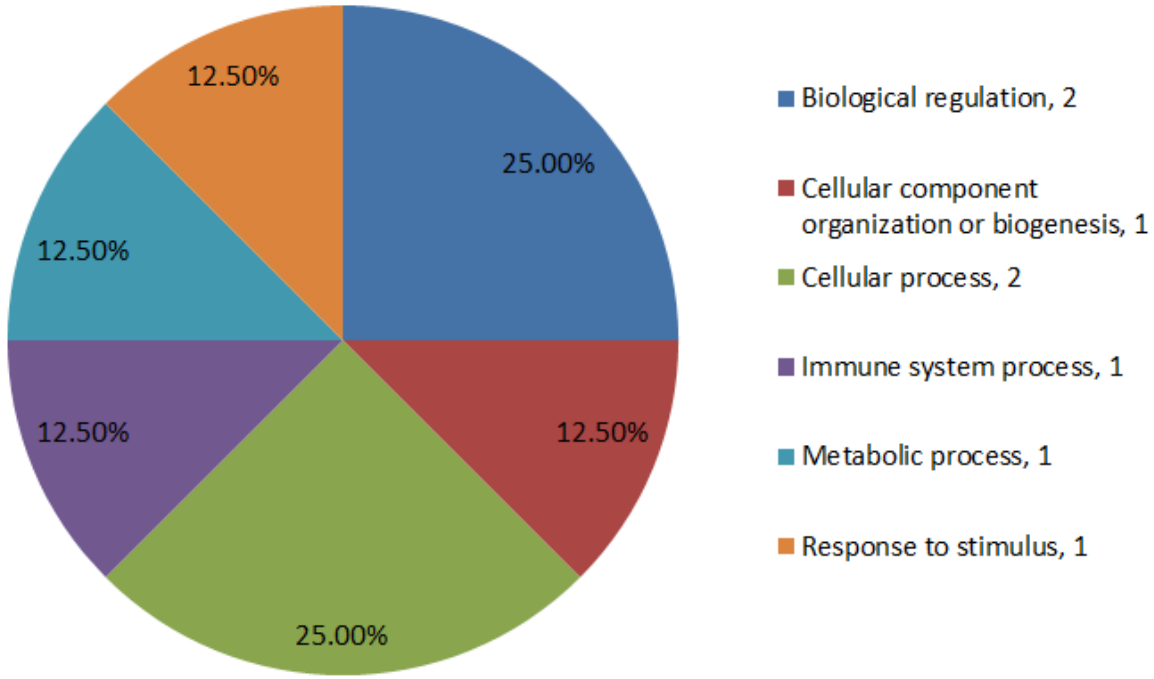

Figure 37: PANTHER analysis of biological processes associated with proteins down-regulated in HSC-5$^{N\text{-}WASP}$ cells compared to HSC-5^{CTR} cells from protein microarray. Percentages in pie chart represent number of genes of interest against total identifications. "Biological regulation, X" signify X number of genes of interest identified for the biological process of biological regulation.

3.3.3 RNA-Seq of HSC-5 sublines identifies candidate regulators

RNA-Seq is a next generation sequencing high-throughput technology capable of mapping and quantifying transcripts [166]. It identifies potential novel targets, microRNAs and differentially expressed genes [167]. It provides more clues of changes at the transcriptional level when HSC-5 cells overexpress N-WASP. RNA of both HSC-5 sublines were isolated, packaged and submitted to Omega Bioservices (Georgia, USA) for cDNA generation using the Illumina TruSeq Total RNA kit. Libraries were directly sequenced and aligned to the Illumina BaseSpace cloud server *Homo sapiens* genome reference using the Illumina Hi-Seq 2500 platform [166].

In both HSC-5 sublines, RNA-Seq analyzed the expression of 25276 genes, each individually quantified using the fragments per kilobase of transcript per million mapped reads (FPKM) unit. Each gene in HSC-5^{CTR} and HSC-5$^{N\text{-}WASP}$ data reads were aligned and their FPKM values were compared. Genes considered up-regulated or down-regulated in HSC-5$^{N\text{-}WASP}$ compared to HSC-5^{CTR} cells must have an HSC-5$^{N\text{-}WASP}$/HSC-5^{CTR} FPKM value ratio of equal or more ($\geq$) than 1.5 and equal or less ($\leq$) than 0.5,

respectively. 4708 genes were up-regulated and 4412 genes were down-regulated in HSC-5$^{N\text{-}WASP}$ cells compared to HSC-5^{CTR} cells. The biological processes associated with up-regulated microarray protein hits (Fig. 38) and down-regulated microarray protein hits (Fig. 39) was identified with the PANTHER database under *Homo sapiens* setting. Also shown is a list of genes that are up-regulated, or are of interest, in HSC-5$^{N\text{-}WASP}$ cells compared to HSC-5^{CTR} cells (Table 5).

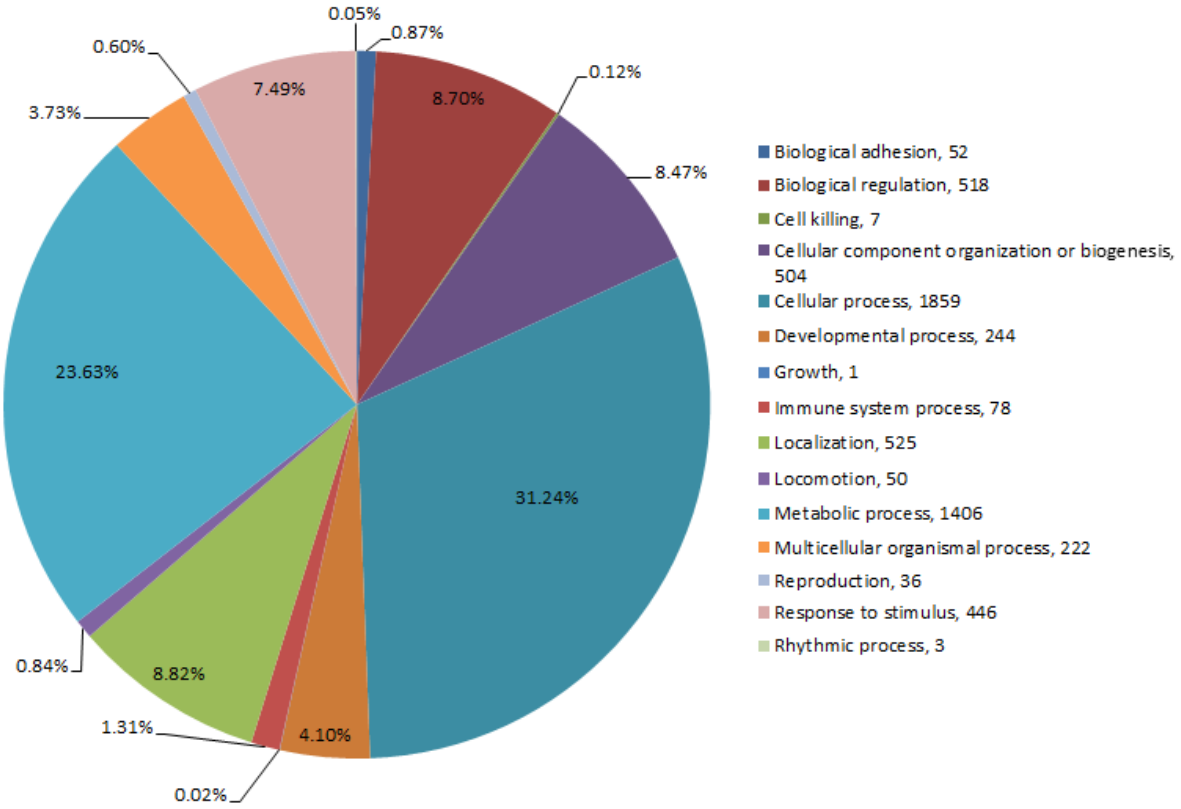

Figure 38: PANTHER analysis of biological processes associated with gene expressions up-regulated in HSC-5$^{N\text{-}WASP}$ cells compared to HSC-5^{CTR} cells from RNA-Seq. Percentages in pie chart represent number of genes of interest against total identifications. "Biological adhesion, X" signify X number of genes of interest identified for the biological process of biological adhesion.

Table 5: List of genes up-regulated or are of interest in HSC-5$^{N\text{-}WASP}$ cells in comparison to HSC-5^{CTR} cells from RNA-Seq. Genes that are up-regulated have their names in bold, but genes of interest do not have names in bold.

Gene of Interest	HSC-5^{CTR} FPKM	HSC-5$^{N\text{-}WASP}$ FPKM	HSC-5$^{N\text{-}WASP}$/HSC-5^{CTR} FPKM Ratio
SGK1	19.777	65.971	**3.336**
JNK1	3.481	10.846	**3.120**
ERK2	42.875	98.658	**2.300**
CSNK1A1	28.477	64.978	**2.282**
SOS1	3.172	6.910	**2.179**
JNK2	5.282	11.142	**2.110**
FOXO1	5.139	8.486	**1.651**
TXNIP	42.111	66.902	**1.589**
CDKN1A	36.935	58.356	**1.580**
PTEN	5.359	7.827	**1.461**
AKT3	14.925	19.863	**1.331**
MDM2	7.270	9.688	**1.330**
FAK	32.417	42.624	**1.315**
CCND1	38.036	48.789	**1.283**
mTOR	10.064	12.870	**1.279**
JNK3	1.137	1.158	**1.018**
GRB2	27.184	22.278	**0.820**
4E-BP1	63.615	51.999	**0.817**
AKT2	13.441	10.862	**0.808**
AKT1	48.061	33.874	**0.704**
SKP2	22.891	14.618	**0.639**
SRC	41.130	25.238	**0.613**
ERK1	16.010	8.706	**0.544**

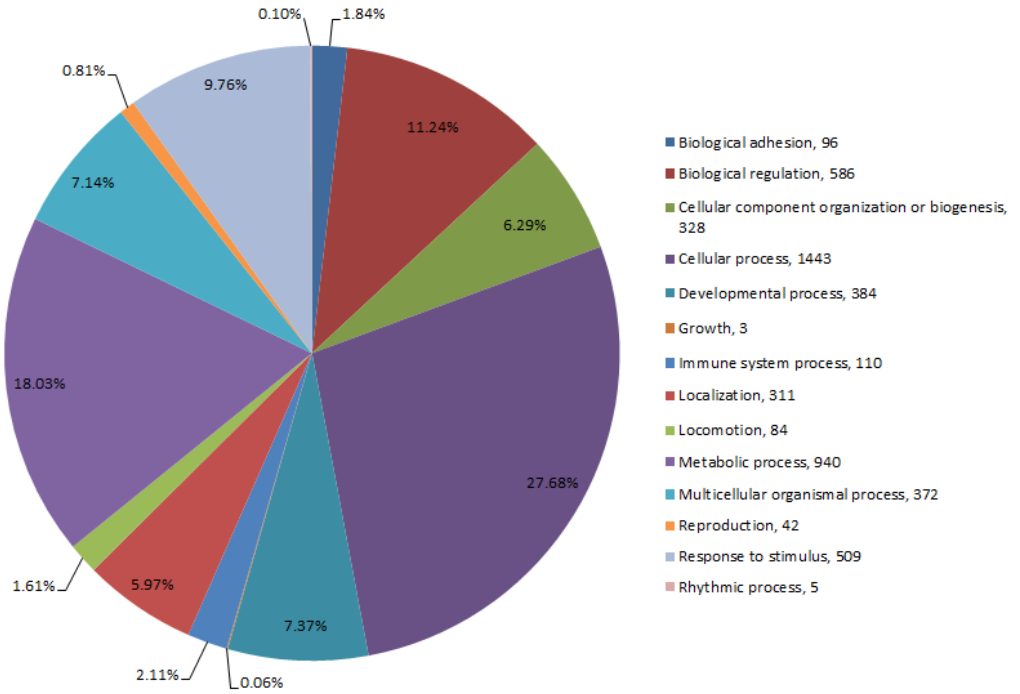

Figure 39: PANTHER analysis of biological processes associated with gene expressions down-regulated in HSC-5$^{N\text{-}WASP}$ cells compared to HSC-5^{CTR} cells from RNA-Seq. Percentages in pie chart represent number of genes of interest against total identifications. "Biological adhesion, X" signify X number of genes of interest identified for the biological process of biological adhesion.

3.3.4 Comparative Ingenuity Pathway Analysis of proteomics, protein microarray and RNA-Seq datasets

Many signalling pathways regulate cell growth and metabolism, such as the MAPK, AKT and mTOR pathways to name a few [168]. Given the multiple datasets generated, analysis of individual proteins and gene expressions will not give sufficient clues as to how N-WASP reduces cell proliferation in HSC-5 cells. The IPA software is an online tool able to analyse multiple datasets and identify candidate biomarkers and signalling axes [169]. The proteomics, protein microarray and RNA-Seq data were uploaded onto the IPA platform and analyzed individually and comparatively. This is to identify candidate pathways and functional molecules involved in HSC-5$^{N\text{-}WASP}$ cell proliferation reduction compared to that of HSC-5^{CTR} cells.

Individual dataset analysis was performed to align the list of proteins or genes identified to those known to be associated with certain signalling axes. However, the datasets' previous definition of up- or down-regulation in HSC-5$^{N\text{-}WASP}$ cells ($X \geq 1.500$ or $X \leq 0.500$) was not used, instead being $X \geq 1.000$ or $X \leq 1.000$ to allow for generating a

broader picture of what portions of an established pathway in HSC-5$^{N\text{-}WASP}$ cells have changed.

The IPA software also uses colour codes as graphical representation of the degree of targets being up-regulated (coloured as red) and down-regulated (coloured as green). To illustrate, the individual IPA analyses of proteomics (Fig. 40), protein microarray (Fig. 41) and RNA-Seq data (Fig. 42) with respect to the mTOR pathway are shown. Protein microarray analysis showed red icons for insulin receptor substrate 1 (IRS1) and 4E-BP1 ($X \geq 1.500$) compared to the pink ERK1/2 ($X \geq 1.000$), showing which parts of mTOR pathway is more affected (Fig. 41). However, discrepancies were observed. There were increases ($X \geq 1.000$) and up-regulation of many components ($X \geq 1.500$) in the protein microarray mTOR pathway (Fig. 41), whereas many components in the RNA-Seq mTOR pathway are highlighted as light pink, showing very mild increases in protein activity detected (Fig. 42). The proteins of AMPK and PI3K are considered down-regulated (icons are green) in the protein microarray mTOR pathway (Fig. 41), but both are considered being increased slightly (lights in light pink) in the RNA-Seq mTOR pathway (Fig. 42).

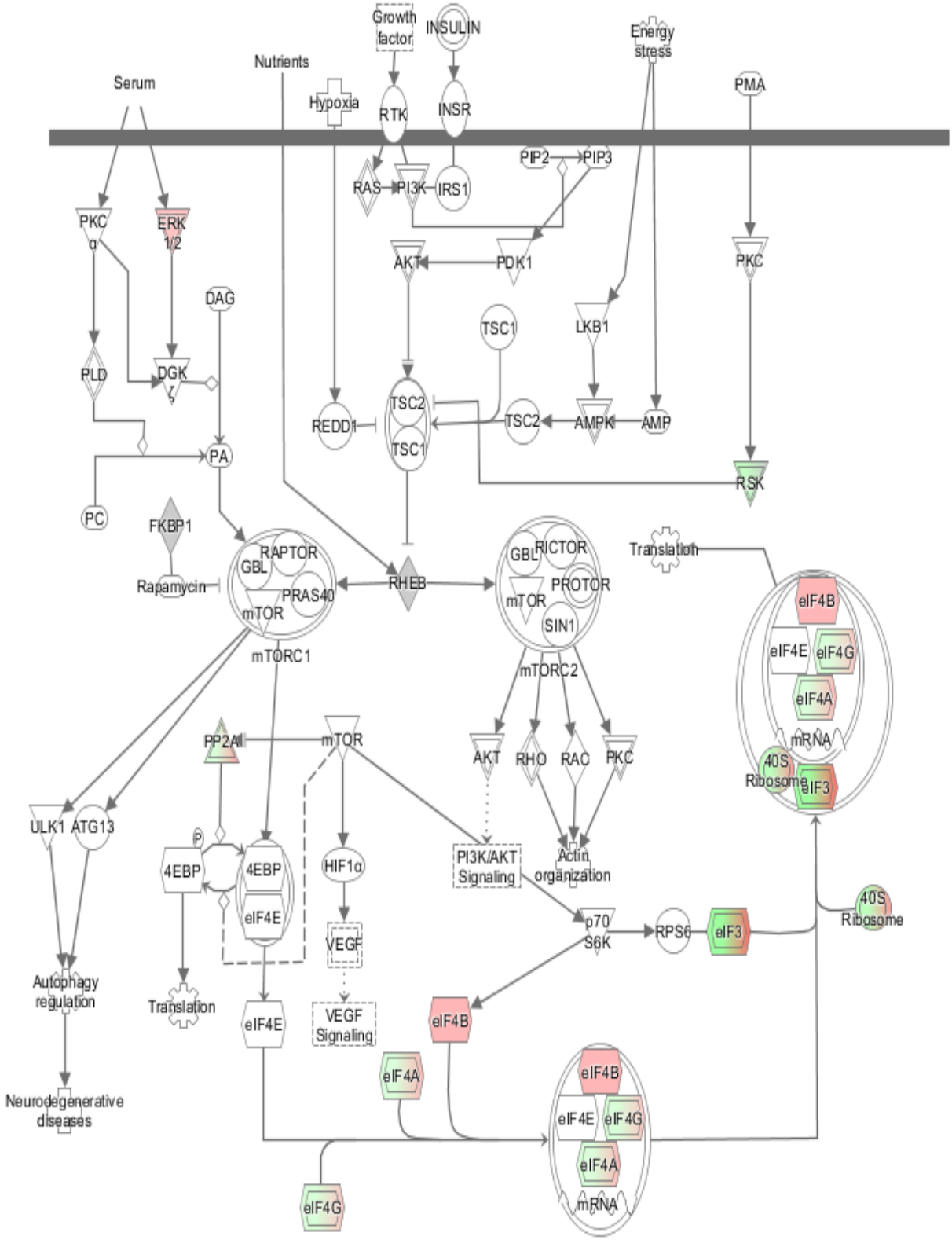

Figure 40: Individual analysis of proteomics data with respect to the mTOR pathway in the IPA software. Proteins detected and identified as up-regulated or down-regulated are labelled as red-coloured or green-coloured icons, respectively. Proteins not detected by IPA from the provided list are labelled as uncoloured icons.

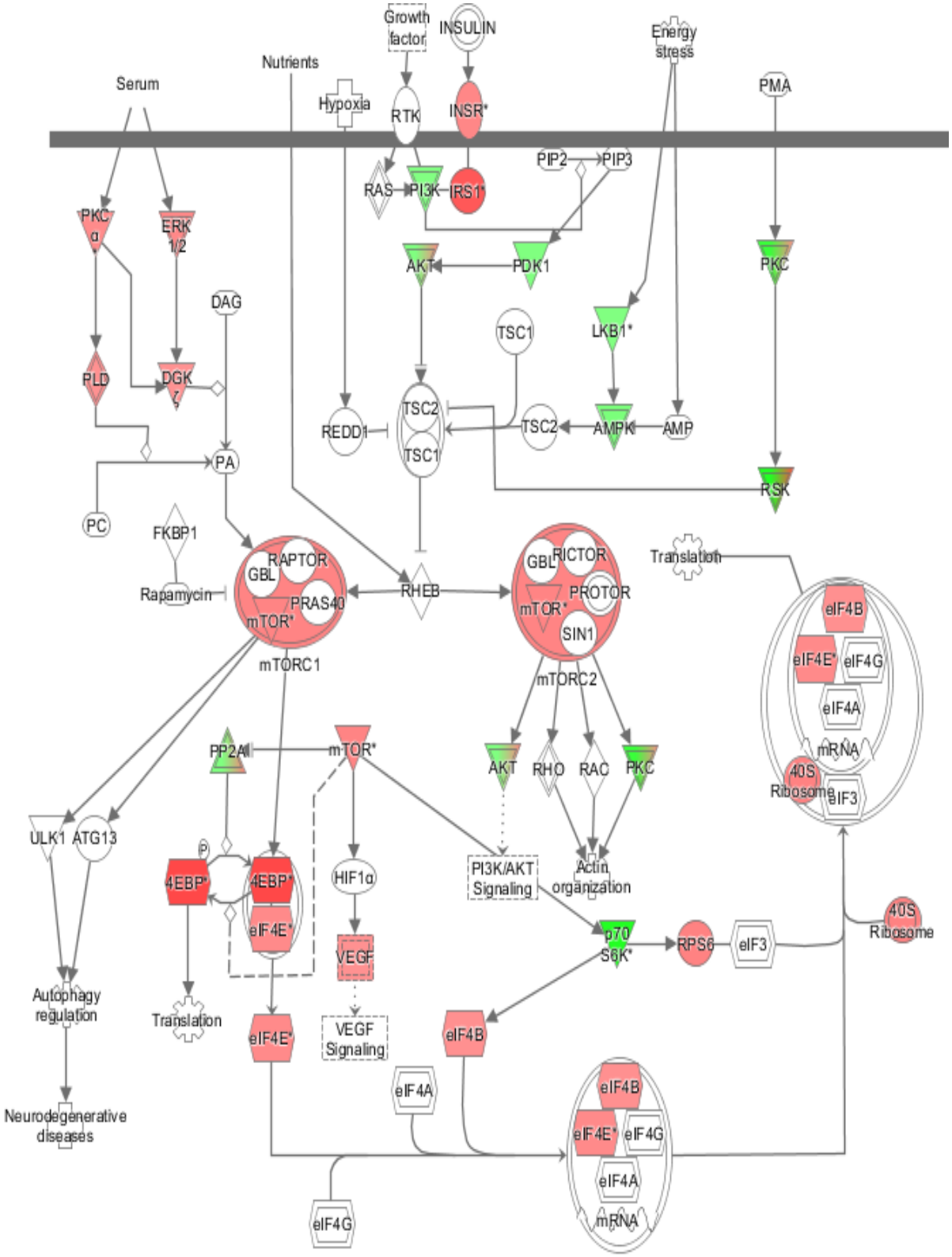

Figure 41: Individual analysis of protein microarray data with respect to the mTOR pathway in the IPA software. Proteins detected and identified as up-regulated or down-regulated are labelled as red-coloured or green-coloured icons, respectively. Proteins not detected by IPA from the provided list are labelled as uncoloured icons.

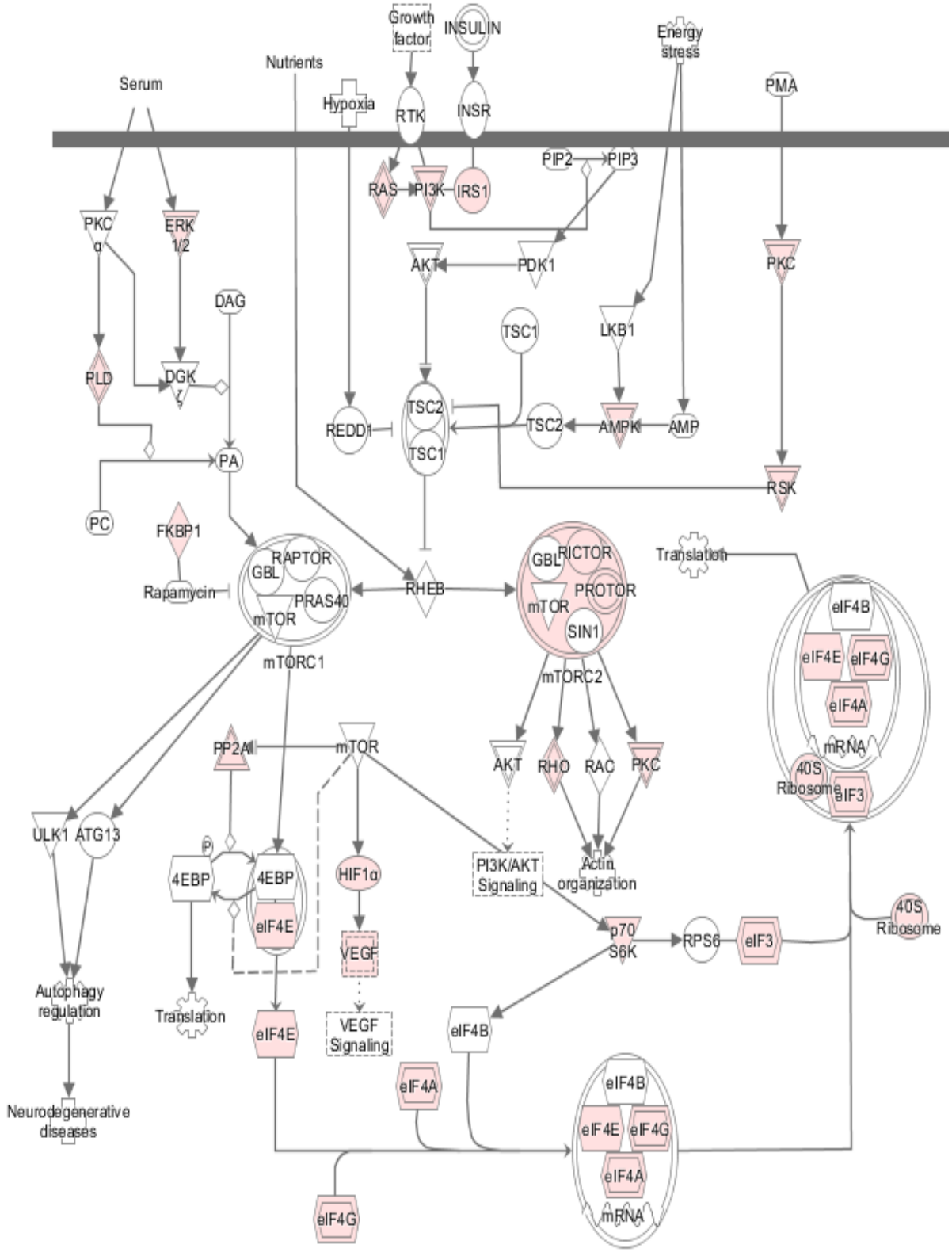

Figure 42: Individual analysis of RNA-Seq data with respect to the mTOR pathway in the IPA software. Proteins detected and identified as up-regulated or down-regulated are labelled as red-coloured or green-coloured icons, respectively. Proteins not detected by IPA from the provided list are labelled as uncoloured icons.

IPA comparative analysis of all datasets identifies candidate pathways or functional molecules when N-WASP is overexpressed in HSC-5 cells. This is helpful since many signalling axes and pathways often mutually cross-talk and integrate with one another to jointly regulate biological processes and maintain cell well-being [170]. For example, the mTOR pathway is flanked outside-to-inside by receptor tyrosine kinase (RTK) receptors (including EGFR) which can pass signals to RAS and PI3K, members of RAS-RAF and PI3K/AKT signalling axes [171] (Fig. 40-42). These signals, with ERK1/2 of the ERK/MAPK signalling axis [172], can jointly or independently influence mTOR protein to form mTOR complex 1 (mTORC1) or 2 (mTORC2) which influences further protein biosynthesis activity and even acts as a feedback loop to AKT signalling and PKCl signalling, respectively [173,174]. A phosphorylated protein in a signalling axis can lead to activation or inactivation of other proteins of other signalling axes [169], thus any phenotype is a combination of multiple signalling pathways.

The IPA software assigns activation Z-scores to any pathway or molecule identified from comparative analysis of multiple datasets, but they are all ranked based on software calculations from the most likely to the least likely in a descending order. Activation Z-scores are also colour coded graphical representation of the degree of targets being up-regulated (coloured as orange) and down-regulated (coloured as blue). 194 pathways were ranked, with a list of top 15 shown (Fig. 43), implicating actin cytoskeleton and Integrin pathways, as well as PI3K/AKT, ERK/MAPK and JNK pathways (not shown). 296 functional molecules were ranked, with a list of top 15 shown (Fig. 44), implicating FOXO1 very highly, as well as AKT, JNK, ERK1/2 (not shown).

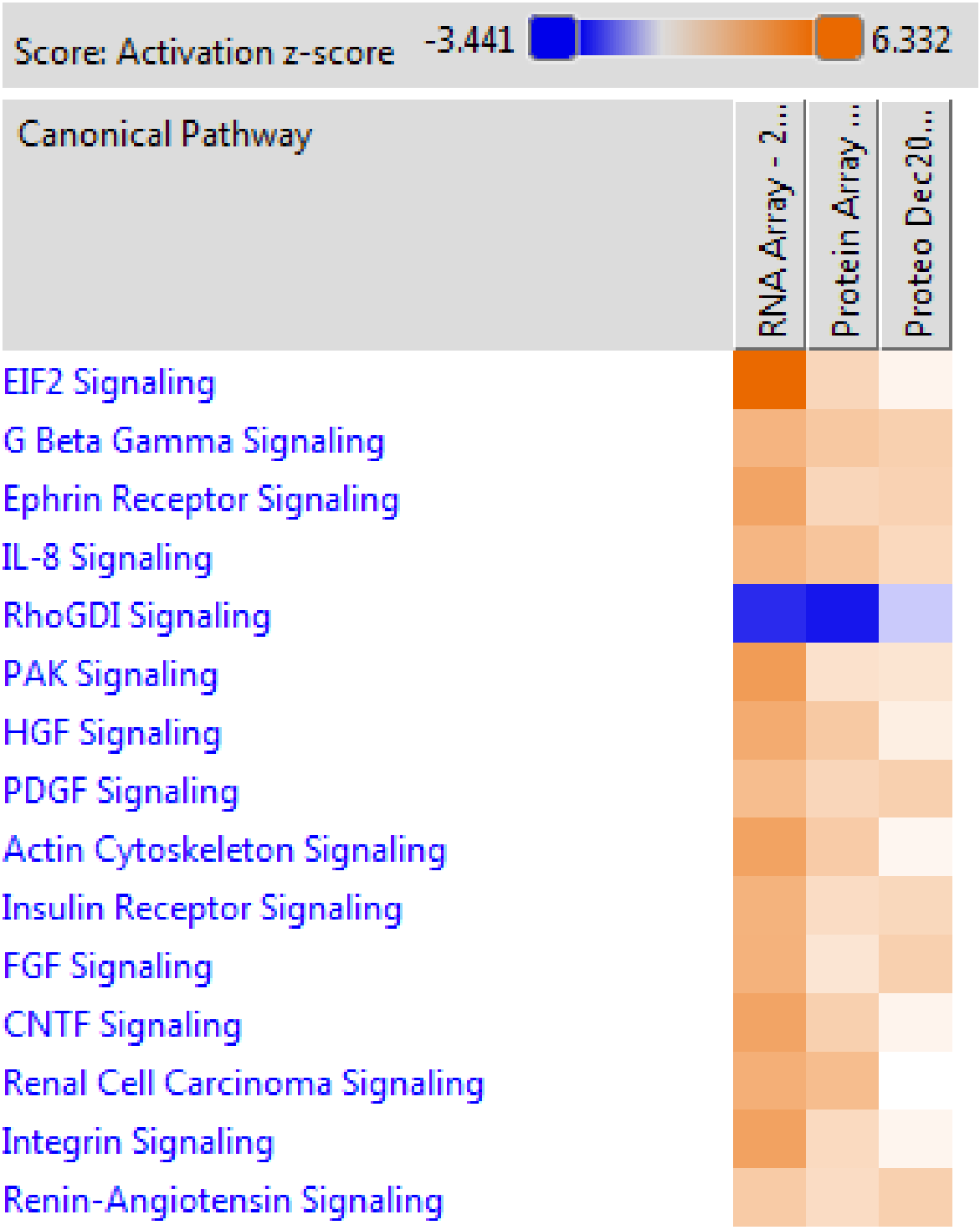

Figure 43: Graphical presentation of the top 15 pathways identified in HSC-5$^{N\text{-}WASP}$ cells compared to HSC-5^{CTR} cells from IPA software comparative analysis. The IPA software provides an activation Z-score for each pathway based on data from each dataset but ranks them from the highest likely relevance in descending order. Note 'actin cytoskeleton signaling' and 'Integrin signaling' are ranked in 9th and 14th place, respectively, and the order of datasets from left to right – RNA-Seq, protein array and proteomics.

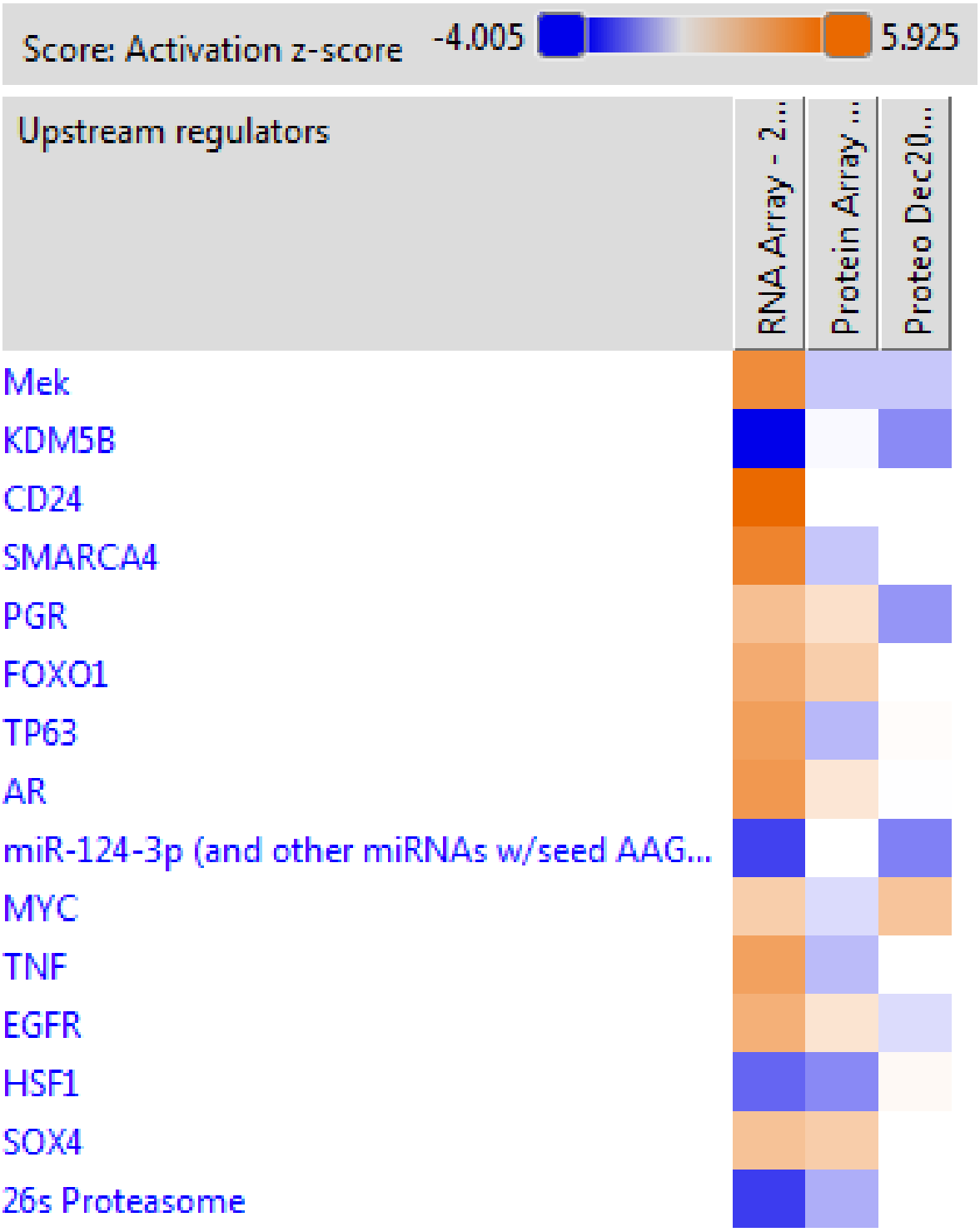

Figure 44: Graphical presentation of the top 15 functional molecules identified in HSC-5$^{N\text{-}WASP}$ cells compared to HSC-5^{CTR} cells from IPA software comparative analysis. The IPA software provides an activation Z-score for each regulator based on data from each dataset but ranks them from the highest likely relevance in descending order. Note 'FOXO1' is ranked in 6th place and and the order of datasets from left to right – RNA-Seq, protein array and proteomics.

3.3.5 Summary

To identify causes for reduced cell proliferation observed in HSC-5$^{N\text{-}WASP}$ cells compared to HSC-5^{CTR} cells, multiple analyses were performed. Proteomic analysis suggests that out of the four candidate signalling pathways responsible for cell proliferation, N-WASP influences the Integrin, EGF and Wnt pathways to cause changes in focal adhesion complex, cell migration and proliferation. Protein microarray and RNA-Seq suggest that N-WASP reduces cell proliferation by influencing activities of regulators responsible for cell growth, metabolism and protein biosynthesis, such as JNK, ERK1/2, FOXO1, p70S6K and various others. IPA comparative analysis of all proteomic, protein microarray and RNA-Seq data suggest a likelihood of N-WASP-influenced signalling that reduce cell proliferation in HSC-5 cells via Integrin-mediated signalling and FOXO1-dependent signalling.

Chapter 4: Results Part 2 – Characterizing the Role of TXNIP in Skin Cancer

4.1 Validation of candidate pathways and regulators identified in HSC-5 sublines

Overexpression of N-WASP in HSC-5 cells reduced cell proliferation (Fig. 18), migration (Fig. 22) and paxillin patches (Fig. 25), but increased E-cadherin localizations (Fig. 20) and vinculin patches (Fig. 23). IPA comparative analysis of proteomics, protein microarray and RNA-Seq highlighted up to 15 pathways likely responsible for HSC-$5^{N\text{-}WASP}$ cell reduced proliferation and migration, including the candidate Integrin pathway to fibroblast growth factor (FGF) and actin cytoskeleton signalling pathways (Fig. 43). It is possible that changes to the Integrin pathway are responsible for the observed phenotypic differences in HSC-$5^{N\text{-}WASP}$ cells compared to HSC-5^{CTR} cells.

It is possible metabolic changes caused by increased Integrin-mediated pathway signalling in HSC-$5^{N\text{-}WASP}$ cells compared to HSC-5^{CTR} cells are mediated by various functional molecules. IPA comparative analysis of proteomics, protein microarray and RNA-Seq highlighted a list of top functional molecules including FOXO1 (Fig. 44), when HSC-5 cells overexpress N-WASP. RNA-Seq and protein microarray showed up-regulated FOXO1 expression (HSC-$5^{N\text{-}WASP}$/HSC-5^{CTR} FPKM ratio: 1.651) and up-regulated phospho-Ser319 FOXO1 levels (HSC-$5^{N\text{-}WASP}$/HSC-5^{CTR} protein ratio: 1.619), respectively. This suggests that a form of negative regulation of FOXO1 is also responsible for the observed phenotypic differences between HSC-5^{CTR} and HSC-$5^{N\text{-}WASP}$ cells.

4.1.1 Integrin pathway and FOXO1 protein are central regulators

Validation of the Integrin pathway was performed. HSC-$5^{N\text{-}WASP}$ cells had increased vinculin patches (Fig. 23) and reduced paxillin patches (Fig. 25) than HSC-5^{CTR} cells. Regulation of cell adhesion and migration by vinculin and paxillin interactions require cell-ECM interactions via Integrin receptors [153]. A study by Hasegawa *et al.* [175] found significant up-regulation of integrins α2, α6 and β1 in HSC-5 cells compared to HaCaT cells. Individual search of the above-mentioned integrins in RNA-Seq data showed HSC-$5^{N\text{-}WASP}$ cells having slight increase (ratio $1.000 \leq X \leq 1.500$) or up-regulation ($X \geq 1.500$) of four of five integrin subunits (Table 6). These suggest the Integrin pathway plays an important role in HSC-5 cell processes.

Table 6: List of Integrin gene expressions up-regulated or are of interest in HSC-5$^{N\text{-}WASP}$ cells in comparison to HSC-5^{CTR} cells from RNA-Seq.

Gene of Interest	HSC-5^{CTR} FPKM	HSC-5$^{N\text{-}WASP}$ FPKM	HSC-5$^{N\text{-}WASP}$/HSC-5^{CTR} FPKM Ratio
Integrin α2 (ITGA2)	25.182	113.893	**4.523**
Integrin α3 (ITGA3)	42.963	52.303	**1.217**
Integrin α6 (ITGA6)	31.783	76.495	**2.407**
Integrin β1 (ITGB1)	121.700	316.477	**2.600**
Integrin β4 (ITGB4)	164.447	104.245	**0.634**

Since N-WASP interacts with Arp2/3 and is critical for actin cytoskeleton remodelling [56], the focal adhesion complex utilizes actin cytoskeleton to regulate cell-ECM interaction and the adherens junctions utilizes actin cytoskeleton to regulate cell-cell adhesion [39], the actin cytoskeleton signalling and Integrin pathway are mutually cooperating. The other 13 pathways from eukaryotic translation initiation factor 2 (EIF2) signalling to renal cell carcinoma signalling all have one common aspect – they depend on signals from the Integrin receptor to stimulate, repress or regulate their activities [176-188]. In other words, the ciliary neurotrophic factor (CNTF) [186], Rho GDP (guanosine diphosphate) dissociation inhibitor (RhoGDI) [180] and platelet-derived growth factor (PDGF) [183] pathways, even in context of other cell lines investigated, all interact with Integrin signalling in order to promote or repress cellular proliferation and migration.

Integrin receptors exhibit bidirectional signalling, as inside-out cell signalling influences integrin activity towards the external environment and outside-in cell signalling towards the intracellular environment [156]. Growth factor pathways, such as HGF [182] and interleukin-8 (IL-8) [179], utilize integrins to operate in this manner. Integrin receptors are held in place by focal adhesion complex, which is the key convergence point for multiple signalling [183]. Key components include FAK, SRC, vinculin, paxillin, integrin-linked kinase (ILK), talin and the kindlins [189], and GRB2 and SOS1 to name a few [190]. Signalling interplay from these components are relayed down to many downstream signalling axes, include RAS/RAF, PI3K/AKT, ERK/MAPK and mTOR

that proceed to regulate cellular activity [158]. These signalling interplay is summarized visually (Fig. 45).

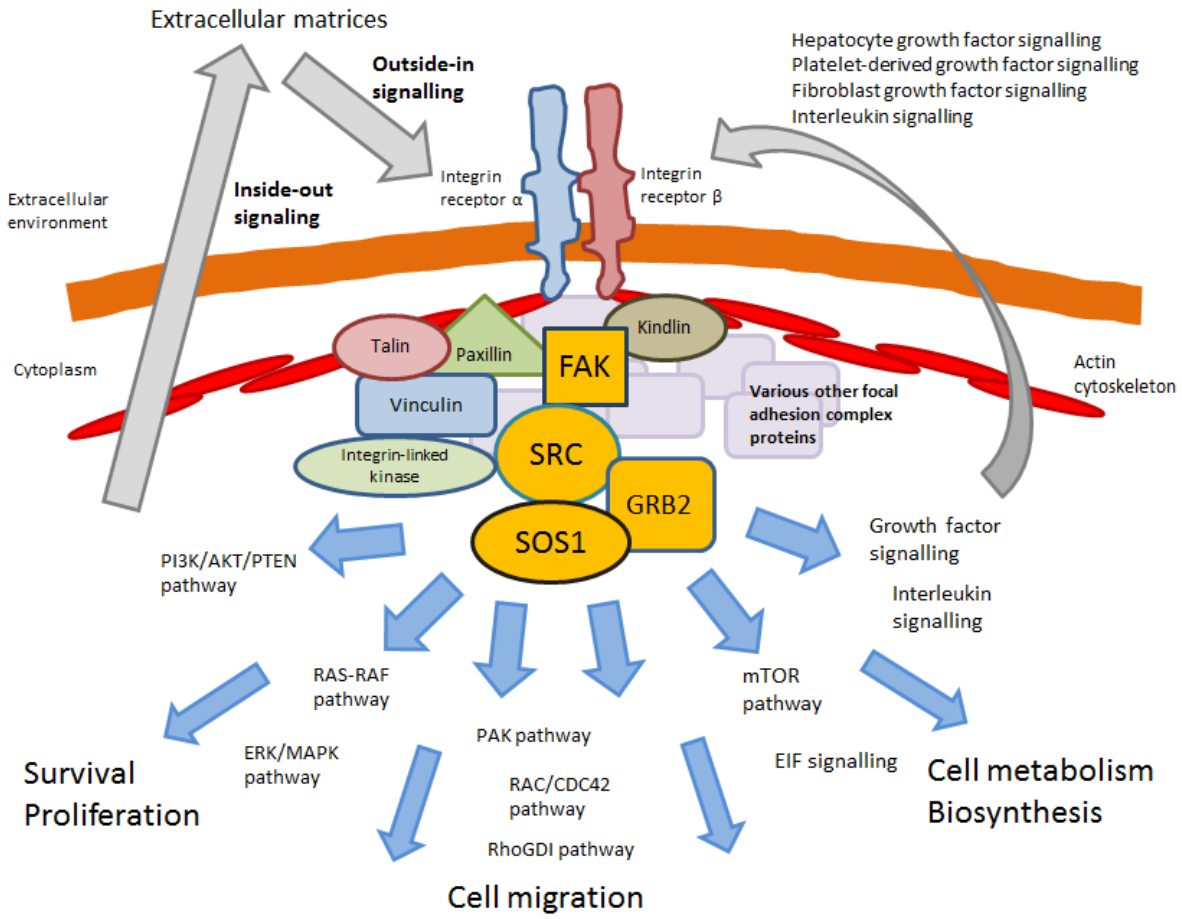

Figure 45: Integrin signalling via the focal adhesion complex is the key point for regulating many signalling pathways in the cell. Integrin receptors interact with the focal adhesion complex, and the interplay of signalling at the focal adhesion complex and outside-in cell signalling determine to which pathways these signals are relayed to. Adapted from Harburger and Calderwood [191] and Wieduwilt and Moasser [171].

14 pathways were considered up-regulated (coloured as orange) by IPA comparative analysis in HSC-$5^{N\text{-}WASP}$ cells compared to HSC-5^{CTR} cells, but one pathway, the RhoGDI pathway was considered down-regulated (coloured as blue) (Fig. 43). This initially suggests that Integrin-mediated down-regulation of the RhoGDI pathway reduced cell proliferation in HSC-$5^{N\text{-}WASP}$ cells. The Rho family of GTPases are a subgroup of the Ras superfamily of GTPases which regulate cytoskeletal dynamics, cell movement, cell growth and proliferation, and the three best-studied Rho GTPases are RhoA, RAC1 and CDC42 [192]. They are stimulated by signals from Integrin-ECM interactions, RTK receptors and G-protein-coupled receptors (GPCRs), among others

[193] and are negatively regulated by RhoGDIs, which consist of RhoGDI isoforms α, β, and γ (ARHGDIA, ARHGDIB and ARHGDIG, respectively) [194].

RNA-Seq data of individual searches for these six RhoGDI proteins with the respective mRNA levels in HSC-5^{CTR} and HSC-5$^{N\text{-}WASP}$ cells are shown (Table 7). ARHGDIB, RhoA and RAC1 do not seem to be affected by changes in N-WASP levels as shown by the FPKM ratio being around 1. As ARHGDIG is known to interact with RhoA and CDC42 in human cells [195], given no changes of RhoA mRNA levels were observed and that increased CDC42 mRNA levels likely correlate with N-WASP overexpression, ARHGDIG is not likely responsible for reduced HSC-5$^{N\text{-}WASP}$ cell proliferation. In general, the role of RhoGDIs in cancer is controversial because they were found to be up- and down-regulated in various cancers and pathological diseases [196]. ARHGDIA is the best-studied and characterized RhoGDI, yet scientific opinion on its role in cell proliferation is divided [197]. ARHGDIA overexpression promoted liver cancer cell proliferation, but repressed cardiac muscle cell proliferation [196,198], for example. Altogether, based on these results, the RhoGDI pathway was not investigated in this dissertation, and only the Integrin pathway was validated.

Table 7: List of RhoGDI pathway gene expressions of interest in HSC-5$^{N\text{-}WASP}$ cells in comparison to HSC-5^{CTR} cells from RNA-Seq.

Gene of Interest	HSC-5^{CTR} FPKM	HSC-5$^{N\text{-}WASP}$ FPKM	HSC-5$^{N\text{-}WASP}$/HSC-5^{CTR} FPKM Ratio
ARHGDIA	113.280	56.500	**0.499**
ARHGDIB	58.422	56.038	**0.959**
ARHGDIG	0.161	0	**0**
RhoA	88.956	97.704	**1.098**
RAC1	85.534	87.334	**1.021**
CDC42	47.268	85.209	**1.803**

Validation of the candidate functional molecule FOXO1 was also performed. FOXO1 is considered as one of the most likely functional molecules responsible for the phenotypic differences observed thus far between HSC-5^{CTR} and HSC-5$^{N\text{-}WASP}$ cells (Fig. 44). There were an additional five regulators ranked higher than FOXO1 by IPA comparative

analysis, with their respective mRNA levels in HSC-$5^{N\text{-}WASP}$ cells compared to HSC-5^{CTR} cells shown (Table 8). These proteins contribute to cancer development in other cell lines by promoting proliferation, reducing cell adhesion and increasing cell migration [199-207]. The effects from up- or down-regulation (or increase or reduction in expression) of these proteins can be correlated with the reduced cell proliferation and migration phenotypes in HSC-$5^{N\text{-}WASP}$ cells compared to and HSC-$5^{N\text{-}WASP}$ cells.

Table 8: List of Ingenuity comparative analysis regulators identified as ranking higher than FOXO1 and their mRNA expressions in HSC-$5^{N\text{-}WASP}$ cells in comparison to HSC-5^{CTR} cells from RNA-Seq.

Gene of Interest	HSC-5^{CTR} FPKM	HSC-$5^{N\text{-}WASP}$ FPKM	HSC-$5^{N\text{-}WASP}$/HSC-5^{CTR} FPKM Ratio
Mek (SMEK1) (protein phosphatase 4 regulatory subunit 3A (PPP4R3A))	7.139	15.099	**2.115**
KDM5B (lysine-specific demethylase 5B)	32.990	25.290	**0.767**
CD24 (cluster of differentiation 24)	61.460	142.133	**2.313**
SMARCA4 (transcription activator BRG1)	50.038	23.581	**0.471**
PGR (progesterone receptor / NR3C3)	1.240	1.527	**1.231**

However, similar to findings about Integrin pathway, these five candidate molecules have one common aspect, which is their connection to FOXO1 as either a target of FOXO1 or a regulator of FOXO1 in order to assert phenotype changes (Fig. 46A). For example, SMEK1 acts upon FOXO1 to stimulate gluconeogenesis in liver cells [199], while triple negative breast tumours exhibit low levels of the cell adhesion molecule CD24 due to high levels of nuclear FOXO1 repressing its levels [205]. This suggests FOXO1 plays a crucial role for changing phenotypes in HSC-$5^{N\text{-}WASP}$ cells compared to HSC-5^{CTR} cells. The mechanism of action in general of kinases known to phosphorylate FOXO1 in the nucleus and cause either nuclear ubiquitination or cytoplasmic translocation for ubiquitination and proteasomal degradation is shown (Fig. 46B). Given the body of knowledge established on how FOXO proteins are regulated by kinases, it

was of interest to study the role of FOXO1 in HSC-5 cells and identify the kinase regulating its activity.

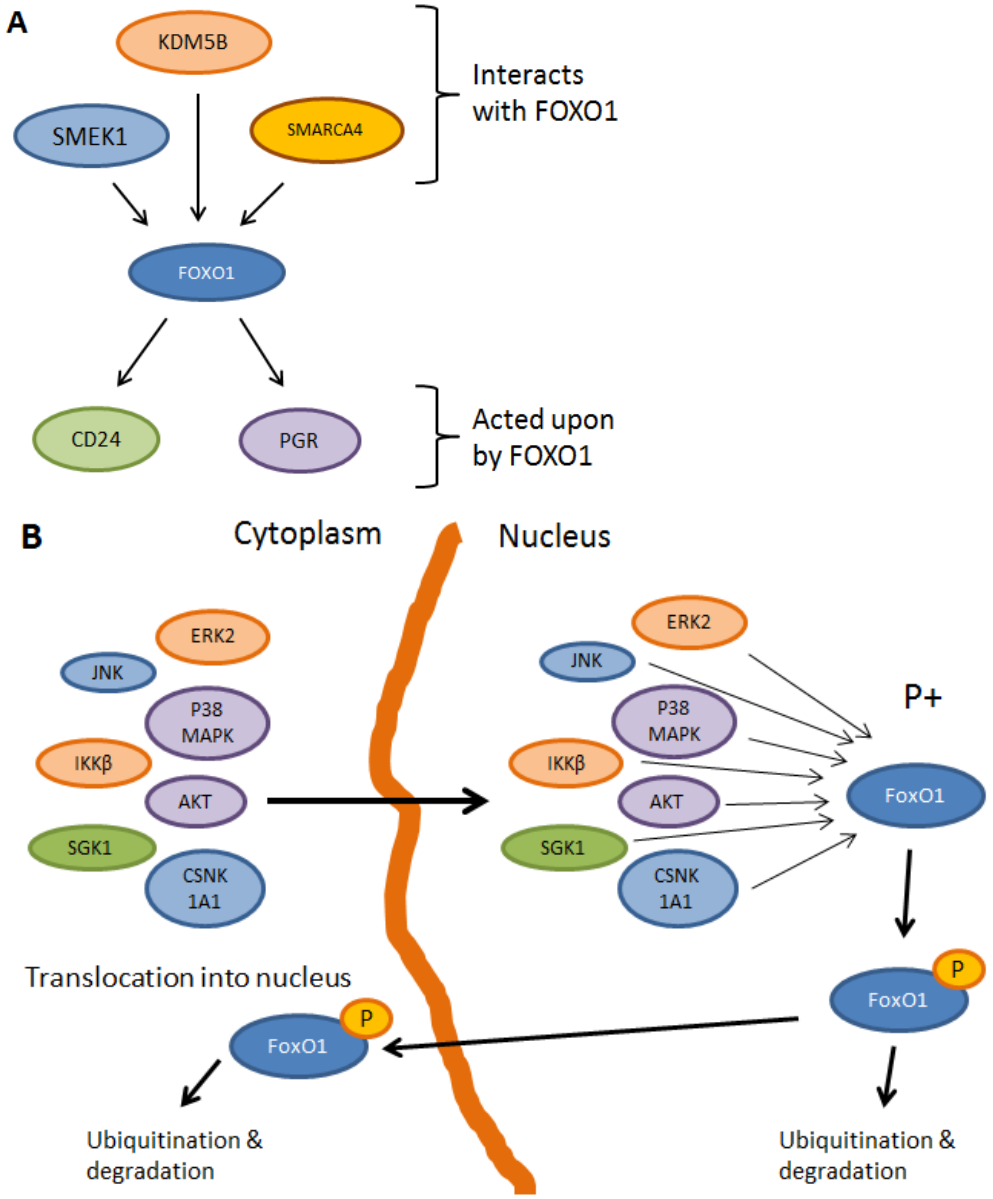

Figure 46: FOXO1 is the key protein for regulating signals among the functional molecules identified, and is usually regulated via phosphorylation to be degraded. A) SMEK1, KDM5B and SMARCA4 intereact with FOXO1 upstream of it, whereas FOXO1 interacts with CD24 and PGR downstream of it [199-207], establishing FOXO1 as a central nexus of protein-signal regulation. B) Numerous kinases such as AKT, SGK1, and JNK translocate from the cytoplasm to the nucleus to phosphorylate FOXO proteins. Generally, this causes FOXO proteins to be inactive and they either translocate to the cytoplasm for ubiquitination and proteasomal degradation or remain in the nucleus for ubiquitination and degradation. Adapted from Lam *et al.* [112] and Huang and Tindall [114].

4.1.2 Real-time PCR shows Integrin pathway is dysregulated in HSC-5$^{N\text{-}WASP}$ cells compared to HSC-5^{CTR} cells

N-WASP interacts with the Wnt and Integrin signalling pathways to influence or modulate cellular growth and development [59,61,88]. N-WASP may indirectly influence the EGF and Hippo pathways via influencing the actions of other proteins interacting with these pathways [89,208]. Proteomics data analysis using the PANTHER software showed the likelihood of Integrin, EGF and Wnt pathways being involved and Hippo pathway not likely involved in HSC-5$^{N\text{-}WASP}$ cells (Fig. 31,32). A real-time PCR study was performed on HSC-5 sublines to study if N-WASP influences any of these pathways in HSC-5 cells. The FOXO1 gene was chosen to represent the Integrin pathway, the pyruvate kinase muscle isozyme M2 (PKM2) gene for EGF pathway, the cMyc gene for Wnt pathway, and the CTGF gene for Hippo pathway. The only significant difference in mRNA levels was found for the FOXO1 gene representing the Integrin pathway (Fig. 47). Together with PANTHER analysis of proteomics (Fig. 31,32), these results suggest that phenotypic differences observed in HSC-5 sublines are likely expressed through N-WASP influencing the Integrin pathway.

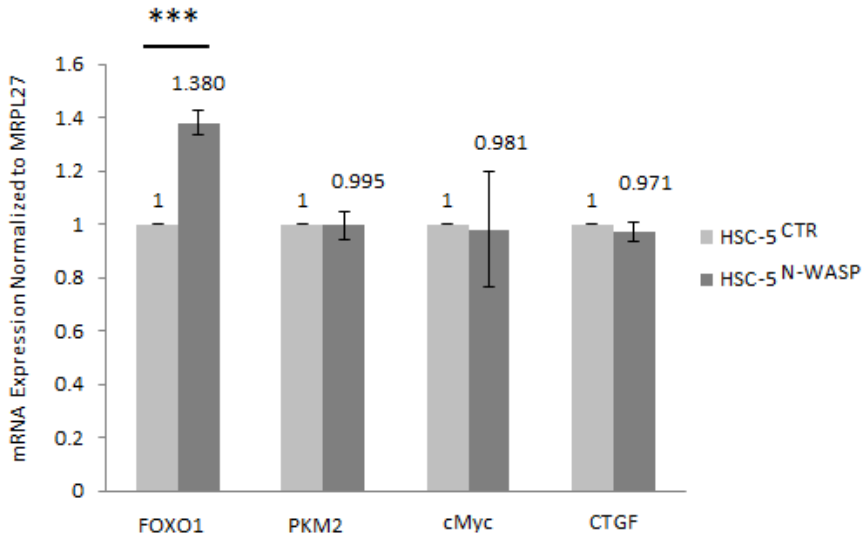

Figure 47: The Integrin pathway is dysregulated in HSC-5$^{N\text{-}WASP}$ cells compared to HSC-5^{CTR} cells. Total RNA was extracted from HSC-5^{CTR} and HSC-5$^{N\text{-}WASP}$ cells, followed by cDNA generation and real-time PCR analysis. cDNAs were diluted and the same amount (in volume) were used for real-time PCR. They were probed for FOXO1, PKM2, cMyc, and CTGF, representing the Integrin, EGF, Wnt and Hippo pathways, respectively. All cDNA values were normalized to MRPL27, and compared to HSC-5^{CTR} cells. Experiments were performed in triplicates. Significance: ***P<0.001 (Student's t-test).

4.1.3 The Integrin pathway is dysregulated in HSC-5$^{N\text{-}WASP}$ cells compared to HSC-5^{CTR} cells

The Integrin pathway was validated by characterizing some of the key components of the focal adhesion complex that is anchored to Integrin receptors, including FAK, SRC, GRB2 and SOS1 [189,190]. FAK is a key regulator in the focal adhesion complex known to cause cancer development of many cells when overexpressed [176]. FAK phosphorylated at Tyr397 residue is crucial in breast cancer for promotion of cell migration activity [209], for example. FAK interaction with vinculin and paxillin determines whether cell migration occurs or cell adhesion occurs [153,154]. A Western blot of HSC-5^{CTR} and HSC-5$^{N\text{-}WASP}$ cells for phospho-Tyr397 FAK and pan-FAK was performed to determine if N-WASP-mediated phenotypic differences were caused via altered FAK expression or activity, even though RNA-Seq data shows FAK is only increased slightly (HSC-5$^{N\text{-}WASP}$/HSC-5^{CTR} FPKM ratio: 1.312) (Table 5). Both HSC-5 sublines had similar pan-FAK expression but HSC-5$^{N\text{-}WASP}$ cells had a slightly reduced phospho-FAK expression compared to HSC-5^{CTR} cells (Fig. 48A). Densitometric quantification of FAK phospho-to-pan-specific bands against GAPDH bands showed a significant reduction of FAK activity (Fig. 48B).

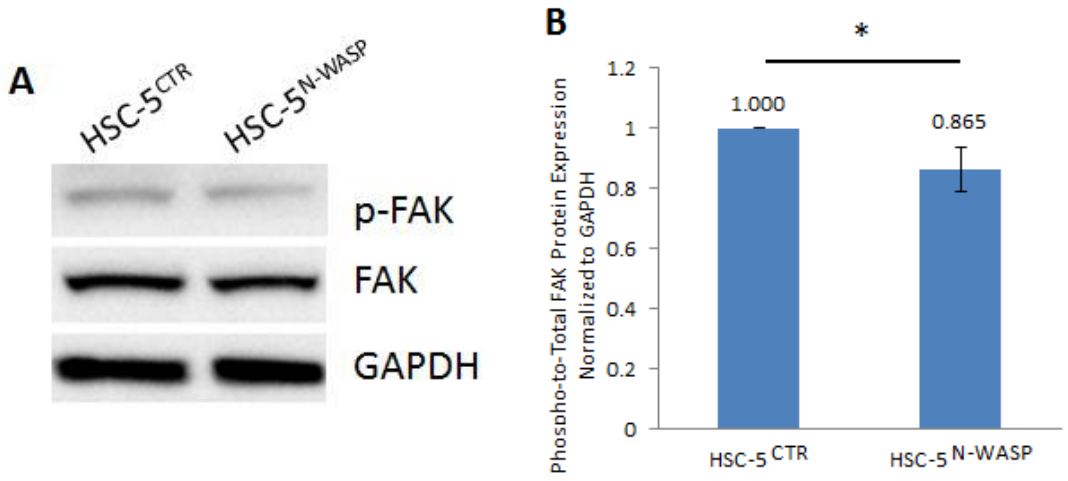

Figure 48: HSC-5$^{N\text{-}WASP}$ cells have reduced FAK activity compared to HSC-5^{CTR} cells. A) Equal amounts of HSC-5^{CTR} and HSC-5$^{N\text{-}WASP}$ cell protein lysates were loaded for Western blot analysis using anti-phospho-Tyr397 FAK, anti-pan-FAK and anti-GAPDH antibodies. B) Densitometric quantifications show significant reduction of active FAK levels in HSC-5$^{N\text{-}WASP}$ cells compared to HSC-5^{CTR} cells. Experiments were performed in triplicates. Significance: *P<0.05 (Student's t-test).

SRC kinase is important for moderating focal adhesion complex signalling [189]. SRC and FAK often interact and activate each other [210], and this binding and its phosphorylation-based activity stimulates integrin-focal adhesion complex signalling in epithelial cells among others [211]. Similar to FAK, SRC regulates cell signalling for proliferation, migration, adhesion and invasion in cancer cells [212]. Even though SRC mRNA levels in HSC-5$^{N\text{-}WASP}$ are slightly reduced and not considered down-regulated (HSC-5$^{N\text{-}WASP}$/HSC-5^{CTR} FPKM ratio: 0.613), the role of SRC in HSC-5 sublines was studied to determine the role of Integrin pathway in HSC-5 cell proliferation. It is possible that reduced SRC levels are responsible for reduced HSC-5 cell proliferation. A Western blot of both HSC-5 sublines for SRC was performed. HSC-5$^{N\text{-}WASP}$ cells had slightly a reduced SRC expression compared to HSC-5^{CTR} cells (Fig. 49A). Densitometric quantification of SRC bands against GAPDH bands showed a significant reduction of SRC protein levels (Fig. 49B).

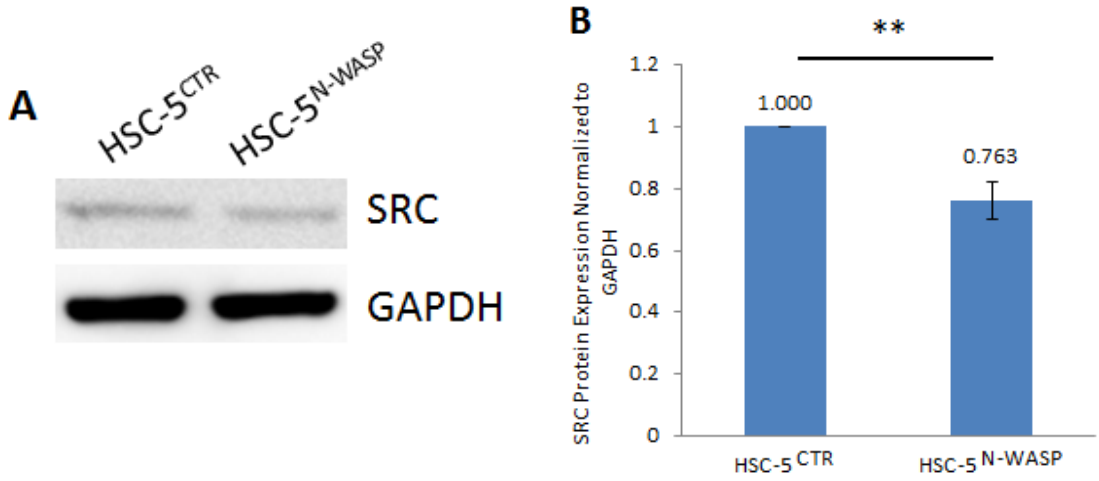

Figure 49: SRC expression is reduced in HSC-5$^{N\text{-}WASP}$ cells compared to HSC-5^{CTR} cells. A) Equal amounts of HSC-5^{CTR} and HSC-5$^{N\text{-}WASP}$ cell protein lysates were loaded for Western blot analysis using anti-SRC and anti-GAPDH antibodies. B) Densitometric quantifications show significant reduction of SRC protein levels in HSC-5$^{N\text{-}WASP}$ cells compared to HSC-5^{CTR} cells. Experiments were performed in triplicates. Significance: $^{**}P<0.01$ (Student's *t*-test).

GRB2 is another focal adhesion complex protein that regulates cell motility in normal and cancer cells, and even metastasis in cancer cells [213]. GRB2 acts downstream of both FAK and SRC joint signalling [210], or acts upstream of FAK by inducing Integrin receptor-mediated phospho-Tyr397 FAK activity and FAK-SRC complex formation for further signal relaying [214]. GRB2 plays a role in cell EMT via the RAS-RAF-MEK-

MAPK pathway following SRC-induced changes to cell adhesion activity [215]. GRB2 activity in HSC-5 sublines was studied, even if RNA-Seq shows that GRB2 mRNA levels are slightly reduced (HSC-$5^{N\text{-}WASP}$/HSC-5^{CTR} FPKM ratio: 0.820). It is possible that reduced GRB2 levels are responsible for reduced HSC-5 cell proliferation. A Western blot of both HSC-5 sublines for GRB2 was performed. HSC-$5^{N\text{-}WASP}$ cells had a slightly reduced GRB2 expression compared to HSC-5^{CTR} cells (Fig. 50A). Densitometric quantification of GRB2 bands against GAPDH bands showed a significant reduction of GRB2 protein levels (Fig. 50B).

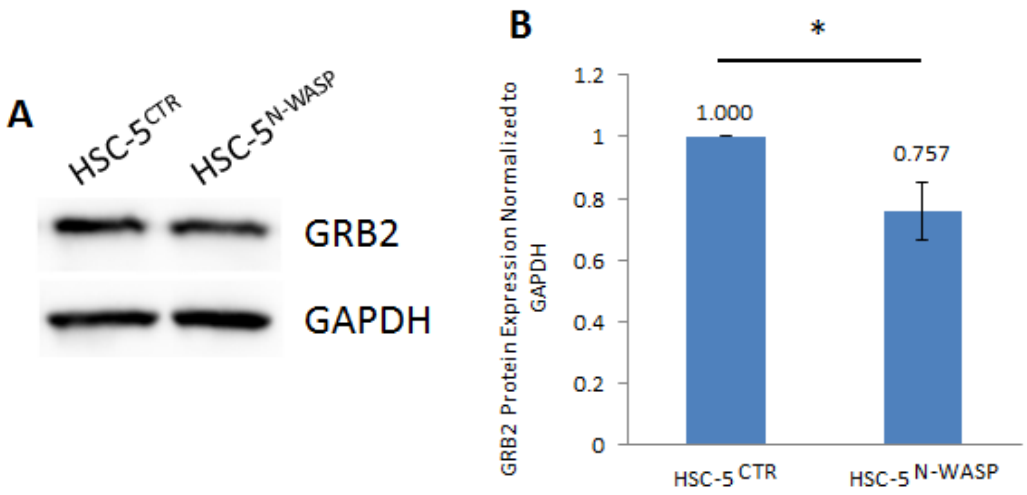

Figure 50: GRB2 expression is reduced in HSC-$5^{N\text{-}WASP}$ cells compared to HSC-5^{CTR} cells. A) Equal amounts of HSC-5^{CTR} and HSC-$5^{N\text{-}WASP}$ cell protein lysates were loaded for Western blot analysis using anti-GRB2 and anti-GAPDH antibodies. B) Densitometric quantifications show significant reduction of GRB2 protein levels in HSC-$5^{N\text{-}WASP}$ cells compared to HSC-5^{CTR} cells. Experiments were performed in triplicates. Significance: *P<0.05 (Student's t-test).

SOS1 is another protein recruited by the focal adhesion complex to mediate cell signalling. SOS1 usually forms a complex with GRB2 [216], and relays Integrin-mediated signalling via the RAS-RAF-MEK-MAPK axis to mediate cell growth, migration and survival [180]. Although much effort has gone into characterizing the structure and domains of SOS1 and its other isoform SOS2 in both humans and mice [217], few studies have been performed to elucidate its role with cell carcinogenesis. It is generally understood that SOS1 levels correlates with cancer development [218] and has a critical role in T-cell development [219]. RNA-Seq showed HSC-$5^{N\text{-}WASP}$ cells with up-regulated SOS1 mRNA levels (HSC-$5^{N\text{-}WASP}$/HSC-5^{CTR} FPKM ratio: 2.179), suggesting increased SOS1 protein levels and a different function in HSC-5 cells than other cell

lines. A Western blot of both HSC-5 sublines for SOS1 was performed. HSC-$5^{N\text{-}WASP}$ cells had increased SOS1 expression compared to HSC-5^{CTR} cells (Fig. 51A). Densitometric quantification of SOS1 bands against GAPDH bands showed a significant increase of SOS1 protein levels (Fig. 51B). As the role of SOS1 in skin cells has not been characterized yet, it is possible SOS1 may be tumour suppressor in HSC-5 cells. SOS1 activity correlated inversely to those of FAK, SRC and GRB2 in HSC-5 cells. Altogether, these results suggest that N-WASP overexpression reduces HSC-5 cell proliferation via changes of Integrin-mediated FAK-SRC-GRB2-SOS1 signalling.

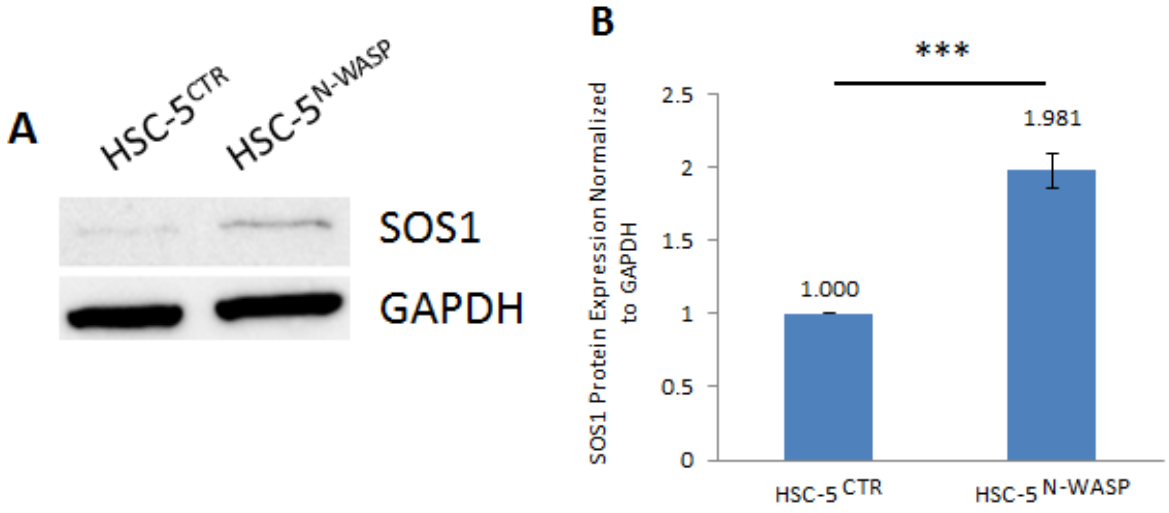

Figure 51: SOS1 expression is increased in HSC-$5^{N\text{-}WASP}$ cells compared to HSC-5^{CTR} cells. A) Equal amounts of HSC-5^{CTR} and HSC-$5^{N\text{-}WASP}$ cell protein lysates were loaded for Western blot analysis using anti-SOS1 and anti-GAPDH antibodies. B) Densitometric quantifications show significant increase of SOS1 protein levels in HSC-$5^{N\text{-}WASP}$ cells compared to HSC-5^{CTR} cells. Experiments were performed in triplicates. Significance: ***$P<0.001$ (Student's *t*-test).

4.1.4 The mTOR pathway is not affected in HSC-5 sublines

The mTOR pathway is a network that incorporates input from numerous upstream pathways and both intracellular and extracellular signals and conditions to manage protein synthesis necessary for cell metabolism and growth [163,220]. The pathway consists of two complexes, mTORC1 and mTORC2. mTORC1 interacts with components of the EIF protein synthesis apparatus to regulate protein biosynthesis and general cell metabolism [173,221], while mTORC2 interacts with pathways such as AKT to regulate cell proliferation, cell metabolism and even actin cytoskeleton remodelling [174,221].

Since IPA analysis highlighted the actin cytoskeleton signalling pathway, RNA-Seq stated HSC-5$^{N\text{-}WASP}$ cells have slightly increased mTOR mRNA (HSC-5$^{N\text{-}WASP}$/HSC-5^{CTR} FPKM ratio: 1.279) and reduced AKT signalling compared to HSC-5^{CTR} cells (Fig. 27,28), mTOR may be responsible for reduced HSC-5 cell proliferation when N-WASP is overexpressed. mTOR activity may be reduced in HSC-5$^{N\text{-}WASP}$ cells, altering proliferative signals or EIF2 protein biosynthesis apparatus via the mTORC1 complex or altering AKT-dependent signalling via the mTORC2 complex. A Western blot of HSC-5 sublines for phospho-Ser2448 mTOR and pan-mTOR was performed. mTOR phospho-Ser2448 levels determine mTOR's activity and its association with mTORC1 and 2 complexes [222]. However, phospho- and pan-mTOR expressions in both HSC-5 sublines are similar (Fig. 52A), and densitometric quantification of mTOR phospho-to-pan-specific bands against GAPDH bands showed no significant differences in active mTOR levels between the HSC-5 sublines (Fig. 52B).

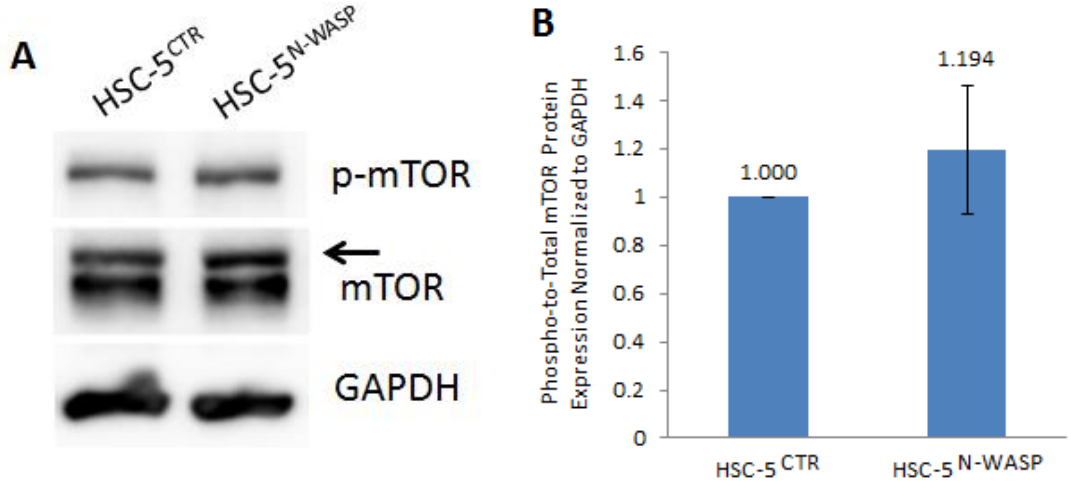

Figure 52: HSC-5^{CTR} and HSC-5$^{N\text{-}WASP}$ cells have similar active mTOR. A) Equal amounts of HSC-5^{CTR} and HSC-5$^{N\text{-}WASP}$ cell protein lysates were loaded for Western blot analysis using anti-phospho-Ser2448 mTOR, anti-pan-mTOR and anti-GAPDH antibodies. B) Densitometric quantifications show no significant difference of active mTOR levels in HSC-5$^{N\text{-}WASP}$ cells compared to HSC-5^{CTR} cells. Experiments were performed in triplicates. Significance: $P>0.05$ (Student's *t*-test).

Protein microarray showed up-regulated phospho-p70S6K, phospho-RSK1/2/3 and phospho-4E-BP1 levels in HSC-5$^{N\text{-}WASP}$ cells compared to HSC-5^{CTR} cells (Table 3). While these proteins are downstream of mTORC1 complex and no changes in mTOR activity were observed, p70S6K and RSK1/2/3 phospho-levels correlate with increased protein synthesis [223], and 4E-BP1 phospho-levels correlate with reduced or inhibited

protein synthesis [164]. RNA-Seq also showed HSC-5$^{N\text{-}WASP}$ cells exhibit slightly reduced 4E-BP1 expression (HSC-5$^{N\text{-}WASP}$/HSC-5^{CTR} FPKM ratio: 0.817). It is possible these downstream signalling might be regulated by N-WASP independently of mTOR.

A Western blot of both HSC-5 sublines for phospho-Thr37/46 4E-BP1 and pan-4E-BP1 was performed. HSC-5^{CTR} and HSC-5$^{N\text{-}WASP}$ cells had similar phospho- and pan-4E-BP1 expressions (Fig. 53A). Densitometric quantification of 4E-BP1 phospho-to-pan-specific bands against GAPDH bands showed no significant differences in active 4E-BP1 levels between the HSC-5 sublines (Fig. 53B). Based on these results, the mTOR pathway is not likely affected by N-WASP overexpression in HSC-5 cells. Reduction of cell proliferation is not caused by changes in mTOR pathways or by reduced protein biosynthesis activity for proliferative functions, but via Integrin signalling relaying anti-proliferative signals.

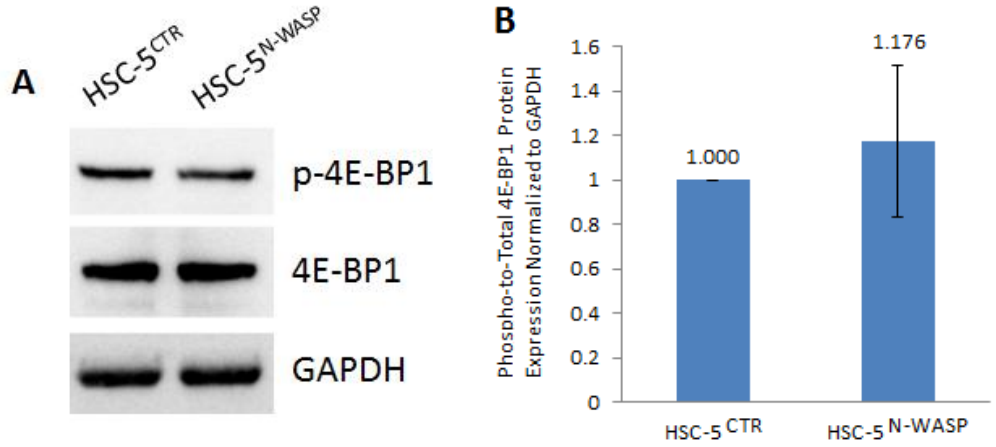

Figure 53: HSC-5^{CTR} and HSC-5$^{N\text{-}WASP}$ cells have similar active 4E-BP1. A) Equal amounts of HSC-5^{CTR} and HSC-5$^{N\text{-}WASP}$ cell protein lysates were loaded for Western blot analysis using anti-phospho-Thr37/46 4E-BP1, anti-pan-4E-BP1 and anti-GAPDH antibodies. B) Densitometric quantifications show no significant difference of 4E-BP1 phosphorylation levels in HSC-5$^{N\text{-}WASP}$ cells compared to HSC-5^{CTR} cells. Experiments were performed in triplicates. Significance: $P>0.05$ (Student's *t*-test).

4.1.5 STAT1 and cytokine signalling are not affected in HSC-5 sublines

Protein microarray identified many phospho- and pan-specific proteins as up- and down-regulated in HSC-5$^{N\text{-}WASP}$ cells. Phospho-Ser727 STAT1, Tyr-40 BMX, Tyr-1230/4/5 Met and Thr-567 Ezrin were up-regulated (Table 3) while pan-specific PTPD1 and PKCl were down-regulated (Table 4). These proteins regulate cell proliferation [224-229] and operate via cytokine-induced receptor signalling [230-236]. STAT1 is well-known for its

Janus kinase 1 (JAK1)-STAT1 pathway of cytokine-mediated signalling [230], and PKCl has been reported to stimulate Type 2 helper T cell cytokine production in an autocrine manner to stimulate cell proliferation [236]. N-WASP knockout in mice fibroblast cells showed increased keratinocyte growth factor (FGF7)-induced cell proliferation [237], suggesting that N-WASP could reduce HSC-5 cell proliferation via cytokine-induced anti-proliferative signalling. To determine if STAT1 and cytokine signalling play a role in reducing HSC-5 cell proliferation, cell proliferation assays were performed on both HSC-5 sublines with and without serum (FBS).

As FBS content is usually not well-defined, can vary in composition and can cause undesired cell stimulation [238], HSC-5$^{N\text{-}WASP}$ cells were cultured in serum-free DMEM. This is to determine if a serum-free environment could rescue HSC-5$^{N\text{-}WASP}$ cell proliferation defects back to that of HSC-5^{CTR} cells. While HSC-5$^{N\text{-}WASP}$ cells proliferated at slower rates compared to HSC-5^{CTR} cell in complete DMEM (Fig. 54), similar to previous observations (Fig. 18), the HSC-5 sublines had significantly severe reduction of cell proliferation in a serum-free environment. This suggested that HSC-5$^{N\text{-}WASP}$ cell reduced proliferation is not due to altered cytokine-mediated and STAT1 signalling.

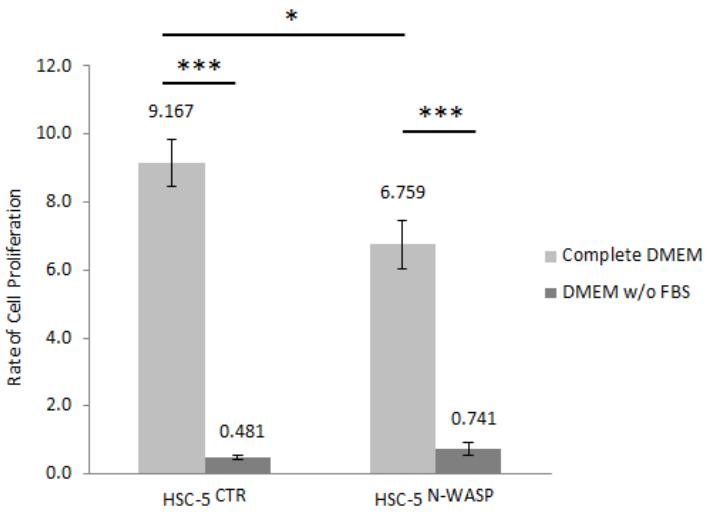

Figure 54: HSC-5 sublines proliferate poorly in DMEM without FBS compared to complete DMEM. 7.5 x 10^3 cells of each cell line were seeded in 24-well plates, incubated for 5 days, trypsinized and counted using a hemacytometer. The rate of proliferation was obtained by comparing total cell counted after 5 days against the number of cells seeded. Experiments were performed in triplicates. Significance: *P<0.05, ***P<0.001 (Student's t-test).

4.1.6 FOXO1 expression is reduced in HSC-5$^{N\text{-}WASP}$ cells compared to HSC-5^{CTR} cells

FOXO proteins are known to reduce cell proliferation by repressing CCND1 and promoting anti-proliferative signalling such as that of CDKN1A [112]. Suppression of CD24 by FOXO1 has been suggested to be responsible for triple negative breast cancer cell migration [205]. These suggest FOXO1 is a repressor of many gene expressions in many cell types. Protein microarray of HSC-5 sublines showed increased phospho-Ser319 FOXO1 levels in HSC-5$^{N\text{-}WASP}$ cells (Table 3), suggesting increased N-WASP expression in HSC-5 cells causes FOXO1 phosphorylation, leading to FOXO1 expulsion from the nucleus and cytoplasmic proteasomal degradation [113]. RNA-Seq showed that HSC-5$^{N\text{-}WASP}$ cells had increased CDKN1A and FOXO1 mRNA levels compared to HSC-5^{CTR} cells (HSC-5$^{N\text{-}WASP}$/HSC-5^{CTR} FPKM value ratios: 1.651 and 1.580 respectively) (Table 5). Real-time PCR of FOXO1 gene in HSC-5^{CTR} and HSC-5$^{N\text{-}WASP}$ cells to determine if Integrin pathway was responsible for reduced cell proliferation showed increased FOXO1 mRNA levels (Fig. 47). Altogether, these suggest that FOXO1 degradation leads to reduced proliferation signals in HSC-5 cells, and the increased FOXO1 transcription may be a compensatory mechanism for reduced protein levels and maintaining the minimum FOXO1-dependent signalling needed.

To determine if this notion of FOXO1 degradation in HSC-5 cells is true, a real-time PCR of HSC-5 sublines for FOXO1 cDNA was repeated. An additional real-time PCR for CDKN1A was simultaneously performed to validate RNA-Seq results as well. HSC-5$^{N\text{-}WASP}$ cells had significant increases of FOXO1 and CDKN1A mRNA levels compared to HSC-5^{CTR} cells (Fig. 55). This suggests that real-time PCR results correlate with RNA-Seq results. A Western blot of both HSC-5 sublines for FOXO1 was also performed. HSC-5$^{N\text{-}WASP}$ cells had a slightly reduced FOXO1 expression compared to HSC-5^{CTR} cells (Fig. 56A). Densitometric quantification of FOXO1 bands against GAPDH bands showed a significant reduction of FOXO1 protein levels in HSC-5$^{N\text{-}WASP}$ cells compared to HSC-5^{CTR} cells (Fig. 56B). Additional imagery and average values of phospho-Ser319 FOXO1 detection spots from the protein microarray (arrows in Fig. 33-35) is shown as well (Fig. 57).

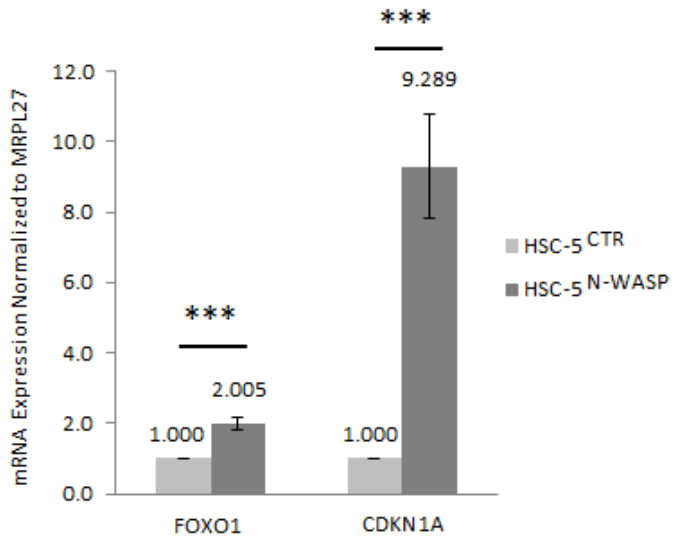

Figure 55: FOXO1 and CDKN1A mRNA expressions are increased in HSC-5$^{N\text{-}WASP}$ cells compared to HSC-5^{CTR} cells. Equal amounts of cDNA from HSC-5^{CTR} and HSC-5$^{N\text{-}WASP}$ cells were subjected to real-time PCR analysis of FOXO1 and CDKN1A cDNA, normalized to MRPL27, showing significant increase of both FOXO1 and CDKN1A mRNA levels in HSC-5$^{N\text{-}WASP}$ cells, compared to HSC-5^{CTR} cells. Experiments were performed in triplicates. Significance: ***P<0.001 (Student's t-test).

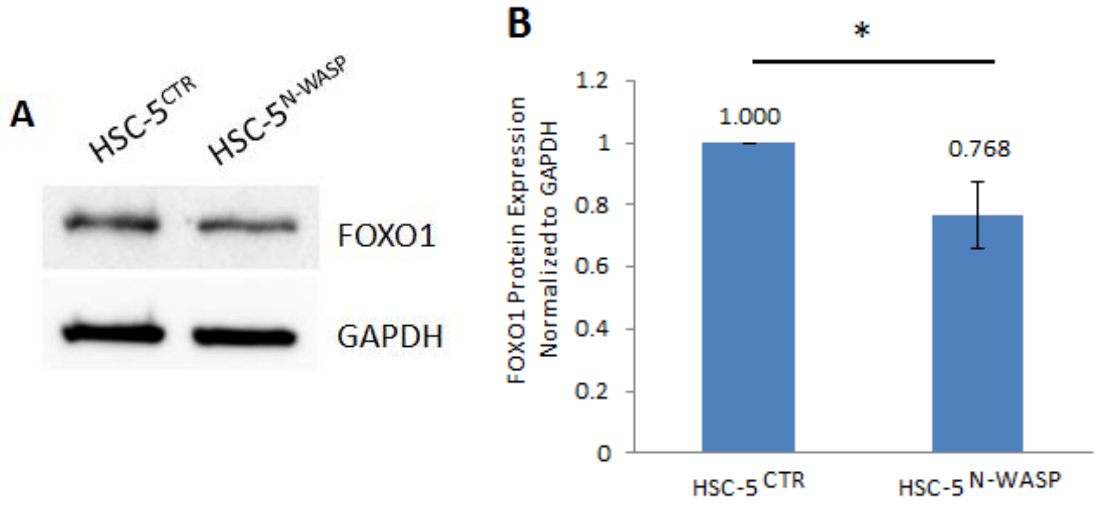

Figure 56: FOXO1 expression is reduced in HSC-5$^{N\text{-}WASP}$ cells compared to HSC-5^{CTR} cells. A) Equal amounts of HSC-5^{CTR} and HSC-5$^{N\text{-}WASP}$ cell protein lysates were loaded for Western blot analysis using anti-FOXO1 and anti-GAPDH antibodies. B) Densitometric quantifications show significant reduction of FOXO1 protein levels in HSC-5$^{N\text{-}WASP}$ cells compared to HSC-5^{CTR} cells. Experiments were performed in triplicates. Significance: *P<0.05 (Student's t-test).

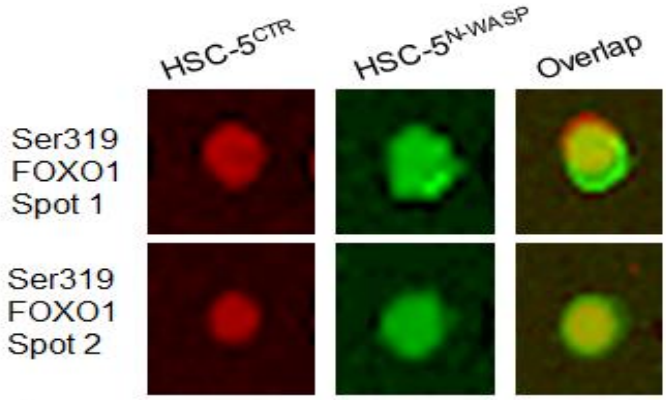

Average HSC-5^{CTR} Value	Average HSC-5^{N-WASP} Value	HSC-5^{N-WASP}/HSC-5^{CTR} Value Ratio
2.286	3.700	1.619

Figure 57: Fluorescence images of protein microarray for phospho-Ser319 FOXO1 of HSC-5^{CTR} and HSC-5^{N-WASP} cells. Equal amounts of HSC-5^{CTR} and HSC-5^{N-WASP} cell protein lysates were subjected to the Kinex KAM-880 Antibody Microarray kit according to manufacturer instructions. The microarrays were read with the GenePix 4000B reader using the Gene Pix Pro 6.0 program, and the values of each duplicate spots were measured, averaged and compared to that of HSC-5^{CTR} cells. These focused spots are derived from the microarray images of HSC-5^{CTR} and HSC-5^{N-WASP} cells (Fig. 33-35).

To determine if phosphorylated FOXO1 is proteasomally-degraded in HSC-5 cells, both HSC-5 sublines were treated with either DMSO as a control or MG132, an inhibitor that prevents proteasomal degradation of ubiquitinated proteins [239]. The MG132 (Sigma) optimized working concentration was 10 µM. A Western blot for probing FOXO1 in cell lysates of all treated HSC-5 sublines and 293T cells transfected with empty pTT2-Neo vector or pTT2-FOXO1g-Neo, sourced from pcDNA-FLAG-FKHR (Addgene #13507) by Prof Kunliang Guan (Massachusetts Institute of Technology, USA) [240] to overexpress exogenous FOXO1, was performed. DMSO-treated HSC-5^{N-WASP} cells had reduced FOXO1 expression compared to DMSO-treated HSC-5^{CTR} cells, but both these expressions are less than those of MG132-treated HSC-5 sublines (arrow for FOXO1 size, around 75 kDa) (Fig. 58A). Densitometric quantification of FOXO1 bands against GAPDH bands showed significant increases in FOXO1 protein levels in MG132-treated HSC-5 sublines compared to DMSO-treated HSC-5 sublines (Fig. 58B). Altogether, these results suggest that when HSC-5 cells overexpress N-WASP, FOXO1 is phosphorylated and translocated to the cytoplasm for proteasomal degradation.

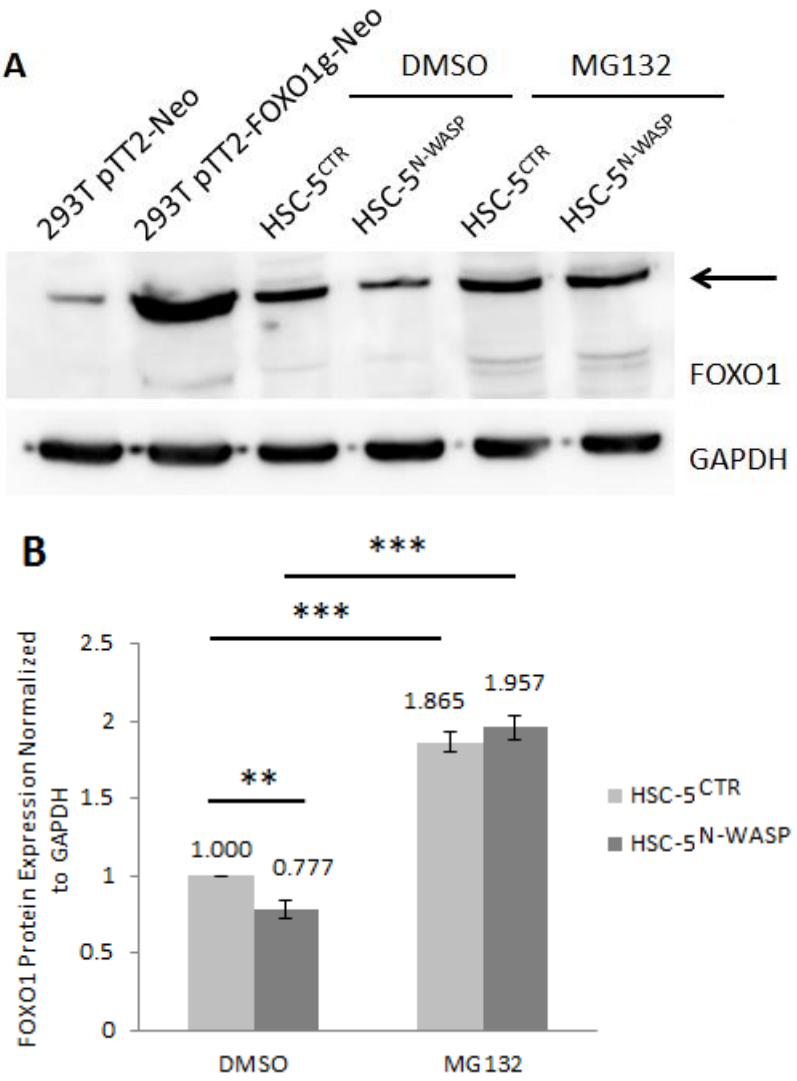

Figure 58: MG132-treated HSC-5 sublines have similar FOXO1 expressions, which are higher than that of DMSO-treated HSC-5 sublines. Both HSC-5^{CTR} and HSC-$5^{N\text{-}WASP}$ cells were first incubated with either DMSO or MG132 for 6 hours prior to cell lysis. A) Equal amounts of HSC-5 sublines' total protein lysates were loaded for Western blot analysis using anti-FOXO1 and anti-GAPDH antibodies. B) Densitometric quantifications show no significant difference of FOXO1 protein levels between HSC-5^{CTR} and HSC-$5^{N\text{-}WASP}$ cells incubated with MG132, compared to HSC-5^{CTR} cells treated with DMSO. Experiments were performed in triplicates. Significance: $^{**}P<0.01$, $^{***}P<0.001$ (Student's *t*-test).

4.1.7 HSC-$5^{N\text{-}WASP}$ cells have reduced nuclear FOXO1 compared to HSC-5^{CTR} cells

Phosphorylation of FOXO proteins lead to their translocation from the nucleus to the cytoplasm for proteasomal degradation [112,113]. N-WASP overexpression in HSC-5 cells correlated with reduced FOXO1 protein levels (Fig. 56). To determine if FOXO1 translocation from the nucleus to the cytoplasm occurs in HSC-5 cells, immunohistochemistry to visualize FOXO1 and the nucleus was performed on HSC-5^{CTR}

and HSC-5$^{N\text{-}WASP}$ cells. HSC-5^{CTR} cells had high green fluorescence corresponding to FOXO1 in the nuclear and perinuclear regions, whereas HSC-5$^{N\text{-}WASP}$ cells had far reduced nuclear FOXO1, and FOXO1 appears more prominently in the perinuclear region and likely spread further within the cytoplasm (Fig. 59). The immunohistochemistry assay was repeated on the HSC-5 sublines with DMSO and MG132 treatment. FOXO1 localizations in DMSO-treated and MG132-treated HSC-5$^{N\text{-}WASP}$ cells are similar, while FOXO1 localizations in DMSO-treated and MG132-treated HSC-5^{CTR} cells are also similar (Fig. 60). These results suggest that FOXO1 translocation from nucleus to cytoplasm in HSC-5 cells does occur.

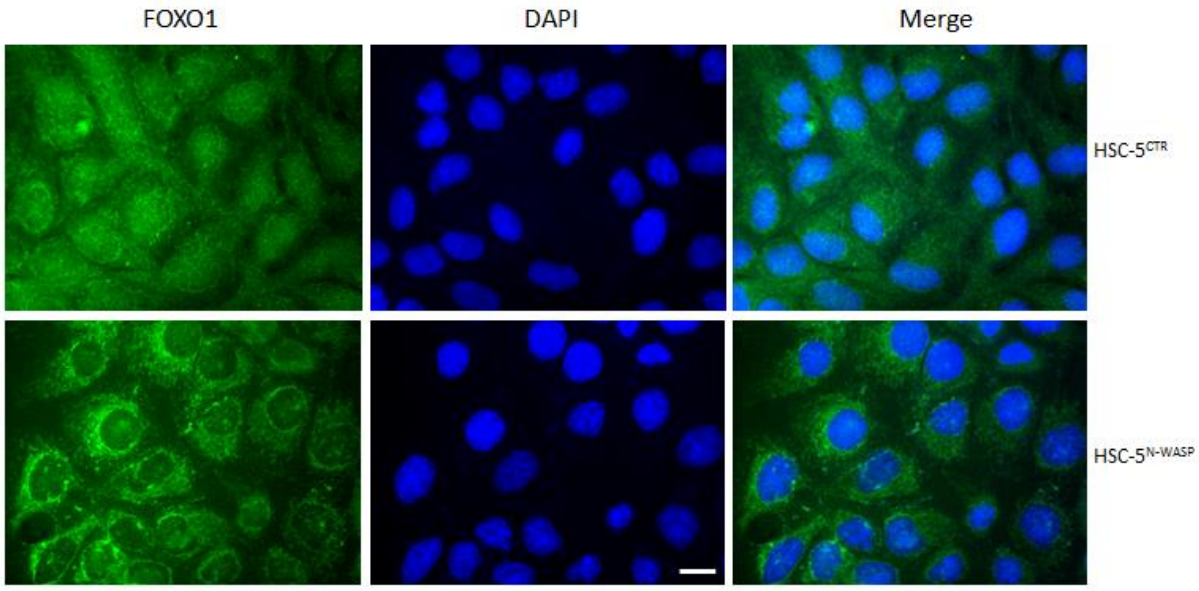

Figure 59: HSC-5$^{N\text{-}WASP}$ cells have reduced nuclear FOXO1 compared to HSC-5^{CTR} cells. Both HSC-5 sublines were seeded on coverslips in 6-well plates, incubated, then fixed and probed with anti-FOXO1 (1°) antibody and Alexa488 conjugates (2°), and with DAPI, under view of 40X objectives lens. Note the difference in green fluorescence in both cell lines where the nucleus is concerned; HSC-5$^{N\text{-}WASP}$ cells have observable areas where nuclei are present and the intensity correlating with levels of FOXO1 localization. Scale bar represents 20 µm. Experiments were performed in triplicates.

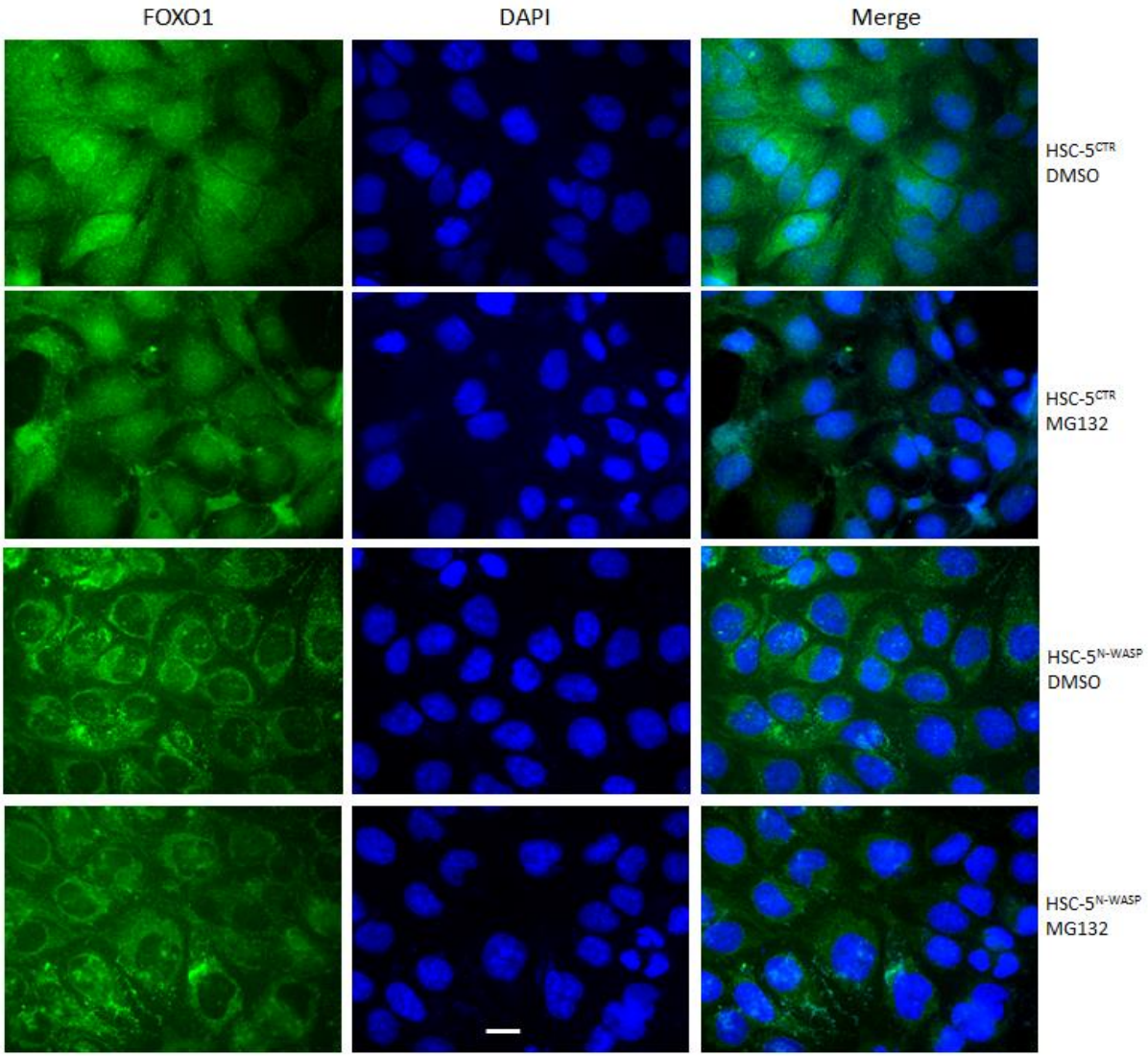

Figure 60: MG132 treatment of HSC-5 sublines does not stabilize nuclear FOXO1. Both HSC-5 sublines were seeded on coverslips in 6-well plates, incubated in presence of DMSO or MG132, then fixed and probed with anti-FOXO1 (1°) antibody and Alexa488 conjugates (2°), and with DAPI, under view of 40X objective lens. Note the difference in green fluorescence in cell lines where the nucleus is concerned; HSC-$5^{N\text{-}WASP}$ cells have observable areas where nuclei are present and the intensity correlating with levels of FOXO1 localization. Scale bar represents 20 µm. Experiments were performed in triplicates.

4.1.8 Exogenous overexpression of FOXO1 does not increase proliferation of HSC-$5^{N\text{-}WASP}$ cells, but does increase proliferation of HaCaT cells

Studies about FOXO1 role in cell signalling have been performed in liver cell lines [116], although studies in glial and lung cell lines have been done too [118,201]. To our knowledge, no studies of the role of FOXO1 in human SCC skin cells have been performed. Since HSC-$5^{N\text{-}WASP}$ cells had reduced cell proliferation (Fig. 18) and FOXO1 protein levels (Fig. 56) compared to HSC-5^{CTR} cells, it is possible FOXO1

overexpression in HSC-5$^{N\text{-}WASP}$ cells may rescue FOXO1 protein levels and cell proliferation defects to that of HSC-5^{CTR} cells.

FOXO1 was overexpressed in both HSC-5 sublines and HaCaT cells to study the role of FOXO1 in human skin cells. Both cell lines were infected with third-generation lentivirus derived from empty pTT2-Neo vector or pTT2-FOXO1g-Neo to overexpress exogenous FOXO1, and selected with neomycin. Western blots of all four HSC-5 sublines and two HaCaT sublines for FOXO1 and cell proliferation assays were performed. HSC-5$^{CTR\text{-}FOXO1}$ and HSC-5$^{N\text{-}WASP\text{-}FOXO1}$ cells had increased FOXO1 expressions compared to HSC-5$^{CTR\text{-}CTR}$ and HSC-5$^{N\text{-}WASP\text{-}CTR}$ cells, and HSC-5$^{N\text{-}WASP\text{-}FOXO1}$ cells had FOXO1 expression exceeding those of HSC-5$^{CTR\text{-}CTR}$ cells (Fig. 61A). Densitometric quantification of FOXO1 bands against GAPDH bands showed the increases in FOXO1 protein levels are significant (Fig. 61B). However, HSC-5$^{N\text{-}WASP\text{-}FOXO1}$ cells proliferated similarly like HSC-5$^{N\text{-}WASP\text{-}CTR}$ cells, while HSC-5$^{CTR\text{-}FOXO1}$ cells proliferated at significantly reduced rates compared to HSC-5$^{CTR\text{-}CTR}$ cells (Fig. 61C). In contrast, HaCaT^{FOXO1} cells had increased FOXO1 expression compared to HaCaT^{CTRN} cells (Fig. 62A), and densitometric quantifications of FOXO1 bands against GAPDH bands showed HaCaT^{FOXO1} cells had significantly increased FOXO1 protein levels than HaCaT^{CTRN} cells (Fig. 62B). HaCaT^{FOXO1} cells had significantly increased proliferation rates than HaCaT^{CTRN} cells (Fig. 62C). These suggested that FOXO1 plays different roles in the cell proliferation of HSC-5 and HaCaT cells.

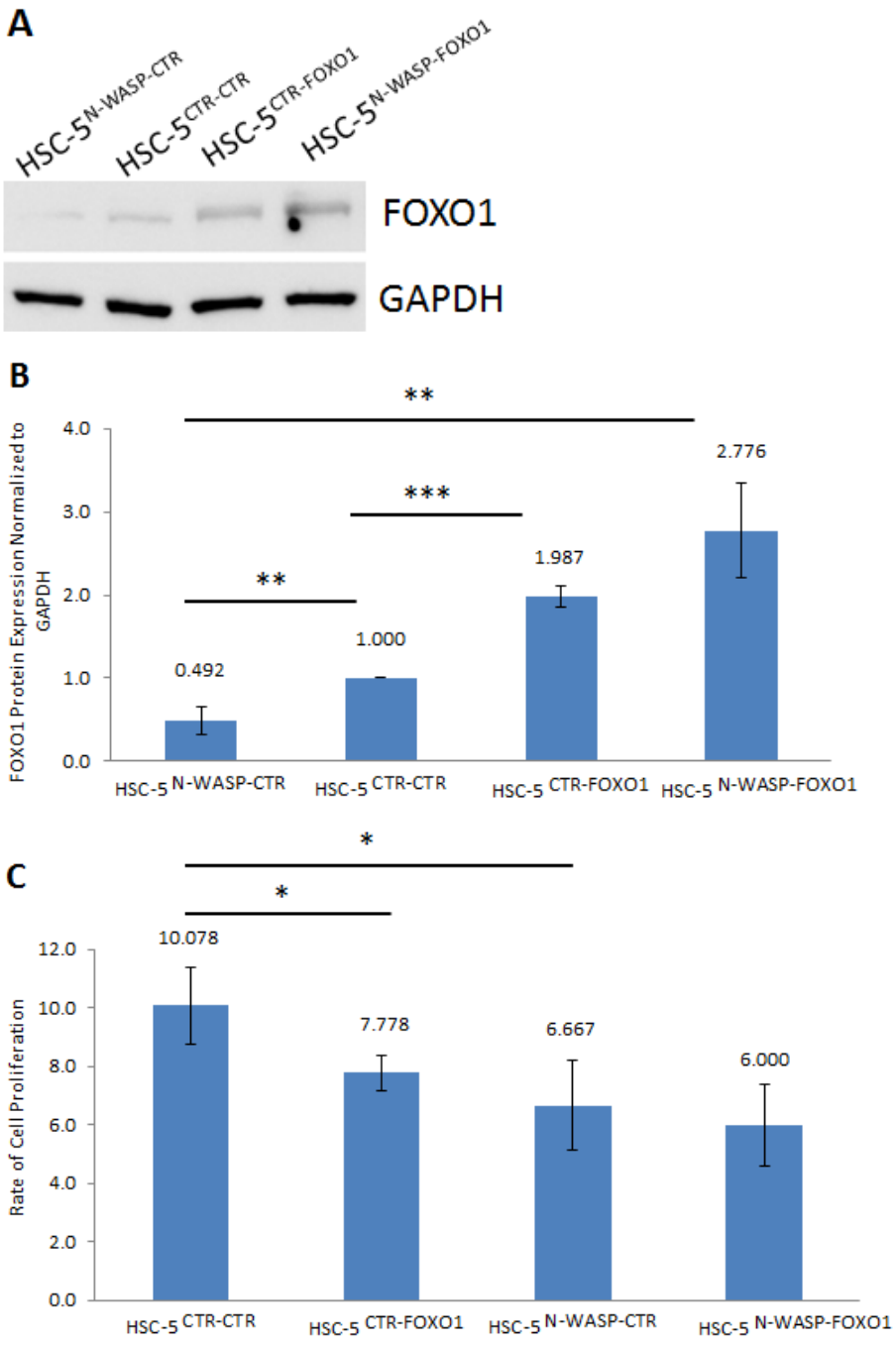

Figure 61: HSC-5 sublines overexpressing FOXO1 in general have reduced cell proliferation compared to control HSC-5 sublines. HSC-5^{CTR} and HSC-$5^{N\text{-}WASP}$ cells were made to overexpress FOXO1 against controls. A) Equal amounts of the four HSC-5 sublines' protein lysates were loaded for Western blot analysis using anti-FOXO1 and anti-GAPDH antibodies. B) Densitometric quantifications show significant increase of FOXO1 protein levels in HSC-5 sublines overexpressing FOXO1 compared to HSC-$5^{CTR\text{-}CTR}$ cells. C) 7.5 x 10^3 cells of each cell line were seeded in 24-well plates, incubated for 5 days, trypsinized and counted using a hemacytometer. The rate of proliferation was obtained by comparing total cell counted after 5 days against the number of cells seeded. Experiments were performed in triplicates. Significance: **P*<0.05, ***P*<0.01, ****P*<0.001 (Student's *t*-test).

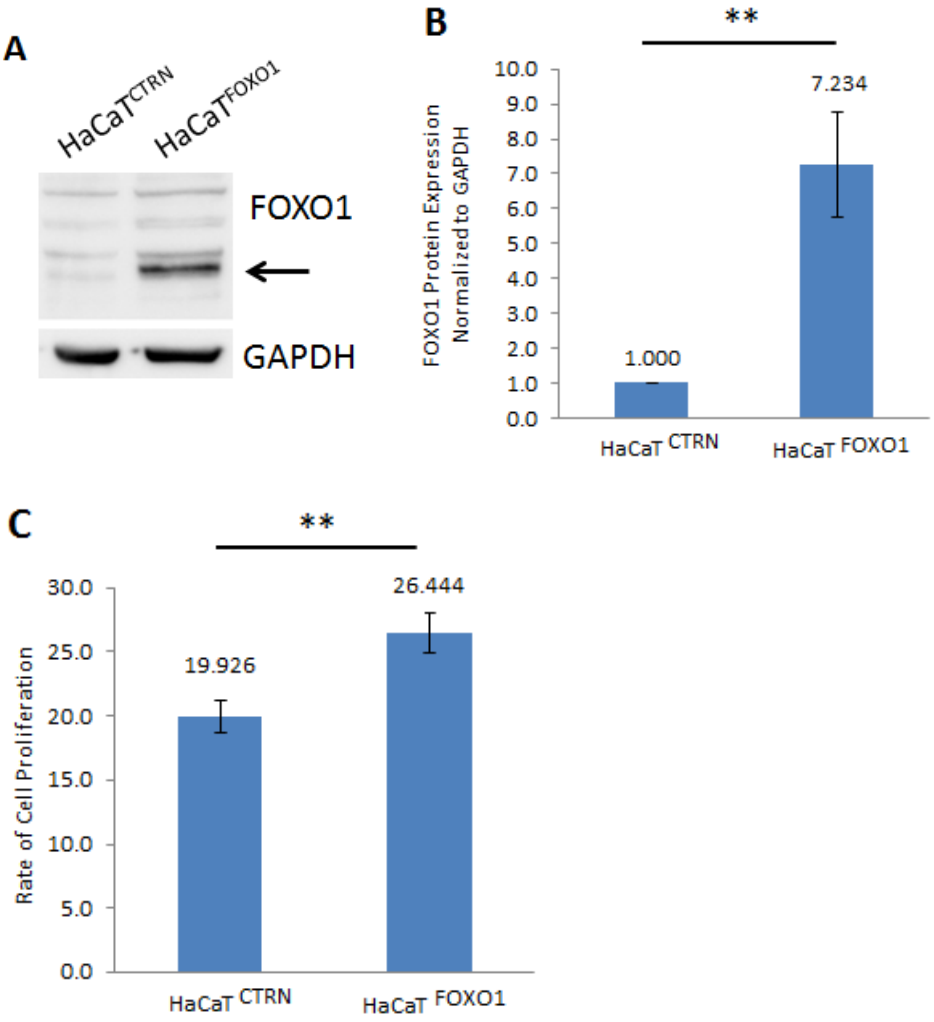

Figure 62: HaCaT^{FOXO1} cells have increased cell proliferation compared to HaCaT^{CTRN} cells. A) Equal amounts of HaCaT^{CTR-N} and HaCaT^{FOXO1} cell protein lysates were loaded for Western blot analysis using anti-FOXO1 and anti-GAPDH antibodies. B) Densitometric quantifications show significant increase of FOXO1 protein levels in HaCaT^{FOXO1} cells compared to HaCaT^{CTR-N} cells. C) 7.5 x 10^3 cells of each cell line were seeded in 24-well plates, incubated for 5 days, trypsinized and counted using a hemacytometer. The rate of proliferation was obtained by comparing total cell counted after 5 days against the number of cells seeded. Experiments were performed in triplicates. Significance: $^{**}P<0.01$ (Student's *t*-test).

4.1.9 Reduction of cell proliferation of HSC-5^{N-WASP} cells compared to HSC-5^{CTR} cells is not caused by the kinases SGK1 and JNKs 1, 2 and 3

It is generally accepted that AKT-phosphorylated FOXO proteins translocate out of the nucleus [241]. AKT1 and AKT3 specifically phosphorylate FOXO3, while AKT2 specifically phosphorylates FOXO1 [242,243]. Other kinases also phosphorylate the FOXOs. SGK1 phosphorylates FOXO1 to cause similar nuclear translocation and cytoplasmic degradation [117,243,244]. The JNKs phosphorylate FOXO1 in pancreatic

cancer cells, resulting in cell apoptosis [116]. Protein microarray analysis showed up-regulated phospho-JNK activity (HSC-$5^{N\text{-}WASP}$/HSC-5^{CTR} value ratio: 1.778) (Table 3), although RNA-Seq data showed up-regulated JNK1 and 2 mRNA levels and JNK3 mRNA levels are slightly increased (HSC-$5^{N\text{-}WASP}$/HSC-5^{CTR} value ratio: 3.120, 2.110 and 1.018 respectively) (Table 5). RNA-Seq data showed up-regulated SGK1 mRNA levels (HSC-$5^{N\text{-}WASP}$/HSC-5^{CTR} value ratio: 3.336) (Table 5). Any of these kinases could be regulating FOXO1 in HSC-5 cells.

HSC-$5^{N\text{-}WASP}$ cells have reduced AKT activity (Fig. 27,28) and reduced cell proliferation (Fig. 18) compared to HSC-5^{CTR} cells. When N-WASP was overexpressed in HSC-5 cells, FOXO1 protein levels are reduced via kinase-dependent nuclear translocation and cytoplasmic proteasomal degradation (Fig. 56-59). These suggest that AKTs do not cause FOXO1 phosphorylation and reduction of protein levels in HSC-5 cells when N-WASP is overexpressed. If AKT-dependent reduction of HSC-5 cell proliferation occurs, this is possibly due to N-WASP-mediated reduced FOXO1 protein levels. Therefore, AKT isoform studies were not performed here.

To determine if SGK1 mRNA expression changes are valid, a real-time PCR on both HSC-5 sublines for SGK1 was performed. HSC-$5^{N\text{-}WASP}$ cells had significantly increased SGK1 mRNA levels compared to HSC-5^{CTR} cells (Fig. 63A). Real-time PCR results thus correlate with RNA-Seq results. To evaluate the effects of SGK1 activity on HSC-5 cell proliferation, SGK knockdown (KD) was performed by infecting both HSC-5 sublines with third-generation lentivirus derived from empty pTT2-Neo vector or pTT2-SGK1sh-Neo to knock down SGK1, and selected with neomycin. Cell proliferation assays were performed on the four HSC-5 sublines before further assays such as Western blot and wound healing were done, to determine if SGK1 knockdown can rescue HSC-$5^{N\text{-}WASP}$ cell proliferation defects. However, SGK1 knockdown in HSC-5^{CTR} and HSC-$5^{N\text{-}WASP}$ cells did not increase cell proliferation rates, instead causing further reduction of cell proliferation rates which were significant compared to HSC-$5^{CTR\text{-}CTR}$ and HSC-$5^{N\text{-}WASP\text{-}CTR}$ cells (Fig. 63B).

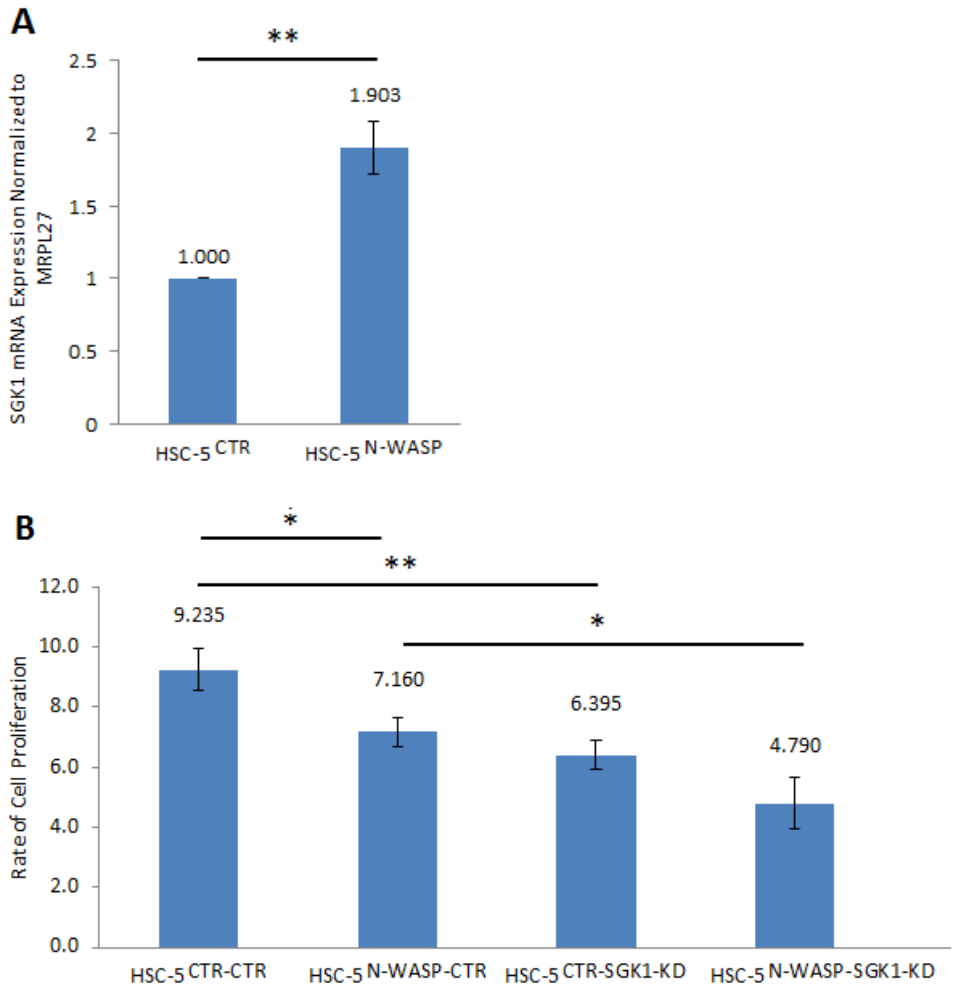

Figure 63: HSC-5 sublines with SGK1 knockdown via shRNA have reduced cell proliferation compared to control HSC-5 sublines. A) Equal amounts of cDNA from HSC-5^{CTR} and HSC-5$^{N\text{-}WASP}$ cells were subjected to real-time PCR analysis of SGK1 cDNA, normalized to MRPL27, showing significant increase of SGK1 mRNA levels in HSC-5$^{N\text{-}WASP}$ cells, compared to HSC-5^{CTR} cells. B) 7.5 x 10^3 cells of each cell line were seeded in 24-well plates, incubated for 5 days, trypsinized and counted using a hemacytometer. The rate of proliferation was obtained by comparing total cell counted after 5 days against the number of cells seeded. Experiments were performed in triplicates. Significance: *P<0.05, **P<0.01 (Student's t-test).

Concerning the role of JNK proteins, as generating multiple lentiviruses targeting each JNK1, JNK2 and JNK3 may cause immense stress on HSC-5 sublines after multiple antibiotic selections, an inhibitor capable of targeting all three JNK isoforms simultaneously, SP600125 (Santa Cruz), was employed. SP600125 selectively inhibits all three JNK isoforms in a dose-dependent manner between 20 to 50 µM working concentrations at recommended increments of 10 µM [245]. HSC-5^{CTR} and HSC-5$^{N\text{-}WASP}$ cells were treated with either DMSO as a control or SP600125 in varying concentrations. Cell proliferation assays performed with 20 µM SP600125 showed HSC-5 sublines with

similar proliferation rates when compared to DMSO control (Fig. 64A). HSC-5^{CTR} cells still proliferated at a higher rate compared to HSC-$5^{N\text{-}WASP}$ cells, both even in DMSO. However, when 50 µM SP600125 was employed to both HSC-5 sublines, cell proliferation rates did not increase but instead were reduced further and significantly compared to DMSO-treated HSC-5 sublines (Fig. 64B). These results suggest the SGK1 and JNK kinases are not responsible for causing reduced HSC-$5^{N\text{-}WASP}$ cell proliferation.

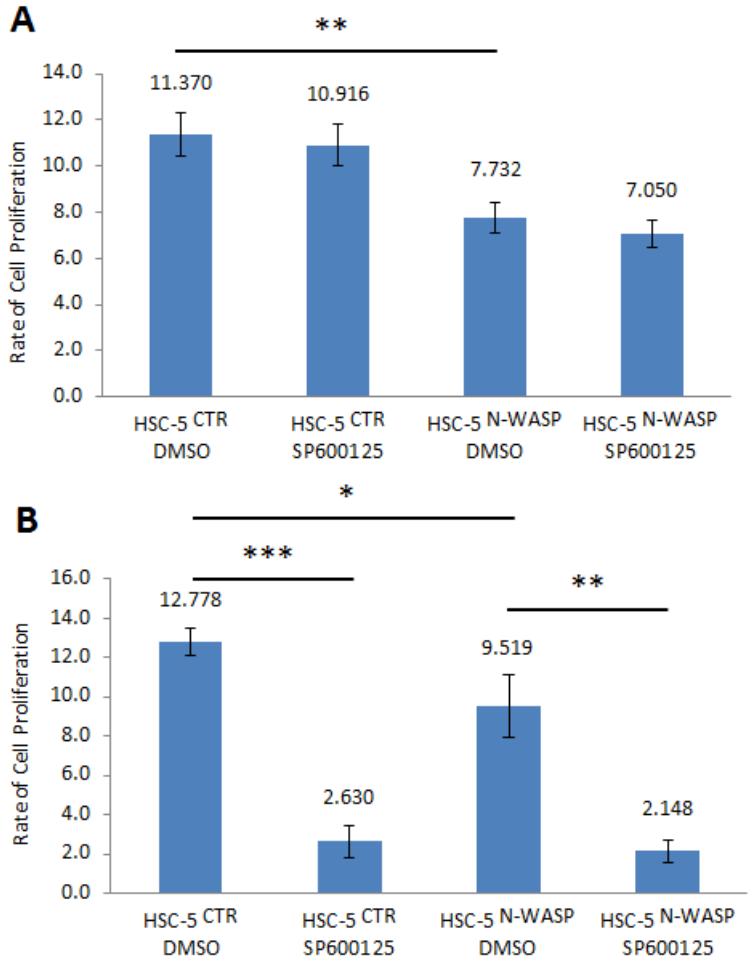

Figure 64: SP600125-treated HSC-5 sublines have reduced cell proliferation in a dose-dependent manner compared to DMSO-treated HSC-5 sublines. Both HSC-5 sublines were incubated in DMSO and A) 20 µM SP600125 or B) 50 µM SP600125. 7.5 x 10^3 cells of each cell line were seeded in 24-well plates, incubated for 5 days, trypsinized and counted using a hemacytometer. The rate of proliferation was obtained by comparing total cell counted after 5 days against the number of cells seeded. Experiments were performed in triplicates. Significance: **P*<0.05, ***P*<0.01, ****P*<0.001 (Student's *t*-test).

4.1.10 HSC-5$^{N\text{-}WASP}$ cells have increased ERK2 activity compared to HSC-5^{CTR} cells

The MAPKs ERK1/2 are well-known to promote cell proliferative activity. This signalling is made mainly through the RAS-RAF-MEK-MAPK signalling axis, where kinases activating other kinases (MAPK kinase kinase (MAP3K) phosphorylating MAP2K phosphorylating MAPKs) lead to translocation into the nucleus to phosphorylate targets and either induce or inhibit specific cell signaling [172]. In HepG2 liver cells, increased SOS1 levels correlated with increased ERK1/2-dependent cell proliferative activity [217]. Knockdown studies on either ERK1 or 2 or both suggest that true proliferative stimulation comes from ERK2 alone, that ERK1 activity may be either silent or is a back-up for ERK2 knockout, although lack of ERK1 activity is suggested to be due to its expression being lower than that of ERK2 [246,247]. RNA-Seq showed HSC-5$^{N\text{-}WASP}$ cells with up-regulated ERK2 mRNA levels but very reduced ERK1 mRNA levels (HSC-5$^{N\text{-}WASP}$/HSC-5^{CTR} FPKM value ratio: 2.300 and 0.544, respectively) (Table 5).

A Western blot of HSC-5^{CTR} and HSC-5$^{N\text{-}WASP}$ cells for phospho-Thr202/Tyr204 ERK1/2 and pan-ERK1/2 was performed to study ERK1/2 expression in HSC-5 cells. HSC-5$^{N\text{-}WASP}$ cells had slight increases of pan-ERK2 and pan-ERK1 expressions compared to HSC-5^{CTR} cells, whereas its phospho-ERK2 expression was increased compared to HSC-5^{CTR} cells (Fig. 65A). Phospho-ERK1 bands were not observed at all. Densitometric quantification of ERK2 phospho-to-pan-specific bands against GAPDH bands showed HSC-5$^{N\text{-}WASP}$ cells with a significantly increased active ERK2 compared to HSC-5^{CTR} cells (Fig. 65B).

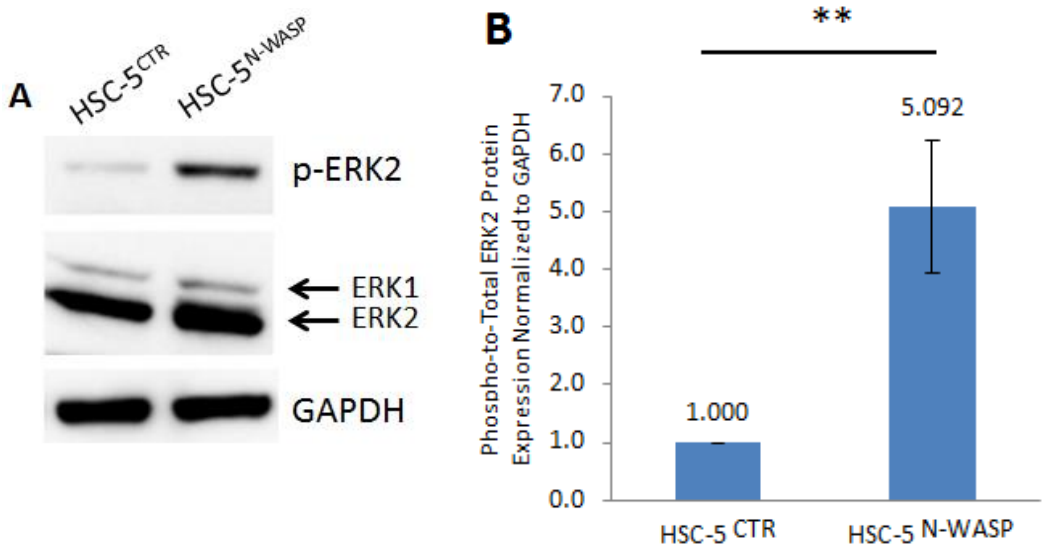

Figure 65: HSC-5$^{N\text{-}WASP}$ cells have increased active ERK2 compared to HSC-5^{CTR} cells. A) Equal amounts of HSC-5^{CTR} and HSC-5$^{N\text{-}WASP}$ cell protein lysates were loaded for Western blot analysis using anti-phospho-Thr202/Tyr204 ERK1/2, anti-pan-ERK1/2 and anti-GAPDH antibodies. B) Densitometric quantifications show significant increase of active ERK2 levels in HSC-5$^{N\text{-}WASP}$ cells compared to HSC-5^{CTR} cells. Experiments were performed in triplicates. Significance: $^{**}P<0.01$ (Student's *t*-test).

4.1.11 Inhibition of ERK2 in HSC-5$^{N\text{-}WASP}$ cells increased proliferation rates

It was reported that inhibition of ERK1/2 in MCF7 lung cells restored protein synthesis and ERK1/2 is a potential therapeutic target for tuberous sclerosis treatment [248]. It is possible increased ERK2 activity in HSC-5 cells reduced cell proliferative activity. To confirm this possibility, cell proliferation assays of HSC-5^{CTR} and HSC-5$^{N\text{-}WASP}$ cells were performed in presence of DMSO as a control and the ERK2-specific inhibitor, sc-222229 (Santa Cruz). sc-222229 is highly selective for ERK2 with a recommended working concentration of 2 nM. sc-222229-treated HSC-5$^{N\text{-}WASP}$ cells had cell proliferation rates similar to that of DMSO-treated HSC-5^{CTR} cells and significantly higher than that of DMSO-treated HSC-5$^{N\text{-}WASP}$ cells (Fig.66). HSC-5$^{N\text{-}WASP}$ cells still proliferated at a significantly slower rate than HSC-5^{CTR} cells.

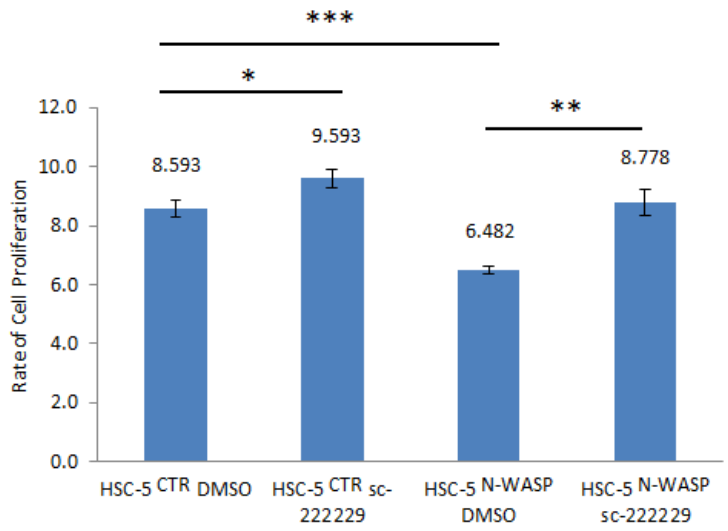

Figure 66: sc-222229-treated HSC-5$^{N\text{-}WASP}$ cells and DMSO-treated HSC-5^{CTR} cells have similar cell proliferation rates. Both HSC-5 sublines were incubated in DMSO or sc-222229. 7.5 x 10^3 cells of each cell line were seeded in 24-well plates, incubated for 5 days, trypsinized and counted using a hemacytometer. The rate of proliferation was obtained by comparing total cell counted after 5 days against the number of cells seeded. Experiments were performed in triplicates. Significance: **P*<0.05, ***P*<0.01, ****P*<0.001 (Student's *t*-test).

4.1.12 Inhibition of ERK2 in HSC-5$^{N\text{-}WASP}$ cells partially rescued Cyclin D1 levels

As stated earlier, Cyclin D1 (CCND1) is a cell proliferation marker, since elevated expressions caused increased RB phosphorylation and promoted cell cycle transit past the G1 phase [155]. Since sc-222229-treated HSC-5$^{N\text{-}WASP}$ cells had similar cell proliferation to that of DMSO-treated HSC-5$^{CTR\text{-}CTR}$ cells (Fig. 66), and CCND1 protein levels in HSC-5^{CTR} and HSC-5$^{N\text{-}WASP}$ cells correlated with their cell proliferation rates (Fig. 18,19), it is possible sc-222229 treatment restored HSC-5$^{N\text{-}WASP}$ cell CCND1 protein levels to that of DMSO-treated HSC-5^{CTR} cells. A Western blot of DMSO- and sc-222229-treated HSC-5 sublines for CCND1 expression was performed. sc-222229-treated HSC-5$^{N\text{-}WASP}$ cells had higher CCND1 expression than DMSO-treated HSC-5$^{N\text{-}WASP}$ cells but lower than DMSO-treated HSC-5^{CTR} cells (Fig. 67A). DMSO-treated HSC-5$^{N\text{-}WASP}$ cells had reduced CCND1 expression compared to DMSO-treated HSC-5^{CTR} cells, similar to previous observations (Fig. 19). Densitometric quantifications of CCND1 bands against GAPDH bands showed that any comparisons between two of these three was significantly different to one another (Fig. 67B).

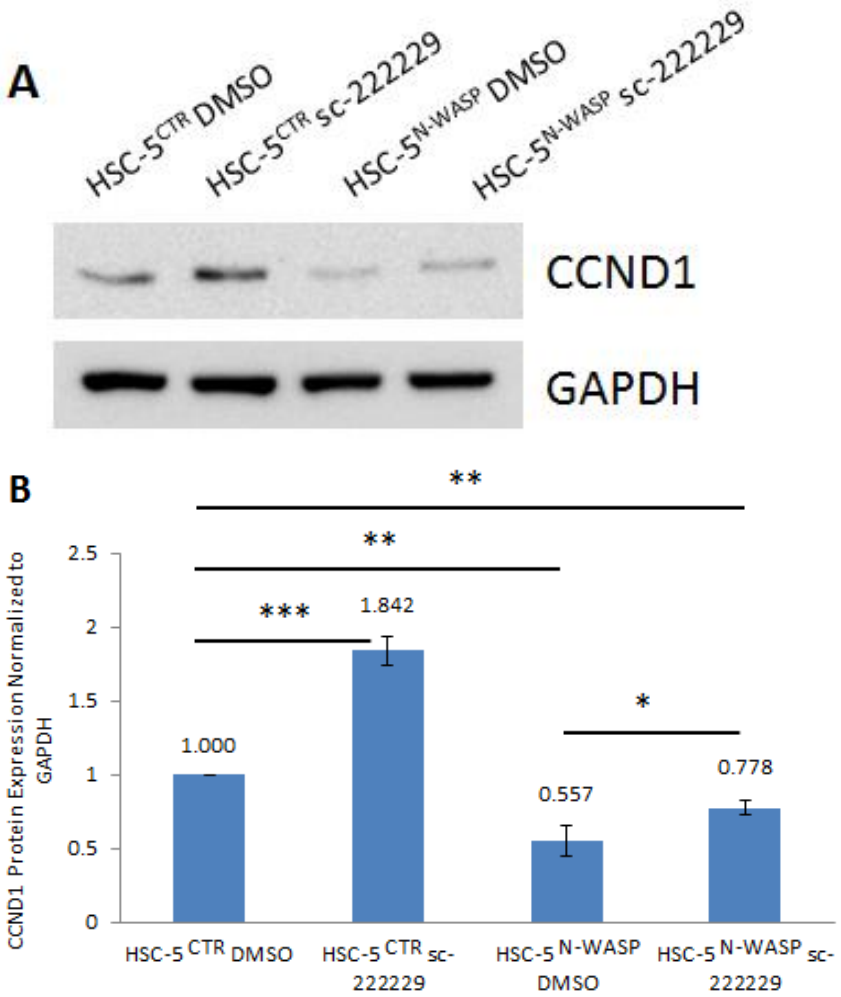

Figure 67: sc-222229-treated HSC-5$^{N\text{-}WASP}$ cells have CCND1 levels higher than that of DMSO-treated HSC-5$^{N\text{-}WASP}$ cells but lower than that of DMSO-treated HSC-5^{CTR} cells. Both HSC-5 sublines were incubated in DMSO or sc-222229 prior to cell lysis. A) Equal amounts of HSC-5^{CTR} and HSC-5$^{N\text{-}WASP}$ cell protein lysates were loaded for Western blot analysis using anti-CCND1 and anti-GAPDH antibodies. B) Densitometric quantifications show significant difference in CCND1 levels when sc-222229-treated HSC-5$^{N\text{-}WASP}$ cells were compared to both DMSO-treated HSC-5^{CTR} and HSC-5$^{N\text{-}WASP}$ cells. Experiments were performed in triplicates. Significance: *P<0.05, **P<0.01, ***P<0.001 (Student's t-test).

4.1.13 Inhibition of ERK2 in HSC-5$^{N\text{-}WASP}$ cells increased FOXO1 expression

Since sc-222229 treatment reversed HSC-5$^{N\text{-}WASP}$ cell proliferation rates to that of DMSO-treated HSC-5^{CTR} cells, it is possible that sc-222229 treatment restored FOXO1 protein levels of HSC-5$^{N\text{-}WASP}$ cells to that of HSC-5^{CTR} cells. Studies showed that ERK1/2 inhibited FOXO proteins via phosphorylation and MDM2 ubiquitination [249], and ERK2 phosphorylated FOXO1 at many other residues than Ser256 and Ser319 in NIH3T3 cells [250]. It is possible that ERK2 is the kinase phosphorylating FOXO1 in HSC-5 cells.

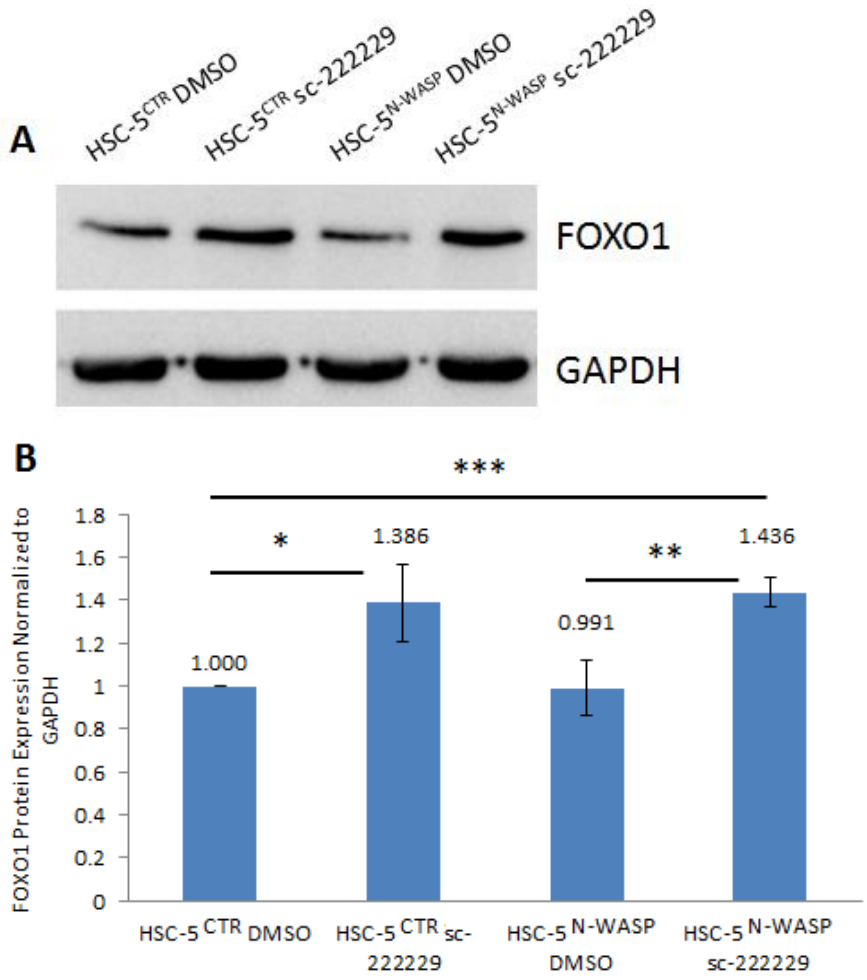

Figure 68: sc-222229-treated HSC-5 sublines have similar FOXO1 expressions, which are higher than those of DMSO-treated HSC-5 sublines. Both HSC-5 sublines were incubated in DMSO or sc-222229 prior to cell lysis. A) Equal amounts of HSC-5^{CTR} and HSC-$5^{N\text{-}WASP}$ cell protein lysates were loaded for Western blot analysis using anti-FOXO1 and anti-GAPDH antibodies. B) Densitometric quantifications show no significant difference of FOXO1 protein levels between HSC-5^{CTR} and HSC-$5^{N\text{-}WASP}$ cells incubated with sc-222229, as well as of protein levels between HSC-5^{CTR} and HSC-$5^{N\text{-}WASP}$ cells incubated with DMSO, compared to HSC-5^{CTR} cells treated with DMSO. Experiments were performed in triplicates. Significance: **P*<0.05, ***P*<0.01, ****P*<0.001 (Student's *t*-test).

A Western blot of DMSO- and sc-222229-treated HSC-5 sublines for FOXO1 expression was performed. FOXO1 expressions of DMSO-treated HSC-5 sublines were similar, in contrast to previous observations (Fig. 56), but sc-222229-treated HSC-5 sublines had similar FOXO1 expressions which were higher than those of DMSO-treated HSC-5 sublines (Fig. 68A). It is possible that the DMSO-treated HSC-$5^{N\text{-}WASP}$ cells may have successfully increased FOXO1 expression via increased transcription, in order to compensate for the reduced protein levels previously observed due to N-WASP overexpression (Fig. 56). Densitometric quantifications of FOXO1 bands against

GAPDH bands show that sc-222229 treatment of each HSC-5 subline had significantly increased the FOXO1 protein levels compared to the respective DMSO treatment (Fig. 68B). These results suggested that ERK2 phosphorylates FOXO1 in HSC-5 cells.

4.1.14 Inhibition of ERK2 in HSC-$5^{N\text{-}WASP}$ cells stabilized nuclear FOXO1 expression

Since sc-222229 treatment reversed HSC-$5^{N\text{-}WASP}$ cell proliferation rates to that of DMSO-treated HSC-5^{CTR} cells, it is possible that FOXO1 localizations in sc-222229-treated HSC-$5^{N\text{-}WASP}$ cells have changed or at least become similar to those of DMSO-treated HSC-5^{CTR} cells. Immunohistochemistry to visualize FOXO1 and the nucleus on both HSC-5 sublines with and without sc-222229 treatment was performed. Similar to previous observations (Fig. 59,60), DMSO-treated HSC-$5^{N\text{-}WASP}$ cells had reduced nuclear FOXO1 compared to DMSO-treated HSC-5^{CTR} cells (Fig. 69). sc-222229-treated HSC-5^{CTR} cells have increased FOXO1 localized in the nuclear and perinuclear regions. However, sc-222229 treatment of HSC-$5^{N\text{-}WASP}$ cells appears to have stabilized nuclear FOXO1 compared to DMSO treatment, making it similar to that of DMSO-treated HSC-5^{CTR} cells. This suggested that ERK2-dependent FOXO1 phosphorylation and cytoplasmic translocation occurs in HSC-5 cells.

This was elaborated with performance of cell lysate fractionation and Western blot of both cytosolic and nuclear fractions of both HSC-5 sublines treated with DMSO and sc-222229 for FOXO1 expression, to determine if ERK2 influences FOXO1 translocation to the cytoplasm in HSC-5 cells. DMSO-treated HSC-$5^{N\text{-}WASP}$ cells had a higher cytosolic FOXO1 expression compared to DMSO-treated HSC-5^{CTR} cells (left arrow, around 75 kDa), wheras sc-222229-treated HSC-5 sublines had reduced cytosolic FOXO1 expressions compared to DMSO-treated HSC-5 sublines (Fig. 70A). Nuclear fractions of DMSO- and sc-222229-treated HSC-5 sublines had FOXO1 expressions of a bigger size (right arrow) and other sizes, suggesting that FOXO1 ubiquitination occurred in the nucleus. GAPDH mainly localizes in the cytoplasm, while Lamin B1 localizes in the nucleus. Ponceau S staining showed the equal loading of cell lysate fraction proteins, even though Lamin B1 expressions differ between each nuclear fraction. Densitometric quantifications of cytosolic FOXO1 bands against GAPDH bands show a significant reduction of cytosolic FOXO1 protein levels in sc-222229-treated HSC-5 sublines compared to DMSO-treated HSC-5 sublines (Fig. 70B).

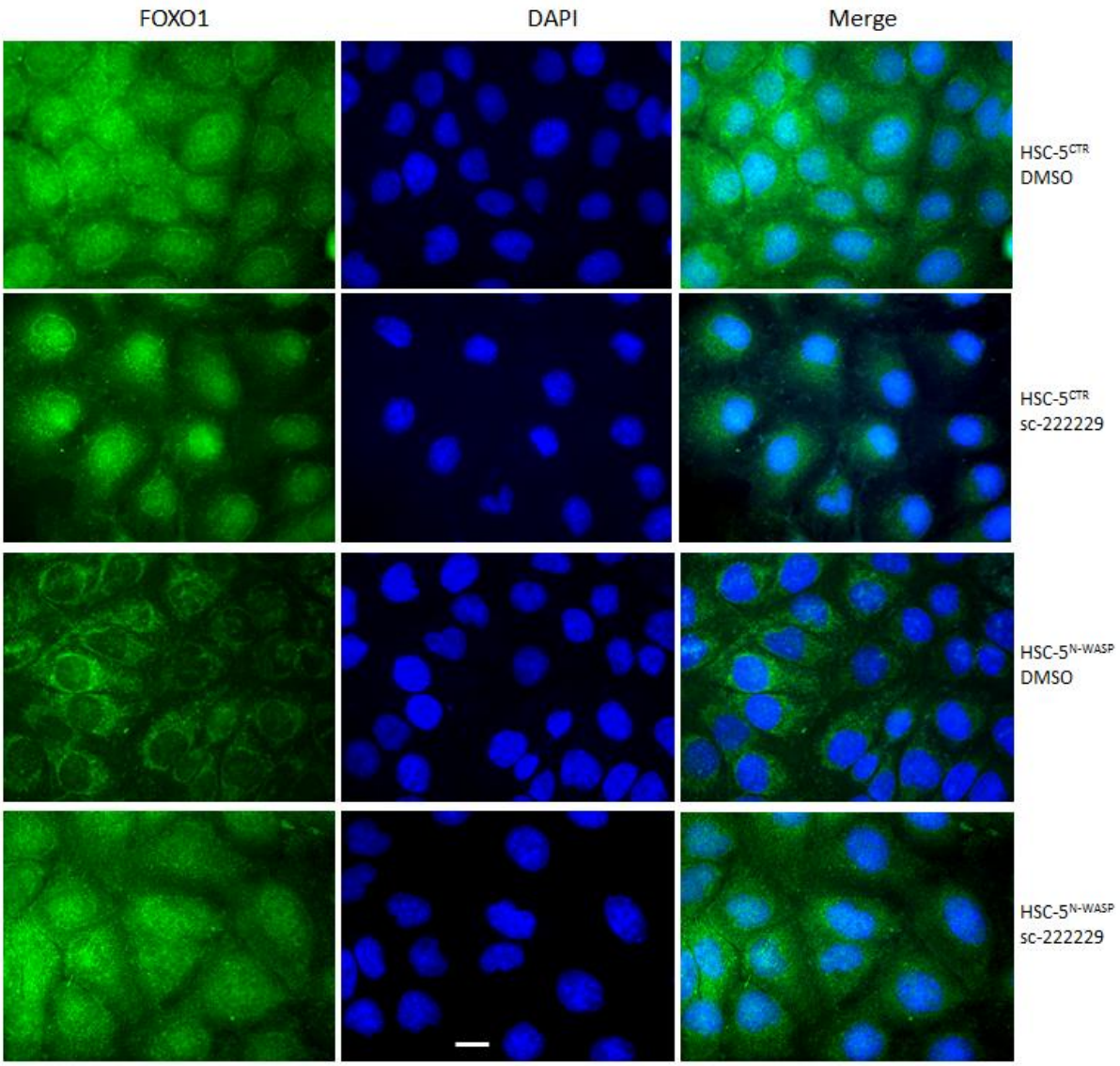

Figure 69: sc-222229-treated HSC-5$^{N\text{-}WASP}$ cells and DMSO-treated HSC-5^{CTR} cells have similar nuclear FOXO1. Both HSC-5 sublines were seeded on coverslips in 6-well plates, incubated in presence of DMSO or sc-222229, then fixed and probed with anti-FOXO1 (1°) antibody and Alexa488 conjugates (2°), and with DAPI, under view of 40X objective lens. Note the difference in green fluorescence in cell lines where the nucleus is concerned; HSC-5$^{N\text{-}WASP}$ cells have observable areas where nuclei are present and the intensity correlating with levels of FOXO1 localization. Scale bar represents 20 µm. Experiments were performed in triplicates.

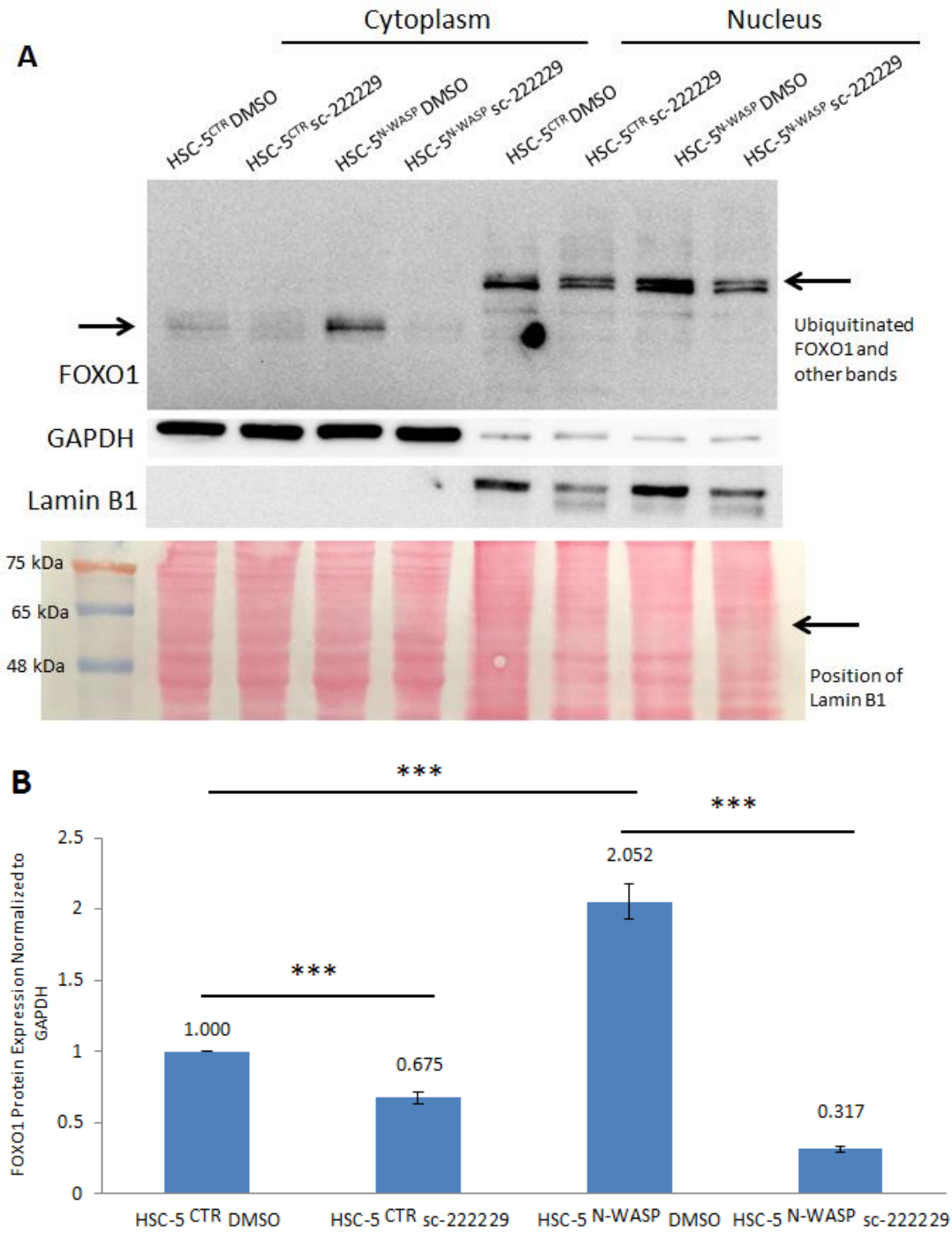

Figure 70: sc-222229-treated HSC-5 sublines have reduced cytosolic FOXO1 compared to DMSO-treated HSC-5 sublines. Both HSC-5 sublines were incubated in DMSO and sc-222229 prior to cell lysis and cell lysate fractionation. A) Equal amounts of HSC-5^{CTR} and HSC-$5^{N\text{-}WASP}$ cell protein lysates were loaded for Western blot analysis using anti-FOXO1, anti-GAPDH and anti-Lamin B1 antibodies. The nitrocellulose membrane was also subjected to Ponceau S staining to reflect loading of equal cell lysate protein amounts. B) Densitometric quantifications show significant reduction of FOXO1 protein levels in cytoplasmic fraction of HSC-5 sublines with sc-222229 compared to HSC-5 sublines with DMSO, compared to HSC-5^{CTR} cells with DMSO. Experiments were performed in triplicates. Significance: ***$P<0.001$ (Student's *t*-test).

4.1.15 HSC-5$^{N\text{-}WASP}$ cells with ERK2 inhibition have reduced E-cadherin localizations to levels that of HSC-5^{CTR} cells

The reversal of cell proliferation rate of HSC-5$^{N\text{-}WASP}$ cells after sc-222229 treatment to that of DMSO-treated HSC-5^{CTR} cells raised the possibility that a similar reversal could occur to E-cadherin localizations in HSC-5 cells. Immunohistochemistry to visualize E-cadherin and actin in DMSO- and sc-222229-treated HSC-5 sublines was performed. DMSO-treated HSC-5$^{N\text{-}WASP}$ cells had the highest fluorescence representing E-cadherin localizations at the cell cortex, followed by both sc-222229-treated HSC-5$^{N\text{-}WASP}$ cells and DMSO-treated HSC-5^{CTR} cells which appear to have the same fluorescence, and sc-222229-treated HSC-5^{CTR} cells which had the least fluorescence (Fig. 71A). Quantification of average E-cadherin fluorescence intensities of all DMSO- and sc-222229-treated HSC-5 sublines also showed similar results (Fig. 71B).

This was followed with a Western blot of all four tested HSC-5 sublines for E-cadherin expression, which showed all four tested HSC-5 sublines having similar E-cadherin expressions (Fig. 72A). Densitometric quantifications of E-cadherin bands against GAPDH bands showed no significant differences in E-cadherin protein levels between all four tested HSC-5 sublines (Fig. 72B), suggesting that the reduction of E-cadherin localizations in skin cancer cells is not due to reduction of protein levels.

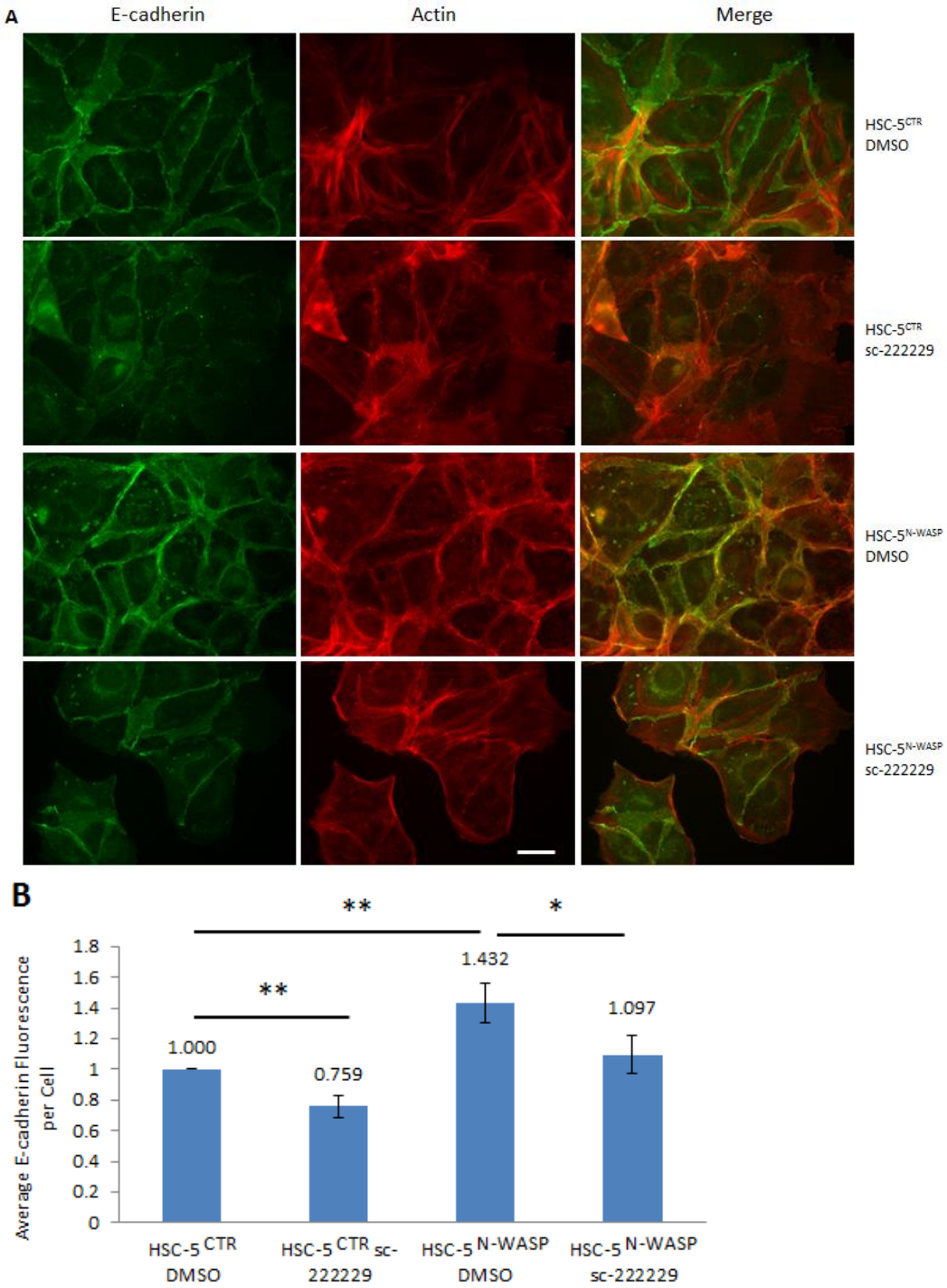

Figure 71: sc-222229-treated HSC-5$^{N\text{-}WASP}$ cells and DMSO-treated HSC-5^{CTR} cells have similar E-cadherin localizations. A) Both HSC-5 sublines were seeded on coverslips in 6-well plates, incubated in presence of DMSO or sc-222229, then fixed and probed with anti-E-cadherin (1°) antibody and Alexa488 conjugates (2°), and with Alexa568 conjugated phalloidin, under view of 40X objective lens. Note the difference in green fluorescence in all cell lines; the intensity correlating with levels of E-cadherin localization. Scale bar represents 20 µm. B) E-cadherin fluorescence was quantified by quantifying the fluorescence in hand-drawn regions of interest for each cell, each fluorescence value was divided by 2, and the total values were then averaged. The average fluorescence intensity was obtained from 20 random cells. Experiments were performed in triplicates. Significance: **P*<0.05, ***P*<0.01 (Student's *t*-test).

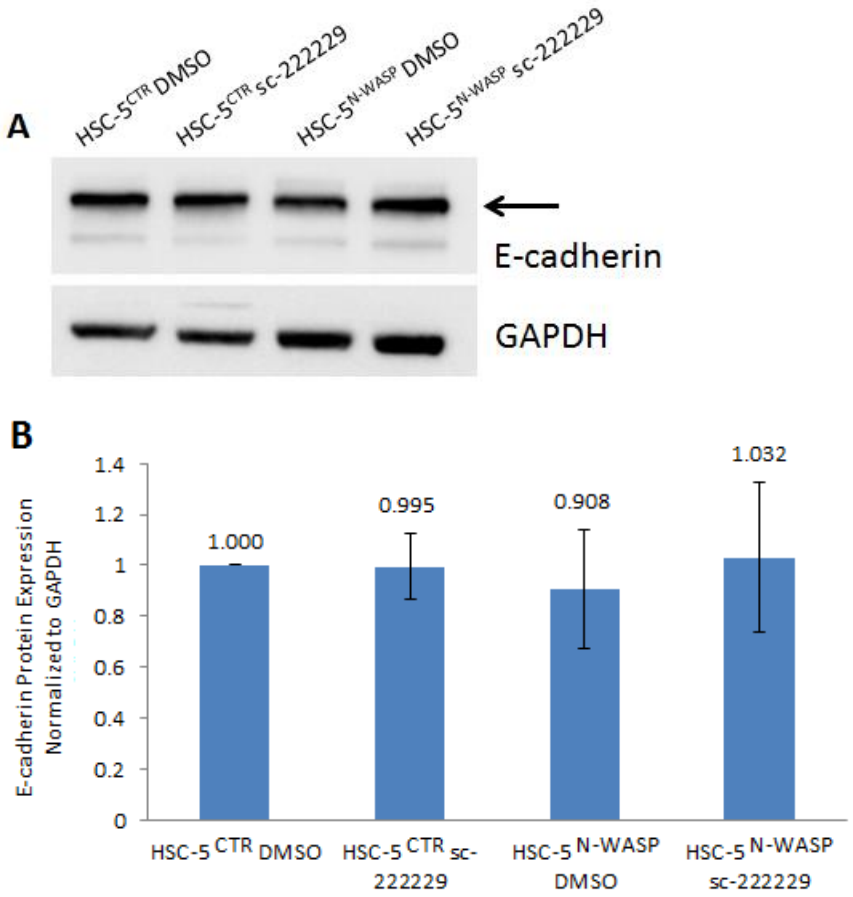

Figure 72: DMSO- and sc-222229-treated HSC-5 sublines have similar E-cadherin expressions. Both HSC-5 sublines were incubated in DMSO or sc-222229 prior to cell lysis. A) Equal amounts of cell protein lysates of HSC-5^{CTR} and HSC-5$^{N\text{-}WASP}$ cells were loaded for Western blot analysis using anti-E-cadherin and anti-GAPDH antibodies. B) Densitometric quantifications show no significant difference of E-cadherin protein levels between all DMSo- and sc-222229-treated HSC-5 sublines, compared to HSC-5^{CTR} cells with DMSO. Experiments were performed in triplicates. Significance: $P>0.05$ (Student's *t*-test).

4.1.16 HSC-5$^{N\text{-}WASP}$ cells with ERK2 inhibition migrated similarly like HSC-5^{CTR} cells

ERK2 inhibition in HSC-5$^{N\text{-}WASP}$ cells reversed proliferation rates to that of HSC-5^{CTR} cells. This raised the possibility of a reversal of cell migration phenotypes to those previously observed for HSC-5^{CTR} and HSC-5$^{N\text{-}WASP}$ cells (Fig. 22). Wound healing assays were performed on the DMSO- and sc-222229-treated HSC-5 sublines. 24 hours after scratches were made, DMSO-treated HSC-5$^{N\text{-}WASP}$ cells closed the wound gap the slowest (Fig. 73A). Naturally, DMSO-treated HSC-5$^{N\text{-}WASP}$ cells had the largest wound surface area, which was very significant (Fig. 73B). To dispel concerns that HSC-5 cell migration may be affected by cell proliferative activity, wound healing assays were

repeated with the cell proliferation inhibitor, cytosine arabinoside, or AraC [251]. The optimal concentration for AraC to inhibit HSC-5 cell proliferation was found to be 5 μM. Similar to earlier observations (Fig. 73A), 24 hours after scratches were made, DMSO-treated HSC-$5^{N\text{-}WASP}$ cells closed the wound gap the slowest (Fig. 74A). DMSO-treated HSC-$5^{N\text{-}WASP}$ cells had the largest wound surface area, which was very significant (Fig. 74B).

A closer observation on sc-222229-treated HSC-5^{CTR} cells at 24 hours that its cell population was heavily packed against each other (border of closed wound gap drawn in black lines) (Fig. 73A,74A), in comparison to both sc-222229-treated HSC-$5^{N\text{-}WASP}$ cells and DMSO-treated HSC-5^{CTR} cells which appear not too packed. This suggested that sc-222229-treated HSC-5^{CTR} cells closed the wound gap earlier than the 24-hour timepoint. To determine if this was true, wound healing assays of DMSO- and sc-222229-treated HSC-5 sublines with and without AraC were repeated for only 12 hours. sc-222229-treated HSC-5^{CTR} cells had the smallest wound surface area, followed by both sc-222229-treated HSC-$5^{N\text{-}WASP}$ cells and DMSO-treated HSC-5^{CTR} cells, and DMSO-treated HSC-$5^{N\text{-}WASP}$ cells which had the largest wound surface area (Fig. 75A,76A). The wound surface areas of sc-222229-treated HSC-$5^{N\text{-}WASP}$ cells and DMSO-treated HSC-5^{CTR} cells were not significantly different from one another, but sc-222229-treated HSC-$5^{N\text{-}WASP}$ cell wound surface area was significantly smaller than that of DMSO-treated HSC-$5^{N\text{-}WASP}$ cells (Fig. 75B,76B).

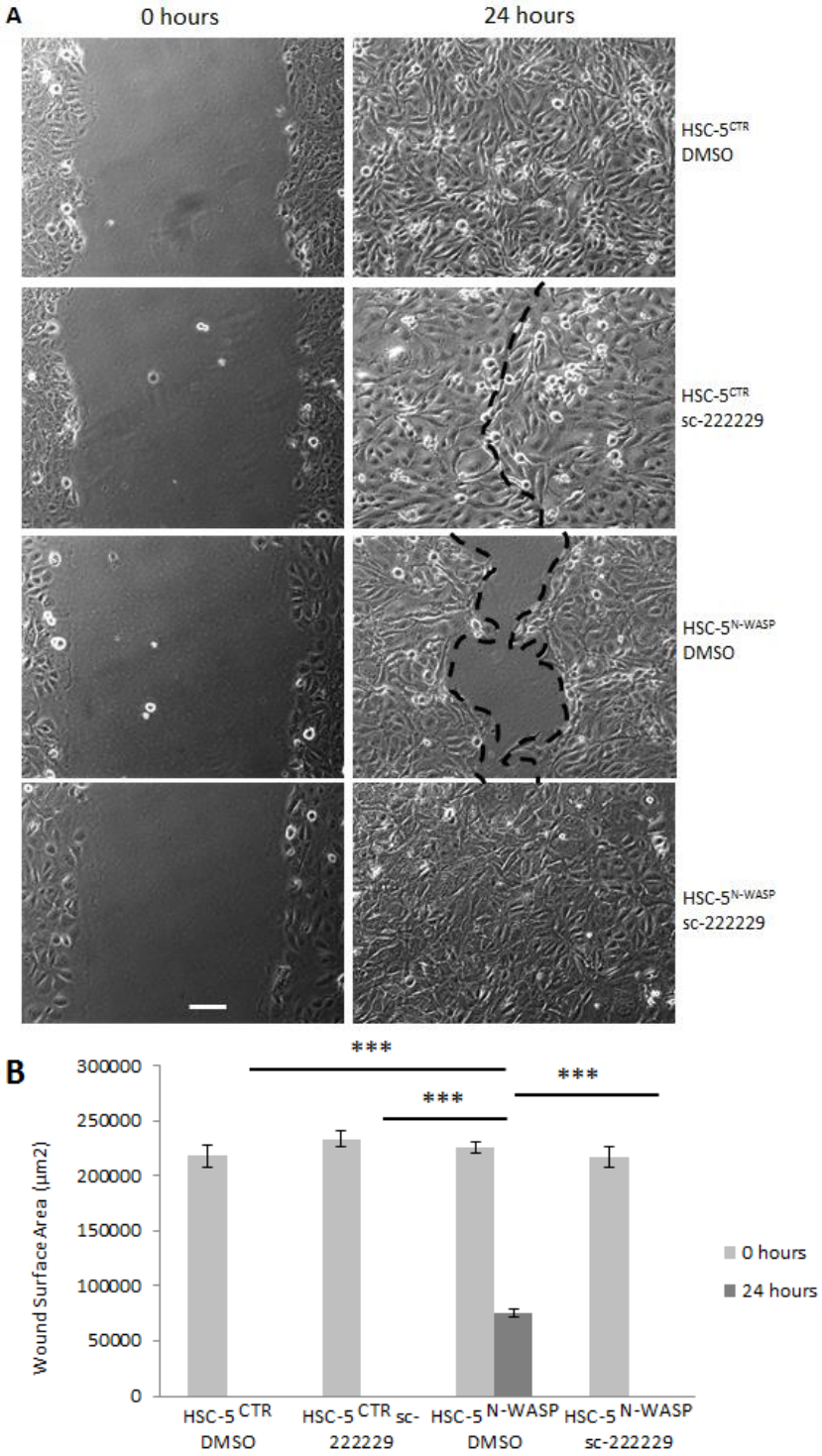

Figure 73: sc-222229-treated HSC-5$^{N\text{-}WASP}$ cells migrated similarly like DMSO-treated HSC-5^{CTR} cells. A) Cells were seeded such that prior to wound healing assay, the cell confluency would be 100%. Cells were incubated in complete DMEM supplemented with 2 nM sc-222229 after scratches were made and for the duration of the assay. Images were taken of the cells 0 hours and 24 hours after the scratches were made, under view of 10X objective lens. Scale bar represents 50 µm. B) Surface areas of wounds were measured at respective time points and compared, whereby sc-222229-treated HSC-5$^{N\text{-}WASP}$ cells closed the gap at a similar pace to DMSO-treated HSC-5^{CTR} cells. Experiments were performed in triplicates. Significance: ***P<0.001 (Student's *t*-test).

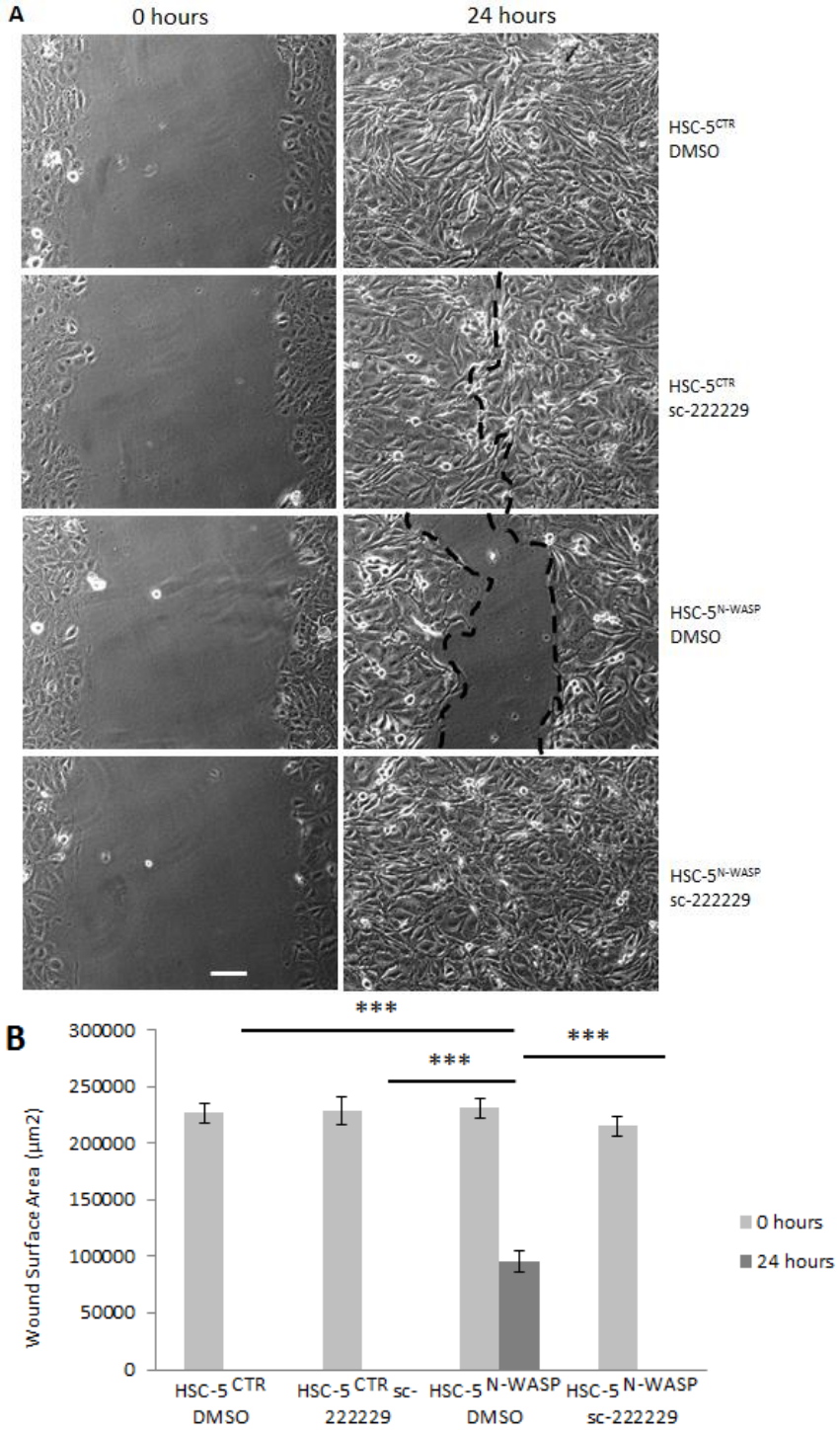

Figure 74: sc-222229-treated HSC-5$^{N\text{-}WASP}$ cells migrated similarly like DMSO-treated HSC-5^{CTR} cells even with AraC. A) Cells were seeded such that prior to wound healing assay, the cell confluency would be 100%. Cells were incubated in complete DMEM supplemented with 2 nM sc-222229 and 5 µM AraC after scratches were made and for the duration of the assay. Images were taken of the cells 0 hours and 24 hours after the scratches were made, under view of 10X objective lens. Scale bar represents 50 µm. B) Surface areas of wounds were measured at respective time points and compared, whereby sc-222229-treated HSC-5$^{N\text{-}WASP}$ cells closed the gap at a similar pace to DMSO-treated HSC-5^{CTR} cells. Experiments were performed in triplicates. Significance: ***P<0.001 (Student's t-test).

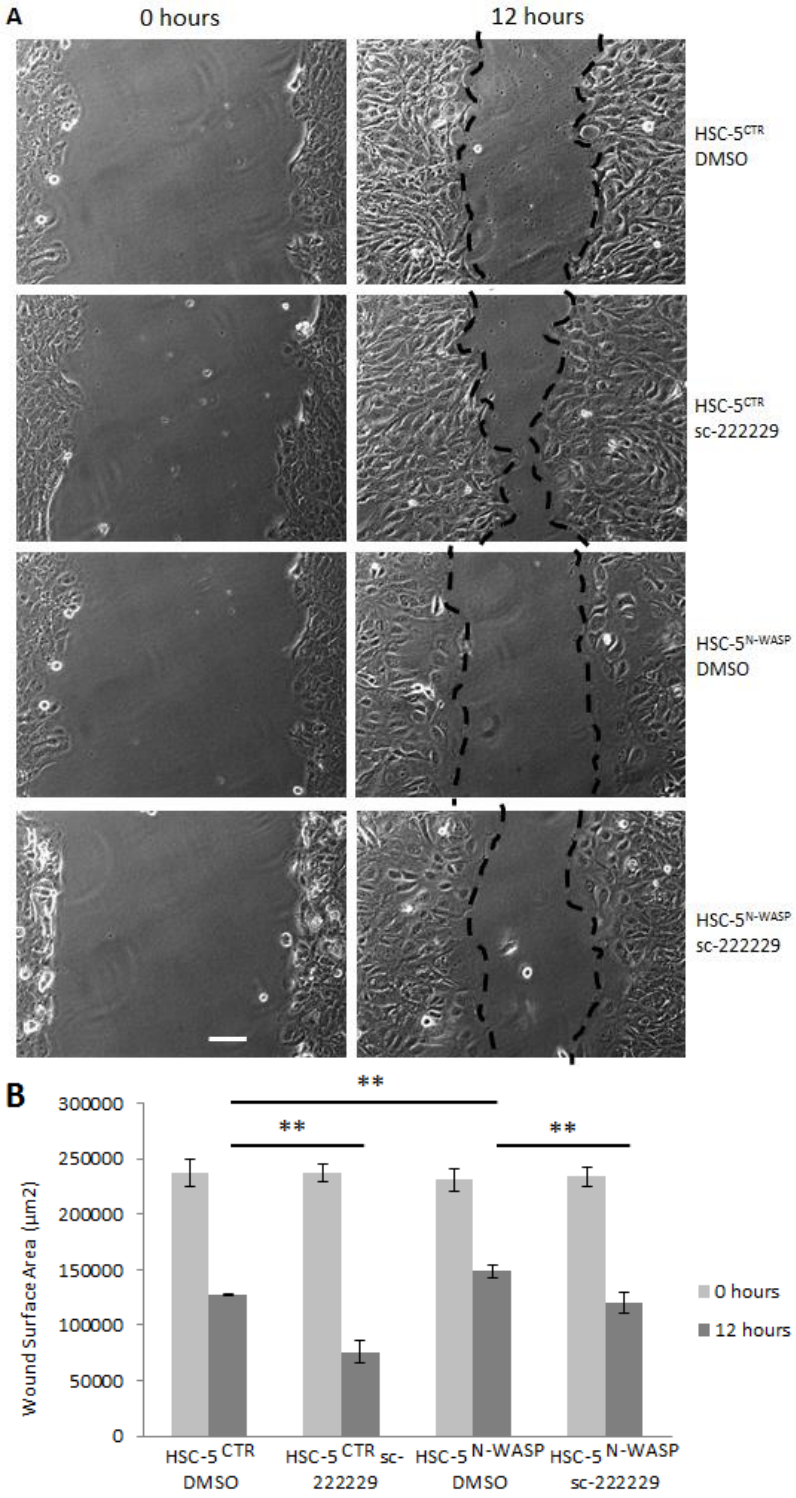

Figure 75: sc-222229-treated HSC-5^{CTR} cells migrated the fastest. A) Cells were seeded such that prior to wound healing assay, the cell confluency would be 100%. Cells were incubated in complete DMEM supplemented with 2 nM sc-222229 after scratches were made and for the duration of the assay. Images were taken of the cells 0 hours and 12 hours after the scratches were made, under view of 10X objective lens. Scale bar represents 50 µm. B) Surface areas of wounds were measured at respective time points and compared, whereby sc-222229-treated HSC-5^{CTR} cells close the gap fastest compared to the other three HSC-5 cell lines tested. Experiments were performed in triplicates. Significance: $^{**}P<0.01$ (Student's *t*-test).

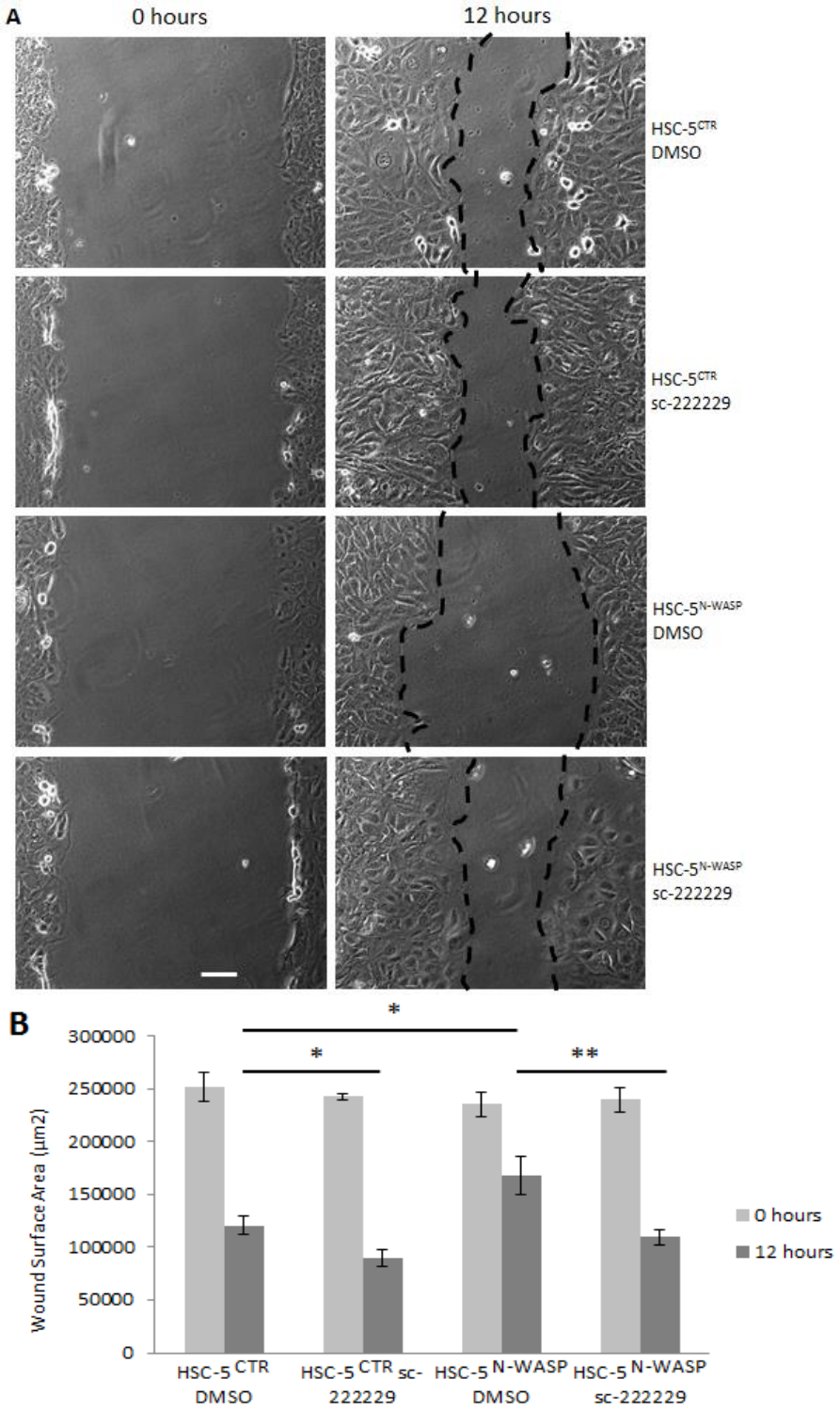

Figure 76: sc-222229-treated HSC-5^{CTR} cells migrated the fastest even with AraC. A) Cells were seeded such that prior to wound healing assay, the cell confluency would be 100%. Cells were incubated in complete DMEM supplemented with 2 nM sc-222229 and 5 µM AraC after scratches were made and for the duration of the assay. Images were taken of the cells 0 hours and 12 hours after the scratches were made, under view of 10X objective lens. Scale bar represents 50 µm. B) Surface areas of wounds were measured at respective time points and compared, whereby sc-222229-treated HSC-5^{CTR} cells close the gap fastest compared to the other three HSC-5 cell lines tested. Experiments were performed in triplicates. Significance: *P<0.05, **P<0.01 (Student's t-test).

4.1.17 HSC-5$^{N\text{-}WASP}$ cells with ERK2 inhibition have reduced vinculin localizations to levels that of HSC-5^{CTR} cells

Since inhibition of ERK2 in HSC-5$^{N\text{-}WASP}$ cells reversed cell migration phenotype to that of HSC-5^{CTR} cells, it is likely that vinculin localization phenotype was reversed in order to facilitate increased cell migration. Immunohistochemistry to visualize vinculin and actin in DMSO- and sc-222229-treated HSC-5 sublines and cell vinculin patch counts were performed. DMSO-treated HSC-5$^{N\text{-}WASP}$ cells had the most vinculin patches at the focal adhesion, followed by both sc-222229-treated HSC-5$^{N\text{-}WASP}$ cells and DMSO-treated HSC-5^{CTR} cells which had similar patch counts, and sc-222229-treated HSC-5^{CTR} cells which had the least patch count (Fig. 77A). The patch counts of sc-222229-treated HSC-5$^{N\text{-}WASP}$ cells and DMSO-treated HSC-5^{CTR} cells were not significant different from one another, but any other comparison was significantly different from one another (Fig. 77B).

This was followed with a Western blot of all four tested HSC-5 sublines for vinculin expression to determine if changes in vinculin localizations were due to changes in protein levels. All four tested HSC-5 sublines had similar vinculin expressions (Fig. 78A). Densitometric quantifications of vinculin bands against GAPDH bands showed no significant differences in vinculin protein levels between all four tested HSC-5 sublines (Fig. 78B), suggesting that the reduction of vinculin patches in skin cancer cells is not due to reduction of protein levels.

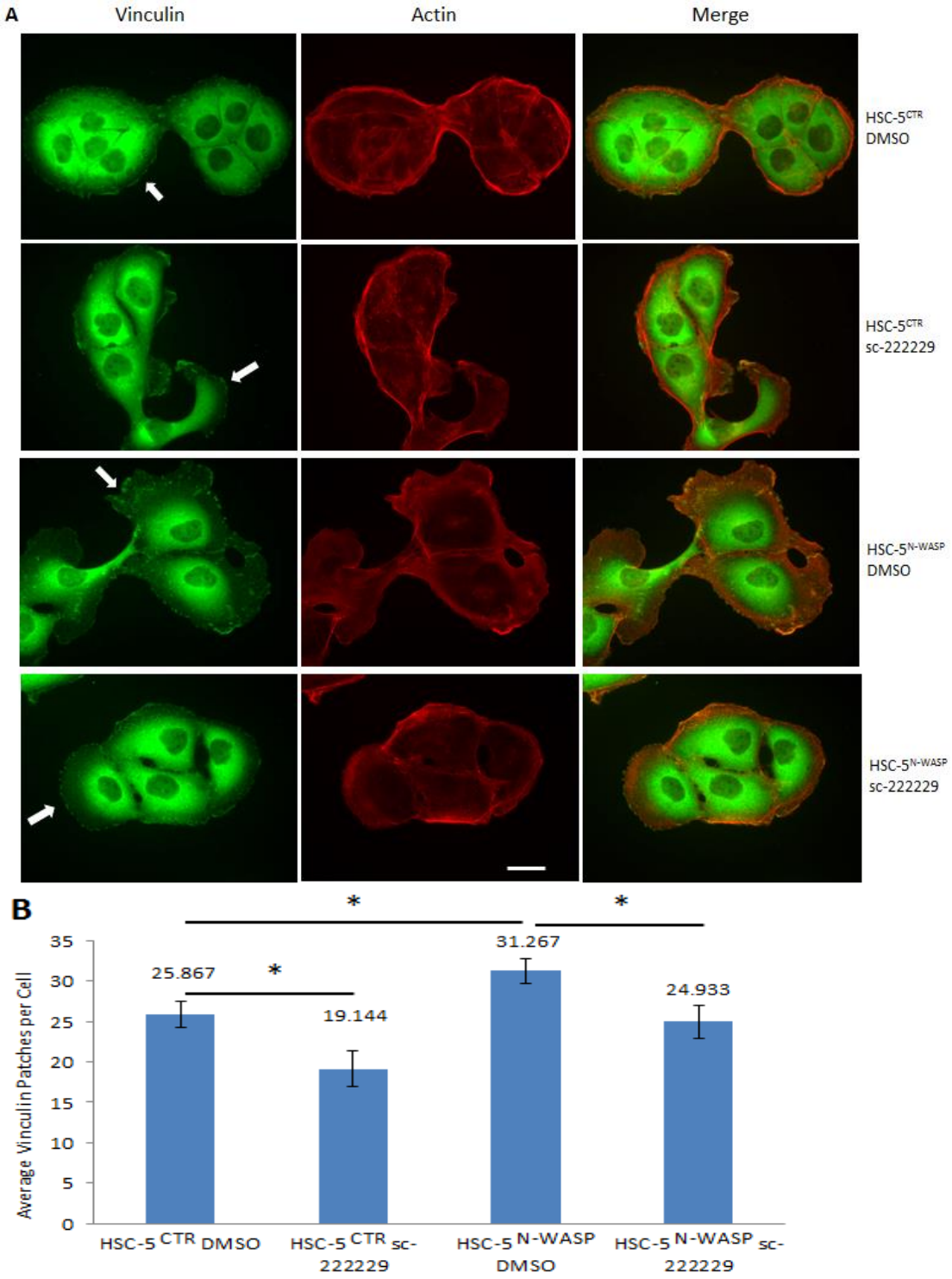

Figure 77: sc-222229-treated HSC-5$^{N\text{-}WASP}$ cells and DMSO-treated HSC-5^{CTR} cells have a similar number of vinculin patches. Both HSC-5 sublines were seeded on coverslips in 6-well plates, incubated in presence of DMSO or sc-222229, then fixed and probed with anti-vinculin (1°) antibody and Alexa488 conjugates (2°), and with Alexa568 conjugated phalloidin, under view of 40X objective lens. Note the difference in the number of observable green fluorescence streaks and dots at the cell membrane. Scale bar represents 20 µm. B) Vinculin patch count was performed by counting number of observable vinculin patches in 30 random cells, averaged, and compared to each other. Experiments were performed in triplicates. Significance: *P<0.05 (Student's t-test).

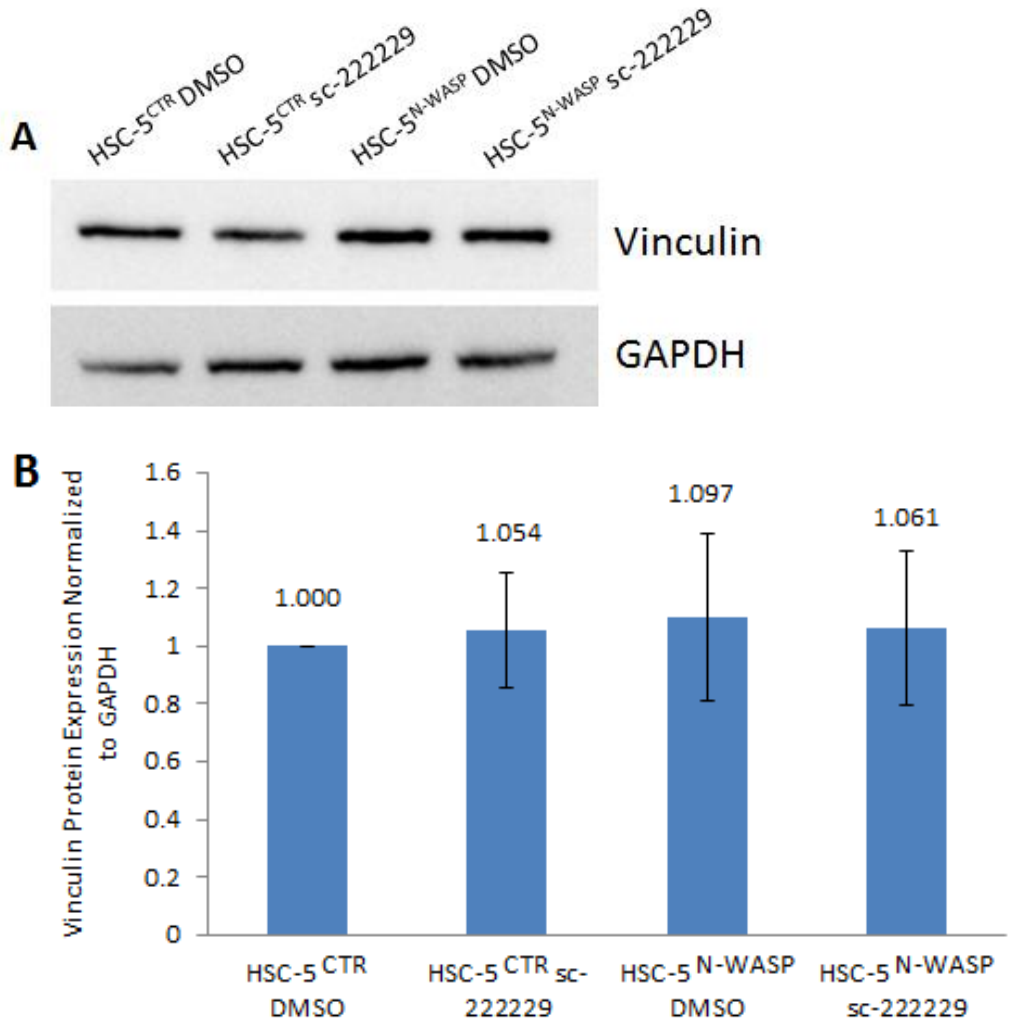

Figure 78: DMSO- and sc-222229-treated HSC-5 sublines have similar vinculin expressions. Both HSC-5 sublines were incubated in DMSO or sc-222229 prior to cell lysis. A) Equal amounts of cell protein lysates of HSC-5^{CTR} and HSC-$5^{N\text{-}WASP}$ cells were loaded for Western blot analysis using anti-vinculin and anti-GAPDH antibodies. B) Densitometric quantifications show no significant difference of vinculin protein levels between all DMSO- and sc-222229-treated HSC-5 sublines, compared to HSC-5^{CTR} cells with DMSO. Experiments were performed in triplicates. Significance: $P>0.05$ (Student's *t*-test).

4.1.18 HSC-5$^{N\text{-}WASP}$ cells with ERK2 inhibition have increased paxillin localizations to levels that of HSC-5^{CTR} cells

Since inhibition of ERK2 in HSC-5$^{N\text{-}WASP}$ cells reversed cell migration phenotype to that of HSC-5^{CTR} cells, it is likely that paxillin localization phenotype was also reversed in order to facilitate increased cell migration. Immunohistochemistry to visualize paxillin and actin in DMSO- and sc-222229-treated HSC-5 sublines and cell paxillin patch counts were performed. sc-222229-treated HSC-5^{CTR} cells had the most paxillin patches at the focal adhesion, followed by both sc-222229-treated HSC-5$^{N\text{-}WASP}$ cells and DMSO-treated HSC-5^{CTR} cells which had similar patch counts, and DMSO-treated HSC-5$^{N\text{-}WASP}$ cells which had the least patch count (Fig. 79A). The patch counts of sc-222229-treated HSC-5$^{N\text{-}WASP}$ cells and DMSO-treated HSC-5^{CTR} cells were not significant different from one another, but any other comparison was significantly different from one another (Fig. 79B).

This was followed with a Western blot of all four tested HSC-5 sublines for paxillin expression to determine if changes in paxillin localizations were due to changes in protein levels. All four tested HSC-5 sublines had similar paxillin expressions (Fig. 80A). Densitometric quantifications of paxillin bands against GAPDH bands showed no significant differences in paxillin protein levels between all four tested HSC-5 sublines (Fig. 80B), suggesting that the reduction of paxillin patches in skin cancer cells is not due to reduction of protein levels.

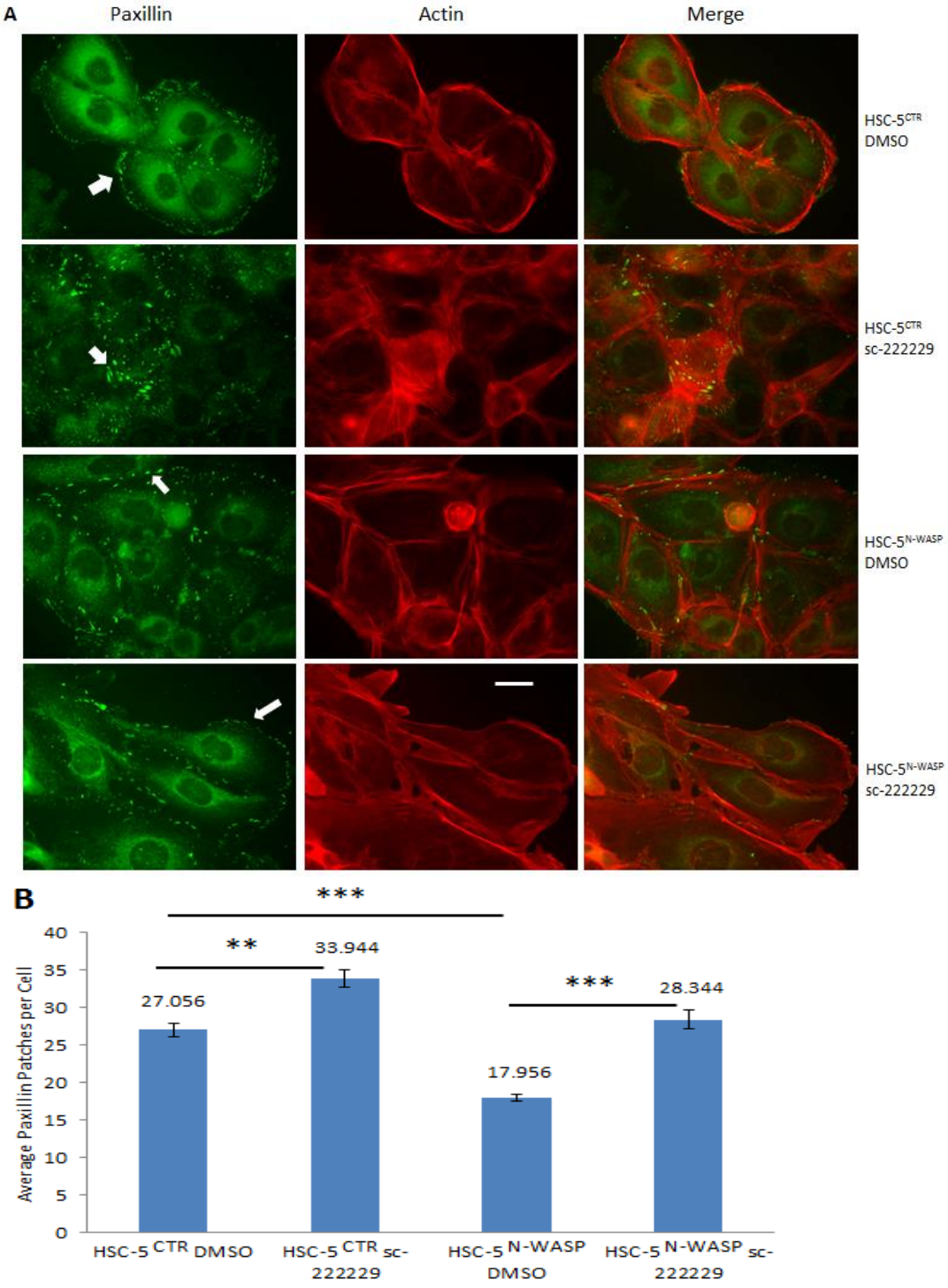

Figure 79: sc-222229-treated HSC-5$^{N\text{-}WASP}$ cells and DMSO-treated HSC-5^{CTR} cells have a similar number of paxillin patches. Both HSC-5 sublines were seeded on coverslips in 6-well plates, incubated in presence of DMSO or sc-222229, then fixed and probed with anti-paxillin (1°) antibody and Alexa488 conjugates (2°), and with Alexa568 conjugated phalloidin, under view of 40X objective lens. Note the difference in the number of observable green fluorescence streaks and dots at the cell membrane. Scale bar represents 20 µm. B) Paxillin patch count was performed by counting number of observable paxillin patches in 30 random cells, averaged, and compared to each other. Experiments were performed in triplicates. Significance: $^{**}P<0.01$, $^{***}P<0.001$ (Student's *t*-test).

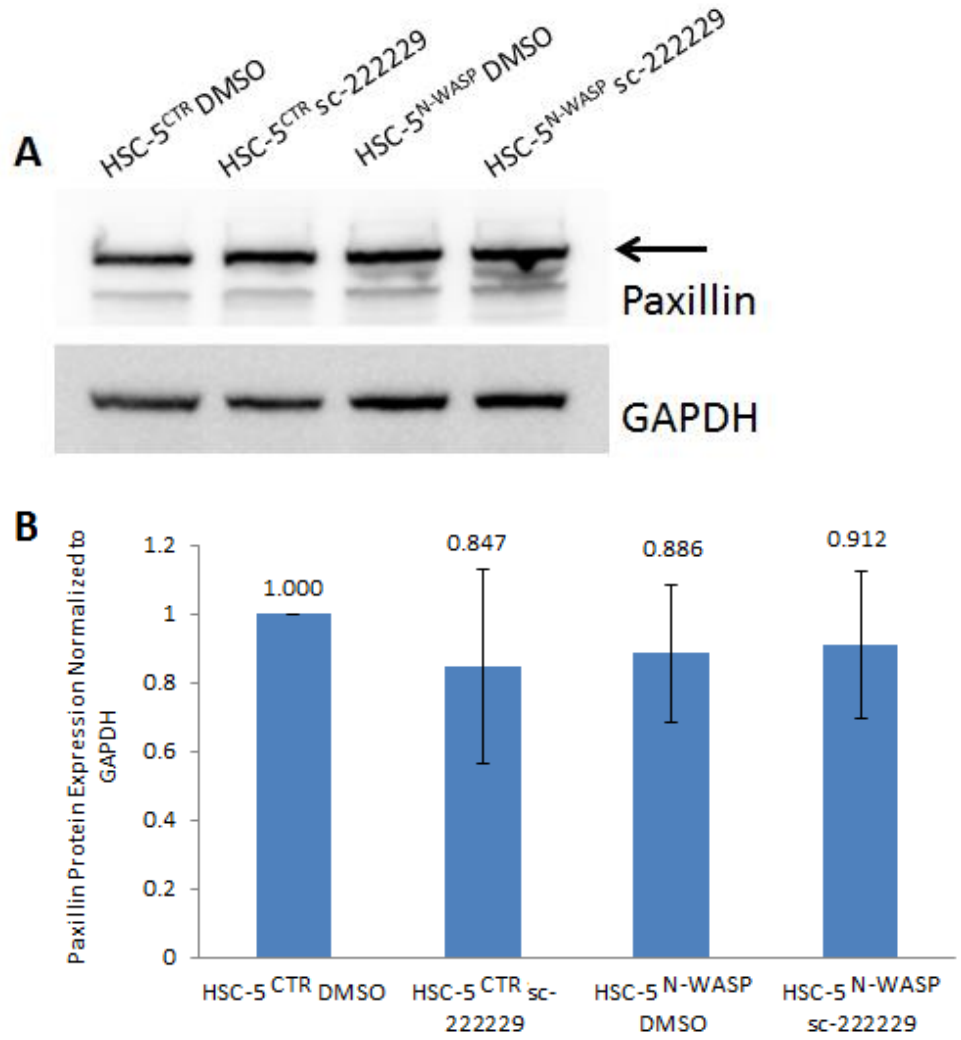

Figure 80: DMSO- and sc-222229-treated HSC-5 sublines have similar paxillin expressions. Both HSC-5 sublines were incubated in DMSO or sc-222229 prior to cell lysis. A) Equal amounts of cell protein lysates of HSC-5^{CTR} and HSC-$5^{N\text{-}WASP}$ cells were loaded for Western blot analysis using anti-paxillin and anti-GAPDH antibodies. B) Densitometric quantifications show no significant difference of paxillin protein levels between all DMSO- and sc-222229-treated HSC-5 sublines, compared to HSC-5^{CTR} cells with DMSO. Experiments were performed in triplicates. Significance: $P>0.05$ (Student's *t*-test).

4.1.19 ERK2 knockdown via shRNA in HSC-5$^{N\text{-}WASP}$ cells reduces cell proliferation further compared to HSC-5^{CTR} cells

ERK2 inhibitor studies performed so far suggest that ERK2 plays an inhibitory role in HSC-5 cells by phosphorylating FOXO1 and increasing expression of an unknown anti-proliferative signal when N-WASP is overexpressed. To study ERK2 activity in presence of sc-222229 in HSC-5 cells, a Western blot of DMSO- and sc-22229-treated HSC-5 sublines for phospho-Thr202/Tyr204 ERK1/2 and pan-ERK1/2 was performed. DMSO-treated HSC-5$^{N\text{-}WASP}$ cells had increased phospho-ERK2 expression compared to DMSO-treated HSC-5^{CTR} cells, similar to previous observations (Fig. 65); however, sc-222229-treated HSC-5 sublines had increased phospho-ERK2 expressions compared to DMSO-treated HSC-5 sublines (Fig. 81A). Densitometric quantification of ERK2 phospho-to-pan-specific bands against GAPDH bands showed significant increases of sc-222229-induced ERK2 activity in HSC-5 cells compared to treatment with DMSO (Fig. 81B).

To further characterize the role of ERK2 in HSC-5 cell proliferation, knockdown of ERK2 was performed by infecting HSC-5^{CTR} and HSC-5$^{N\text{-}WASP}$ cells with third-generation lentivirus derived from empty pTT2-Neo vector or pTT2-ERK2sh-Neo to knock down ERK2, and selected with neomycin. Western blots of all four HSC-5 sublines for ERK1/2 expression and cell proliferation assays were then performed. ERK2 knockdown in HSC-5 sublines was successful, with knockdown sublines having reduced pan-ERK2 expressions compared to control sublines (Fig. 82A). Densitometric quantification of ERK2 bands against GAPDH bands showed significant reductions of pan-ERK2 protein levels in knockdown cells compared to control cells (Fig. 82B). HSC-5 sublines with ERK2 knockdown had significantly reduced proliferation rates compared to HSC-5 sublines without knockdown (Fig. 83), instead of HSC-5$^{N\text{-}WASP\text{-}ERK2\text{-}KD}$ cells exhibiting rescued cell proliferation rates to that of HSC-5$^{CTR\text{-}CTR}$ cells. These results suggest the presence of an ERK2 complex with ERK2-interacting proteins in HSC-5 cells that regulate cell proliferation. ERK2 knockdown via shRNA disrupts the complex, severely reducing cell proliferation, but sc-222229 inhibits ERK2 substrate phosphorylation, leading to rescue of HSC-5$^{N\text{-}WASP}$ cell proliferation and reversal of phenotypes tested to that of HSC-5^{CTR} cells.

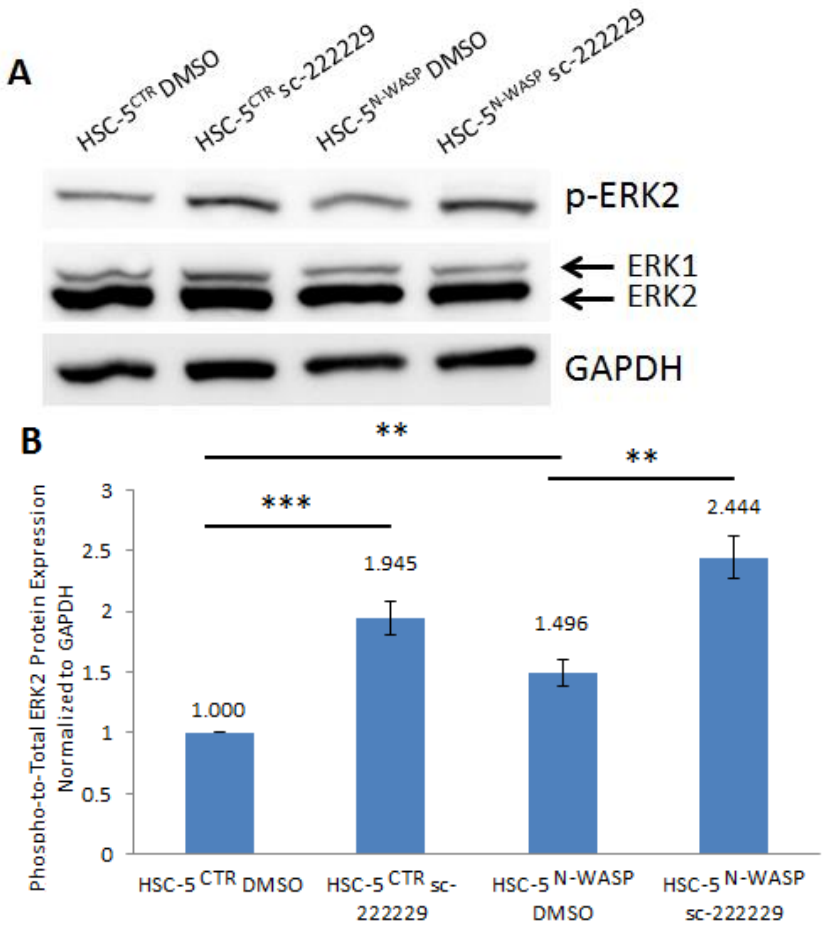

Figure 81: sc-222229-treated HSC-5 sublines have increased active ERK2 compared to DMSO-treated HSC-5 sublines. Both HSC-5 sublines were incubated in DMSO and sc-222229 prior to cell lysis. A) Equal amounts of HSC-5^{CTR} and HSC-$5^{N\text{-}WASP}$ cell protein lysates were loaded for Western blot analysis using anti-phospho-Thr202/Tyr204 ERK1/2, anti-pan-ERK1/2 and anti-GAPDH antibodies. B) Densitometric quantifications show significant increase of active ERK2 levels in HSC-5 sublines with sc-222229 compared to HSC-5 sublines with DMSO, all compared to HSC-5^{CTR} cells with DMSO. Experiments were performed in triplicates. Significance: $^{**}P<0.01$, $^{***}P<0.001$ (Student's *t*-test).

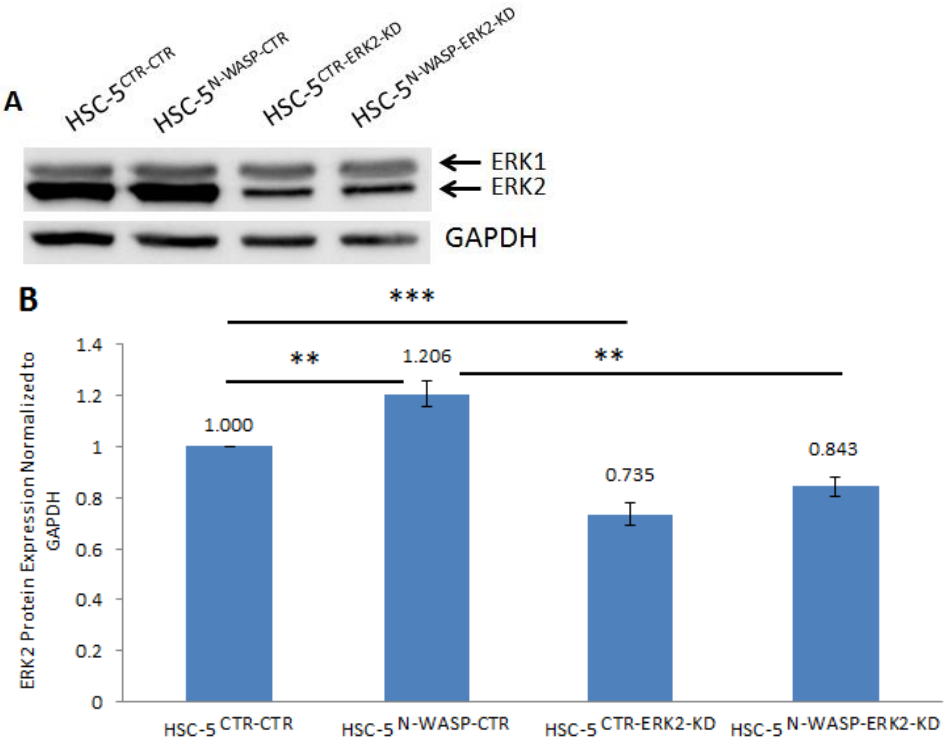

Figure 82: HSC-5 sublines with ERK2 knockdown via shRNA have reduced ERK2 expression compared to control HSC-5 sublines. A) Equal amounts of HSC-5 subline protein lysates were loaded for Western blot analysis using anti-ERK1/2 and anti-GAPDH antibodies. B) Densitometric quantifications show significant reduction of pan-ERK2 protein levels in HSC-5 sublines with shRNA-induced knockdown compared to control cells, compared to HSC-$5^{CTR-CTR}$ cells. Experiments were performed in triplicates. Significance: ***P*<0.01, ****P*<0.001 (Student's *t*-test).

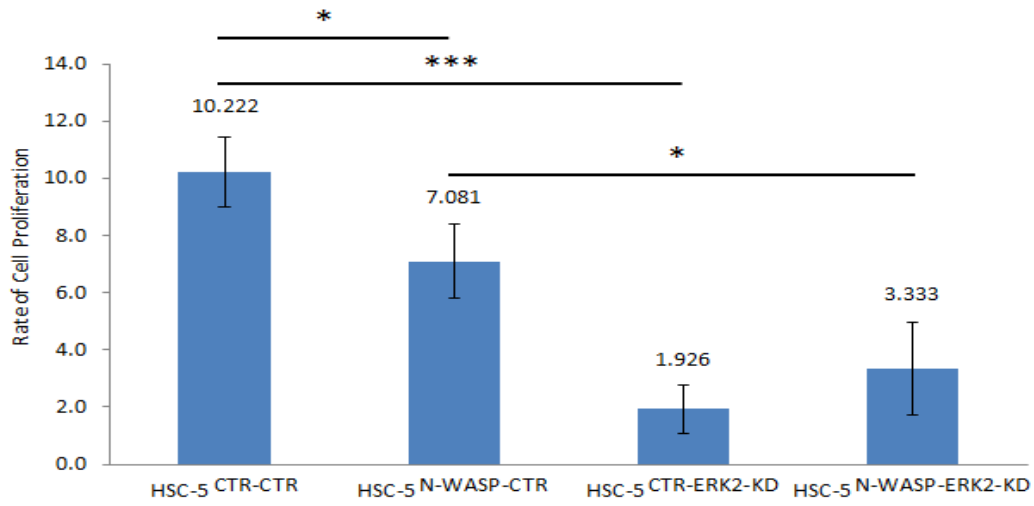

Figure 83: HSC-5 sublines with ERK2 knockdown via shRNA have further reduced cell proliferation compared to control HSC-5 sublines. 7.5 x 10^3 cells of each cell line were seeded in 24-well plates, incubated for 5 days, trypsinized and counted using a hemacytometer. The rate of proliferation was obtained by comparing total cell counted after 5 days against the number of cells seeded. Experiments were performed in triplicates. Significance: **P*<0.05, ****P*<0.001 (Student's *t*-test).

4.1.20 Summary

IPA comparative analysis of proteomics, protein microarray and RNA-Seq data of HSC-5^{CTR} and HSC-$5^{N\text{-}WASP}$ cells suggested the Integrin pathway and FOXO1 as the pathway and functional molecule mediating observed phenotypic changes. The Integrin-mediated FAK-SRC-GRB2-SOS1 signalling is dysregulated in HSC-$5^{N\text{-}WASP}$ cells. HSC-$5^{N\text{-}WASP}$ cells have reduced FOXO1 protein levels probably due to increased ERK2-dependent phosphorylation and translocation from the nucleus for cytoplasmic proteasomal degradation. ERK2 inhibition via sc-222229 treatment rescued HSC-$5^{N\text{-}WASP}$ cell proliferation, cell migration and localizations of E-cadherin, vinculin and paxillin to that of HSC-5^{CTR} cells, although CCND1 was partially rescued and there were excess FOXO1 protein levels. ERK2 knockdown via shRNA reduced HSC-$5^{N\text{-}WASP}$ cell proliferation further, suggesting that sc-222229 inhibit phosphorylation of ERK2 substrates by ERK2 to rescue all phenotypes tested. Identification of a FOXO1 target gene causing phenotypic changes observed in HSC-$5^{N\text{-}WASP}$ cells compared to HSC-5^{CTR} cells is to be performed.

4.2 Characterization of TXNIP levels and phenotypes in HSC-5 sublines

Protein microarray and RNA-Seq analysis showed FOXO1 levels are reduced in HSC-$5^{N\text{-}WASP}$ cells, suggesting that FOXO1 may be responsible for mediating phenotypic changes in HSC-5 cells. FOXO1 regulates expression of genes responsible for cell metabolism and growth, such as pyruvate dehydrogenase lipoamide kinase isozyme 4 (PDK4), all-trans-retinol 13,14-reductase (RETSAT) and TXNIP [252]. TXNIP is also regulated by AKT to control liver cell glucose uptake [253]. TXNIP prevents scavenging of ROS, leading to its build-up and increasing degree of cell damage [125,133]. FOXO1 expression was found to correlate inversely with TXNIP expression in liver cells [254]. Many cancers have reduced or silenced TXNIP expression [134]. RNA-Seq showed up-regulated TXNIP mRNA levels in HSC-$5^{N\text{-}WASP}$ cells (HSC-$5^{N\text{-}WASP}$/HSC-5^{CTR} FPKM value ratio: 1.589) (Table 5). HSC-$5^{N\text{-}WASP}$ cells proliferate at a slower rate than HSC-5^{CTR} cells (Fig. 18). All these suggest that TXNIP may play a role in skin carcinogenesis.

4.2.1 TXNIP expression is increased in HSC-$5^{N\text{-}WASP}$ cells compared to HSC-5^{CTR} cells

A Western blot of HSC-5^{CTR} and HSC-$5^{N\text{-}WASP}$ cells for TXNIP was performed to evaluate its expression in HSC-5 cells. HSC-$5^{N\text{-}WASP}$ cells had increased TXNIP

expression compared to HSC-5^{CTR} cells (Fig. 84A). Densitometric quantifications of TXNIP bands against GAPDH bands showed HSC-5$^{N\text{-}WASP}$ cells with significantly increased TXNIP protein levels compared to HSC-5^{CTR} cells (Fig. 84B).

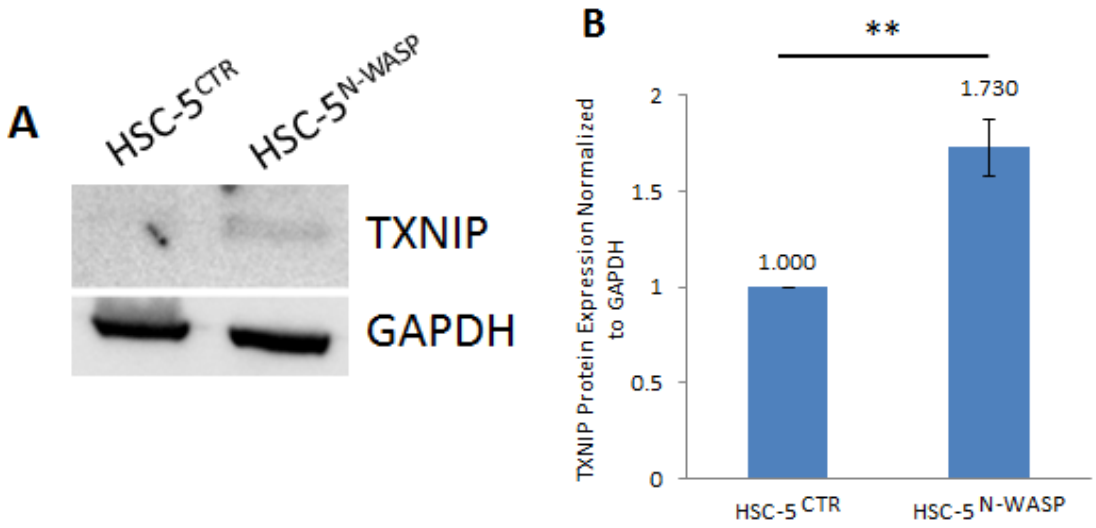

Figure 84: TXNIP expression is increased in HSC-5$^{N\text{-}WASP}$ cells compared to HSC-5^{CTR} cells. A) Equal amounts of HSC-5^{CTR} and HSC-5$^{N\text{-}WASP}$ cell protein lysates were loaded for Western blot analysis using anti-TXNIP and anti-GAPDH antibodies. B) Densitometric quantifications show significant increase of TXNIP protein levels in HSC-5$^{N\text{-}WASP}$ cells compared to HSC-5^{CTR} cells. Experiments were performed in triplicates. Significance: ***P*<0.01 (Student's *t*-test).

4.2.2 Generation of HSC-5 sublines with TXNIP knockdown

The role of TXNIP in HSC-5 cells was studied by generating TXNIP knockdown in HSC-5^{CTR} and HSC-5$^{N\text{-}WASP}$ cells. HSC-5 sublines were infected with third-generation lentivirus derived from empty pTT2-Neo vector or pTT2-TXNIPsh-Neo to knock down TXNIP, and selected with neomycin. A Western blot of all four HSC-5 sublines for TXNIP was then performed. TXNIP knockdown in HSC-5 sublines was successful, with HSC-5$^{N\text{-}WASP\text{-}CTR}$ cells having the highest TXNIP expression, followed by HSC-5$^{CTR\text{-}CTR}$ cells, and both HSC-5$^{CTR\text{-}TXNIP\text{-}KD}$ and HSC-5$^{N\text{-}WASP\text{-}TXNIP\text{-}KD}$ cells with the lowest TXNIP expression (Fig. 85A). Densitometric quantifications of TXNIP bands against GAPDH bands found that HSC-5 sublines with TXNIP knockdown had significantly reduced TXNIP protein levels compared to control HSC-5 sublines (Fig. 85B). To determine if TXNIP mRNA levels correlate with protein levels, a real-time PCR in all four HSC-5 sublines for TXNIP was performed. HSC-5$^{N\text{-}WASP\text{-}TXNIP\text{-}KD}$ cells had TXNIP mRNA levels which are significantly reduced compared to HSC-5$^{N\text{-}WASP\text{-}CTR}$ cells but similar to

HSC-5$^{CTR-CTR}$ cells (Fig. 85C). HSC-5$^{N-WASP-CTR}$ cells had the highest TXNIP mRNA levels, which were significantly higher than that of HSC-5$^{CTR-CTR}$ cells. These results suggest that TXNIP mRNA levels correlated with protein levels in skin cancer cells.

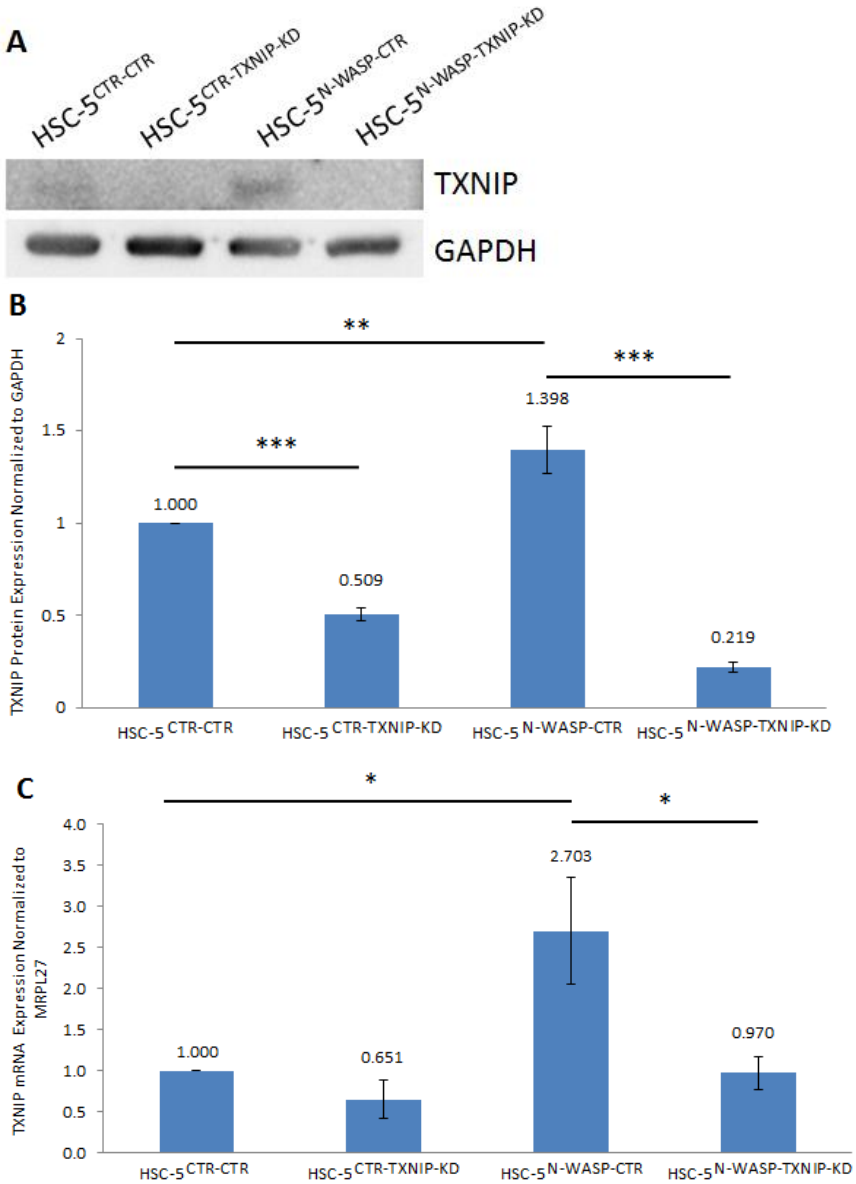

Figure 85: TXNIP knockdown was performed successfully in both HSC-5 sublines. A) Equal amounts of all four HSC-5 sublines' protein lysates were loaded for Western blot analysis using anti-TXNIP and anti-GAPDH antibodies. B) Densitometric quantifications show significant reduction of TXNIP protein levels in HSC-5$^{CTR-TXNIP-KD}$ and HSC-5$^{N-WASP-TXNIP-KD}$ cells compared to HSC-5$^{CTR-CTR}$ and HSC-5$^{N-WASP-CTR}$ cells, compared to HSC-5$^{CTR-CTR}$ cells. C) Equal amounts of cDNA from all four HSC-5 sublines were subjected to real-time PCR analysis of TXNIP cDNA, normalized to MRPL27, showing significant reduction of TXNIP mRNA levels in HSC-5$^{N-WASP-TXNIP-KD}$ cells compared to HSC-5$^{N-WASP-CTR}$ cells, compared to HSC-5$^{CTR-CTR}$ cells. Experiments were performed in triplicates. Significance: **P*<0.05, ***P*<0.01, ****P*<0.001 (Student's *t*-test).

4.2.3 HSC-5$^{N\text{-}WASP}$ cells with TXNIP knockdown have increased cell proliferation

TXNIP levels are down-regulated in many cancers [134], and increased TXNIP expression correlates with increased ROS levels, leading to cell apoptosis [136]. HSC-5$^{N\text{-}WASP}$ cells proliferated slower than HSC-5^{CTR} cells (Fig. 18), possibly due to increased TXNIP protein levels. Cell proliferation assays were performed for the four HSC-5 sublines. HSC-5$^{N\text{-}WASP\text{-}TXNIP\text{-}KD}$ cells had proliferation rates that are similar to that of HSC-5$^{CTR\text{-}CTR}$ cells but that are significantly higher than that of HSC-5$^{N\text{-}WASP\text{-}CTR}$ cells (Fig. 86).

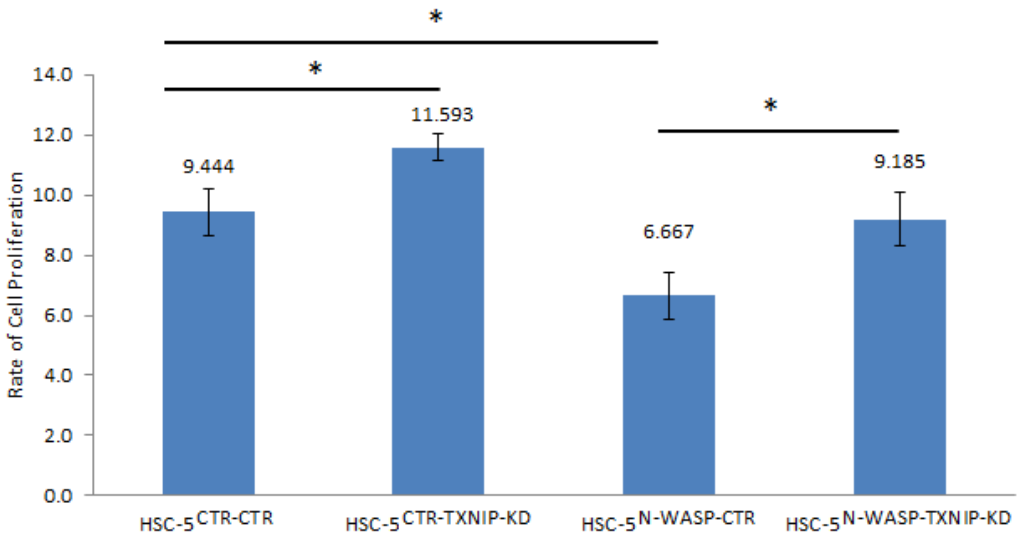

Figure 86: HSC-5$^{CTR\text{-}CTR}$ and HSC-5$^{N\text{-}WASP\text{-}TXNIP\text{-}KD}$ cells have similar cell proliferation rates. 7.5 x 10^3 cells of each cell line were seeded in 24-well plates, incubated for 5 days, trypsinized and counted using a hemacytometer. The rate of proliferation was obtained by comparing total cell counted after 5 days against the number of cells seeded. Experiments were performed in triplicates. Significance: *P<0.05 (Student's t-test).

4.2.4 HSC-5$^{N\text{-}WASP\text{-}TXNIP\text{-}KD}$ cells have further reduced Cyclin D1 expression

CCND1 is a marker for cell proliferation, whereby elevated expressions cause increased RB phosphorylation which promotes cell cycle transit past G1 phase [155]. Since HSC-5$^{N\text{-}WASP\text{-}TXNIP\text{-}KD}$ cells exhibited increased cell proliferation similar to that of HSC-5$^{CTR\text{-}CTR}$ cells (Fig. 86), and CCND1 protein levels in HSC-5^{CTR} and HSC-5$^{N\text{-}WASP}$ cells correlated with their respective cell proliferation rates (Fig. 18,19), a Western blot of all four HSC-5 sublines for CCND1 expression was performed to study its expression. HSC-5$^{N\text{-}WASP\text{-}CTR}$ cells had a lower CCND1 expression than HSC-5$^{CTR\text{-}CTR}$ cells, similar with previous observations (Fig. 19); however, HSC-5$^{N\text{-}WASP\text{-}TXNIP\text{-}KD}$ cells had the lowest

CCND1 expression, which does not correlate with its increased cell proliferation rate (Fig. 87A). Densitometric quantification of CCND1 bands against GAPDH bands showed significant a difference in CCND1 protein levels between HSC-5$^{CTR\text{-}TXNIP\text{-}KD}$ cells and any other three HSC-5 sublines (Fig. 87B).

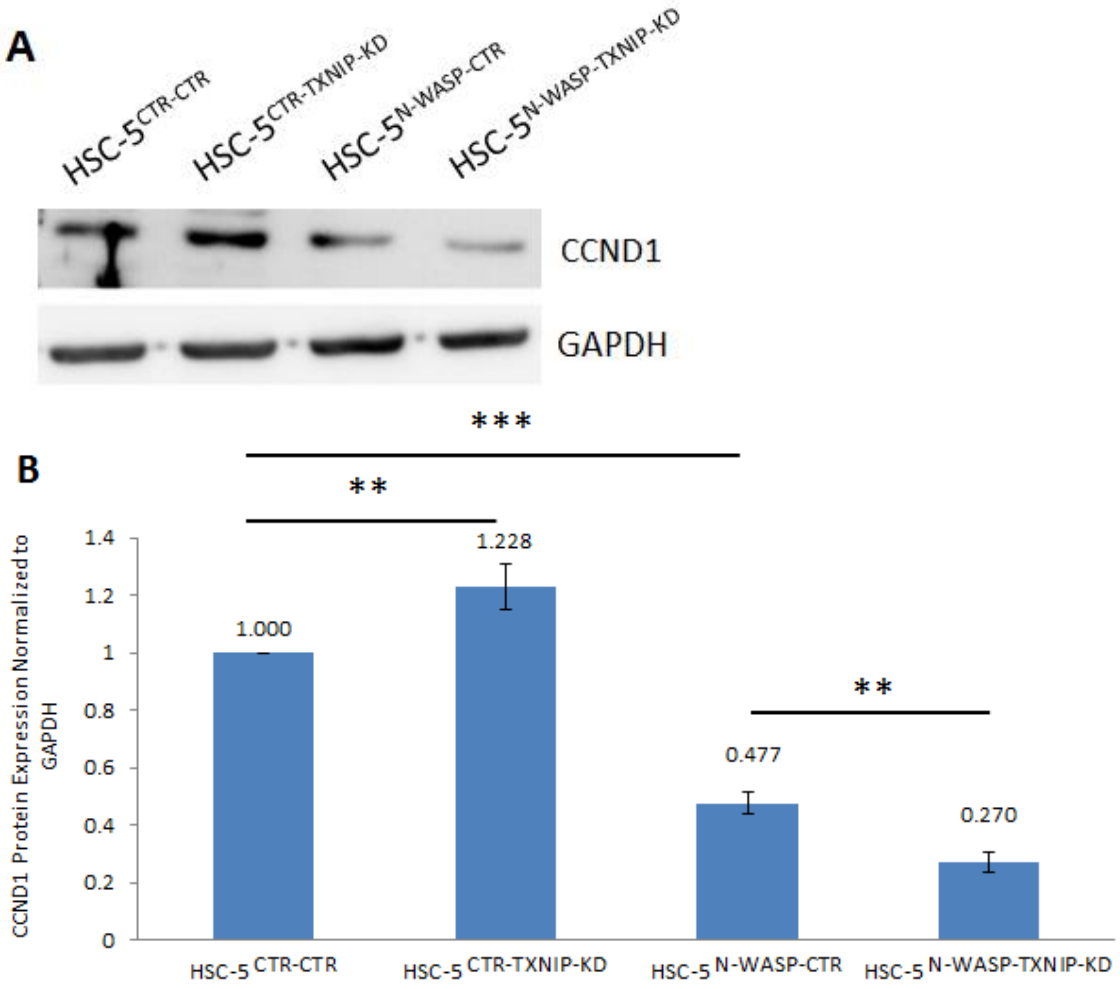

Figure 87: HSC-5$^{N\text{-}WASP\text{-}TXNIP\text{-}KD}$ cells have further reduced CCND1 expression compared to HSC-5$^{CTR\text{-}CTR}$ cells. A) Equal amounts of all four HSC-5 sublines' protein lysates were loaded for Western blot analysis using anti-CCND1 and anti-GAPDH antibodies. B) Densitometric quantifications show significant differences in CCND1 protein levels when any two of the four HSC-5 sublines were compared to each other, compared to HSC-5$^{CTR\text{-}CTR}$ cells. Experiments were performed in triplicates. Significance: ***P*<0.01, ****P*<0.001 (Student's *t*-test).

4.2.5 HSC-5$^{N\text{-}WASP}$ cells with TXNIP knockdown have reduced E-cadherin localizations to levels that of HSC-5^{CTR} cells

The reversal of proliferation rate of HSC-5$^{N\text{-}WASP\text{-}TXNIP\text{-}KD}$ cells to that of HSC-5$^{CTR\text{-}CTR}$ cells suggested the possibility of a reversal of E-cadherin localizations of HSC-5$^{N\text{-}WASP}$ cells to that of HSC-5^{CTR} cells. It is possible that TXNIP plays a role in E-cadherin localization in human skin cancer cells. Immunohistochemistry to visualize E-cadherin and actin was performed on all four HSC-5 sublines. HSC-5$^{N\text{-}WASP\text{-}CTR}$ cells had the highest fluorescence representing E-cadherin localizations at the cell cortex, followed by both HSC-5$^{N\text{-}WASP\text{-}TXNIP\text{-}KD}$ and HSC-5$^{CTR\text{-}CTR}$ cells which have the same fluorescence, and then HSC-5$^{CTR\text{-}TXNIP\text{-}KD}$ cells with the lowest fluorescence (Fig. 88A). The quantification of average E-cadherin fluorescence intensities of all four HSC-5 sublines also showed similar results (Fig. 88B).

A Western blot of all four HSC-5 sublines for E-cadherin expression was performed to determine if E-cadherin localizations were due to changes in E-cadherin expressions. E-cadherin expressions of all HSC-5 sublines were similar (Fig. 89A) and densitometric quantification of E-cadherin bands against GAPDH bands showed no significant differences in E-cadherin protein levels between all four HSC-5 sublines (Fig. 89B), suggesting that changes in E-cadherin localizations were not due to changes in protein levels.

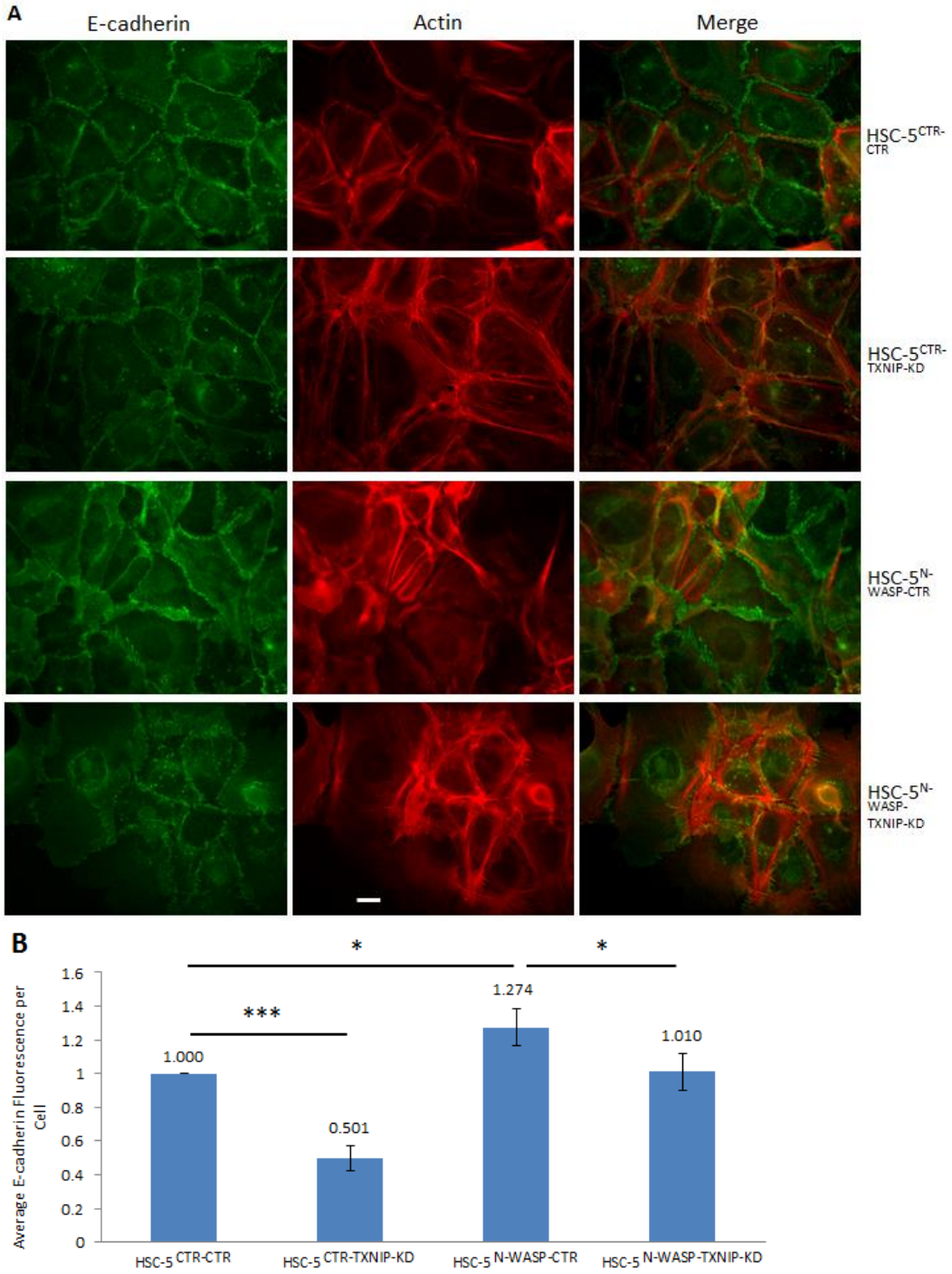

Figure 88: HSC-5$^{CTR-CTR}$ and HSC-5$^{N-WASP-TXNIP-KD}$ cells have similar E-cadherin localizations. A) All four HSC-5 sublines were seeded on coverslips in 6-well plates, incubated, then fixed and probed with anti-E-cadherin (1°) antibody and Alexa488 conjugates (2°), and with Alexa568 conjugated phalloidin, under view of 40X objective lens. Note the difference in green fluorescence in all cell lines; the intensity correlating with levels of E-cadherin localization. Scale bar represents 20 µm. B) E-cadherin fluorescence was quantified by quantifying the fluorescence in hand-drawn regions of interest for each cell, each fluorescence value was divided by 2, and the total values were then averaged. The average fluorescence intensity was obtained from 20 random cells. Experiments were performed in triplicates. Significance: **P*<0.05, ****P*<0.001 (Student's *t*-test).

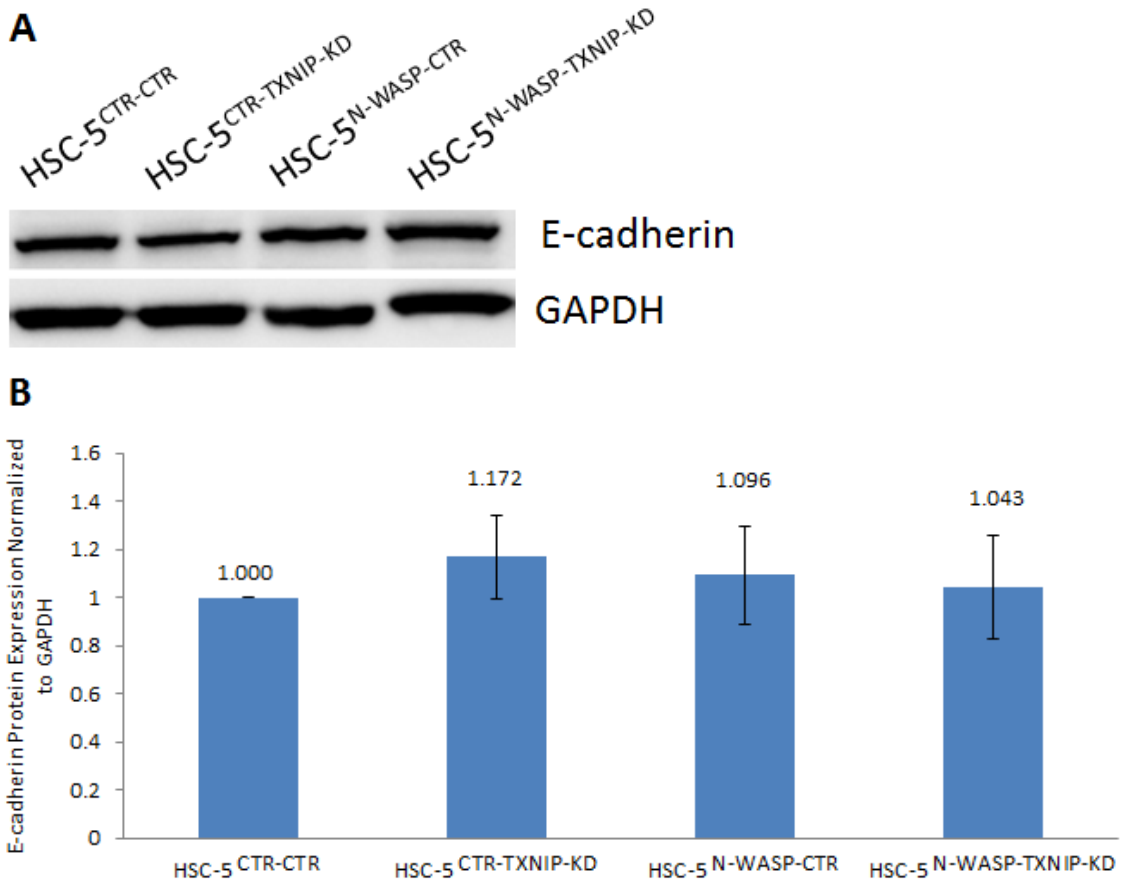

Figure 89: TXNIP knockdown does not affect E-cadherin expression. A) Equal amounts of cell protein lysates of all four HSC-5 sublines were loaded for Western blot analysis using anti-E-cadherin and anti-GAPDH antibodies. B) Densitometric quantifications show no significant difference of E-cadherin protein levels between all four HSC-5 sublines, compared to HSC-5$^{CTR-CTR}$ cells. Experiments were performed in triplicates. Significance: $P>0.05$ (Student's *t*-test).

4.2.6 HSC-5$^{N-WASP-TXNIP-KD}$ cells migrated similarly like HSC-5$^{CTR-CTR}$ cells

TXNIP knockdown in HSC-5^{N-WASP} cells was able to reverse the cell proliferation defect observed in HSC-5^{N-WASP} cells. It is possible that TXNIP knockdown could reverse HSC-5^{N-WASP} cell migration phenotype, and play a role in cell migration of human skin cancer cells. The four HSC-5 sublines were subjected to wound healing assays. 24 hours after scratches were made, all HSC-5 sublines except HSC-5$^{N-WASP-CTR}$ cells closed the wound gap (although a very noticeable small wound gap is present for HSC-5$^{N-WASP-TXNIP-KD}$ cells) (Fig. 90A). Naturally, HSC-5$^{N-WASP-CTR}$ cells had a significantly large wound surface area (Fig. 90B). The wound healing assays for these four HSC-5 sublines were repeated with 5 μM AraC to determine if the cell migration phenotype observed was influenced by differences in cell proliferation. 24 hours after scratches were made,

all HSC-5 sublines except HSC-5$^{N\text{-}WASP\text{-}CTR}$ cells closed the wound gap (Fig. 91A). Naturally, HSC-5$^{N\text{-}WASP\text{-}CTR}$ cells had a significantly large wound surface area (Fig. 91B).

A closer observation on HSC-5$^{CTR\text{-}TXNIP\text{-}KD}$ cells at 24 hours found that its cell population was heavily packed against each other (border of closed wound gap drawn in black lines), in comparison, both HSC-5$^{CTR\text{-}CTR}$ and HSC-5$^{N\text{-}WASP\text{-}TXNIP\text{-}KD}$ cell populations do not appear too packed (Fig. 90A,91A). This suggested that HSC-5$^{CTR\text{-}TXNIP\text{-}KD}$ cells closed the wound gap earlier than the 24-hour timepoint. To determine if this was true, wound healing assays of all four HSC-5 sublines with and without AraC were repeated for only 12 hours. HSC-5$^{CTR\text{-}TXNIP\text{-}KD}$ cells had the smallest wound surface area, followed by both HSC-5$^{CTR\text{-}CTR}$ cells and HSC-5$^{N\text{-}WASP\text{-}TXNIP\text{-}KD}$ cells, and then HSC-5$^{N\text{-}WASP\text{-}CTR}$ cells which had the largest wound surface area (Fig. 92A,93A). The wound surface areas of HSC-5$^{CTR\text{-}CTR}$ cells and HSC-5$^{N\text{-}WASP\text{-}TXNIP\text{-}KD}$ cells were not significantly different from one another, but HSC-5$^{N\text{-}WASP\text{-}TXNIP\text{-}KD}$ cell wound surface area was significantly smaller than that of HSC-5$^{N\text{-}WASP\text{-}CTR}$ cells (Fig. 92B,93B).

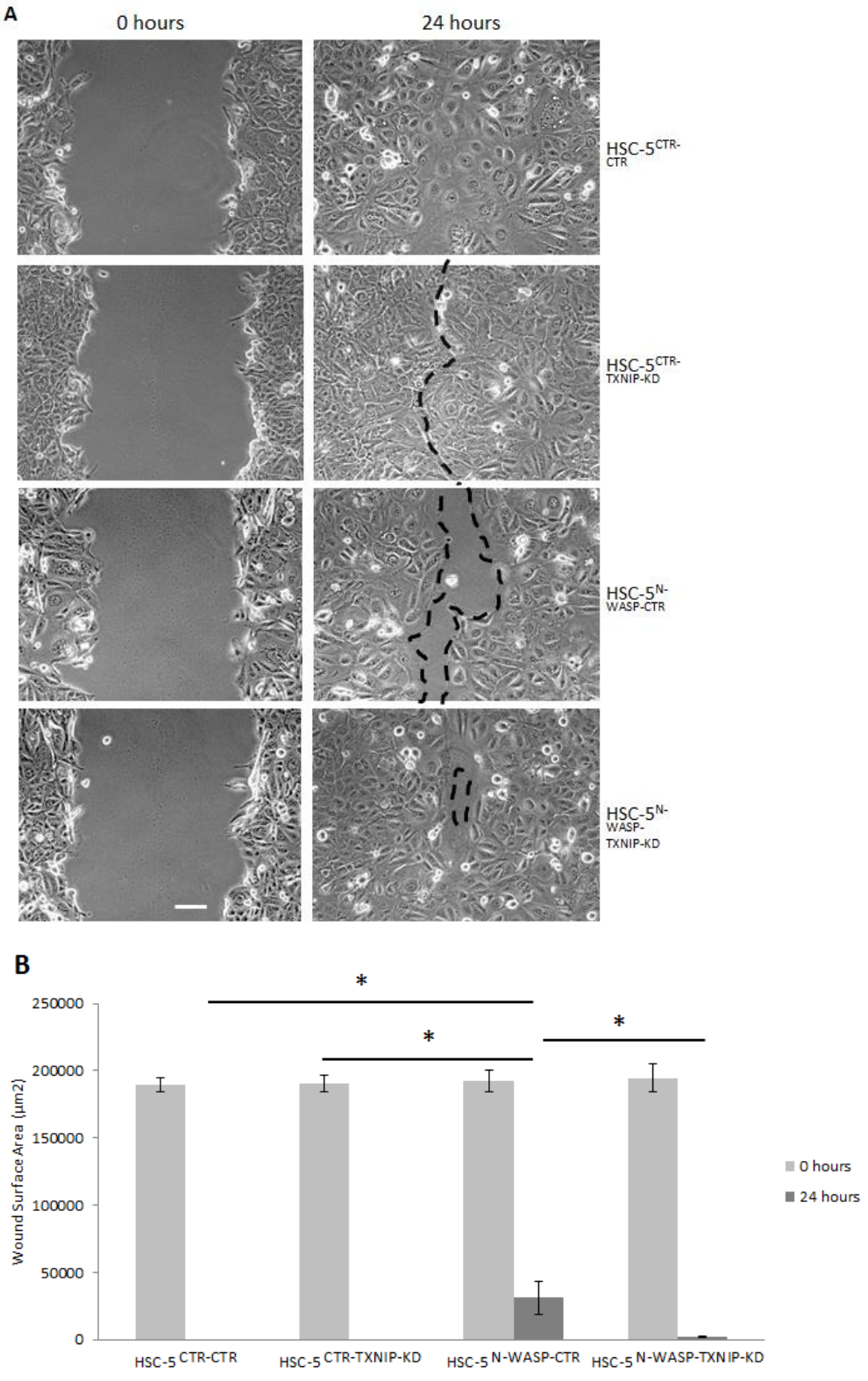

Figure 90: HSC-5$^{\text{N-WASP-TXNIP-KD}}$ cells migrated similarly like HSC-5$^{\text{CTR-CTR}}$ cells. A) Cells were seeded such that prior to wound healing assay, the cell confluency would be 100%. Images were taken of the cells 0 hours and 24 hours after the scratches were made, under view of 10X objective lens. Scale bar represents 50 µm. B) Surface areas of wounds were measured at respective time points and compared, whereby HSC-5$^{\text{N-WASP-TXNIP-KD}}$ cells closed the gap at a similar pace to HSC-5$^{\text{CTR-CTR}}$ cells. Experiments were performed in triplicates. Significance: *P<0.05 (Student's t-test).

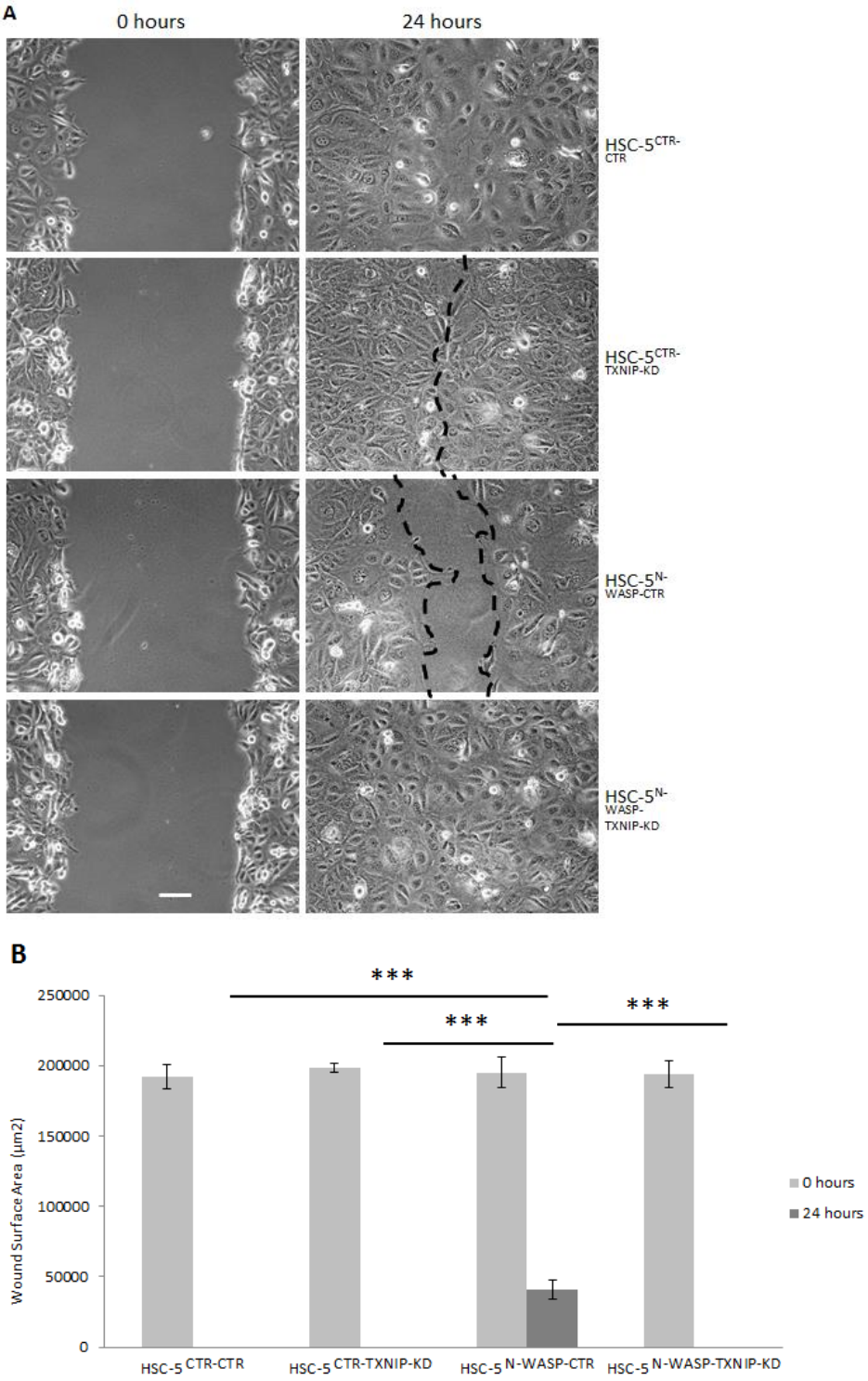

Figure 91: HSC-5$^{\text{N-WASP-TXNIP-KD}}$ cells migrated similarly like HSC-5$^{\text{CTR-CTR}}$ cells even with AraC. A) Cells were seeded such that prior to wound healing assay, the cell confluency would be 100%. Cells were incubated in complete DMEM supplemented with 5 µM AraC after scratches were made and for the duration of the assay. Images were taken of the cells 0 hours and 24 hours after the scratches were made, under view of 10X objective lens. Scale bar represents 50 µm. B) Surface areas of wounds were measured at respective time points and compared, whereby HSC-5$^{\text{N-WASP-TXNIP-KD}}$ cells closed the gap at a similar pace to HSC-5$^{\text{CTR-CTR}}$ cells. Experiments were performed in triplicates. Significance: ***P<0.001 (Student's t-test).

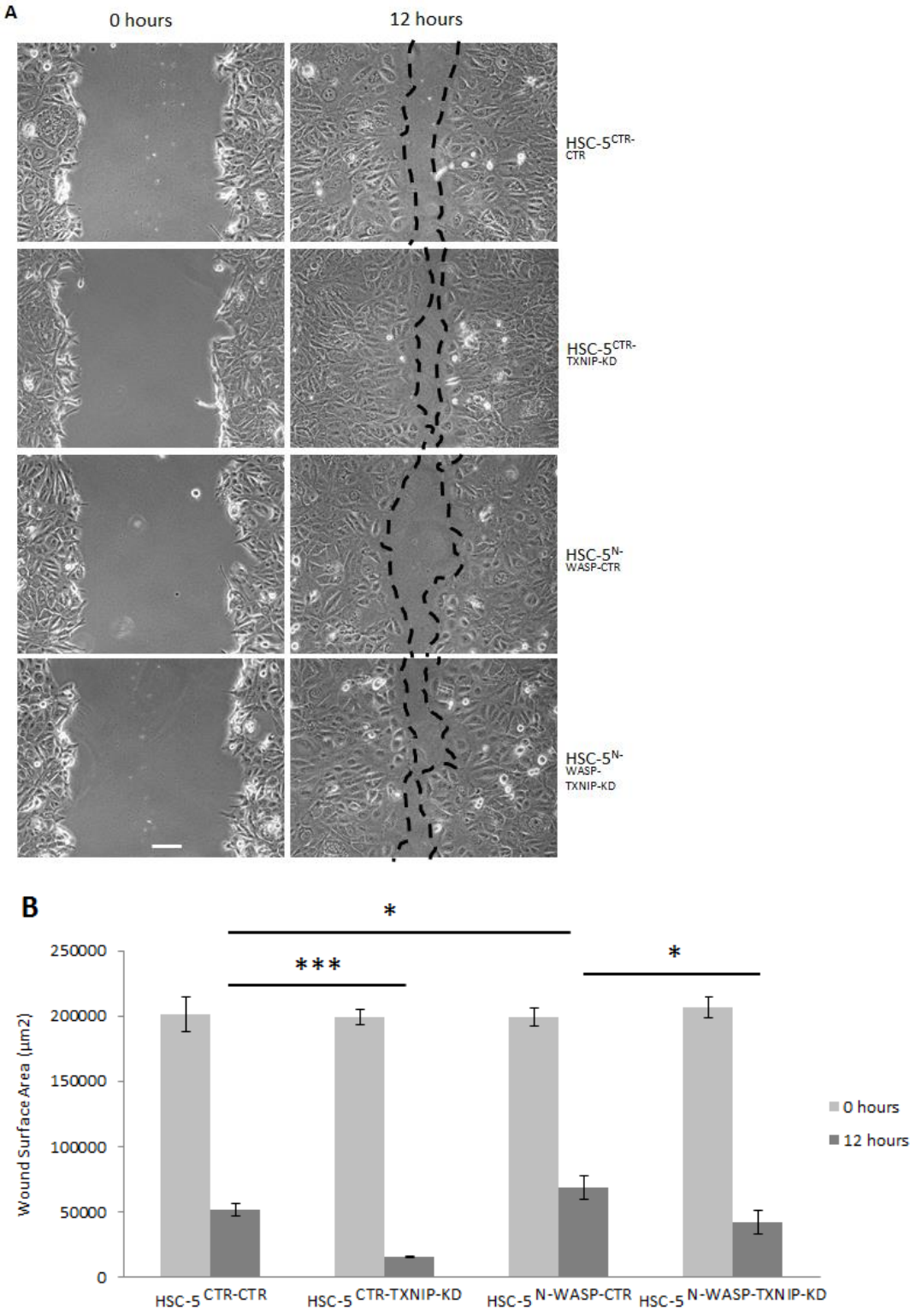

Figure 92: HSC-5$^{CTR\text{-}TXNIP\text{-}KD}$ cells migrated the fastest. A) Cells were seeded such that prior to wound healing assay, the cell confluency would be 100%. Images were taken of the cells 0 hours and 12 hours after the scratches were made on the cells, under view of 10X objective lens. Scale bar represents 50 µm. B) Surface areas of wounds were measured at respective time points and compared, whereby HSC-5$^{CTR\text{-}TXNIP\text{-}KD}$ cells close the gap fastest compared to the other three HSC-5 sublines. Experiments were performed in triplicates. Significance: **P*<0.05, ****P*<0.001 (Student's *t*-test).

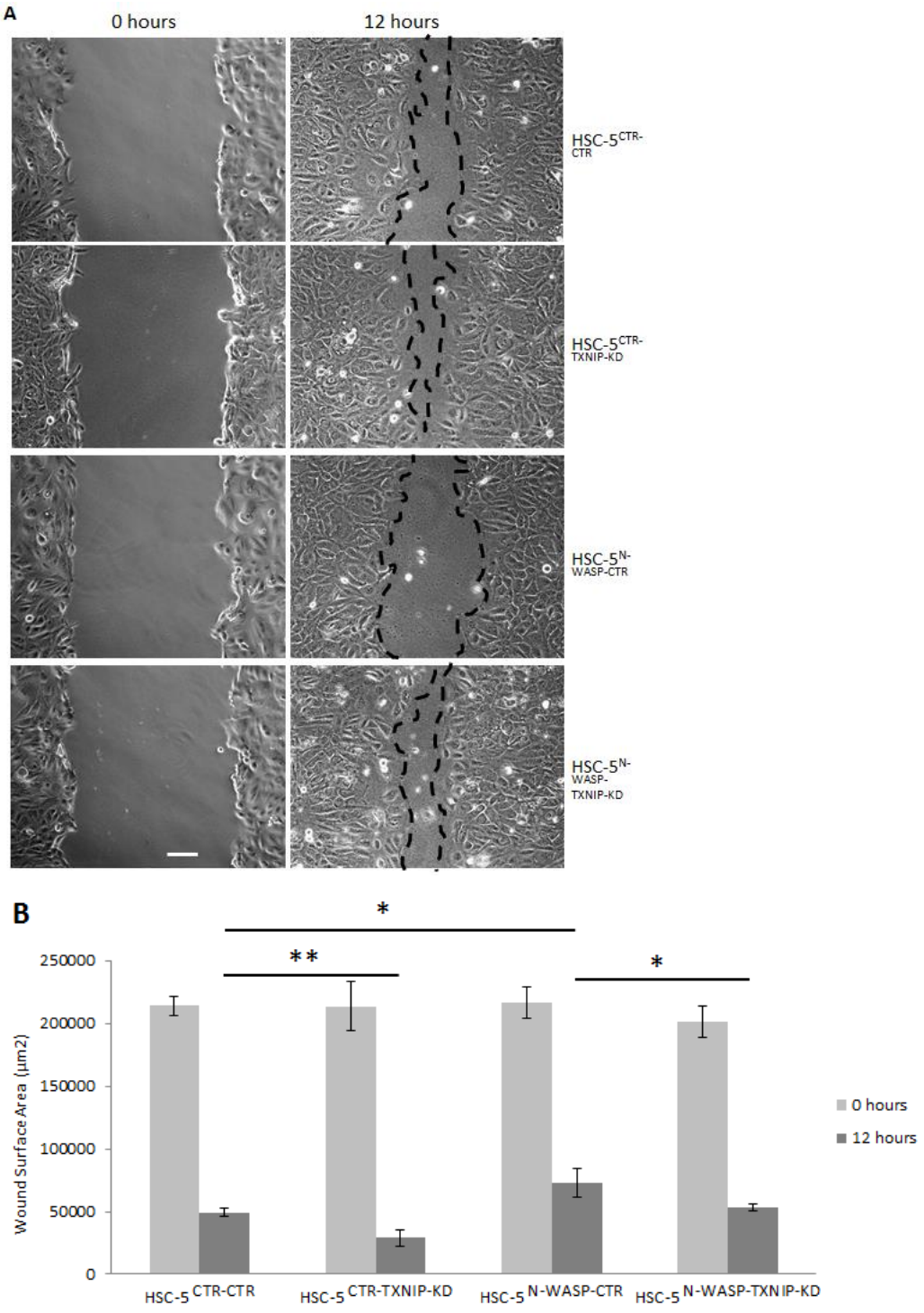

Figure 93: HSC-5$^{CTR\text{-}TXNIP\text{-}KD}$ cells migrated the fastest even with AraC. A) Cells were seeded such that prior to wound healing assay, the cell confluency would be 100%. Cells were incubated in complete DMEM supplemented with 5 µM AraC after scratches were made and for the duration of the assay. Images were taken of the cells 0 hours and 12 hours after the scratches were made on the cells, under view of 10X objective lens. Scale bar represents 50 µm. B) Surface areas of wounds were measured at respective time points and compared, whereby HSC-5$^{CTR\text{-}TXNIP\text{-}KD}$ cells close the gap fastest compared to the other three HSC-5 sublines. Experiments were performed in triplicates. Significance: **P*<0.05, ***P*<0.01 (Student's *t*-test).

4.2.7 HSC-5$^{N\text{-}WASP}$ cells with TXNIP knockdown have reduced vinculin localizations to levels that of HSC-5^{CTR} cells

TXNIP knockdown in HSC-5$^{N\text{-}WASP}$ cells reversed the cell migration phenotype to that of HSC-5^{CTR} cells. It is possible that the vinculin localization phenotype was reversed in order to facilitate increased cell migration activity. Immunohistochemistry to visualize vinculin and actin and cell vinculin patch counts were performed for all four HSC-5 sublines. HSC-5$^{N\text{-}WASP\text{-}CTR}$ cells had the most vinculin patches at the focal adhesion, followed by both HSC-5$^{CTR\text{-}CTR}$ cells and HSC-5$^{N\text{-}WASP\text{-}TXNIP\text{-}KD}$ cells, and HSC-5$^{CTR\text{-}TXNIP\text{-}KD}$ cells which had the least vinculin patches (Fig. 94A). The difference in vinculin patch count between HSC-5$^{CTR\text{-}CTR}$ and HSC-5$^{N\text{-}WASP\text{-}TXNIP\text{-}KD}$ cells were not significant, while HSC-5$^{N\text{-}WASP\text{-}TXNIP\text{-}KD}$ cell vinculin patch count was significantly reduced compared to that of HSC-5$^{N\text{-}WASP\text{-}CTR}$ cells (Fig. 94B).

A Western blot of all four HSC-5 sublines for vinculin expression was performed to determine if vinculin localizations were due to changes in vinculin protein levels. The vinculin expressions of all four HSC-5 sublines were similar (Fig. 95A). Densitometric quantification of vinculin bands against GAPDH bands showed no significant difference in vinculin protein levels between all four HSC-5 sublines (Fig. 95B). These results suggest that changes in vinculin localization were not due to changes in protein levels.

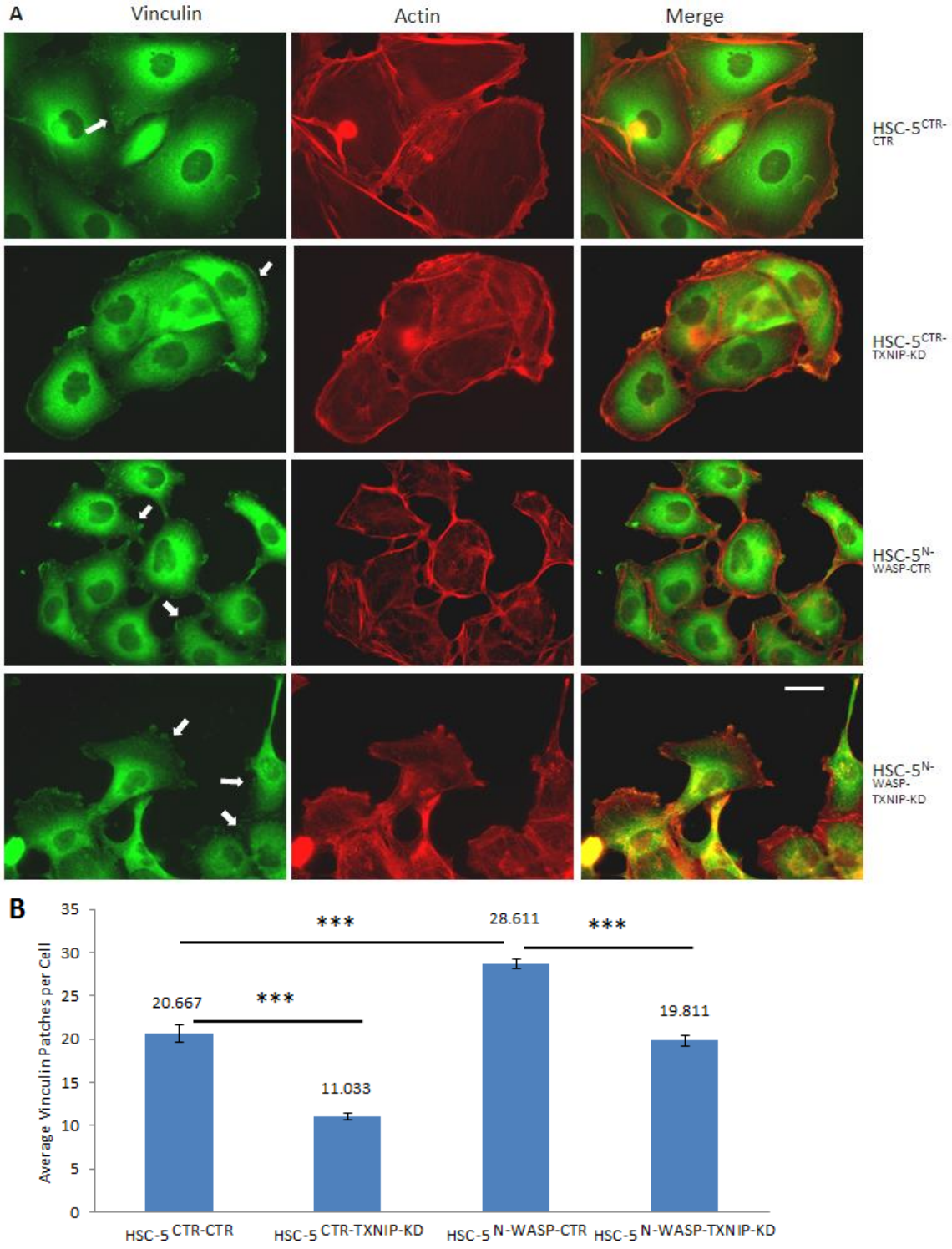

Figure 94: HSC-5$^{CTR-CTR}$ and HSC-5$^{N-WASP-TXNIP-KD}$ cells have a similar number of vinculin patches. A) All four HSC-5 sublines were seeded on coverslips in 6-well plates, incubated, then fixed and probed with anti-vinculin (1°) and Alexa488 conjugates (2°), and with Alexa568 conjugated phalloidin, under view of 40X objective lens. Note the difference in the number of observable green fluorescence streaks and dots at the cell membrane. Scale bar represents 20 µm. B) Vinculin patch count was performed by counting number of observable vinculin patches in 30 random cells, averaged, and compared to each other. Experiments were performed in triplicates. Significance: ***P<0.001 (Student's t-test).

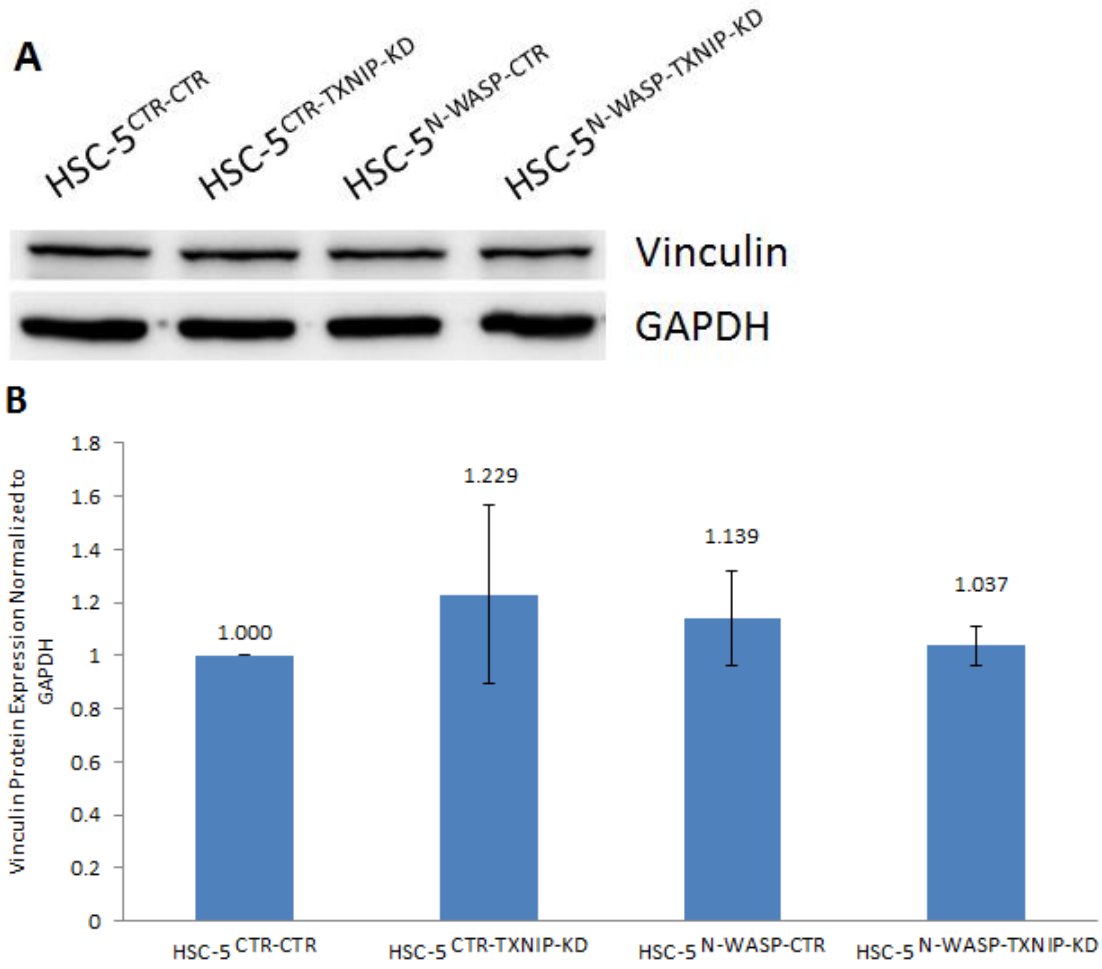

Figure 95: TXNIP knockdown does not affect vinculin expression. A) Equal amounts of cell protein lysates of all four HSC-5 sublines were loaded for Western blot analysis using anti-vinculin and anti-GAPDH antibodies. B) Densitometric quantifications show no significant difference of vinculin protein levels between all four HSC-5 sublines, compared to HSC-5$^{CTR-CTR}$ cells. Experiments were performed in triplicates. Significance: $P>0.05$ (Student's *t*-test).

4.2.8 HSC-5$^{N\text{-}WASP}$ cells with TXNIP knockdown have increased paxillin localizations to levels that of HSC-5^{CTR} cells

TXNIP knockdown in HSC-5$^{N\text{-}WASP}$ cells reversed the cell migration phenotype to that of HSC-5^{CTR} cells. It is possible that the paxillin localization phenotype was also reversed in order to facilitate increased cell migration activity. Immunohistochemistry to visualize paxillin and actin and cell paxillin patch counts were performed for all four HSC-5 sublines. HSC-5$^{N\text{-}WASP\text{-}CTR}$ cells had the least paxillin patches at the focal adhesion, followed by both HSC-5$^{CTR\text{-}CTR}$ cells and HSC-5$^{N\text{-}WASP\text{-}TXNIP\text{-}KD}$ cells, and HSC-5$^{CTR\text{-}TXNIP\text{-}KD}$ cells which had the most paxillin patches (Fig. 96A). The difference in paxillin patch count between HSC-5$^{CTR\text{-}CTR}$ and HSC-5$^{N\text{-}WASP\text{-}TXNIP\text{-}KD}$ cells were not significant, while HSC-5$^{N\text{-}WASP\text{-}TXNIP\text{-}KD}$ cell paxillin patch count was significantly increased compared to that of HSC-5$^{N\text{-}WASP\text{-}CTR}$ cells (Fig. 96B).

A Western blot of all four HSC-5 sublines for paxillin expression was performed to determine if paxillin localizations were due to changes in paxillin protein levels. The paxillin expressions of all four HSC-5 sublines were similar (Fig. 97A). Densitometric quantification of paxillin bands against GAPDH bands showed no significant difference in paxillin protein levels between all four HSC-5 sublines (Fig. 97B). These results suggest that changes in paxillin localization were not due to changes in protein levels.

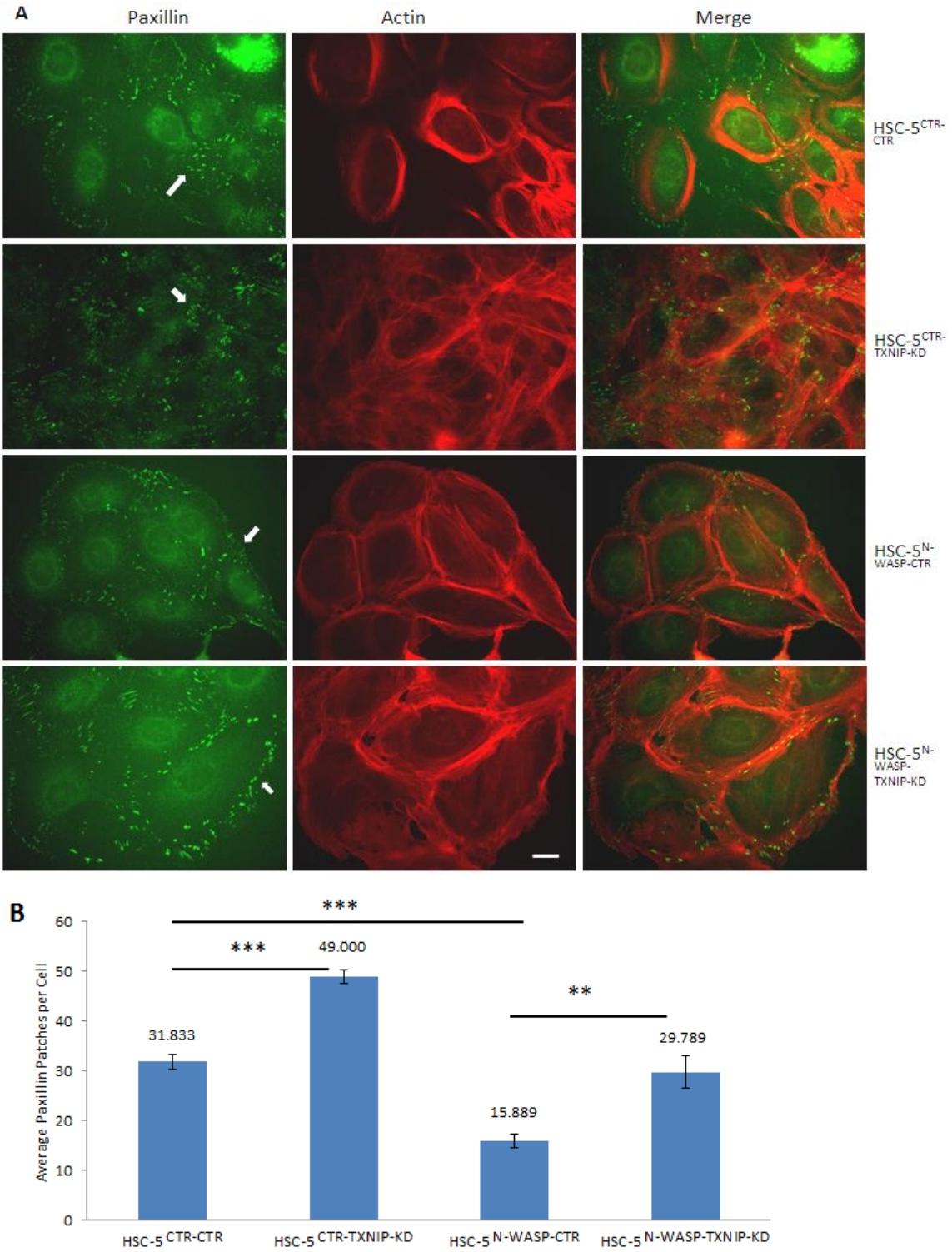

Figure 96: HSC-5$^{CTR-CTR}$ and HSC-5$^{N-WASP-TXNIP-KD}$ cells have a similar number of paxillin patches. A) All four HSC-5 sublines were seeded on coverslips in 6-well plates, incubated, then fixed and probed with anti-paxillin (1°) and Alexa488 conjugates (2°), and with Alexa568 conjugated phalloidin, under view of 40X objective lens. Note the difference in the number of observable green fluorescence streaks and dots at the cell membrane. Scale bar represents 20 µm. B) Paxillin patch count was performed by counting number of observable paxillin patches in 30 random cells, averaged, and compared to each other. Experiments were performed in triplicates. Significance: ** $P<0.01$, *** $P<0.001$ (Student's *t*-test).

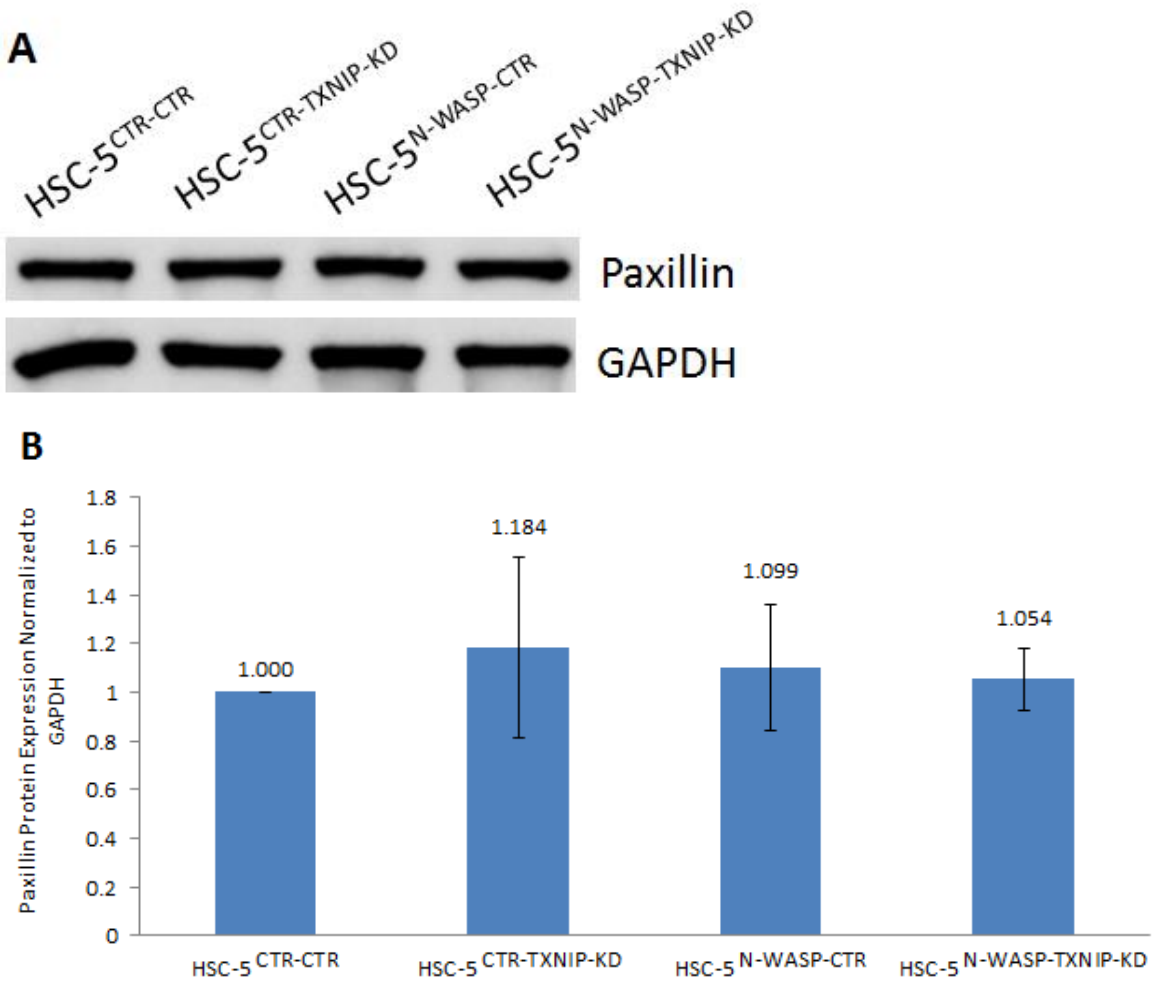

Figure 97: TXNIP knockdown does not affect paxillin expression. A) Equal amounts of cell protein lysates of all four HSC-5 sublines were loaded for Western blot analysis using anti-paxillin and anti-GAPDH antibodies. B) Densitometric quantifications show no significant difference of paxillin protein levels between all four HSC-5 sublines, compared to HSC-5$^{CTR-CTR}$ cells. Experiments were performed in triplicates. Significance: $P>0.05$ (Student's *t*-test).

4.2.9 HSC-5^{N-WASP} cells with TXNIP knockdown have similar ROS levels like that of HSC-5^{CTR} cells

The interaction between TXNIP and thioredoxin influences the rate of ROS scavenging and the rate of damage to cells if left unchecked [137]. TXNIP is down-regulated in many cancer cells [134], suggesting that increased ROS scavenging in cancer cells allows unhindered cell proliferation and that ROS levels influence cell proliferation activity. HSC-5^{N-WASP} cells exhibit reduced cell proliferation compared to HSC-5^{CTR} cells possibly via increased TXNIP-dependent ROS production. The four HSC-5 sublines were subjected to an ROS detection assay to determine if TXNIP influences ROS levels in skin cancer cells. HSC-5$^{N-WASP-CTR}$ cells had the highest ROS levels,

followed by HSC-5$^{CTR\text{-}TXNIP\text{-}KD}$ cells, and both HSC-5$^{CTR\text{-}CTR}$ and HSC-5$^{N\text{-}WASP\text{-}TXNIP\text{-}KD}$ cells with the lowest ROS levels (Fig. 98). HSC-5$^{CTR\text{-}CTR}$ and HSC-5$^{N\text{-}WASP\text{-}TXNIP\text{-}KD}$ cells do not have ROS levels significantly different between each other, but they each are significant compared to that of HSC-5$^{N\text{-}WASP\text{-}CTR}$ cells.

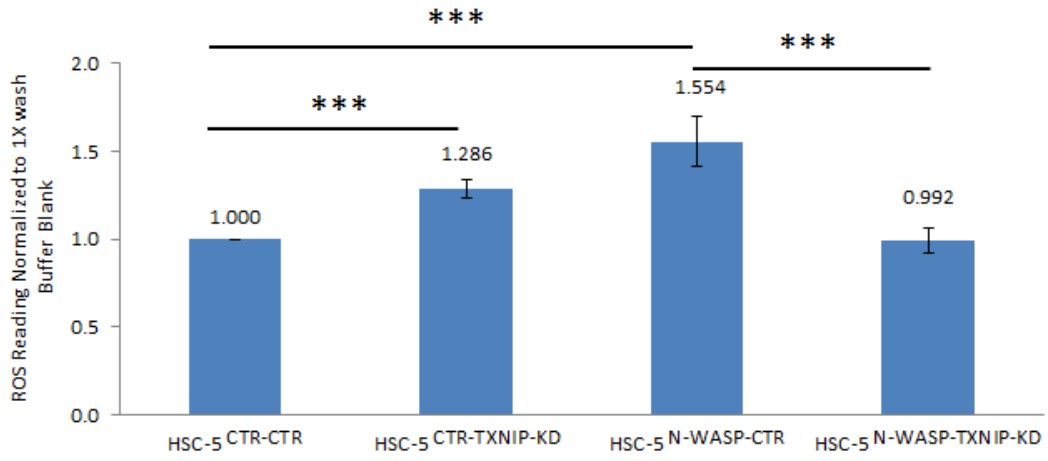

Figure 98: HSC-5$^{CTR\text{-}CTR}$ and HSC-5$^{N\text{-}WASP\text{-}TXNIP\text{-}KD}$ cells have similar reduced ROS levels. All four HSC-5 sublines were first seeded and incubated to grow to 70% confluency in 24-well plates, probed with DCFDA at the optimized 25 µM working concentration, washed with 1X Wash buffer, and read in a microplate reader. The readings were averaged and compared to that of HSC-5$^{CTR\text{-}CTR}$ cells. Experiments were performed in triplicates. Significance: ***P<0.001 (Student's t-test).

Increase of ROS levels appears to be responsible for increased cell apoptosis [135,138]. Cell proliferation assay results suggest that N-WASP overexpression causes approximately 30% reduction of cell proliferation rate (Fig. 18,86). It is possible that reduced proliferation rates in HSC-5$^{N\text{-}WASP}$ cells compared to HSC-5^{CTR} cells is due to increased ROS levels (Fig. 18), and that reversal of proliferation rates in HSC-5$^{N\text{-}WASP\text{-}TXNIP\text{-}KD}$ cells to that of HSC-5$^{CTR\text{-}CTR}$ cells is due to reduction of ROS levels (Fig. 86). It is possible that the cell proliferation rate change of 30% cell proliferation is due to cell apoptosis caused by changes in ROS levels, or ROS levels influencing cell proliferation itself. An Annexin-V/PI assay was performed on all four HSC-5 sublines to determine if cell proliferation rate change was due to cell apoptosis or not. Visually, Annexin-V GFP fluorescence represents cell extracellular phosphatidylserine signalling for macrophage engulfment due to apoptosis, and PI RFP fluorescence represents dead cells. HSC-5$^{N\text{-}WASP\text{-}CTR}$ cells had the highest Annexin V/PI staining compared to the other three HSC-5 sublines, which all have similar visualized staining (Fig. 99). HSC-5$^{N\text{-}WASP\text{-}CTR}$ cells

Annexin-V/PI staining covered approximately 10% of all cells at most. This suggested that the cell proliferation rate change in HSC-5 cells is not due to ROS-induced cell apoptosis, but ROS regulating cell signalling pathways to reduce cell proliferation.

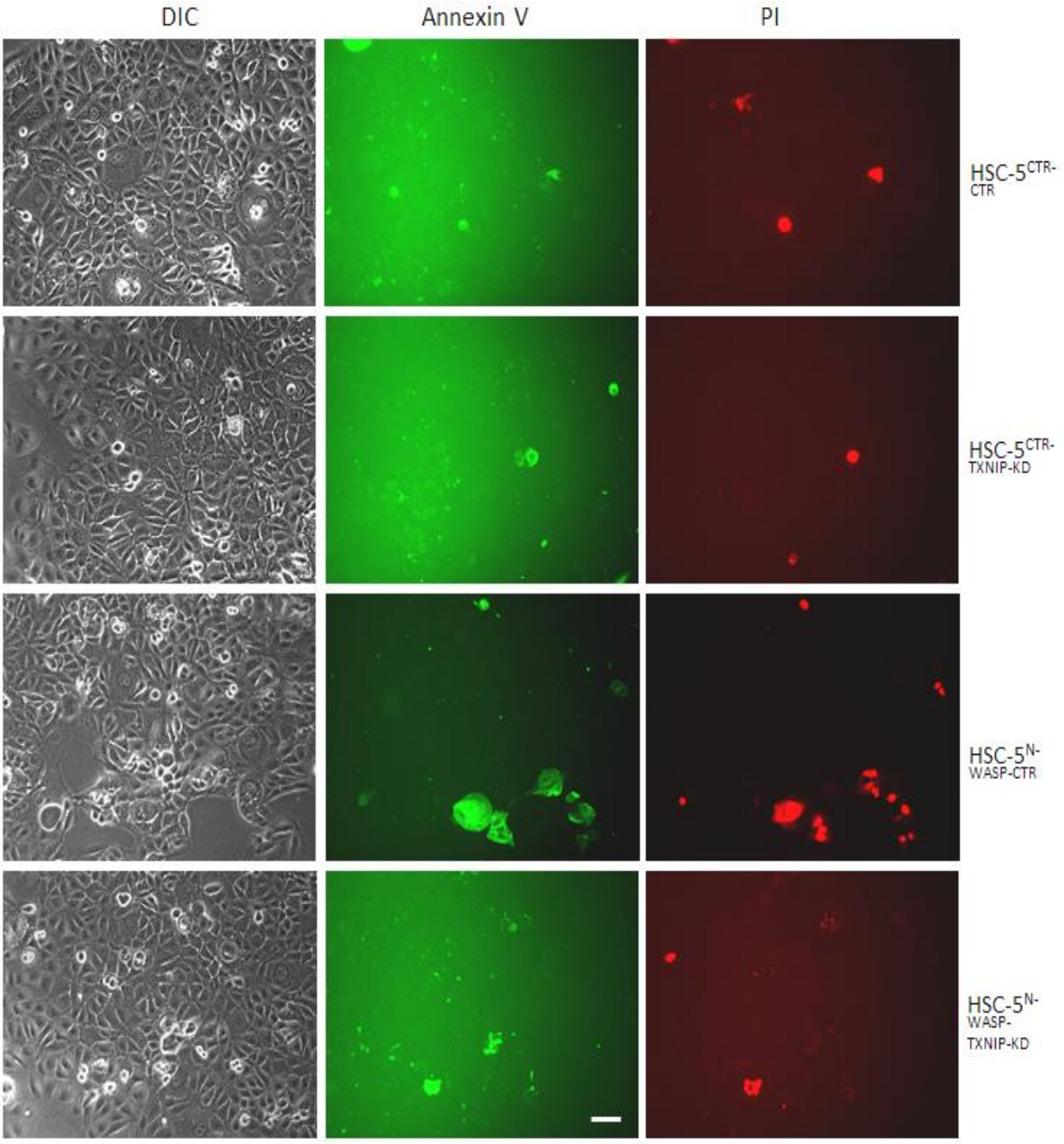

Figure 99: HSC-5$^{N\text{-}WASP\text{-}CTR}$ cells have the highest fluorescence for Annexin-V and PI, while all other HSC-5 sublines have similar Annexin-V and PI fluorescence. All four HSC-5 sublines were first seeded and incubated to grow to 70% confluency in 24-well plates, then probed with Annexin V to visualize phosphatidylserine presence and with PI to visualize dead cells, under view of 10X objective lens. Scale bar represents 50 µm. Experiments were performed in triplicates.

4.2.10 HSC-5$^{N\text{-}WASP\text{-}TXNIP\text{-}KD}$ cells have very reduced nuclear N-WASP

Actin is present in the nucleus, possibly responsible for chromatin remodelling and gene expression regulation [28]. As a regulator of actin branching, N-WASP has been shown to be present in nucleus assisting in RNA polymerase II-mediated transcription and mitotic chromosomal alignment [63,64]. HSC-5$^{N\text{-}WASP\text{-}TXNIP\text{-}KD}$ cells had many similar phenotypes to that of HSC-5$^{CTR\text{-}CTR}$ cells. The N-WASP expressions in cytosolic and nuclear fractions of all four HSC-5 sublines were assessed. Cell lysate fractionation and Western blot of cytosolic and nuclear fractions of all four HSC-5 sublines for N-WASP expression was performed. Cytosolic N-WASP of all four HSC-5 sublines are similar, while nuclear N-WASP of only HSC-5$^{CTR\text{-}CTR}$, HSC-5$^{CTR\text{-}TXNIP\text{-}KD}$ and HSC-5$^{N\text{-}WASP\text{-}CTR}$ cells are similar (arrow for N-WASP size, around 68 kDa) (Fig. 100A). HSC-5$^{N\text{-}WASP\text{-}TXNIP\text{-}KD}$ cell nuclear N-WASP was very reduced compared to that of all other fractions. Various bands or other sizes were also observed in the nuclear fractions, suggesting that N-WASP ubiquitination occurred in the nucleus. GAPDH mainly localizes in the cytoplasm, while Lamin B1 localizes in the nucleus. Ponceau S staining showed the equal loading of cell lysate fraction proteins, even though Lamin B1 band intensities differ between each nuclear fraction. Densitometric quantification of nuclear N-WASP bands against GAPDH bands show a significant reduction of nuclear FOXO1 protein levels in HSC-5$^{N\text{-}WASP\text{-}TXNIP\text{-}KD}$ cells compared to that of the other three HSC-5 sublines (Fig. 100B).

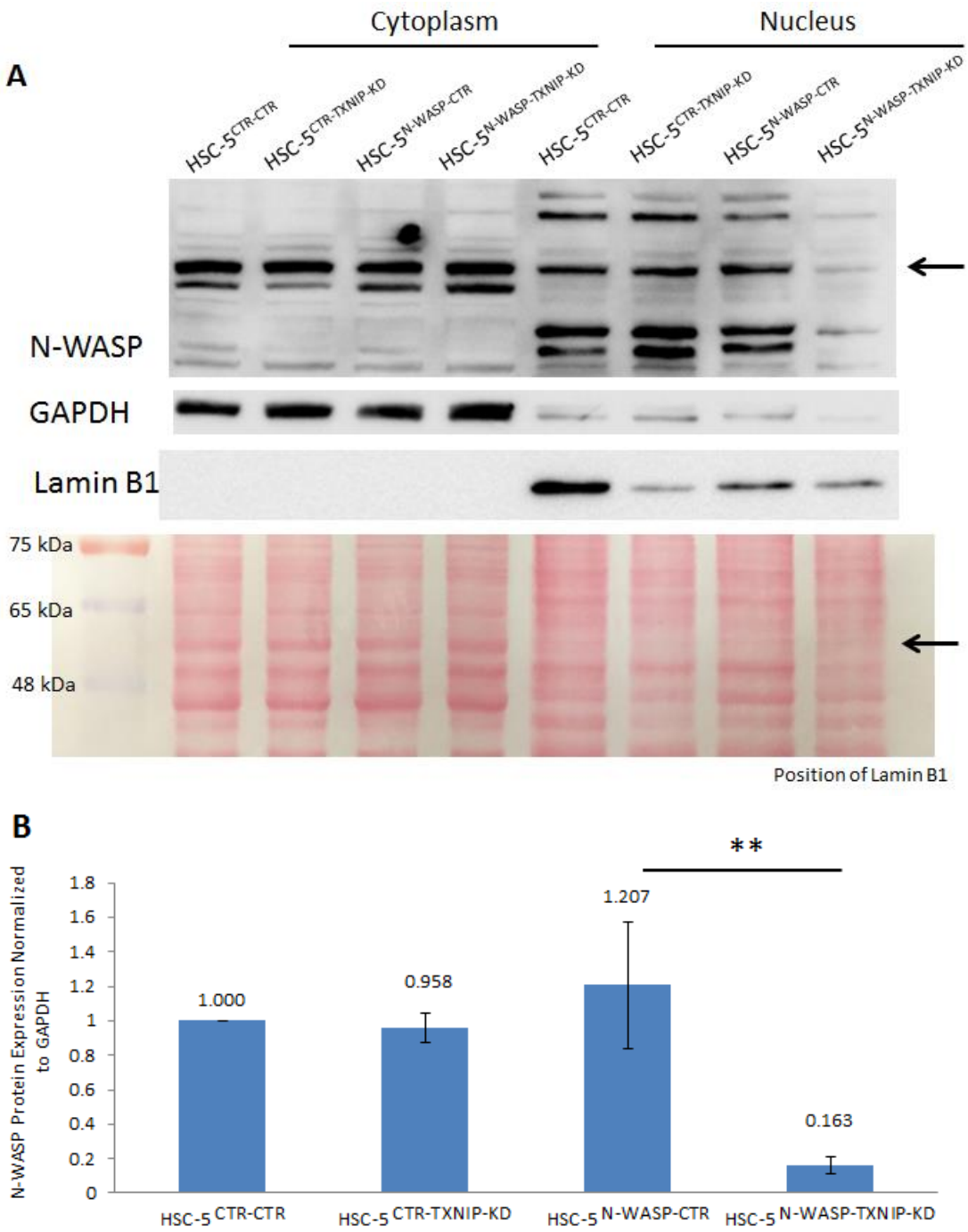

Figure 100: HSC-5$^{\text{N-WASP-TXNIP-KD}}$ cells have very reduced nuclear N-WASP. All four HSC-5 sublines were subjected to cell lysate fractionation and Western blot. A) Equal amounts of each HSC-5 sublines' protein lysates were loaded for Western blot analysis using anti-N-WASP, anti-GAPDH and anti-Lamin B1 antibodies. The nitrocellulose membrane was also subjected to Ponceau S staining to reflect loading of equal cell lysate protein amounts. B) Densitometric quantifications show significant reduction of N-WASP protein levels in nuclear fraction of HSC-5$^{\text{N-WASP-TXNIP-KD}}$ cells compared to the other three HSC-5 sublines, compared to HSC-5$^{\text{CTR-CTR}}$ cells. Experiments were performed in triplicates. Significance: $^{**}P<0.01$ (Student's *t*-test).

4.2.11 Exogenous expression of TXNIP in HSC-5 cells and TXNIP knockdown in HaCaT cells both reduced cell proliferation rates

The reversal of cell proliferation rates of HSC-$5^{N\text{-}WASP}$ cells to that of HSC-5^{CTR} cells was done by TXNIP knockdown. This is because increased TXNIP levels were only observed when HSC-5 cells overexpressed N-WASP (Fig. 84). To study the role of TXNIP in human skin cells, HSC-5 and HaCaT cells were made to overexpress TXNIP. This was done by infecting HSC-5 and HaCaT cells with third-generation lentivirus derived from empty pTT2-Neo vector or pTT2-TXNIPg-Neo to overexpress (OE) TXNIP (sourced from NIH_MGC_310, Mammalian Gene Collection). HaCaT cells were also infected with third-generation lentivirus derived from pTT2-TXNIPsh-Neo to knock down TXNIP to determine if silencing of TXNIP affects HaCaT cell proliferation. All HSC-5 and HaCaT sublines were selected with neomycin.

Cell proliferation assays were performed on these two HSC-5 sublines and three HaCaT sublines. HSC-$5^{TXNIP\text{-}OE}$ cells exhibited significantly reduced proliferation rates compared to HSC-5^{CTRN} cells (Fig. 101). A Western blot of TXNIP expression in HSC-$5^{TXNIP\text{-}OE}$ cells against HSC-5^{CTRN} cells was not possible as HSC-$5^{TXNIP\text{-}OE}$ cells grew very slowly after neomycin selection, this subline could not be expanded into larger culture dishes to get higher cell numbers, and the cell numbers obtained from a 6-well lentiviral infection were sufficient for one proliferation assay per attempt of HSC-5 subline generation. The significance was obtained after performing three separate lentiviral infections for subline generation and proliferation assays. Given the results, it can be inferred that lentiviral infection and neomycin selection successfully overexpressed TXNIP in HSC-5 cells and caused severe reduction of cell proliferation.

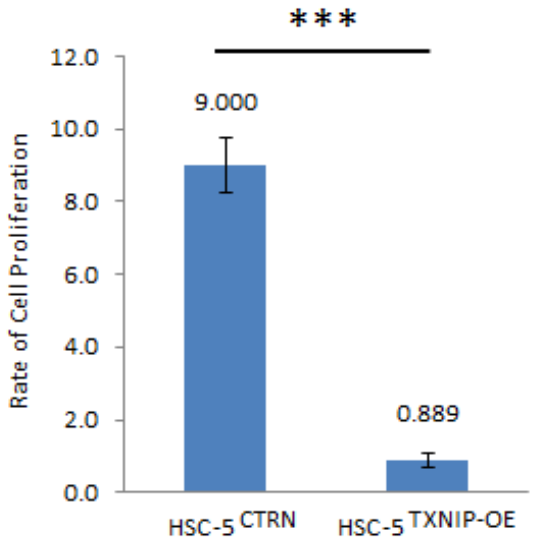

Figure 101: HSC-5$^{TXNIP-OE}$ cells proliferate poorly compared to HSC-5^{CTRN} cells. 7.5 x 10^3 cells of each cell line were seeded in 24-well plates, incubated for 5 days, trypsinized and counted using a hemacytometer. The rate of proliferation was obtained by comparing total cell counted after 5 days against the number of cells seeded. Experiments were performed in triplicates. Significance: ***P<0.001 (Student's t-test).

All three HaCaT sublines generated, however, were successfully expanded for Western blot for TXNIP and cell proliferation assays. Densitometric quantifications of all TXNIP bands observed against GAPDH bands were done. No significant TXNIP overexpression in HaCaT cells was achieved (Fig. 102A), though the cells were still used for proliferation assays. TXNIP knockdown was successfully achieved, and a significant difference in TXNIP protein levels between HaCaT^{CTRN} and HaCaT$^{TXNIP-KD}$ was observed (Fig. 102B). There are no significant differences between proliferation rates of HaCaT$^{TXNIP-OE}$ cells and HaCaT^{CTRN} cells, but there is a significant reduction in cell proliferation rate for HaCaT$^{TXNIP-KD}$ cells compared to HaCaT^{CTRN} cells (Fig. 102C). Given these results, it is possible that TXNIP plays different roles in proliferation of HSC-5 and HaCaT cells.

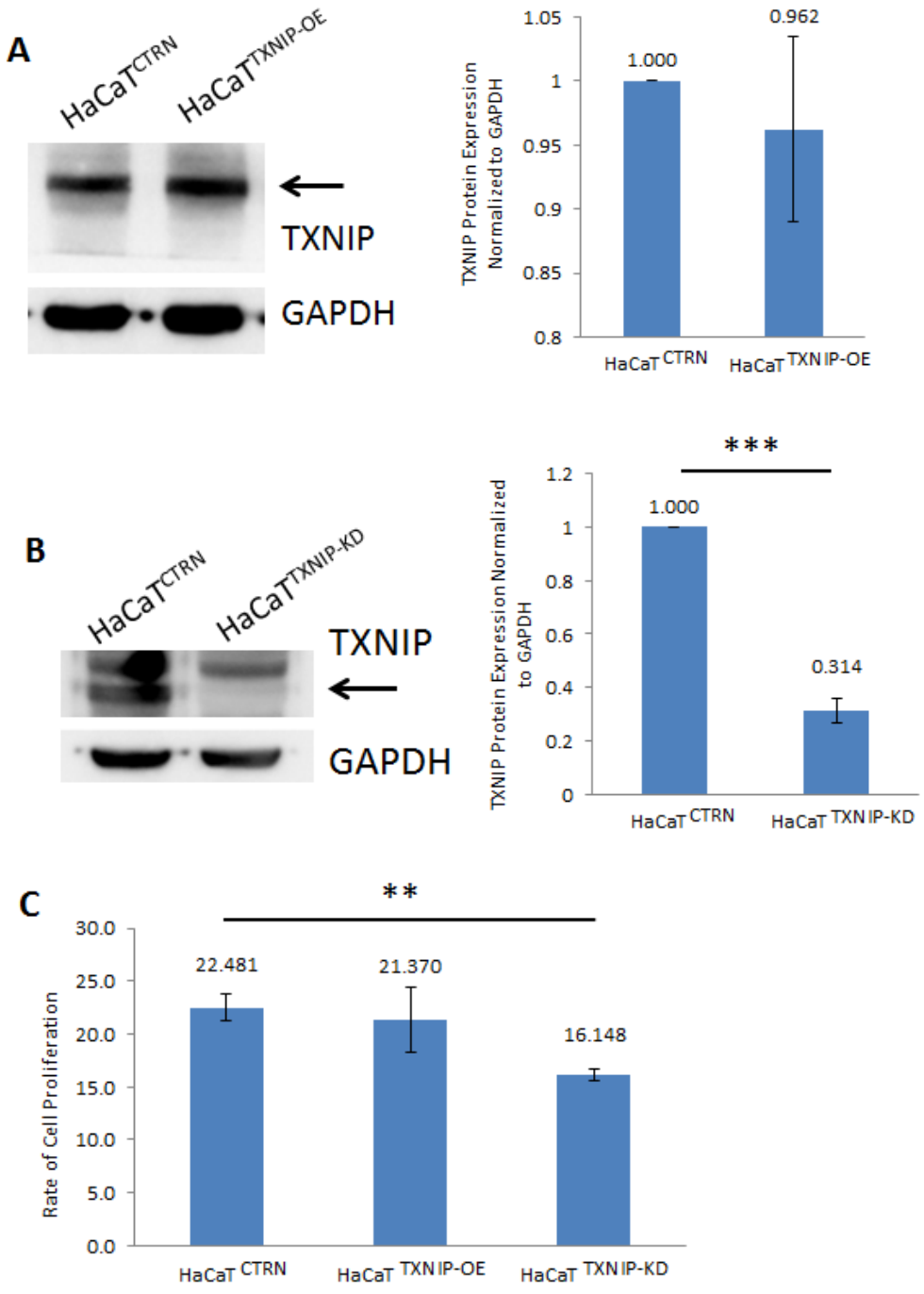

Figure 102: HaCaT$^{TXNIP-KD}$ cells have reduced cell proliferation compared to HaCaT^{CTRN} cells. HaCaT cells were made to A) overexpress TXNIP and B) exhibit knockdown of TXNIP. Equal amounts of all HaCaT sublines' cell protein lysates were loaded for Western blot analysis using anti-TXNIP and anti-GAPDH antibodies, and densitometric quantifications show significant reduction of TXNIP protein levels in HaCaT$^{TXNIP-KD}$ cells compared to HaCaT^{CTRN} cells, although no significant differences were observed in HaCaT$^{TXNIP-OE}$ cells. C) 7.5 x 10^3 cells of each cell line were seeded in 24-well plates, incubated for 5 days, trypsinized and counted using a hemacytometer. The rate of proliferation was obtained by comparing total cell counted after 5 days against the number of cells seeded. Experiments were performed in triplicates. Significance: ***P*<0.01, ****P*<0.001 (Student's *t*-test).

4.2.12 Summary

TXNIP Western blot of HSC-5^{CTR} and HSC-5$^{N\text{-}WASP}$ cells suggests it plays a role in reduced cell proliferation in HSC-5$^{N\text{-}WASP}$ cells. TXNIP knockdown in HSC-5$^{N\text{-}WASP}$ cells increased cell proliferation, reduced E-cadherin localizations, increased cell migration, reduced vinculin patches and increased paxillin patches to levels of that of HSC-5^{CTR} cells. Changes to localizations of E-cadherin, vinculin and paxillin do not correlate with protein levels. HSC-5$^{N\text{-}WASP\text{-}TXNIP\text{-}KD}$ cells had further reduced CCND1 levels, which does not correlate with its increased cell proliferation phenotype. ROS levels were similarly reversed but Annexin-V/PI staining suggested the reduction in HSC-5$^{N\text{-}WASP}$ cell proliferation rate is not due to ROS-induced apoptosis but likely ROS-induced changes to cell signalling pathways regulating cell proliferation. HSC-5$^{N\text{-}WASP\text{-}TXNIP\text{-}KD}$ cells also had reduced nuclear N-WASP compared to the other three HSC-5 sublines. Excess TXNIP protein levels is possibly very harmful to HSC-5 cells, but since TXNIP knockdown correlated with reduced proliferation in HaCaT cells, it is possible that TXNIP plays a part in supporting HaCaT cell proliferation. These suggest that TXNIP plays a role in regulating cell proliferation and other cellular processes in HSC-5 cells, and its effects are manifested by altered Integrin-mediated signalling and AKT signalling.

Chapter 5: Discussion

5.1 The role of N-WASP in HSC-5 and HaCaT cells

N-WASP is critical for actin cytoskeleton remodelling, as it activates the Arp2/3 complex and promotes actin polymerization [26,56]. Reduced N-WASP levels are correlated with cancer progression and poor prognosis in breast and colorectal cancer patients [79,80]. We have found that N-WASP levels are reduced in SCC samples compared to matched skin perilesionals in 33 patients (Swagata's unpublished data) (Fig. 4). These suggest that N-WASP may be a tumour suppressor in skin epithelial cells. This dissertation aims to characterize the role of N-WASP in skin carcinogenesis, using the tumorigenic HSC-5 cell line as a model for early-stage skin cancer and the non-tumorigenic HaCaT cell line as a model for normal human skin keratinocytes.

HSC-5 cell were found to have reduced N-WASP protein levels compared to HaCaT cells, and N-WASP mRNA levels correlated with protein levels (Fig. 7). HSC-5 cells were found to proliferate slower than HaCaT cells *in vitro*, even though HSC-5 cells are cancerous (Fig. 8). N-WASP was shown to be crucial for cell adhesion and inhibiting cell migration in MEF cells [147]. The cell utilizes E-cadherin, integrins and proteins of the focal adhesion complex, such as vinculin and paxillin [151,152], to regulate cell adhesion via cell-cell or cell-ECM adhesion, and thus migration. E-cadherin promotes cell-cell adhesion, and vinculin promotes cell adhesion, while paxillin promotes cell migration [153]; all of which are crucial, as cancer cells require the ability to detach from the ECM and migrate freely in order to proliferate.

It is hypothesized that cell migration requires reduced E-cadherin and vinculin localizations and more paxillin localizations, while cell adhesion requires increased E-cadherin and vinculin localizations and reduced paxillin localizations. HSC-5 cells were found to migrate faster (Fig. 11), have reduced E-cadherin cortical localizations (Fig. 9), reduced vinculin patches (Fig. 12) and increased paxillin patches (Fig. 14) compared to HaCaT cells. Both HSC-5 and HaCaT cells, however, have similar expressions of E-cadherin (Fig. 10), vinculin (Fig. 13) and paxillin (Fig. 15) despite differences in protein localizations. These suggest that N-WASP promotes recruitment of E-cadherin to the cell cortex and vinculin to the focal adhesion, and suppresses recruitment of paxillin from the focal adhesion to facilitate cell migration in skin cells.

5.2 The role of N-WASP in HSC-5 sublines

5.2.1 Characterizing N-WASP phenotypes in HSC-5 sublines

N-WASP is suggested to regulate cell proliferation and migration, and the localizations of E-cadherin, vinculin and paxillin. However, the HSC-5 and HaCaT cell lines used were derived from different individuals with varying genetic backgrounds and mutations, thus the observed phenotypes cannot be attributed to N-WASP expression in HSC-5 and HaCaT cells. The role of N-WASP in skin cancer cells was characterized by overexpressing N-WASP in HSC-5 cells. Several clones of HSC-$5^{N\text{-}WASP}$ cells with varying levels of N-WASP overexpression were generated (Fig. 16). HSC-$5^{N\text{-}WASP}$ clone 86 was found to express N-WASP similar to that of HaCaT cells and was used for the rest of this dissertation. N-WASP mRNA levels correlated with protein levels, though not proportionately (Fig. 17), suggesting that post-transcriptional regulation of N-WASP occurred.

HSC-$5^{N\text{-}WASP}$ cells were found to proliferate slower than HSC-5^{CTR} cells in an N-WASP-dependent manner (Fig. 18), suggesting that N-WASP expression is inversely proportional to cell proliferation rates. This finding corroborates with a report that HRT18 human colorectal cancer cells overexpressing N-WASP proliferated at lower rates compared to control cells [80]. Cyclin D1 (CCND1) is a well-known cell proliferation marker [155], and the AKT pathway is among the most well-established pathways implicated in cancer progression [157]. The expression of CCND1, and those of AKT and PTEN were studied to determine if the activities of these proteins correlate with the reduction of cell proliferation in HSC-$5^{N\text{-}WASP}$ cells. HSC-$5^{N\text{-}WASP}$ cells had reduced CCND1 expression (Fig. 19) and reduced AKT activity (Fig. 27) due to increased inhibition by PTEN (Fig. 28). These results corroborates with recent findings that increased PTEN activity is due to reduced phosphorylation of the PTEN inhibitory residues Ser380/Thr382/383 [255]. These suggest that N-WASP plays a negative role in cell proliferation in skin cancer cells.

Studies of cell migration and protein localizations also found that HSC-$5^{N\text{-}WASP}$ cells migrated slower (Fig. 22), had increased E-cadherin cortical localizations (Fig. 20) and increased vinculin patches (Fig. 23) but had reduced paxillin patches (Fig. 25) compared to HSC-5^{CTR} cells. All these are similar to previous observations where HaCaT cells migrated slower (Fig. 11), had increased E-cadherin cortical localizations (Fig. 9) and

increased vinculin patches (Fig. 12) and had reduced paxillin patches (Fig. 14) compared to HSC-5 cells. Both HSC-5 sublines expressed similar levels of E-cadherin (Fig. 21), vinculin (Fig. 24) and paxillin (Fig. 26) despite differences in protein localizations. These results are also similar to previous observations whereby both HaCaT and HSC-5 cells had similar expression levels of E-cadherin (Fig. 10), vinculin (Fig. 13) and paxillin (Fig. 15). These results suggest that N-WASP does regulate the recruitment of E-cadherin to the cell cortex and vinculin and paxillin to the focal adhesion to regulate cell adhesion and migration in both HSC-5 and HaCaT cells.

5.2.2 Multiple analyses of the 'omics in HSC-5 sublines

HSC-5 cell proliferation is inversely proportional to N-WASP expression (Fig. 18). This phenotype may be due to changes in signalling pathway and regulator activities due to differences in N-WASP expression. Several studies were performed to identify these pathways and functional molecules. First was the individual analysis of proteomics, protein microarray and RNA-Seq, and second was the comparative analysis of results of all three studies using the IPA software. Proteomics identifies changes at the proteomic level, protein microarray identifies changes of various signalling pathway proteins and RNA-Seq identifies changes at the transcription level. The IPA software performs individual dataset analysis and comparative analysis of multiple datasets, identifying putative signalling pathways or functional molecules with the help of its knowledge database that is updated every seven days with the latest findings from the scientific community [170], making results more up-to-date.

Four candidate pathways were chosen to be studied in HSC-5 cells: the Integrin, EGF, Wnt and Hippo pathways. They are among the most well-established pathways implicated in cell proliferation [86,89,91,98]. Analysis of proteomics suggested that all pathways except Hippo may be dysregulated in HSC-$5^{N\text{-}WASP}$ cells (Fig. 31,32). Protein microarray identified many proteins up- and down-regulated such as FOXO1, JNK, p70 S6K and STAT1, to name a few (Table 3,4). RNA-Seq found many individual genes such as FOXO1, ERK2, FAK, SOS1 which were either up-regulated or had mild increases or reduction in expression (Table 5). IPA comparative analysis of all three datasets gave a list of the most likely 15 pathways (Fig. 43) and functional molecules (Fig. 44) involved in phenotypic differences between HSC-5^{CTR} and HSC-$5^{N\text{-}WASP}$ cells, including the Integrin pathway and FOXO1.

5.3 Identifying molecules of interest in HSC-5 sublines

5.3.1 Justification for validating selected pathways and regulators

HSC-$5^{N\text{-}WASP}$ cells had increased vinculin patches (Fig. 23) and migrated slower (Fig. 22) compared to HSC-5^{CTR} cells, suggesting involvement of the Integrin pathway in regulating cell migration [153]. HSC-5 cells were found to express significantly more integrin subunits compared to HaCaT cells [175]. IPA comparative analysis found 15 pathways, including the Integrin pathway, likely responsible for phenotypic differences between HSC-5^{CTR} and HSC-$5^{N\text{-}WASP}$ cells (Fig. 43). The other 14 pathways were found to require interaction with the Integrin pathway to mediate and coordinate all inside-out and outside-in signalling to regulate cell growth [176-188]. This marks the Integrin pathway as a central nexus for these signalling pathways (Fig. 45). Even though down-regulation of RhoDGI pathway was initially considered responsible for reducing proliferation in HSC-$5^{N\text{-}WASP}$ cells, this pathway was ruled out because many of its components are unaffected by N-WASP overexpression (Table 7) and scientific opinion is divided on this pathway's precise role in cell proliferation [196-198]. Proteomics (Fig. 31,32) and protein microarray (Table 3,4) suggested the possibility of EGF, Wnt, mTOR and STAT1 or cytokine-mediated signalling as candidate pathways as well, so these pathways with the Integrin pathway were validated.

FOXO1 was listed as the sixth-likeliest candidate functional molecule effecting change in HSC-$5^{N\text{-}WASP}$ cells (Fig. 44). Above it were SMEK1, KDM5B, PGR, SMARCA4 and CD24. RNA-Seq (Table 5) and protein microarray (Table 3) suggested FOXO1 as a candidate functional molecule. Although SMEK1, KDM5B, PGR, SMARCA4 and CD24 all are considered more likely as candidate molecules than FOXO1 due to their IPA comparative analysis rankings, all five were found to require interaction with FOXO1 as a central nexus for effecting any change, either as targets of FOXO1 or requiring FOXO1 to assert their cellular effects (Fig. 46A) [199-207]. Various kinases are known to regulate FOXO1, such as AKT, ERK, SGK1 and JNK kinases to name a few (Fig. 46B) [112,114], thus studies of FOXO1 and identification of its regulating kinase in HSC-5 cells were performed.

5.3.2 Validating candidate pathways in HSC-5 sublines

IPA comparative analysis identified 15 pathways, including the Integrin pathway, likely responsible for phenotypic differences between HSC-5^{CTR} and HSC-$5^{N\text{-}WASP}$ cells (Fig.

43). However, the 14 pathways identified require the Integrin pathway as the central nexus to regulate all signalling to regulate cell growth [176-188]. It is possible that the Integrin-mediated signalling is dysregulated in HSC-$5^{N\text{-}WASP}$ cells compared to HSC-5^{CTR} cells.

A thorough literature review performed led to the selection of four signalling pathways – Integrin, EGF, Wnt and Hippo – to be validated in HSC-5 sublines. This is because these pathways are known to regulate cell proliferation and interact with signals from N-WASP [59,81,65,98], thus it was crucial to determine if N-WASP overexpression in HSC-5 cells reduced cell proliferation via any of these pathways. Real-time PCR was performed to validate the Integrin, EGF, Wnt and Hippo pathways via representative pathway target genes. Even though the Hippo pathway was not implicated in proteomics analysis (Fig. 31,32), validation of the pathway was still performed to determine if Hippo signalling is affected in HSC-$5^{N\text{-}WASP}$ cells. Integrin signals were reported to cause FOXO phosphorylation [89] and that FOXO1 is involved in skin cell morphogenesis and *stratum basale* keratinocyte proliferation [121,122], thus FOXO1 was chosen to validate the Integrin pathway. The PKM2 gene supports glycolytic processes for DNA synthesis and cell proliferation by the EGF pathway [256]. cMyc is a well-known Wnt pathway target gene that regulates cell proliferation [92] and CTGF is a Hippo pathway target gene vital for development [98]. The only significant change was observed for FOXO1 mRNA levels (Fig. 47), suggesting only the Integrin pathway is influenced by N-WASP in HSC-5 cells.

Validation of Integrin pathway was further carried out by studying the expressions of FAK, SRC, GRB2 and SOS1, components of the Integrin-controlled focal adhesion signalling [189,190]. Expressions of FAK, SRC and GRB2 were found to be reduced in HSC-$5^{N\text{-}WASP}$ compared to HSC-5^{CTR} cells (Fig. 48-50). This is consistent with the reduced proliferation phenotype, since activities of FAK, SRC and GRB2 are known to be proportionate to cell proliferation [209,212,213]. SOS1 expression, however, was found to be increased in HSC-$5^{N\text{-}WASP}$ cells (Fig. 51), suggesting SOS1 may be a tumour suppressor in HSC-5 cells. These studies suggest that N-WASP does regulate HSC-5 cell proliferation via dysregulation of the Integrin-mediated FAK-SRC-GRB2-SOS1 signalling.

Up-regulation of phospho-p70S6K and RSK1/2/3 (Table 3) suggest involvement of mTOR pathway, which regulates cell growth via protein synthesis and is downstream of the AKT pathway [220,221]. It was observed that HSC-5$^{N\text{-}WASP}$ cells had reduced AKT activity but increased PTEN activity (Fig. 27,28), therefore HSC-5$^{N\text{-}WASP}$ cells may have reduced mTOR signalling to cause reduced proliferation. However, since there was no change to active mTOR and 4E-BP1 levels between HSC-5 sublines (Fig. 52,53), this suggests the mTOR pathway is not responsible for reduced proliferation in HSC-5 cells. Changes observed to STAT1, BMX, Met, Ezrin, PTPD1 and PKCl (Table 3,4) suggest a reduction in proliferative signalling and an increase of anti-proliferative signalling in HSC-5$^{N\text{-}WASP}$ cells via the STAT1 and cytokine signalling pathways [224-229]. Cell proliferation assays of HSC-5 sublines with and without FBS were done to investigate the involvement of cytokine-mediated signalling. However, as absence of serum caused further reduction of HSC-5$^{N\text{-}WASP}$ cell proliferation (Fig. 54), this suggests that the STAT1 and cytokine-mediated signalling are not responsible for reduced proliferation in HSC-5 cells. All these results reinforce the notion that Integrin-mediated signalling is affected in HSC-5$^{N\text{-}WASP}$ cells.

5.3.3 Validating FOXO1 and its kinases in HSC-5 sublines

IPA comparative analysis identified FOXO1 and five additional regulators (SMEK1, KDM5B, PGR, SMARCA4, CD24) (Fig. 44) as candidate functional molecules responsile for phenotypic differences between HSC-5^{CTR} and HSC-5$^{N\text{-}WASP}$ cells. FOXO1 is considered a central nexus for the other five regulators to assert cellular effects [199-207] (Fig. 46A). It is possible that FOXO1 expression and activity is dysregulated in HSC-5$^{N\text{-}WASP}$ cells compared to HSC-5^{CTR} cells. Studies of FOXO1 in HSC-5 cells, as well as identification of its regulating kinase and its role in HSC-5 cells, were performed.

FOXO1 expression is reduced in HSC-5$^{N\text{-}WASP}$ cells compared to HSC-5^{CTR} cells (Fig. 56); however, its mRNA levels are increased in HSC-5$^{N\text{-}WASP}$ cells (Fig. 55). Protein microarray of HSC-5 sublines found HSC-5$^{N\text{-}WASP}$ cells had up-regulated phospho-FOXO1 levels (Table 3, Fig. 57). MG132 treatment in HSC-5 sublines raised pan-FOXO1 levels compared to DMSO treatment (Fig. 58). HSC-5$^{N\text{-}WASP}$ cells had reduced nuclear FOXO1 compared to HSC-5^{CTR} cells (Fig. 59,60). These results suggested that increased N-WASP levels caused FOXO1 translocation out of the nucleus and

proteasomal degradation in HSC-5 cells. The observation of reduced expression but increased transcription suggested that HSC-5$^{N\text{-}WASP}$ cells are compensating for reduced FOXO1 protein levels to maintain the minimum FOXO1 signalling needed.

FOXO1 was overexpressed in HSC-5 and HaCaT cells to study its role in both skin cancer and normal cells. FOXO1 overexpression in HSC-5 sublines was achieved, but this reduced cell proliferation further compared to controls (Fig. 61). FOXO1 overexpression in HaCaT cells was achieved, which led to increased cell proliferation compared to controls (Fig. 62). These results suggest that FOXO1 represses HSC-5 cell proliferation but supports HaCaT cell proliferation, corroborating with scientific opinion of FOXO1 being capable of multiple functions across many cell lines and types [112]. FOXO1 knockdown has also been reported to both promote and suppress wound healing of mouse dermal wounds in two separate reports [257,258]. If FOXO1 overexpression in HSC-5$^{N\text{-}WASP}$ cells to levels of that of HSC-5^{CTR} cells was achieved, it is possible that HSC-5$^{N\text{-}WASP}$ cells may proliferate similar to HSC-5^{CTR} cells.

Many kinases have been shown to regulate FOXO1 via phosphorylation [117], including AKT, SGK1, MST1, JNK and ERK2 (Fig. 46). Identification of the regulating kinase allows understanding of the relationship between N-WASP overexpression, FOXO1 activity and changes in Integrin signalling, cell migration and cell proliferation in HSC-5 cells. AKT is ruled out because its reduced activity (Fig. 27,28) is contrary to established notions that increased AKT activity correlates with increased FOXO1 phosphorylation. SGK1 and JNK kinase mRNA levels were found to be increased in HSC-5$^{N\text{-}WASP}$ cells (Table 5). SGK1 knockdown in HSC-5$^{N\text{-}WASP}$ cells did not restore cell proliferation to levels that of HSC-5^{CTR} cells (Fig. 63). JNK inhibition reduced HSC-5 sublines' cell proliferation in a dose-dependent manner compared to that of DMSO treatment (Fig. 64). Thus, SGK1 and JNK kinases are considered not likely the kinases phosphorylating FOXO1 in HSC-5 cells.

ERK2 is well-known to promote cell proliferation [246,247] and was recently established to be able to phosphorylate FOXO1 in NIH3T3 cells [250]. It is possible that active ERK2 is reduced in HSC-5$^{N\text{-}WASP}$ cells compared to HSC-5^{CTR} cells. However, HSC-5$^{N\text{-}WASP}$ cells were found to have increased active ERK2 compared to HSC-5^{CTR} cells (Fig. 65). Inhibition of ERK2 with the ERK2-specific inhibitor sc-222229, blocking

ERK2 substrate phopshorylation [259,260] not only restored HSC-5$^{N\text{-}WASP}$ cell proliferation to that of HSC-5^{CTR} cells (Fig. 66), but raised pan-FOXO1 levels (Fig. 68) and prevented translocation of FOXO1 for cytoplasmic degradation and stabilized nuclear FOXO1 to levels that of HSC-5^{CTR} cells (Fig. 69,70). Cytosolic FOXO1 of HSC-5$^{N\text{-}WASP}$ cells, which was increased compared to that of HSC-5^{CTR} cells, was reduced after sc-222229 treatment (Fig. 70). These results suggest that FOXO1 is necessary for cell proliferation and ERK2 may be responsible for the phosphorylation of FOXO1 in HSC-5 cells.

ERK2 inhibition via sc-222229 treatment in HSC-5$^{N\text{-}WASP}$ cells also restored cell migration (Fig. 73,75) and localizations of E-cadherin (Fig. 71), vinculin (Fig. 77) and paxillin (Fig. 79) to levels that of HSC-5^{CTR} cells. Expressions of E-cadherin (Fig. 72), vinculin (Fig. 78) and paxillin (Fig. 80) were similar despite the differences in protein localizations due to ERK2 inhibition. This reinforces the notion that N-WASP causes ERK2-dependent FOXO1 phosphorylation and cytoplasmic proteasomal degradation in HSC-5 cells. This likely leads to changes in Integrin-mediated signalling and AKT signalling, which lead to changes in cell migration and proliferation phenotypes.

It was debated if reversal of cell migration phenotypes observed following ERK2 inhibition were due to changes of cell proliferation. Wound healing assays of HSC-5 sublines treated with DMSO or sc-222229 were repeated with the anti-proliferative drug AraC, showing the same cell migration patterns (Fig. 74,76) as those observed in wound healing assays carried out without AraC (Fig. 73,75). This suggested that N-WASP regulates both cell migration and proliferation, and cell migration is not influenced by proliferative activity; both phenotypes are independent from one another. ERK2 inhibition of HSC-5$^{N\text{-}WASP}$ cells had rescued cell proliferation rates to HSC-5^{CTR} cells (Fig. 66), but had a partial rescue of CCND1 expression (Fig. 67). It is possible that in presence of sc-222229, partial rescue of CCND1 is sufficient to rescue cell proliferation defects. Similar FOXO1 expressions were observed in DMSO-treated HSC-5 sublines (Fig. 68A), in contrast to the reduced expression previously observed (Fig. 56). It is possible that HSC-5$^{N\text{-}WASP}$ cells have compensated FOXO1 levels for those that were degraded due to N-WASP overexpression.

HSC-5 sublines with ERK2 inhibition had increased active ERK2 compared to DMSO-treated sublines (Fig. 81). Knockdown of ERK2 via shRNA in HSC-5 sublines (Fig. 82), to characterize the role of ERK2 in HSC-5 cells, found further reduction of cell proliferation (Fig. 83). The cell proliferation results (Fig. 66,83) suggested the presence of a complex of ERK2 with ERK2-interacting proteins that regulates HSC-5 cell proliferation. ERK2 knockdown via shRNA possibly disrupted this complex, further reducing HSC-5 cell proliferation (Fig. 83). ERK2 inhibition does not disrupt this ERK2 complex but only inhibits ERK2 substrate phosphorylation by ERK2 which leads to increased active ERK2 in a negative-feedback manner (Fig. 81), restoring HSC-$5^{N\text{-}WASP}$ cell proliferation (Fig. 66). The operation of this hypothesized ERK2 complex, and how N-WASP regulates it and its precise effects on cell migration and proliferation, remain unknown at this point and should be studied eventually.

5.4 The role of TXNIP in HSC-5 sublines

5.4.1 Characterizing TXNIP phenotypes in HSC-5 sublines

RNA-Seq showed up-regulation of a FOXO1 target gene, TXNIP (Table 5), which negatively regulates the ROS-scavenging thioredoxin system [133]. TXNIP expression is reportedly silenced or reduced in many cancers [134]. This could explain the increased cell proliferation rate of cancer cells compared to normal cells. HSC-$5^{N\text{-}WASP}$ cells had increased TXNIP expressions compared to HSC-5^{CTR} cells (Fig. 84). TXNIP mRNA levels correlated with protein levels (Fig. 85), suggesting increased transcription of TXNIP in HSC-$5^{N\text{-}WASP}$ cells. TXNIP knockdown via shRNA in HSC-$5^{N\text{-}WASP}$ cells not only restored cell proliferation (Fig. 86), but also cell migration (Fig. 90,92) and localizations of E-cadherin (Fig. 88), vinculin (Fig. 94) and paxillin (Fig. 96) to levels that of HSC-5^{CTR} cells. Changes of localizations of E-cadherin (Fig. 89), vinculin (Fig. 95) and paxillin (Fig. 97) are not due to any differences in protein levels due to TXNIP knockdown.

It was debated if reversal of cell migration phenotypes observed following TXNIP knockdown were due to changes of cell proliferation. Wound healing assays of HSC-5 sublines treated with or without TXNIP knockdown were repeated with the anti-proliferative drug AraC, showing the same cell migration patterns (Fig. 91,93) as those observed in wound healing assays carried out without AraC (Fig. 90,92). These results reinforce the notion that N-WASP regulates both HSC-5 cell migration and proliferation;

both activities are independent and do not influence one another. CCND1 expression was further reduced in HSC-5$^{N\text{-}WASP\text{-}TXNIP\text{-}KD}$ cells compared to HSC-5$^{N\text{-}WASP}$ cells (Fig. 87). It is possible that this negative regulation of CCND1 in HSC-5$^{N\text{-}WASP\text{-}TXNIP\text{-}KD}$ cells occurred in order to ensure efficient transit of cell cycle past the S phase [261,262] and support the increase of cell proliferative activity. It is possible that CCND1 is able to operate in different ways to support HSC-5 cell proliferation, given its partial rescue of expression following ERK2 inhibition (Fig. 67) and the observed further reduction following TXNIP knockdown (Fig. 87).

A profiling of N-WASP in nuclear and cytosol fractions showed only HSC-5$^{N\text{-}WASP\text{-}TXNIP\text{-}KD}$ cells having very reduced nuclear N-WASP, in contrast to all other sublines which had similar expressions (Fig. 100). FAK phosphorylation of N-WASP at Tyr256 has been reported to prevent N-WASP accumulation in the nucleus [64] and promotes N-WASP-dependent actin polymerization in the cytoplasm [68]. It is possible that TXNIP knockdown restored FAK activity in HSC-5$^{N\text{-}WASP\text{-}TXNIP\text{-}KD}$ cells, and that of SRC as well, since it was reported that increased SRC also prevents N-WASP accumulation in the nucleus [263]. HSC-5$^{N\text{-}WASP\text{-}TXNIP\text{-}KD}$ cells had similar cell proliferation rates (Fig. 86), similar localizations of vinculin (Fig. 94) and paxillin (Fig. 96), and similar cell migration (Fig. 90,92) to that of HSC-5$^{CTR\text{-}CTR}$ cells. These results suggested that altered Integrin-mediated FAK-SRC-GRB2-SOS1 signalling and even AKT signalling are downstream of TXNIP knockdown. The same could be said for ERK2 inhibition, since the observed reversal of phenotypes of cell migration and proliferation in HSC-5 cells are similar, either after ERK2 inhibition or TXNIP knockdown.

ROS studies showed HSC-5$^{N\text{-}WASP}$ cells had increased ROS levels compared to HSC-5^{CTR} cells, and that TXNIP knockdown reverted ROS levels of HSC-5$^{N\text{-}WASP}$ cells back to that of HSC-5^{CTR} cells (Fig. 98). HSC-5$^{N\text{-}WASP}$ cells had the most fluorescence of Annexin-V and PI corresponding to apoptosis and cell necrosis, respectively, whereas the other three HSC-5 sublines had reduced yet similar fluorescence (Fig. 99). These suggest that cell proliferation defects in HSC-5$^{N\text{-}WASP}$ cells compared to HSC-5^{CTR} cells was not due to ROS-induced cell apoptosis due to increased TXNIP expression, but due to ROS-influenced changes of signalling pathways that lead to reduced cell proliferation. It was reported that thioredoxin system influences MCF7 breast cell proliferation via

regulation of ERK1/2 and CCND1 activities [264], supporting the notion that ROS regulation influences HSC-5 cell processes.

Finally, TXNIP was overexpressed in HSC-5 and HaCaT cells to elucidate its role in skin cells. HSC-$5^{TXNIP-OE}$ cells grew very slowly compared to HSC-5^{CTRN} cells and could not be maintained *in vitro* (Fig. 101), probably due to high levels of overexpression of TXNIP. Although TXNIP overexpression in HaCaT cells was not achieved, TXNIP knockdown was successfully performed and HaCaT$^{TXNIP-KD}$ cells had reduced cell proliferation compared to HaCaT^{CTRN} cells (Fig. 102). These suggest that TXNIP operates differently in both HSC-5 and HaCaT cells, since TXNIP represses HSC-5 cell proliferation, but possibly promotes HaCaT cell proliferation. Increased *in vitro* TXNIP levels reduced thioredoxin levels and increased ROS levels [130,137]. FOXO1 accelerates wound healing of mouse dermal wounds by both TGFβ1-dependent and TGFβ1-independent signalling for eliminating ROS-induced oxidative stress [265]. Since TXNIP is negatively regulated by FOXO1, the direct roles of FOXO1, TXNIP and ROS in cellular processes could be studied eventually.

N-WASP overexpression in HSC-5 cells likely changed the phenotypes tested by negatively regulating the interactions of TXNIP and thioredoxin system, and increased ROS build-up instead of ROS scavenging. Increased N-WASP levels in HSC-5 cells (Fig. 17) correlated with reduced FOXO1 levels (Fig. 56), increased active ERK2 (Fig. 65) and increased TXNIP levels (Fig. 84). Increased N-WASP levels also correlated with reduced FAK activity and reduced SRC and GRB2 levels (Fig. 48-50), increased SOS1 levels (Fig. 51) and reduced AKT activity (Fig. 27,28). These suggest that in HSC-5 cells, N-WASP relieves FOXO1 inhibition of TXNIP via ERK2-dependent phosphorylation of FOXO1, leading to FOXO1 degradation, increased TXNIP expression and increased ROS levels. The increase in ROS levels leads to changes in Integrin-mediated signalling causing reduced cell migration and changes in AKT signalling causing reduced cell proliferation.

5.4.2 Proposal of an N-WASP-ERK2- FOXO1-TXNIP mechanism

The results of assays performed to study the role N-WASP in skin cancer cells can be summarized as such – HSC-5^{N-WASP} cells had reduced cell proliferation, cell migration, paxillin patches and AKT activity but increased E-cadherin localizations and vinculin

patches compared to HSC-5^{CTR} cells. IPA comparative analysis of proteomics, protein microarray and RNA-Seq suggested the Integrin pathway and FOXO1 as being responsible for changes in phenotypes between HSC-5^{CTR} and HSC-5$^{N\text{-}WASP}$ cells. Assays performed showed that the Integrin signalling and FOXO1 regulation in HSC-5$^{N\text{-}WASP}$ cells are dysregulated compared to HSC-5^{CTR} cells. ERK2 is the likely kinase regulating FOXO1 in HSC-5 cells with N-WASP overexpression. Both inhibition of ERK2 and knockdown of the FOXO1 target gene TXNIP in HSC-5$^{N\text{-}WASP}$ cells restored cell proliferation, cell migration and localizations of E-cadherin, vinculin and paxillin back to levels that of HSC-5^{CTR} cells. Cell proliferation rate changes between HSC-5^{CTR} and HSC-5$^{N\text{-}WASP}$ cells is probably not due to ROS-induced cell apoptosis, but ROS-induced changes to cell signalling that affect cell proliferation and migration. In other words, this dissertation aims to provide a possible explanation of how skin cancer cells, or early-stage cancerous skin cells, regulate cell proliferation when N-WASP expression is reduced.

It is proposed that in HSC-5 cells, N-WASP levels are reduced, preventing ERK2-dependent FOXO1 nuclear export and cytoplasmic degradation, keeping FOXO1 in the nucleus and repressing TXNIP expression, allowing thioredoxin system-mediated ROS scavenging to go unhindered, affecting Integrin-mediated signalling such as reducing SOS1 activity but increasing FAK, SRC and GRB2 activities to increase cell migration via reduced cell adhesion, and increase cell proliferation via increased AKT activity (Fig. 103). When N-WASP is overexpressed in HSC-5 cells to mimic normal skin keratinocytes with high N-WASP protein levels, N-WASP causes ERK2-dependent FOXO1 nuclear export and cytoplasmic degradation, relieving repression of TXNIP which proceeds to interfere with the thioredoxin system, accumulate ROS and negatively regulate Integrin-mediated signalling such as causing reduced FAK, SRC and GRB2 activities but increased SOS1 activity to reduce cell migration via increased cell adhesion, and reduced cell proliferation via reduced AKT activity (Fig. 104).

It is possible that SCCs are formed from normal skin cells *in vivo* with this mechanism of action. To our knowledge, this is the first study of the roles of N-WASP, ERK2, FOXO1 and TXNIP in skin cell proliferation and migration. *In vivo* studies can help substantiate the proposed *in vitro* mechanism and data into *in vivo* preventive and treatment solutions for skin cancer.

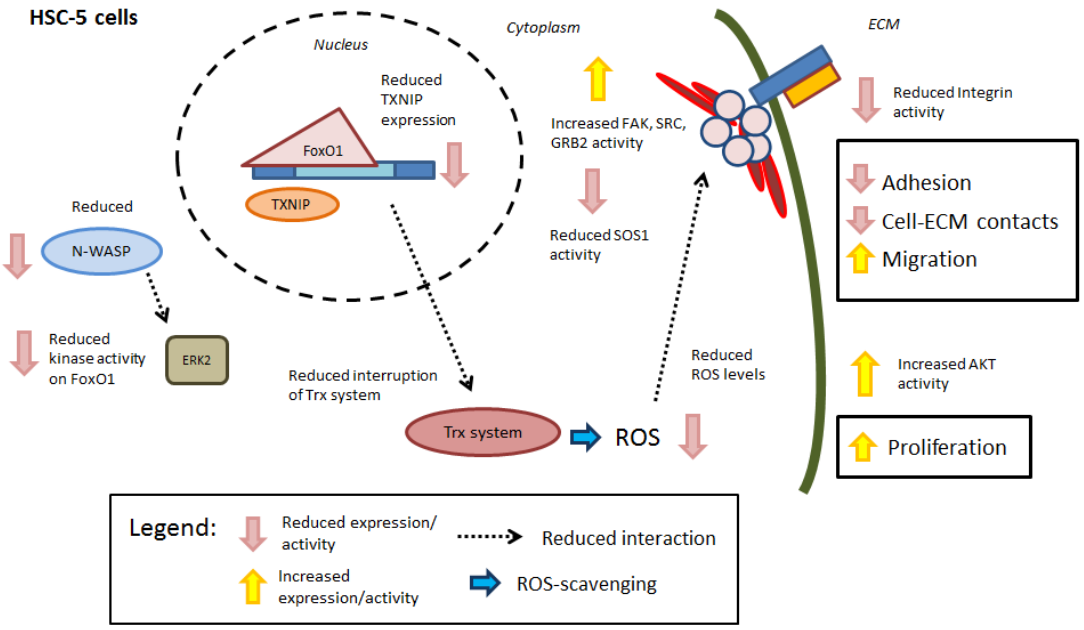

Figure 103: A proposed N-WASP-ERK2-FOXO1-TXNIP mechanism in HSC-5 cells. In HSC-5 cells, low N-WASP levels keep FOXO1 in the nucleus to repress TXNIP, allowing the thioredoxin system to scavenge ROS, leading to promotion of cell migration and proliferation via Integrin-mediated FAK-SRC-GRB2-SOS1 signalling and AKT signalling, thus leading to skin carcinogenesis.

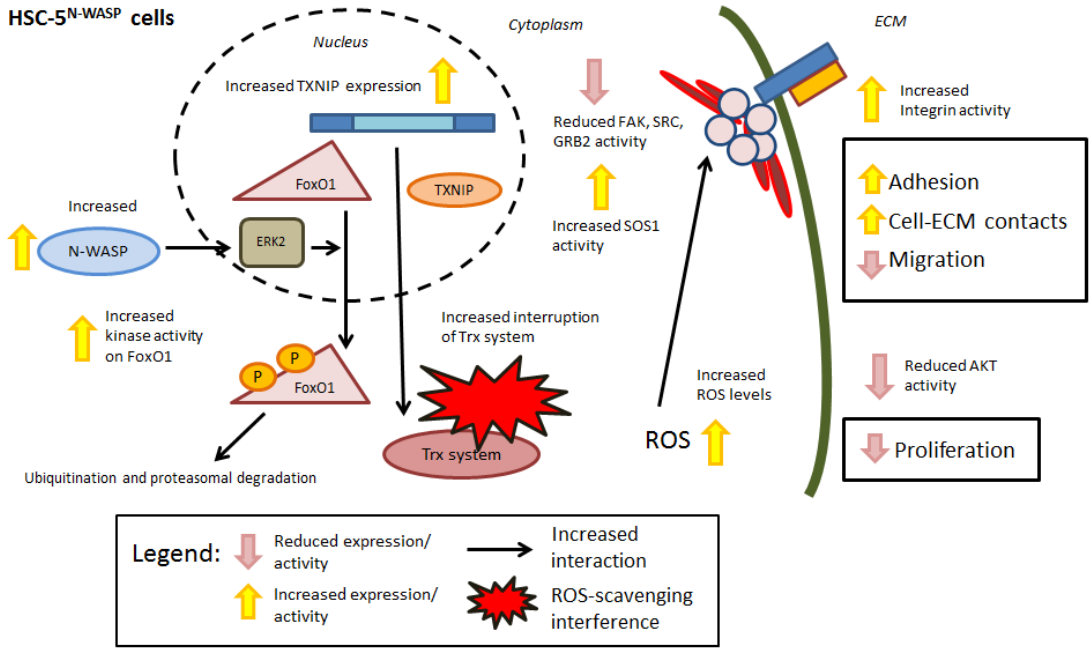

Figure 104: A proposed N-WASP-ERK2-FOXO1-TXNIP mechanism in HSC-5$^{N\text{-}WASP}$ cells. In HSC-5$^{N\text{-}WASP}$ cells, high N-WASP levels cause FOXO1 phosphorylation via ERK2 activity, relieving repression on TXNIP transcription. TXNIP interferes with the thioredoxin system and presence of excess ROS levels alters Integrin-mediated FAK-SRC-GRB2-SOS1 signalling and AKT signalling, suppressing cell migration and proliferation, which interferes with skin carcinogenesis.

Conclusion

The ubiquitously-expressed N-WASP plays a critical role in actin cytoskeleton remodelling. Studies on the HSC-5 and HaCaT skin cell lines suggest that N-WASP plays critical roles in cell proliferation and migration of both cancer and normal skin cells. N-WASP levels are proportionate to localizations of E-cadherin and vinculin, but inversely proportional to cell migration and paxillin localization. HSC-$5^{N\text{-}WASP}$ cells had reduced proliferation, probably due to reduced AKT activity. Multiple analyses of proteomics, protein microarray and RNA-Seq suggest that increased N-WASP levels caused dysregulation of Integrin signalling and down-regulation of FOXO1 signalling, which reduces proliferation in HSC-$5^{N\text{-}WASP}$ cells. Validation of data showed likelihood of an N-WASP-mediated altered Integrin-SRC-FAK-GRB2-SOS1 signalling and ERK2-dependent FOXO1 nuclear translocation and cytoplasmic degradation. Inhibition of ERK2 and knockdown of the FOXO1 target gene, TXNIP, in HSC-$5^{N\text{-}WASP}$ cells *in vitro* both increased cell proliferation, cell migration and paxillin localization but reduced E-cadherin and vinculin localizations, reversing phenotypes tested to that of HSC-5^{CTR} cells. TXNIP knockdown also reduces ROS levels, suggesting that excess ROS in HSC-$5^{N\text{-}WASP}$ cells reduces cell proliferation. It is proposed that in HSC-5 cells, high N-WASP levels causes ERK2-dependent FOXO1 degradation and relieving of repressed TXNIP expression, interference with the thioredoxin system, allowing ROS build-up and suppresses cell migration and proliferation via altered Integrin-SRC-FAK-GRB2-SOS1 and AKT signalling pathways. These *in vitro* findings may be translated into *in vivo* solutions to skin cancer treatment and prevention.

Future Work

The results of this dissertation suggested that N-WASP, ERK2, FOXO1 and TXNIP play crucial roles in normal skin epithelial biology and carcinogenesis. A proposed mechanism is that in skin cells, increased N-WASP levels caused increased ERK2-dependent FOXO1 phosphorylation, relieving repression of TXNIP and increasing transcription of TXNIP which interferes with thioredoxin-mediated ROS scavenging, which affects cell signalling leading to reduced cell proliferation and migration. However, this dissertation is just a small portion of a study into the roles of N-WASP, ERK2, FOXO1 and TXNIP in skin cell biology, especially skin cancer cell biology, since studies were performed on HSC-5 cells.

TXNIP negatively regulates the thioredoxin ROS scavenging system. TXNIP-thioredoxin system interactions are important in regulating cell growth, especially where oxygen species waste is concerned. Long-term or reversible knockdown of any thioredoxin system genes, such as thioredoxin or peroxiredoxin, could be done to study its role in normal skin cells and skin cancer cells. Assays for measuring glycolysis and the specific effects of ROS on cellular processes such as cell adhesion, cell migration and focal adhesion activity by Integrin signalling could be performed to better understand on the role of oxidative stress in *in vitro* cell biology. The role of Integrin signalling can be determined by inhibition, knockdown or knockout of any Integrin subunit or any component of the focal adhesion complex.

The IPA comparative analysis identified the FGF, HGF, PDGF and IL-8 pathways, among others, as candidate pathways regulating HSC-5 cell proliferation and migration. Their profiles in HSC-5 cells are not known at this point, and profiling of these pathways could be performed as a means to further skin cell biology understanding. PKCl levels are known to correlate with cell proliferation rates. HSC-$5^{N\text{-}WASP}$ cells have reduced PKCl expression compared to HSC-5^{CTR} cells, suggesting PKCl as a candidate functional molecule regulating HSC-5 cell proliferation. The role of PKCl can be determined by overexpression studies. Various kinases and proteins regulate FOXO activity, but this dissertation only showed that ERK2 phosphorylates FOXO1 in HSC-5 cells when N-WASP is overexpressed. The profiles of other kinases in HSC-5 cells are not fully characterized. Studies on profiling kinases like AKT, MST1, SGK1 and JNKs in HSC-5 cells can be performed.

In vitro assays in HSC-5 cells represent cellular biology in established human cell lines, but results of these assays should be correlated with *in vivo* biology. Skin SCC and matching skin perilesionals could be isolated from patients for ascertaining the expressions of FOXO1, ERK2, TXNIP and activities of ROS in normal skin cells and skin cancer cells. Oxidative stress due to dysregulation of ROS is an on-going topic of cancer research. The study of ROS levels and other functional molecules such as CD24 and SMARCA4 is an opportunity for further understanding of human skin cell biology and translate *in vitro* findings into *in vivo* treatments and prevention.

Understanding the role N-WASP plays in normal human skin keratinocytes is essential for increasing knowledge of *in vivo* normal skin and skin cancer cell biology. It was shown earlier that in HaCaT cells, FOXO1 overexpression increased cell proliferation rates but TXNIP knockdown reduced such rates. This suggested the presence of complex and cross-talking signalling pathways that promote cell proliferation in HaCaT cells. Proteomics, protein microarray, RNA-Seq, IPA comparative analysis and validation experiments of any candidate pathways or functional molecules identified should be performed on HaCaT cells with N-WASP or TXNIP knockdown, or even FOXO1 overexpression.

References

1. Proksch, E., Brander, J.M., and Jensen, J.M. *The skin: an indispensable barrier*. Exp Dermatol, 2008. 17:1063-1072.
2. McGrath, J.A., et al. In Burns, et al. (eds) *Rook's Textbook of Dermatology*, 7th edn. 2004. Blackwell Publishing:45-128.
3. Ovaere, P., et al. *The emerging roles of serine protease cascades in the epidermis*. Trends Biochem Sci, 2009. 34:453-463.
4. Health, Medicine and Anatomy Reference Pictures. *Labelled skin diagrams*. [Online] 2013. Available from: http://healthfavo.com/labeled-skin-diagrams.html. [Accessed: 20th January 2018].
5. Fuchs, D.A., and Cleveland, D.W. *A structural scaffolding of intermediate filaments in health and disease*. Science, 1998. 279:514-519.
6. Madison, K.C. *Barrier function of the skin: "la raison d'être" of the epidermis*. J Invest Dermatol, 2003. 121:231-241.
7. Agar, N., and Young, A.R. *Melanogenesis: a photoprotective response to DNA damage?* Mutat Res, 2005. 571:121-123.
8. Maricich, S.M., et al. *Merkel cells are essential for light touch response*. Science, 2009. 324:1580-1582.
9. Mitra, A.K., et al. *Drug Delivery*. 2015. Jones & Bartlett Learning:285-286.
10. Croce, C.M. *Oncogenes and cancer*. N Eng J Med, 2008. 358:502-511.
11. Hanahan, D., and Weinberg, R.A. *The hallmarks of cancer*. Cell, 2000. 100:57-70.
12. Bandarchi, B., et al. *From melanocyte to metastatic malignant melanoma*. Dermatol Res Pract, 2010. 583749:1-8.
13. Jemal, A., et al. *Cancer statistics*. CA Cancer J Clin, 2008. 58:71-96.
14. Jerant, A.F., et al. *Early detection and treatment of skin cancer*. Am Fam Physician, 2000. 62:357-368,375-376, 381-382.
15. Runger, T.M., et al. *Comparison of DNA damage responses following equimutagenic doses of UVA and UVB: a less effective cell cycle arrest with UVA may render UVA-induced pyrimidine dimers more mutagenic than UVB-induced ones*. Photochem Photobiol Sci, 2012. 11:207-215.
16. Bataille, V. *Genetic epidemiology of melanoma*. Eur J Cancer, 2003. 39:1341-1347.
17. Smalley, K.S. *A pivotal role for ERK in the oncogenic behaviour of malignant melanoma?* J Int Cancer, 2003. 104:527-532.
18. Humphreys, T.R. *Skin cancer: recognition and management*. Clin Cornerstone, 2001. 4:23-32.
19. Cakir, B.Ö., Adamson, P., and Cingi, C. *Epidemiology and economic burden of nonmelanoma skin cancer*. Facial Plast Surg Clin North Am, 2012. 20:419-422.
20. Han, S., et al. *DNA repair gene XRCC3 polymorphisms and cancer risk: a meta-analysis of 48 case-control studies*. Eur J Hum Genet, 2006. 14:1136-1144.
21. Epstein, E.H., Shepard, J.A., and Flotte, T.J. *Case records of the Massachusetts General Hospita. Case 3-2008. An 80-year-old woman with cutaneous basal-cell carcinoma and cysts of the jaws*. N Engl J Med, 2008. 358:393-401.
22. Janes, S.M., and Watt, F.M. *New roles for integrins in squamous-cell carcinoma*. Nat Rev Cancer, 2006. 6:175-183.
23. Kim, S.A., et al. *Calcium-dependent dynamics of cadherin interactions at cell-cell junctions*. Proc Natl Acad Sci USA, 2011. 108:9857-9862.
24. Fletcher, D.A., and Mullins, R.D. *Cell mechanics and the cytoskeleton*. Nature, 2010. 463:485-492.

25. Doherty, G.J., and McMahon, H.T. *Mediation, modulation and consequences of membrane-cytoskeleton interactions*. Nature, 2008. 37:65-95.
26. Lodish, H., et al. *Molecular Cell Biology*, 4th edn. [Online] 2000. W.H. Freeman. Section 18.1: The Actin Cytoskeleton. Available from https://www.ncbi.nlm.nih.gov/books/ NBK21493/. [Accessed: 1st February 2018].
27. Rotty, J. D., Wu, C., and Bear, J.E. New insights into the regulation and cellular functions of the ARP2/3 complex. *Nat Rev Mol Cell Biol*, 2013. 14:7-12.
28. Visa, N., and Percipalle, P. *Nuclear functions of actin*. Cold Spring Harb Perspect Biol, 2010. 2:a000620.
29. Pollard, T.D., and Borisy, G.G. *Cellular motility driven by assembly and disassembly of actin filaments*. Cell, 2003. 112:453-465.
30. De La Cruz, E.M., et al. *Thymosin-β4 changes the conformation and dynamics of actin monomers*. Biophys J, 2000. 78:2516-2527.
31. Disanza, A., et al. *Actin polymerization machinery: the finish line of signalling networks, the starting point of cellular movement*. Cell Mol Life Sci, 2005. 62:955-970.
32. Egile, C., et al. *Activation of the CDC42 effector N-WASP by the Shigella flexneri IcsA protein promotes actin nucleation by Arp2/3 complex and bacterial actin-based motility*. J Cell Biol, 1999. 146:1319-1332.
33. Chesarone, M.A., and Goode, B.L. *Actin nucleation and elongation factors: mechanisms and interplay*. Curr Opin Cell Biol, 2009. 21:28-37.
34. Lee, S.H., and Dominguez, R. *Regulation of actin cytoskeleton dynamics in cells*. Mol Cells, 2010. 29:311-325.
35. Dayel, M. *How Arp2/3 complex nucleates actin filaments*. [Online] 2015. Available from: http://www.dayel.com/research/arp23-complex/. [Accessed: 28th January 2018].
36. Gumbiner, B.M. *Cell adhesion: the molecular basis of tissue architecture and morphogenesis*. Cell, 1996. 84:345-357.
37. Lampe, P.D., and Lau, A.F. *The effects of connexion phosphorylation on gap junctional communication*. Int J Biochem Cell Biol, 2004. 36:1171-1186.
38. Tsukita, S., Furuse, M., and Itoh, M. *Structural and signalling molecules come together at tight junctions*. Curr Opin Cell Biol, 1999. 11:628-633.
39. Knights, A.J., et al. *Holding tight: cell junctions and cancer spread*. Trends Cancer Res, 2012. 8:61-69.
40. Horwitz, A.R., and Parsons, J.T. *Cell migration – movin' on*. Science, 1999. 286:1102-1103.
41. Huttenlocher, A., and Horwitz, A.R. *Integrins in cell migration*. Cold Spring Harb Perspect Biol, 2001. 3:a005074.
42. Choi, C.K., et al. *Actin and α-actinin orchestrate the assembly and maturation of nascent adhesions in a myosin II motor-independent manner*. Nat Cell Biol, 2008. 10:1039-1050.
43. Petrie, R.J., Doyle, A.D., and Yamada, K.M. *Random versus directionally persistent cell migration*. Nat Rev Mol Cell Biol, 2009. 10:538-549.
44. Rodriguez, O.C. *Conserved microtubule-actin interactions in cell movement and morphogenesis*. Nat Cell Ciol, 2003. 5:599-609.
45. Cory, G.O., and Ridley, A.J. *Cell motility: breaking WAVEs*. Nature, 2002. 418:732-733.
46. Derry, J.M., Ochs, H.D., and Francke, U. *Isolation of a novel gene mutated in Wiskott-Aldrich syndrome*. Cell, 1994. 78:635-644.

47. Thrasher, A.J., and Burns, S.O. *WASP: a key immunological multitasker*. Nat Rev Immunol, 2010. 10:182-192.
48. Imai, K., Nonoyama, S., and Ochs, H.D. *WASP (Wiskott-Aldrich syndrome protein) gene mutations and phenotype*. Curr Opin Allergy Clin Immunol, 2003. 3:427-436.
49. Takenawa, T., and Miki, H. *WASP and WAVE family proteins: key molecules for rapid rearrangement of cortical actin filaments and cell movement*. J Cell Sci, 2001. 114:1801-1809.
50. Zuchero, J.B., et al. *p53-cofactor JMY is a multifunctional actin nucleation factor*. Nat Cell Biol, 2009. 11:451-459.
51. Institut für Molekulare Zellbiologie. *Novel activators of Arp2/3 complex: JMY and WHAMM*. [Online] 2014. Available from: http://www.uni-muenster.de/Biologie.Allgm Zoo/Gruppen/Stradal/Research/arp23act.html. [Accessed: 29th January 2018].
52. Miki, H., Miura, K., and Takenawa, T. N-*WASP a novel actin-depolymerizing protein regulates the cortical cytoskeletal rearrangement in a PIP2-dependent manner downstream of tyrosine kinases*. EMBO J, 1996. 15: 5326-5335.
53. Martinez-Quiles, N., et al. *WIP regulates N-WASP-mediate actin polymerization and filopodium formation*. Nat Cell Biol, 2001. 3:484-491.
54. Weiler, M.C., Smith, J.L., and Masters, J.N. *CR16, a novel proline-rich protein expressed in rat brain neurons, binds to SH3 domains and is a MAP kinase substrate*. J Mol Neurosci, 1996. 7:203-215.
55. Aspenstrom, P. *The WASP-binding protein WIRE has a role in the regulation of the actin filament system downstream of the platelet-derived growth factor receptor*. Exp Cell Res, 2002. 279:21-33.
56. Higgs, H.N., and Pollard, T.D. *Activation by Cdc42 and Pip2 of Wiskott-Aldrich syndrome protein (WASP) stimulates actin nucleation by Arp2/3 complex*. J Cell Biol, 2000. 150:1311-1320.
57. Kowalski, J.R., et al. *Cortactin regulates cell migration through activation of N-WASP*. J Cell Sci, 2005. 118:79-87.
58. Machesky, L.M., and Insall, R.H. *Scar1 and the related Wiskott-Aldrich syndrome protein, WASP, regulate the actin cytoskeleton through the Arp2/3 complex*. Curr Biol, 1998. 8:1347-1356.
59. Wu, X., et al. *Focal adhesion kinase regulation of N-WASP subcellular localization and function*. J Biol Chem, 2004. 279:9565-9576.
60. Padrick, S.B., et al. *The interaction between N-WASP and the Arp2/3 complex links Cdc42-dependent signals to actin assembly*. Cell, 1999. 97:221-231.
61. Kessels, M.M., and Qualmann, B. *Syndapins integrate N-WASP in receptor-mediated endocytosis*. EMBO J, 2002. 21:6083-6094.
62. Benesch, S., et al. *N-WASP deficiency impairs EGF internalization and actin assembly at clathrin-coated pits*. J Cell Sci, 2005. 118:3103-3115.
63. Wu, X., et al. *Regulation of RNA polymerase II dependent transcription by N-WASP and its nuclear-binding partners*. Nat Cell Biol, 2006. 8:756-763.
64. Park, S.J., and Takenawa, T. *Neural Wiskott-Aldrich syndrome protein is required for accurate chromosome congression and segregation*. Mol Cells, 2011. 31:515-521.
65. Lyubimova, A., et al. *Neural Wiskott-Aldrich syndrome protein modulates Wnt signalling and is required for hair follicle cycling in mice*. J Clin Invest, 2010. 120:446-456.

66. Lommel, S., et al. *Actin-pedestal formation by enteropathogenic* Eschrichia coli *and intracellular motility of Shigella flexneri are abolished in N-WASP-defective cells*. EMBO Rep, 2001. 2:850-857.
67. Snapper, S.B. et al. *N-WASP deficiency reveals distinct pathways for cell surface projections and microbial actin-based motility*. Nat Cell Biol, 2001. 3:897-904.
68. Krueger, E.W., et al. *A dynamin-cortactin-Arp2/3 complex mediates actin reorganization in growth factor-stimulated cell*. Mol Biol Cell, 2003. 14:1085-1096.
69. Yamaguchi, H, et al. *Molecular mechanisms of invadopodium formation: the role of the N-WASP-Arp2/3 complex pathway and cofilin*. J Cell Biol, 2005. 168:441-452.
70. Takano, K., et al. *Nebulin and N-WASP cooperate to cause IGF-1-induced sarcomeric actin filament formation*. Science, 2010. 330:1536-1540.
71. Kovacs, E.M., et al. *N-WASP regulates the epithelial junctional actin cytoskeleton through a non-canonical post-nucleation pathway*. Nat Cell Biol, 2011. 13:934-943.
72. Yanagawa, H., et al. *Genome-wide screening of genes showing altered expression in liver metastases of humancolorectal cancers by cDNA microarray*. Neoplasia, 2001. 3:395-401.
73. Frugtniet, B.A., et al. *Neural Wiskott-Adlrich syndrome protein (nWASP) is implicated in human lung cancer invasion*. BMC Cancer, 2017. 17:224.
74. Bourguignon, L.Y.W., et al. *Hyaluronan-CD44 interaction with neural Wiskott-Aldrich syndrome protein (N-WASP) promotes actin polymerization and Erb2 activation leading to β-catenin nuclear translocation, transcriptional up-regulation, and cell migration in ovarian tumour cells*. J Biol Chem, 2007. 282:1265-1280.
75. Chan, G., Nogalski, M.T., and Yurochko, A.D. *Activation of EGFR on monocytes is required for human cytomegalovirus entry and mediates cellular motility*. Proc Natl Acad Sci USA, 2009. 106:22369-22374.
76. Cotta-de-Almeida, V., et al. *Wiskott-Aldrich syndrome protein (WASP) and N-WASP are critical for T cell development*. Proc Natl Acad Sci USA, 2007. 104:15424-15429.
77. Manchanda, N., et al. *The NF2 tumour suppressor Merlin and the ERM proteins interact with N-WASP and regulate its actin polymerization function*. J Biol Chem, 2005. 280:12517-12522.
78. Park, J., et al. *Dyrk1A negatively regulates the actin cytoskeleton through threonine phosphorylation of N-WASP*. J Cell Sci, 2012. 125:67-80.
79. Martin, T.A., et al. *N-WASP is a putative tumour suppressor in breast cancer cells, in vitro and in vivo, and is associated with clinical outcome in patients with breast cancer*. Clin Exp Metastasis, 2008. 25:97-108.
80. Martin, T.A., et al. *The clinical and biological implications of N-WASP expression in human colorectal cancer*. Transl Gastrointest Cancer, 2012. 1:10-20.
81. Misra, A., et al. *Hypoxia activated EGFR signalling induces epithelial to mesenchymal transition (EMT)*. PLoS:One, 2012. 7:e49766.
82. Lorenz, M., et al. Imaging sites of N-WASP activity in lamellipodia and invadopodia of carcinoma cells. Curr Biol, 2004. 14:697-703.
83. Gadea, G., et al. *DOCK10-mediated Cdc42 activation is necessary for amoeboid invasion of melanoma cells*. Curr Biol, 2008. 18:1456-1465.
84. Yu, X., et al. *N-WASP coordinates the delivery and F-actin-mediated capture of MT1-MMP at invasive pseudopods*. J Cell Biol, 2012. 199:527-544.

85. Wang, S., and Huang, C. *N-WASP, a colorectal cancer suppressor?* Transl Gastrointest Cancer, 2012. 1:5-6.
86. Watt, F.M. *Role of integrins in regulating epidermal adhesion, growth and differentiation*. EMBO J, 2002. 22:2324-2333.
87. Calderwood, D.A., Shattil, S.J., and Ginsberg, M.H. *Integrins and actin filaments: reciprocal regulation of cell adhesion and signalling*. J Biol Chem, 2004. 275:22607-22610.
88. Zhang, X., et al. *N-WASP-directed actin polymerization activates Cas phosphorylation and lamellipodium spreading*. J Cell Sci, 2014. 127:1394-1405.
89. Downward, J. *Targeting Ras signalling pathways in cancer therapy*. Nat Rev Cancer, 2003. 3:11-22.
90. Biteau, B., and Jasper, H. *EGF signalling regulates the proliferation of intestinal steam cells in* Drosophila. Development, 2011. 138:1045-1055.
91. Goessling, W., et al. *Genetic interaction of PGE2 and Wnt signalling regulates developmental specification of stem cells and regeneration*. Cell, 2009. 136:1136-1147.
92. Logan, C.Y., and Nusse, R. *The Wnt signalling pathway in development and disease*. Annu Rev Cell Dev Biol, 2004. 20:781-810.
93. Komiya, Y., and Habas, R. *Wnt signal transduction pathways*. Organogenesis, 2008. 4:68-75.
94. Justice, R.W., et al. *The Drosophila tumour suppressor gene Warts encodes a homolog of human myotonic dystrophy kinase and is required for the control of cell shape and proliferation*. Genes Dev, 1995. 9:534-546.
95. Tapon, N., et al. *Salvador promotes both cell cycle exit and apoptosis in* Drosophila *and is mutated in human cancer cell lines*. Cell, 2002. 110:467-478.
96. Jia, J., et al. *The Drosophila Ste20 family kinase dMST functions as a tumour suppressor by restricting cell proliferation and promoting apoptosis*. Genes Dev, 2003. 17:2514-2519.
97. Lai, Z.C., et al. *Control of cell proliferation and apoptosis by Mob-as-tumour-suppressor, Mats*. Cell, 2005. 120:675-685.
98. Pan, D.J. *The Hippo signalling pathway in development and cancer*. Dev Cell, 2010. 19:491-505.
99. Badouel, C., et al. *The FERM-domain protein Expanded regulates Hippo pathway activity via direct interactions with the transcriptional activator Yorkie*. Dev Cell, 2009. 16:411-420.
100. Oh, H., Reddy, B.V., and Irvine, K.D. *Phosphorylation-independent repression of Yorkie in Fat-Hippo signalling*. Dev Biol, 2009. 335:188-197.
101. Dong, J., et al. *Elucidation of a universal size-control mechanism in* Drosophila *and mammals*. Cell, 2007. 130:120-133.
102. Ivkovic, S., et al. *Connective tissue growth factor coordinates chondrogenesis and angiogenesis during skeletal development*. Development, 2003. 130:2779-2791.
103. Karin, M. *Too many transcription factors: positive and negative interactions*. New Biol, 1990. 2:126-131.
104. Lee, T.I., and Young, R.A. *Transcription of eukaryotic protein-coding genes*. Annu Rev Genet, 2000. 34:77-137.
105. Latchman, D.S. *Transcription factors: an overview*. Int J Exp Path, 1993. 74:417-422.
106. Matys, V., et al. *TRANSFAC and its module TRANSCompel: transcriptional gene regulation in eukaryotes*. Nucleic Acids Res, 2006. 34:D-108-110.

107. Stegmaier, P., Kel, A.E., and Wingender, E. *Systematic DNA-binding domain classification of transcription factors*. Genome Inform Int Confer Genome Inform, 2004. 15:276-286.
108. Tuteja, G., and Kaestner, K.H. *SnapShot: forkhead transcription factors I*. Cell, 2007. 130:1160.e1-1160.e2.
109. Lehmann, O.J., et al. *Fox's in development and disease*. Trends Genet, 2003. 19:339-344.
110. Weigel, D., et al. *The homeotic gene fork head encodes a nuclear protein and is expressed in the terminal regions of the* Drosophila *embryo*. Cell, 1989. 57:645-658.
111. Kaestner, K.H., Knochel, W., and Martinez, D.E. *Unified nomenclature for the winged helix/forkhead transcription factors*. Genes Dev, 2000. 14:142-146.
112. Lam, E.W.F., et al. *Forkhead box proteins: tuning forks for transcriptional harmony*. Nat Rev Cancer, 2013. 13:482-495.
113. Golson, M.L., and Kaestner, K.H. *Fox transcription factors: from development to disease*. Development, 2016. 143:4558-4570.
114. Huang, H., and Tindall, D.J. *Regulation of FOXO protein stability via ubiquitination and proteasome degradation*. Biochim Biophys Acta, 2011. 1813:1961-1964.
115. Greer, E.L., and Brunet, A. *FOXO transcription factors at the interface between longevity and tumour suppression*. Oncogene, 2005. 24:7410-7425.
116. Kawamori, D., et al. *The forkhead transcription factor Foxo1 bridges the JNK pathway and transcription factor PDX-1 through its intracellular translocation*. J Biol Chem, 2006. 281:1091-1098.
117. Obsil, T., and Obsilova, V. *Structure/function relationships underlying regulation of FOXO transcription factors*. Oncogene, 2008. 27:2263-2275.
118. Ciechomska, I., et al. *Inhibition of Akt kinase signalling and activation of Forkhead are indispensable for upregulation of FasL expression in apoptosis of glioma cells*. Oncogene, 2003.22:7617-7627.
119. Ferdous, A., et al. *Forkhead factor FoxO1 is essential for placental morphogenesis in the developing embryo*. Proc Natl Acad Sci USA, 2011. 108:16307-16312.
120. Barr, F.G. *Gene fusions involving PAX and FOX family members in alveolar rhabdyomyosarcoma*. Oncogene, 2001. 20:5736-5746.
121. Tsitsipatis, D., Klotz, L.-O., and Steinbrenner, H. *Multifaceted functions of the forkhead box transcription factors FoxO1 and FoxO3 in skin*. Biochim Biophys Acta, 2017. 1861:1057-1064.
122. Gunschmann, C., et al. *Insulin/IGF-1 controls epidermal morphogenesis via regulation of FoxO-mediated p63 inhibition*. Dev Cell, 2013. 26:176-187.
123. Watanabe, R., et al. *Anti-oxidative, anti-cancer and anti-inflammatory actions by thioredoxin 1 and thioredoxin-binding protein-2*. Pharmacol Ther, 2010. 127:261-270.
124. Kang, S.W., Lee, S., and Lee, E.K. *ROS and energy metabolism in cancer cells: alliance for fast growth*. Arch Pharm Res, 2015. 38:338-345.
125. Liu, B., et al. *Dihyodromyricetin induces mouse hepatoma Hepal-6 cell apoptosis via the transforming growth factor-beta pathway*. Mol Med Rep, 2015. 11:1609-1614.
126. Circu, M.L., and Aw, T.Y. *Reactive oxygen species, cellular redox systems and apoptosis*. Free Radic Biol Med, 2010. 48:749-762.
127. Yoshihara, E., et al. *Thioredoxin/Txnip: redoxisome, as a redox switch for the pathogenesis of diseases.* Front Immunol, 2014. 4:514.

128. Rhee, S.G., Chae, H.Z., and Kim, K. *Peroxiredoxins: a historical overview and speculative preview of novel mechanisms and emerging concepts in cell signalling*. Free Radic Biol Med, 2005. 38:1543-1552.
129. Rundlof, A.K., and Arner, E.S. *Regulation of the mammalian selenoprotein thioredoxin reductase 1 in relation to cellular phenotype, growth and signalling events*. Antioxid Redox Signal, 2004. 6:41-52.
130. Nishiyama, A., et al. *Identification of thioredoxin-binding protein-2/vitamin D(3) up-regulated protein 1 as a negative regulator of thioredoxin function and expression*. J Biol Chem, 1999. 31:21645-21650.
131. Chen, K.S., and DeLuca, H.F. *Isolation and characterization of a novel cDNA from HL-60 cells treated with 1,25-dihydroxyvitamin D-3*. Biochim Biophys Acta, 1994. 1219:26-32.
132. Patwari, P., et al. *The interaction of thioredoxin with Txnip: evidence for formation of a mixed disulfide by disulfide exchange*. J Biol Chem, 2006. 281:21884-21891.
133. Patwari, P., et al. *Thioredoxin-independent regulation of metabolism by the α-arrestin proteins*. J Biol Chem, 2009. 284:24996-25003.
134. Zhou, J., Yu, Q., and Chng, W.-J. *TXNIP (VDUP-1, TBP-2): a major redox regulator commonly suppressed in cancer by epigenetic mechanisms*. Int J Biochem Cell Biol, 2011. 43:1668-1673
135. Saxena, G., Chen, J., and Shalev, A. *Intracellular shuttling and mitochondrial function of thioredoxin-interacting protein*. J Biol Chem, 2010. 285:3997-4005.
136. Gao, K., et al. *5'-AMP-activated protein kinase attenuates Adriamycin-induced oxidative podocyte injury through thioredoxin-mediated suppression of the apoptosis signal-regulating kinase 1-P38 signaling pathway*. Mol Pharmacol, 2014. 85:460-471.
137. Junn, E., et al. *Vitamin D3 up-regulated protein 1 mediates oxidative stress via suppressing the thioredoxin function*. J Immunol, 2000. 164:6287-6295.
138. Su, C., et al. *Fenofibrate suppressed proliferation and migration of human neuroblastoma cells via oxidative stress dependent of TXNIP upregulation*. Biochem Biophys Res Commun, 2015. 460:983-988.
139. Jin, H.O., et al. *TXNIP potentiates Redd1-induced mTOR suppression through stabilization of Redd1*. Oncogene, 2011.
140. Nishinaka, Y., et al. *Loss of thioredoxin-binding protein-2/vitamin D3 up-regulated protein 1 in human T-cell leukemia virus type I-dependent T-cell transformation: implications for adult T-cell leukemia leukemogenesis*. Cancer Res, 2004. 64:1287-1292.
141. Bodnar, J.S., et al. *Positional cloning of the combined hyperlipidemia gene Hyplip1*. Nat Genet, 2002. 30:110-116.
142. Sheth, S.S., et al. *Thioredoxin-interacting protein deficiency disrupts the fasting-feeding metabolic transition*. J Lipid Res, 2005. 46:123-134.
143. Moffat, J., et al. *A lentiviral RNAi library for human and mouse genes applied to an arrayed viral high-content screen*. Cell, 2006. 124:1283-1298.
144. Sancak, Y., et al. *The Rag GTPases bind Raptor and mediate amino acid signalling to mTORC1*. Science, 2008. 320:1496-1501.
145. Dutta, B., et al. *Elucidating the temporal dynamics of chromatin-associated protein release upon DNA digestion by quantitative proteomic approach*. J Proteom, 2012. 75:5493-5506.
146. Mi, H., et al. *Large-scale gene function analysis with the PANTHER classification system*. Nat Protoc, 2013. 8:1551-1566.

147. Misra, A., et al. *N-WASP plays a critical role in fibroblast adhesion and spreading*. Biochem Biophys Res Commun, 2007. 364:908-912.
148. Hozumi, Y., et al. *Human squamous cell carcinoma from skin: establishment and characterization of a new cell line (HSC-5)*. J Dermatol, 1990. 17:143-148.
149. Boukamp, P., et al. *Normal keratinization in a spontaneously immortalized aneuloid human keratinocyte cell line*. J Cell Biol, 1988. 106:761-771.
150. Wheelock, M.J., and Jensen, P.J. *Regulation of keratinocyte intercellular junction organization and epidermal morphogenesis by E-cadherin*. J Cell Biol, 1992. 117:415-425.
151. Peng, X., et al. *Vinculin regulates cell-surface E-cadherin expression by binding to beta-catenin*. J Cell Sci, 2010. 123:567-577.
152. Xu, W., Baribault, H., and Adamson, E.D. *Vinculin knockout results in heart and brain defects during embryonic development*. Development, 1998. 125:325-337.
153. Zemljic-Harpf, A.E., et al. *Cardiac-myocyte-specific excision of the vinculin gene disrupts cellular junctions, causing sudden death or dilated cardiomyopathy*. Mol Cell Biol, 2007. 27:7522-7537.
154. Jagadeeswaran, R., et al. *Paxillin is a target for somatic mutations in lung cancer: implications for cell growth and invasion*. Cancer Res, 2008. 68:132-142.
155. Mamay, C.L., et al. *Cyclin D1 as a proliferative marker regulating retinoblastoma phosphorylation in mouse lung epithelial cells*. Cancer Lett, 2001. 168:165-172.
156. Hynes, R.O. *Integrins: bidirectional, allosteric signalling machines*. Cell, 2002. 110:673-687.
157. Lawlor, M.A., and Alessi, D.R. *PKB/Akt: a key mediator of cell proliferation, survival and insulin responses?* J Cell Sci, 2001. 114:2903-2910.
158. Mitsiades, C.S., Mitsiades, N., and Koutsilleris, M. *The Akt pathway: molecular targets for anti-cancer drug development*. Curr Cancer Drug Targets, 2004. 4:235-256.
159. Chu, E.C., and Tarnawski, A.S. *PTEN regulatory functions in tumour suppression and cell biology*. Med Sci Monitor, 2004. 10:RA235-RA241.
160. Ross, A.H., and Gericke, A. *Phosphorylation keeps PTEN phosphatase closed for business*. Proc Natl Acad Sci USA, 2009. 106:1297-1298.
161. Nalivaeva, N.N., and Turner, A.J. *Post-translational modifications of proteins: acetylcholinesterase as a model system*. Proteomics, 2001. 1:735-747.
162. Khoury, G.A., Baliban, R.C., and Floudas, C.A. *Proteome-wide post-translational modification statistics: frequency analysis and curation of the swiss-prot database*. Sci Rep, 2011. 1:90.
163. Hay, N., and Sonenberg, N. *Upstream and downstream of mTOR*. Genes Dev, 2004. 18:1926-1945.
164. Gingras, A.C., et al. *Regulation of 4E-BP1 phosphorylation: a novel two-step mechanism*. Genes Dev, 1999. 13:1422-1437.
165. Fields, A.P., and Regala, R.P. *Protein kinase C iota: human oncogene, prognostic marker and therapeutic target*. Pharmacol Res, 2007. 55:487-497.
166. Nagalakshmi, U., Waern, K., and Snyder, M. *RNA-Seq: a method for comprehensive transcriptome analysis*. Curr Protoc Mol Biol, 2010. Chapter 4:Unit 4.11.1-4.11.13.
167. Nookaew, I., et al. *A comprehensive comparison of RNA-Seq-based transcriptome analysis from reads to differential gene expression and cross-comparison with microarrays: a case study in Saccharomyces cerevisiae*. Nucleic Acids Res, 2012. 40:10084-10097.

168. Tocris. *Signaling pathways*. [Online] 2018. Available from: https://www.tocris.com /signaling-pathways#.WD6R8FyoN0w. [Accessed: 16th April 2018].
169. Nishi, H., Demir, E., and Panchenko, A.R. *Crosstalk between signalling pathways provided by single and multiple protein phosphorylation sites*. J Mol Biol, 2015. 427:511-520.
170. Krämer, A., et al. *Causal analysis approaches in Ingenuity Pathway Analysis*. Bioinformatics, 2014. 30:523-530.
171. Wieduwilt, M.J., and Moasser, M.M. *The epidermal growth factor receptor family: biology driving targeted therapeutics*. Cell Mol Life Sci, 2008. 65:1566-1584.
172. Hilger, R.A., Scheulen, M.E., and Strumberg, D. *The Ras-Raf-MEK-ERK pathway in the treatment of cancer. Onkologie*, 2002. 25:511-518.
173. Kim, D.H., et al. *mTOR interacts with raptor to form a nutrient-sensitive complex that signals to the cell growth machinery*. Cell, 2002. 110:163-175.
174. Sarbassov, D.D., et al. *Rictor, a novel binding partner of mTOR, defines a rapamycin-insensitive and raptor-independent pathway that regulates the cytoskeleton*. Curr Biol, 2004. 14:1296-1302.
175. Hasegawa, M., et al. *CD151 dynamics in carcinoma-stroma interaction: integrin expression, adhesion strength and proteolytic activity*. Lab Investig, 2007. 87:882-892.
176. Gorrini, C., et al. *Fibronectin controls cap-dependent translation through β1 integrin and eukaryotic initiation factors 4 and 2 coordinated pathways*. Proc Natl Acad Sci USA, 2005. 102:9200-9205.
177. Ahmed, S.M., et al. *G protein betagamma subunits regulate cell adhesion through Rap1a and its effector Radil*. J Biol Chem, 2010. 285:6538-6551.
178. Park, I., and Lee, H.S. *EphB/ephrinB signalling in cell adhesion and migration*. Mol Cells, 2015. 38:14-19.
179. Cohen-Hillel, E., et al. *Interleukin 8 and cell migration to inflammatory sites: the regulation of focal adhesion kinase under conditions of migratory desensitization*. Isr Med Assoc J, 2007. 9:579-583.
180. Lawson, C.D., and Burridge, K. *The on-off relationship of Rho and Rac during integrin-mediated adhesion and cell migration*. Small GTPases, 2014. 5:e27958.
181. Chan, P.M., Lim, L., and Manser, E. *PAK is regulated by PI3K, PIX, Cdc42, and PP2αC and mediates focal adhesion turnover in the hyperosmotic stress-induced p38 pathway*. J Biol Chem, 2008. 283:24949-24961.
182. Beviglia, L., and Kramer, B.H. *HGF induces FAK activation and integrin-mediated adhesion in MTLn3 breast carcinoma cells*. Int J Cancer, 1999. 83:640-649.
183. Carloni, V., et al. *Tyrosine phosphorylation of focal adhesion kinase by PDGF is dependent on ras in human stellate cells*. Hepatology, 2000. 31:131-140.
184. Lebrun, P., et al. *Cell adhesion and focal adhesion kinase regulate insulin receptor substrate-1 expression*. J Biol Chem, 2000. 275:38371-38377.
185. Korah, R., et al. *Expression of FGF-2 alters focal adhesion dynamics in migration-restricted MDA-MB-231 breast cancer cells*. Breast Cancer Res Treat, 2004. 88:17-28.
186. Keasey, M.P., et al. *Inhibition of a novel specific neuroglial integrin signaling pathway increases STAT3-mediated CNTF expression*. Cell Commun Signal, 2013. 11:35.
187. Sakamoto, S., Schwarze, S., and Kyprianou, N. *Anoikis disruption of focal adhesion-Akt signaling impairs renal cell carcinoma*. Eur Urol, 2011. 59:734-744.

188. Chen, J.K., et al. *Angiotensin IV induces tyrosine phosphorylation of focal adhesion kinase and paxillin in proximal tubule cells*. Am J Physiol Renal Physiol, 2001. 280:F980-F988.
189. Duperret, E.K., and Ridky, T.W. *Focal adhesion complex proteins in epidermis and squamous cell carcinoma*. Cell Cycle, 2013. 12:3272-3285.
190. Findlay, G.M., et al. *Interaction domains of Sos1/Grb2 are finely tuned for cooperative control of embryonic stem cell fate*. Cell, 2013. 152:1008-1020.
191. Harburger, D.S., and Calderwood, D.A. *Integrin signalling at a glance*. J Cell Sci, 2009. 122:159-163.
192. Boureax, A., et al. *Evolution of the Rho family of the ras-like GTPases in eukaryotes*. Mol Biol Evol, 2007. 24:203-216.
193. Schwartz, M. *Rho signalling at a glance*. J Cell Sci, 2004. 117:5457-5458.
194. Dovas, A., and Couchman, J.R. *RhoGDI: multiple functions in the regulation of Rho family GTPase activities*. Biochem J, 2005. 390:1-9.
195. Adra, C.N., et al. *RHOGDIγ: a GDP-dissociation inhibitor for Rho proteins with preferential expression in brain and pancreas*. Proc Natl Acad Sci USA, 1997. 94:4279-4284.
196. Wang, H., et al. *Overexpression of RhoGDI, a novel predictor of distant metastasis, promotes cell proliferation and migration in hepatocellular carcinoma*. FEBS Lett, 2014. 588:503-508.
197. Garcia-Mata, R., Boulter, E., and Burridge, K. *The invisible hand: regulation of RHO GTPases by RHOGDIs*. Nat Rev Mol Cell Biol, 2011. 12:493-504.
198. Wei, L., et al. *Inhibition of Rho family GTPases by Rho GDP dissociation inhibitor disrupts cardiac morphogenesis and inhibits cardiomyocyte proliferation*. Development, 2002. 129:1705-1714.
199. Yoon, Y.S., et al. *Suppressor of MEK null (SMEK)/protein phosphatase 4 catalytic subunit (PP4C) is a key regulator of hepatic gluconeogenesis*. Proc Natl Acad Sci USA, 2010. 107:17704-17709.
200. Wang, D., et al. *Depletion of histone demethylase KDM5B inhibits cell proliferation of hepatocellular carcinoma by regulation of cell cycle checkpoint proteins p15 and p27*. J Exp Clin Cancer Res, 2016. 35:37.
201. Ma, J., et al. *KDM6B elicits cell apoptosis by promoting nuclear translocation of FoxO1 in non-small cell lung cancer*. Cell Physiol Biochem, 2015. 37:201-213.
202. Zhang, L.H., et al. *Histone demethylase JARID1B promotes cell proliferation but is downregulated by N-Myc oncoprotein*. Oncol Rep, 2014. 31:1935-1939.
203. Wong, P.P., et al. *Histone demethylase KDM5B collaborates with TFAP2C and Myc to repress the cell cycle inhibitor p21cip (CDKN1A)*. Mol Cell Biol, 2012. 32:1633-1644.
204. Ma, Y.H., et al. *Forkhead box O1 promotes INS-1 cell apoptosis by reducing the expression of CD24*. Mol Med Rep, 2016. 13:2991-2998.
205. Wu, Y.Y., et al. *Triple negative breast tumours in African-American and Hispanic/Latina women are high in CD44+, low in CD24+, and have loss of PTEN*. PLoS One, 2013. 8:e78259.
206. Choi, J., et al. *MicroRNA-139-5p regulates proliferation of hematopoietic progenitors and is repressed during BCR-ABL-mediated leukemogenesis*. Blood, 2016. 128:2117-2129.
207. Diep, C.H., Knutson, T.P., and Lange, C.A. *Active FoxO1 is a key determinant of isoform-specific progesterone receptor transactivation and senescence programming*. Mol Cancer Res, 2016. 14:141-162.

208. Zhao, B., Tumaneng, K., and Guan, K. *The Hippo pathway in organ size control, tissue regeneration and stem cell self-renewal*. Nat Cell Biol, 2011. 13:877-883.
209. Yoon, H., et al. *Understanding the roles of FAK in cancer: inhibitors, genetic models and new insights*. J Histochem Cytochem, 2015. 63:114-128.
210. Mitra, S.K., and Schlaepfer, D.D. *Integrin-regulated FAK-Src signalling in normal and cancer cells*. Curr Opin Cell Biol, 2006. 18:516-523.
211. Schlaepfer, D.D., Mitra, S.K., and Ilic, D. *Control of motile and invasive cell phenotypes by focal adhesion kinase*. Biochim Biophys Acta, 2004. 1692:77-102.
212. Je, D.W., et al. *The inhibition of Src family kinase suppresses pancreatic cancer cell proliferation, migration and invasion*. Pancreas, 2014. 43: 768-776.
213. Giubellino, A., et al. *Grb2 signalling in cell motility and cancer*. Expert Opin Ther Targets, 2008. 12:1021-1033.
214. Cheng, S.Y.S., et al. *Grb2 promotes integrin-induced focal adhesion (FAK) autophosphorylation and directs the phosphorylation of protein tyrosine phosphastase α by the Src-FAK kinase complex*. Mol Cell Biol, 2014. 34:348-361.
215. McLean, G.W., et al. *The role of focal-adhesion kinase in cancer – a new therapeutic opportunity*. Nat Rev Cancer, 2005. 5:505-515.
216. Innocenti, M., et al. *Mechanisms through which Sos-1 coordinates the activation of Ras and Rac*. J Cell Biol, 2002. 156:125-136.
217. Pierre, S., Bats, A.S., and Coumoul, X. *Understanding SOS (son of sevenless)*. Biochem Pharmacol, 2011. 82:1049-1056.
218. De, S., Dermawan, J.K.T., and Stark, G.S. *EGF receptor uses Sos1 to drive constitutive activation of NFκB in cancer cells*. Proc Natl Acad Sci USA, 2014. 111:11721-11726.
219. Kortum, R.L., et al. *Targeted Sos1 deletion reveals its critical role in early T-cell development*. Proc Natl Acad Sci USA, 2011. 108:12407-12412.
220. Tokunaga, C., Yoshino, K., and Yonezawa, K. *mTOR integrates amino acid and energy-sensing pathways*. Biochem Biophys Res Commun, 2004. 313:443-446.
221. Laplante, M., and Sabatini, D.M. *mTOR signalling at a glance*. J Cell Sci, 2009. 122:3589-3594.
222. Rosner, M., et al. *mTOR phosphorylated at S2448 binds to raptor and rictor*. Amino Acids, 2010. 38:223-228.
223. Chung, J., et al. *PDGF and insulin-dependent pp70S6K activation mediated by phosphatidylinositol-3-OH kinase*. Nature, 1994. 370:71-75.
224. Wang, H., et al. *STAT1 activation regulates proliferation and differentiation of renal progenitors*. Cell Signal, 2010. 22:1717-1726.
225. Dai, B., et al. *Compensatory upregulation of tyrosine kinase Etk/BMX in response toandrogen deprivation promotes castration-resistant growth of prostate cancer cells*. Cancer Res, 2010. 70:5587-5596.
226. Organ, S.L., and Tsao, M.S. *An overview of the c-MET signalling pathway*. Ther Adv Med Oncol, 2011. 3:S7-S19.
227. Ward, IV, R.E., et al. *The protein 4.1, ezrin, radixin, moesin (FERM) domain of Drosophila Coracle, a cytoplasmic component of the septate junction, provides functions essential for embryonic development and imaginal cell proliferation*. Genetics, 2001. 159:219-228.
228. Cardone, L., et al. *Mitochondrial AKAP121 binds and targets protein tyrosine phosphatase D1, a novel positive regulator of Src signalling*. Mol Cell Biol, 2004. 24:4613-4626.
229. Pillai, P., et al. *A novel PKC-l inhibitor abrogates cell proliferation and induces apoptosis in neuroblastoma*. Int J Biochem Cell Biol, 2011. 43:784-794.

230. Sun, L., et al. *JAK1-STAT1-STAT3, a key pathway promoting proliferation and preventing premature differentiation of myoblasts*. J Cell Biol, 2007. 179:129-138.
231. Li, Y., et al. *BMX/Etk promotes cell proliferation and tumorigenicity of cervical cancer cells through PI3K/AKT/mTOR and STAT3 pathways*. Oncotarget, 2017. 8:49238-49252.
232. Gui, Y., et al. *Regulation of MET receptor tyrosine kinase signaling by suppressor of cytokine signalling 1 in hepatocellular carcinoma*. Oncogene, 2015. 34:5718-5728.
233. Jiang, W.G., and Hiscox, S. *Cytokine regulation of ezrin expression in the human colon cancer cell line HT29*. Anticancer Res, 1996. 16:861-865.
234. Jui, H.Y., et al. *Protein-tyrosine phosphatase D1, a potential regulator and effector for Tec family kinases*. J Biol Chem, 2000. 275:41124-41132.
235. Carlucci, A., et al. *PTPD1 supports receptor stability and mitogenic signalling in bladder cancer cell*. J Biol Chem, 2010.285:39260-39270.
236. Yang, J.Q., et al. *Loss of PKC lambda/iota impairs Th2 establishment and allergic airway inflammation in vivo*. Proc Natl Acad Sci USA, 2009. 106:1099-1104.
237. Jain, N., et al. *Conditional knockout of N-WASP in mouse fibroblast caused keratinocyte hyper proliferation and enhanced wound closure*. Sci Rep, 2016. 6:38109.
238. Antypas, H., Libberton, B., and Melican, K. *Reducing background cytokine expression in epithelial cells without serum starvation*. Methods X, 2014. 1:251-253.
239. Han, Y.H., et al. *The effect of MG132, a proteasome inhibitor on HeLa cells in relation to cell growth, reactive oxygen species and GSH*. Oncol Rep, 2009. 22:215-221.
240. Tang, E.D., et al. *Negative regulation of the forkhead transcription factor FKHR by Akt*. J Biol Chem, 1999. 274:16741-16746.
241. Matheny, R.W., Jr., and Adamo, M.L. *Effects of PI3K catalytic subunit and Akt isoform deficiency on mTOR and p70S6K activation in myoblasts*. Biochem Biophys Res Commun, 2009. 390:252-257.
242. Arboleda, M.J., et al. *Overexpression of AKT2/Protein Kinase Bβ leads to up-regulation of β1 Integrins, increased invasion, and metastasis of human breast and ovarian cancer cells*. Cancer Res, 63. 63:196-206
243. Rudd, M.D., et al. *Constitutively active FoxO1a and a DNA-binding domain mutant exhibit distinct co-regulatory functions to enhance progesterone receptor A activity*. J Mol Endocrinol, 2007. 38:673-690.
244. Wang, Y., Zhou, Y., and Graves, D.T. *FOXO transcription factors: their clinical significance and regulation*. Biomed Res Int, 2014. 2014:925350
245. Bennett, B.L., et al. *SP600125, an anthrapyrazolone inhibitor of Jun N-terminal kinase*. Proc Natl Acad Sci USA, 2001. 98:13681-13686.
246. Lefloch, R., Pouysségur, J., and Lenormand, P. *Single and combined silencing of ERK1 and ERK2 reveals their positive contribution to growth signalling depending on their expression levels*. Mol Cell Biol, 2008. 28:511-527.
247. Lefloch, R., Pouysségur, J., and Lenormand, P. *Total ERK1/2 activity regulates cell proliferation*. Cell Cycle, 2009. 85:705-711.
248. Pal, R., et al. *Inhibition of ERK1/2 restores GSK3 activity and protein synthesis levels in a model of tuberous sclerosis*. Sci Rep, 2017. 7:4174.
249. Yang, J.Y., et al. *ERK promotes tumorigenesis by inhibiting FoxO3a via Mdm2-mediated degradation*. Nat Cell Biol, 2008. 10:138-148.

250. Asada, S., et al. *Mitogen-activated protein kinases, Erk and p38, phosphorylate and regulate FoxO1*. Cell Signal, 2007. 19:519-527.
251. Liu, L., Halfter, W., and Layer, P.G. *Inhibition of cell proliferation by cytosine-arabinoside and its interference with spatial and temporal differentiation patterns in the chick retina*. Cell Tissue Res, 1986. 244:501-513.
252. Shin, D.J., et al. *Genome-wide analysis of FoxO1 binding in hepatic chromatin: potential involvement of FoxO1 in linking retinoid signalling to hepatic gluconeogenesis*. Nucleic Acids Res, 2012. 40:11499-11509.
253. Waldhart, A.N., et al. *Phosphorylation of TXNIP by AKT mediates acute influx of glucose in response to insulin*. Cell Rep, 2017. 19:2005-2013.
254. Kibbe, C., et al. *FoxO1 competes with carbohydrate response element-binding protein (ChREBP) and inhibits thioredoxin-interacting protein (TXNIP) transcription in pancreatic beta cells*. J Biol Chem, 2013. 288:23194-23202.
255. Yang, Z., et al. *Phosphorylation and inactivation of PTEN at residues Ser380/Thr382/383 induced by Helicobacter pylori promotes gastric epithelial cell survival through PI3K/Akt pathway*. Oncotarget, 2015. 6:31916-31926.
256. Chaneton, B., et al. *Serine is a natural ligand and allosteric activator of pyruvate kinase M2*. Nature, 2012. 491:458-462.
257. Zhang, C.Y., et al. *FoxO1 expression in keratinocytes promotes connective tissue healing*. Sci Rep, 2017. 7:42834.
258. Mori, R., et al. *Reduced FoxO1 expression accelerates skin wound healing and attenuates scarring*. Am J Pathol, 2014. 184:2465-2479.
259. Dochi, T., et al. *Phosphorylation of human immunodeficiency virus type 1 capsid protein at serine 16, required for peptidyl-prolyl isomerase-dependent uncoating, is mediated by virion-incorporated extracellular signal-regulated kinase 2*. J Gen Virol, 2014. 95:1156-1166.
260. Samadani, R., et al. *Small-molecule inhibitors of ERK-mediated immediate early gene expression and proliferation of melanoma cells expressing mutated BRAF*. Biochem J, 2015. 467:425-438.
261. Nishi, K., et al. *Cyclin D1 downregulation is important for permanent cell cycle exit and initiation of differentiation induced by anchorage-deprivation in human keratinocytes*. J Cell Biochem, 2009. 106:63-72.
262. Yang, K., Hitomi, M., and Stacey, D.W. *Variations in cyclin D1 levels through the cell cycle determine the proliferative fate of a cell*. Cell Div, 2006. 1:32.
263. Suetsugu, S., and Takenawa, T. *Translocation of N-WASP by nuclear localization and export signals into the nucleus modulates expression of HSP90*. J Biol Chem, 2003. 278:42515-42523.
264. Mochizuki, M., et al. *Thioredoxin regulates cell cycle via the ERK1/2-Cyclin D1 pathway*. Antioxid Redox Signal, 2009. 11:2957-2971.
265. Ponugoti, B., et al. *FoxO1 promotes wound healing through the up-regulation of TGF-β1 and prevention of oxidative stress*. J Cell Bio, 2013. 203:327-343.

Appendix 1: List of plasmids cloned for this study

Main vector used for plasmid cloning

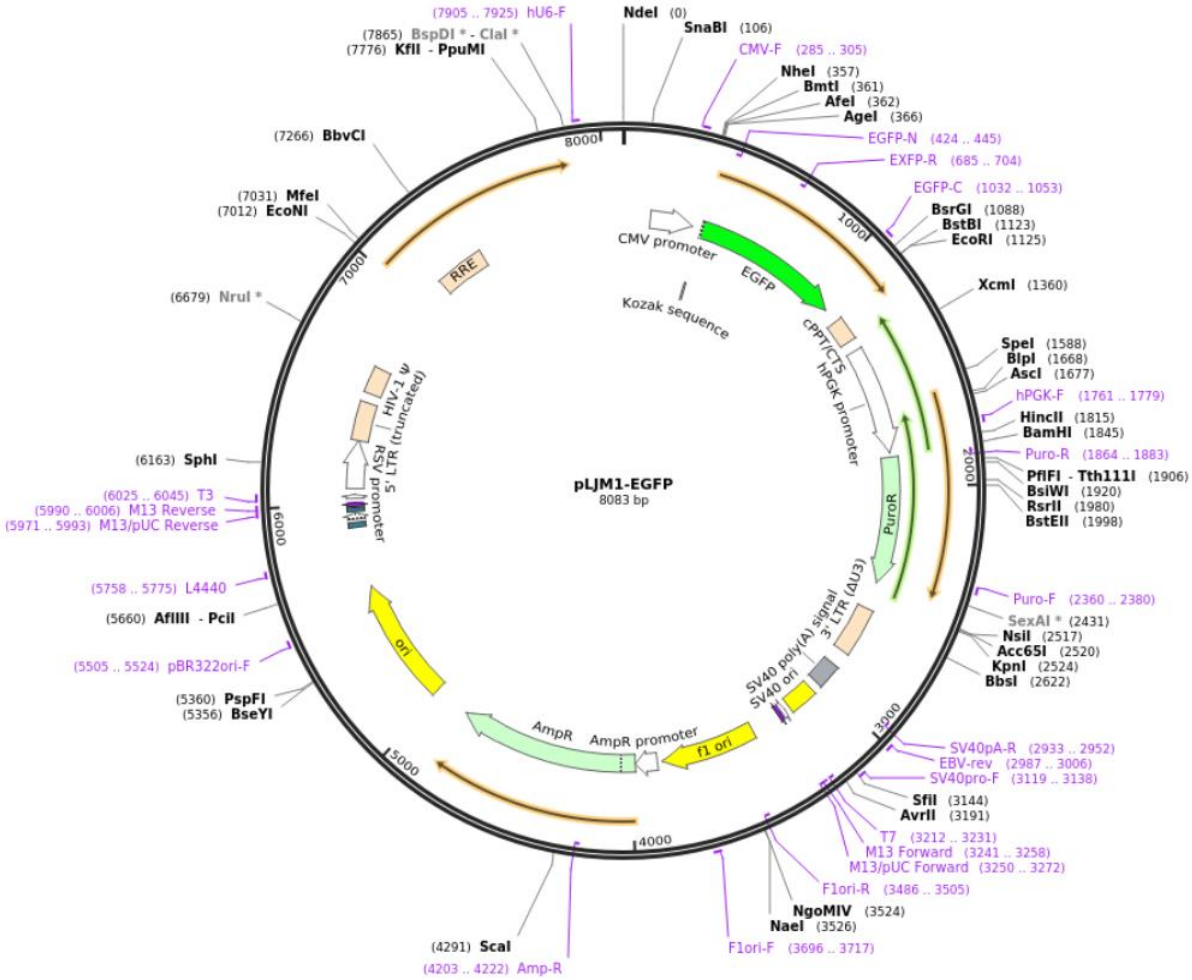

Map of the original pLJM1-EGFP vector. Areas representing sequences for puromycin resistance (PuroR in light green) and EGFP (EGFP in dark green) are shown. Original pLJM1-EGFP vector was from Prof David Sabatini (Addgene #19319) [143].

The pTT1-Puro vector for subsequent DNA cloning was constructed by replacing EGFP sequences in pLJM1-EGFP with an MCS. The pTT2-Neo vector for subsequent DNA cloning was constructed by replacing pTT1-Puro PuroR sequences with sequences for neomycin resistance.

Names of plasmids cloned and details

pTT2-SGK1sh-Neo	Human specific SGK1 shRNA under U6 promoter, with constitutively expressed CMV promoter, with neomycin selection marker; insert source: queried BlastN human RefSeq RNA.
pTT2-TXNIPsh-Neo	Human specific TXNIP shRNA under U6 promoter, with constitutively expressed CMV promoter, with neomycin selection marker; insert source: queried BlastN human RefSeq RNA.
pTT2-ERK2sh-Neo	Human specific ERK2 shRNA under U6 promoter, with constitutively expressed CMV promoter, with neomycin selection marker; insert source: queried BlastN human RefSeq RNA.
pTT2-FOXO1g-Neo	Human specific FoxO1 cDNA clone under constitutively expressed CMV promoter, with neomycin selection marker; insert source: Addgene #13507 [239].
pTT2-TXNIPg-Neo	Human specific TXNIP cDNA clone under constitutively expressed CMV promoter, with neomycin selection marker; insert source: NIH_MGC_310, Mammalian Gene Collection.

Names of other plasmids used and details

pTT1-Puro	Empty vector with multiple cloning site under constitutively expressed CMV promoter, with puromycin selection marker
pTT1-N-WASP-Puro	Human specific N-WASP cDNA clone under constitutively expressed CMV promoter, with puromycin selection marker; insert source: Dr Amrita Salvi, former colleague.
pTT2-Neo	Empty vector with multiple cloning site under constitutively expressed CMV promoter, with neomycin selection marker

Appendix 2: List of shRNAs generated for this study

Names of genes targeted, reverse primers R1 and R2, and sequences in lower case

Human SGK1 shRNA	GTTCTCGAGaacagtgtgcaataagattgcCCGGTGTTTCGTCCTTTCCAC
	CGGAATTCCATGGCAAAAAAgcaatcttattgcacactgttCTCGAGAACAGTGTG
Human CK1A1 shRNA	TAACTCGAGttatagagttaatgcagagtcCCGGTGTTTCGTCCTTTCCAC
	CGGAATTCCATGGCAAAAAgactctgcattaactctataaCTCGAGTTA
Human ERK2 shRNA	CATCTCGAGatgttctcatgtctgaagcgcCCGGTGTTTCGTCCTTTCCAC
	CGGAATTCCATGGCAAAAAAgcgcttcagacatgagaacatCTCGAGATGTTCTCATGTC
Human TXNIP shRNA	TTCCTCGAGgaatattcaactcgaaggatgCCGGTGTTTCGTCCTTTCCAC
	CGGAATTCCATGGCAAAAAcatccttcgagttgaatattcCTCGAGGAA

Appendix 3: List of real-time PCR primers for this study

Names of genes targeted and forward and reverse primer sequences

Human MRPL27	CTGGTGGCTGGAATTGACCGCTA
	CAAGGGGATATCCACAGAGTACCTTG
Human PKM2	CAGAGGCTGCCATCTACCAC
	CCAGACTTGGTGAGGACGAT
Human CTGF	TTGGCCCAGACCCAACTA
	GCAGGAGGCGTTGTCATT
Human N-WASP	AAGGATGGGAAACTATTGTGGGA
	GACGGCCCAAAAGGTCTGTAA
Human cMyc	CTTCTCTCCGTCCTCGGATTCT
	GAAGGTGATCCAGACTCTGACCTT
Human SGK1	CATAGGAGTTATTGGCAAT
	CTTCCATCTCACTAACCA
Human TXNIP	ACTCGTGTCAAAGCCGTTAGG
	TCCCTGCATCCAAAGCACTT
Human FOXO1	TTATGACCGAACAGGATGATCTTG
	TGTTGGTGATGAGAGAAGGTTGAG